



## STRATEGIES TO INCREASE THE CELL-TO-ELECTRODE ELECTRON TRANSFER OF BIOANODES FOR THEIR APPLICATION IN CELLULAR-BASED BIOPHOTOVOLTAICS

Zaida Nair Herrero Medina

**ADVERTIMENT.** L'accés als continguts d'aquesta tesi doctoral i la seva utilització ha de respectar els drets de la persona autora. Pot ser utilitzada per a consulta o estudi personal, així com en activitats o materials d'investigació i docència en els termes establerts a l'art. 32 del Text Refós de la Llei de Propietat Intel·lectual (RDL 1/1996). Per altres utilitzacions es requereix l'autorització prèvia i expressa de la persona autora. En qualsevol cas, en la utilització dels seus continguts caldrà indicar de forma clara el nom i cognoms de la persona autora i el títol de la tesi doctoral. No s'autoritza la seva reproducció o altres formes d'explotació efectuades amb finalitats de lucre ni la seva comunicació pública des d'un lloc aliè al servei TDX. Tampoc s'autoritza la presentació del seu contingut en una finestra o marc aliè a TDX (framing). Aquesta reserva de drets afecta tant als continguts de la tesi com als seus resums i índexs.

**ADVERTENCIA.** El acceso a los contenidos de esta tesis doctoral y su utilización debe respetar los derechos de la persona autora. Puede ser utilizada para consulta o estudio personal, así como en actividades o materiales de investigación y docencia en los términos establecidos en el art. 32 del Texto Refundido de la Ley de Propiedad Intelectual (RDL 1/1996). Para otros usos se requiere la autorización previa y expresa de la persona autora. En cualquier caso, en la utilización de sus contenidos se deberá indicar de forma clara el nombre y apellidos de la persona autora y el título de la tesis doctoral. No se autoriza su reproducción u otras formas de explotación efectuadas con fines lucrativos ni su comunicación pública desde un sitio ajeno al servicio TDR. Tampoco se autoriza la presentación de su contenido en una ventana o marco ajeno a TDR (framing). Esta reserva de derechos afecta tanto al contenido de la tesis como a sus resúmenes e índices.

**WARNING.** Access to the contents of this doctoral thesis and its use must respect the rights of the author. It can be used for reference or private study, as well as research and learning activities or materials in the terms established by the 32nd article of the Spanish Consolidated Copyright Act (RDL 1/1996). Express and previous authorization of the author is required for any other uses. In any case, when using its content, full name of the author and title of the thesis must be clearly indicated. Reproduction or other forms of for profit use or public communication from outside TDX service is not allowed. Presentation of its content in a window or frame external to TDX (framing) is not authorized either. These rights affect both the content of the thesis and its abstracts and indexes.

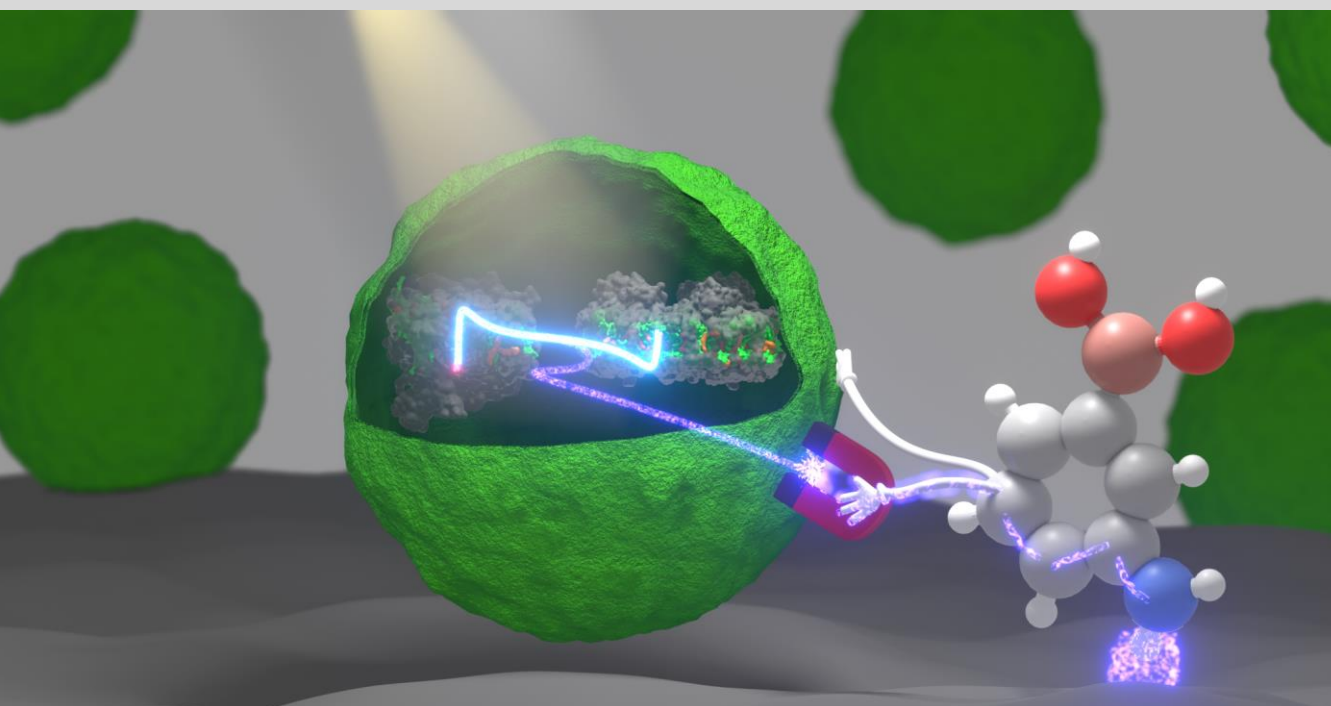


UNIVERSITAT  
ROVIRA i VIRGILI

# Strategies to increase the cell-to-electrode electron transfer of bioanodes for their application in cellular-based biophotovoltaics

---

ZAIDA NAIR HERRERO MEDINA



DOCTORAL THESIS  
2022





Zaida Nair Herrero Medina

STRATEGIES TO INCREASE THE CELL-TO-ELECTRODE  
ELECTRON TRANSFER OF BIOANODES FOR THEIR  
APPLICATION IN CELLULAR-BASED BIOPHOTOVOLTAICS

DOCTORAL THESIS

supervised by Dr. Ioanis Katakis

Departament d'Enginyeria Química



UNIVERSITAT ROVIRA I VIRGILI

Tarragona

2022





UNIVERSITAT  
ROVIRA I VIRGILI

Departament d'Enginyeria Química  
Universitat Rovira i Virgili  
Campus Sescelades,  
Avda. Països Catalans, 26  
43007 Tarragona  
Tel: 977 55 85 79  
Fax: 977 55 96 67

Prof. Dr. Ioanis Katakis

CERTIFIES:

That the present study, entitled “**Strategies to increase the cell-to-electrode electron transfer of bioanodes for their application in cellular-based biophotovoltaics**” presented by Zaida Nair Herrero Medina for the award of the degree of Doctor, has been carried out under my supervision at the Department of Chemical Engineering of Universitat Rovira i Virgili, and that it fulfils the requirements to obtain the International Mention.

Tarragona, May 31<sup>st</sup> 2022.

Prof. Dr. Ioanis Katakis

**To my beloved father, Agustín Herrero Otorel.**



## **Acknowledgements**

My sincere gratitude to my supervisor Dr. Ioanis Katakis for giving me the opportunity to pursue this thesis and for his guidance.

I am very grateful for the Martí Franquès scholarship of the Department of Chemical Engineering of the Universitat Rovira i Virgili and to the King Abdulaziz Univestity for providing the funds to execute this project.

I should thank Nuria Juanpere for her diligence and efficient work and her willingness to help with every administrative issue I had. I would like to thank Álex for always being available to help me with my doubts regarding the doctorate.

I would like to thank Rita and Núria from the scientific & technical resources service (SRCIT) of the URV for their help and training in microcopy techniques.

I am very grateful to Dr. Schuhmann for finding a place for me in his group, for being so close and dedicating time to me. I also want to express my gratitude to Dr. Conzuelo for helping me and guiding me in my stage at the group of Dr. Schuhmann.

My special gratitude to all my colleagues of the Interfibio group: Barbara for helping me with all administrative issues and purchases. Mari Carmen for patiently accompanying me so many times to change nitrogen gas cylinders. Vasso for turning a blind eye to my disorder in lab 223. Ivan for those unexpected jokes and always trying to make a group and my PhD colleagues Xhensila, Nihad, Nassif and Cansu for the moments shared. I am extremely grateful to

my co-worker Ester, for sharing her deep knowledge about algae with me.

I would like to especially thank the colleagues in the group that I consider my friends: Mayreli, who has been my mom at work, always helping me altruistically and giving me a more calm and pragmatic view of life. Mabel for the eternal laughs. Miriam, for so many good times outside of work. Laura “mi comadre nunca incomadre”, we have both walked this path at the same time. For the laughs, the dances, the support, thank you “usurpadora”.

I would also like to thank my friends Anabel and Judit, for taking care of me, hugging me and supporting me for so long.

I am very grateful to Mari and Miguel for bringing into the world and raising one of the most important people in my life. For welcoming me so well into your family. I want also to thank Omaira for taking care of everyone so much.

I am extremely fortunate to rely on a great family that has always supported me. I would like to express my gratitude to my brothers Rodri and Manu and especially to my sisters Alba, who has been like a second mother and my "gemelier" Mariem for always accompanying me in everything since I was little and being so positive. I love you all very much and without your help I would not have been able to carry out this work. I would also like to thank my sister Laura for listening to my podcasts and my brothers-in-law Meri and Ricardo for all the good times. I want to thank my brother-in-law and friend Roger, because even though I drive you a little crazy, I know you like me. I am very grateful to have as a friend my sister-

in-law Reme who listens to me, encourages me and gives me free therapy so many times. I am deeply grateful to have my beautiful nieces Emma, Aitana, Ingrid, Anna, Bruna and Vega who fill me with joy and love. I would also like to thank Antonio for taking care of my mother.

I am deeply indebted to my dear mother, the most positive and strong person I know. For raising us with so much love and patience. From you I have learned what resilience is and I did not know that I would put it into practice so much during this thesis. I love you very much and this work is also dedicated to you. I am very grateful to the most generous person I have ever known, my father. For always encouraging me to do what I proposed, for believing in me and teaching me to care and love. I miss you and I know you would be so proud of all of us.

Finally, I would like to thank my travel companion, Julio. For helping me and taking care of me so much. For knowing better than me what I need at all times. For cheering me up in the low moments. For the bad chemistry jokes, which only here I will admit that make me laugh. Thanks for coming to volleyball. Love you.

## **List of publications derived from the present Doctoral Thesis**

1. Z. Herrero-Medina, P. Wang, A. Lielpetere, A.S. Bashammakh, A.O. Alyoubi, I. Katakis, F. Conzuelo, W. Schuhmann, A biophotoelectrode based on boronic acid-modified *Chlorella vulgaris* cells integrated within a redox polymer, *Bioelectrochemistry*. 146 (2022) 108128. <https://doi.org/10.1016/j.bioelechem.2022.108128>.

## Abbreviations

**μ-BPV:** micro-BPV

**2-ABA:** [REDACTED]

**2-PDA:** [REDACTED]

**3-AP:** [REDACTED]

**3-APBA:** [REDACTED]  
[REDACTED]

**3-PDA:** [REDACTED]

**4-ABA:** [REDACTED]

**ACN:** acetonitrile

**ADQS:** 9,10-anthraquinone-  
2,6-disulfonate

**AHSA:** [REDACTED]  
[REDACTED]

**AMSA:** [REDACTED]  
[REDACTED]

**ANI:** aniline

**APS:** ammonium persulfate

**APX:** ascorbate peroxidase

**ATO:** antimony-tin oxide

**ATP:** adenosine triphosphate

**BBM:** Bold's basal medium

**BES:** bioelectrochemical  
system

**BOD:** bilirubin oxidase

**BPV:** biophotovoltaic

**BSA:** bovine serum albumin

**CA:** chronoamperometry

**CBA:** carbon-based anode

**CBB:** Calvin-Benson-  
Bassham cycle

**CCCP:** carbonyl cyanide m-  
chlorophenylhydrazone

**CE:** coulombic efficiency

**CET:** cyclic electron  
transport

**Chl *a*:** chlorophyll *a*

**CPA:** conducting polymer-  
based anode

**CV:** cyclic voltammetry

**Cyt *b<sub>6</sub>f*:** cytochrome *b<sub>6</sub>f*

**D:** immobilization by  
desiccation

**DBMIB:** 2,5-dibromo-  
3-methyl-6-isopropyl-p-  
benzoquinone

**DCBQ:** 2,6-dichloro-1,4-  
benzoquinone

**DCHQ:** 2,6-dichloro-1,4-  
hydroquinone

**DCMU:** 3-(3,4-dichlorophenyl)-1,1-dimethyl urea

**Dd**: [REDACTED]  
[REDACTED]  
[REDACTED]

**D**: [REDACTED]  
[REDACTED]  
[REDACTED]

**DEET:** direct extracellular electron transfer

**d**: [REDACTED] deficient

**DG:** doping degree

**DMF:** N, N-dimethylformamide

**d**: [REDACTED]-deficient

**DOS:** density of states

**E<sub>F</sub>:** Fermi level

**EFC:** enzymatic fuel cell

**EPS:** extracellular polymeric substances

**EQF:** photon flux

**EROI:** energy return on investment

**ESEM:** environmental scanning electron microscopy

**ET:** electron transfer

**F:** steady state fluorescence in the light before SP

**F<sub>0</sub>:** minimum fluorescence level in the dark

**F<sub>0</sub>':** minimum fluorescence level upon light

**Fd:** ferredoxin

**Flv A/B:** flavodiiron proteins

**F<sub>M</sub>:** maximum fluorescence level in the dark

**F<sub>M</sub>':** maximum fluorescence level in the light

**FNR:** ferredoxin-NADP<sup>+</sup> reductase

**FTO:** fluorine-doped tin oxide

**F<sub>v</sub>/F<sub>M(D)</sub>:** F<sub>v</sub>/F<sub>M</sub> of cells grown in replete medium immobilized by desiccation

**F<sub>v</sub>/F<sub>M(S)</sub>:** F<sub>v</sub>/F<sub>M</sub> of cell suspension grown in replete medium

**F<sub>v</sub>/F<sub>M(W)</sub>:** F<sub>v</sub>/F<sub>M</sub> of cells grown in replete medium immobilized by wet immobilization

**F<sub>v</sub>/F<sub>M</sub>:** maximum photochemical quantum yield of PSII

**FWHM:** Full width at half maximum

**GCE/oCNT/PAPBA:**  
GCE/oCNT modified with  
PAPBA

**GCE/oCNT/PAPBA\_C.**  
*vulgaris*: *C. vulgaris*  
immobilized on  
GCE/oCNT/PAPBA

**GCE/oCNT:** GCE modified  
with oCNT

**GCE/PAPBA:** GCE modified  
with PAPBA

**GCE:** glassy carbon electrode

**GHG:** greenhouse gas

**GOX:** glucose oxidase

**HNQ:** 2-hydroxy-1,4-  
naphthoquinone

**HQNO:** 2-heptyl-4-  
hydroxyquinoline n-oxide

**HSD:** honest significant  
difference

**ICP:** intrinsically conducting  
polymer

**IEET:** indirect extracellular  
electron transfer

**IO:** inverse opal ITO

**IO-ITO:** inverse opal ITO

**ITO:** indium tin oxide

**KB/WPCC:** ketjen Black-  
modified waterproof carbon  
cloth

**LET:** linear electron transport

**LHCI:** light harvesting  
complex I

**LHCII:** light harvesting  
complex II

**MBA:** metal-based anode

**MDC:** microbial desalination  
cell

**MEC:** microbial  
electrosynthesis cell

**MFC:** microbial fuel cell

**ML:** measuring light

**MSC:** microbial solar cell

**MV:** methyl-viologen

**Mv-BOD:** *Myrothecium*  
*verrucaria* bilirubin oxidase

**MWCNT:** multiwalled  
carbon nanotube

**MWCO:** molecular weight  
cut off

**NADP<sup>+</sup>:** nicotinamide  
adenine dinucleotide  
phosphate

**NADPH:** reduced  
nicotinamide adenine  
dinucleotide phosphate

**NEM:** N-ethylmaleimide

**Nhd-2:** type II NADH  
dehydrogenase

**NO:** non-regulated non-photochemical quenching

**NPQ:** light-induced non-photochemical quenching

**oCNT:** oxidized multi-walled carbon nanotubes

**OCV:** open circuit voltage

**OD<sub>680</sub>:** optical density at 680 nm

**OEC:** oxygen evolving complex

**OL:** oxidation level

**OMC:** outer membrane cytochrome

**ORP:** open raceway pond

**ORR:** oxygen reduction reaction

**OTA:** optically transparent anode

**P2ABA:** [REDACTED]

**P2PDA:** [REDACTED]

**P3AP:** [REDACTED]

**P3PDA:** [REDACTED]

**P4ABA:** [REDACTED]

**P680:** PSII-reaction center chlorophyll

**P700:** PSI-reaction center chlorophyll

**PAHSA:** [REDACTED]

**PAM:** pulse amplitude modulation

**PAMSA:** [REDACTED]

**PANI:** polyaniline

**PAPBA:** poly-(3-aminophenylboronic acid)

**PAR:** photosynthetic active radiation

**PB:** phosphate buffer

**p-BQ:** p-benzoquinone

**PBS:** phosphate buffer saline

**PBSE:** 1-pyrenebutyric acid N-hydroxysuccinimide ester

**PC:** plastocyanin

**PCA:** pyrenecarboxylic acid

**PEDGE:** poly(ethylene glycol) diglycidyl ether

**PEDOT:PSS:** poly(3,4-ethylenedioxythiophene):poly styrene sulfonate



**PEM:** proton exchange membrane

**PETC:** photosynthetic electron transport chain

**PFP:** poly(fluorene-alt-phenylene)

**PGR5:** proton gradient regulation 5

**PGRL1:** proton gradient regulation-like 1

**PMA:** phenylmercuric acetate

**PMFC:** photosynthetic microbial fuel cell

**P-Os G43:** poly(1-vinylimidazole-co-allylamine)-[Os(bpy)<sub>2</sub>Cl]Cl

**P-Os:** Os-complex modified redox polymer

**PP:** polypyrrole

**PPFD:** photosynthetic photon flux density

**PQ:** plastoquinone

**PQH2:** plastoquinol

**PSI:** photosystem I

**PSII:** photosystem II

**PT:** theoretical achievable power output

**PV:** photovoltaic

**P-vio:** viologen modified polymer

**QA:** plastoquinone intermediate A

**QB:** plastoquinone intermediate B

**qE:** high-energy-state quenching

**qI:** photoinhibitory quenching

**q<sub>p</sub>:** coefficient of photochemical fluorescence quenching

**qT:** state transition quenching

**QY:** quantum yield

**RCII:** reaction center of PSII

**RE:** renewable energy

**RGO:** reduced graphene oxide

**RH:** relative humidity

**ROS:** reactive oxygen species

**RT:** room temperature

**RuBisCO:** ribulose-1,5-biphosphate carboxylase-oxygenase

**s.u.:** shake-up

**S:** cell suspension grown in replete media

**SHE:** standard hydrogen electrode

**SN\***: concentrated supernatant

**SOD**: superoxide dismutase

**SP**: saturation pulse

**SRG**: solar radiation at the ground state level


**SS**: stainless-steel

**SWV**: square-wave voltammetry

**TEM**: transmission electron microscopy

**UNFCCC**: United Nations Framework Convention on Climate Change

**UPS**: Ultraviolet Photoelectron Spectroscopy

**W**:  immobilization

**Wd**:   
  


**Wd**:   
  


**XPS**: X-Ray Photoelectron Spectroscopy

$\Gamma_{\text{PAPBA}}$ : surface area coverage of PAPBA

$\Phi \text{NO}_{(D)}$ :  $\Phi$  NO of cells grown in replete medium immobilized by desiccation

$\Phi \text{NO}_{(W)}$ :  $\Phi$  NO of cells grown in replete medium immobilized by wet immobilization

$\Phi \text{NO}$ : quantum yield of NO

$\Phi \text{NPQ}_{(D)}$ :  $\Phi$  NPQ of cells grown in replete medium immobilized by desiccation

$\Phi \text{NPQ}_{(S)}$ :  $\Phi$  NPQ of cell suspension grown in replete medium

$\Phi \text{NPQ}_{(W)}$ :  $\Phi$  NPQ of cells grown in replete medium immobilized by wet immobilization

$\Phi \text{NPQ}$ : quantum yield of NPQ

$\Phi \text{PSII}_{(D)}$ :  $\Phi$  PSII of cells grown in replete medium immobilized by desiccation

$\Phi \text{PSII}_{(S)}$ :  $\Phi$  PSII of cell suspension grown in replete medium

$\Phi \text{PSII}_{(W)}$ :  $\Phi$  PSII of cells grown in replete medium immobilized by wet immobilization

$\Phi \text{PSII}$ : effective photochemical quantum yield of PSII

## **Table of contents**

<b>Summary</b> .....	<b>1</b>
<b>Chapter 1. Introduction</b> .....	<b>5</b>
<b>Chapter2. Boronic acid modified electrodes for electrochemical communication with <i>Chlorella vulgaris</i></b> .....	<b>59</b>
<b>Chapter 3. Derivatives of polyanilines as platforms to construct biophotoelectrodes</b> .....	<b>91</b>
<b>Chapter 4. A biophotoelectrode based on boronic acid-modified <i>Chlorella vulgaris</i> cells integrated within a redox polymer</b> .....	<b>133</b>
<b>Chapter 5. Exoelectrogenesis of <i>C. vulgaris</i>-based biophotoelectrodes due to stress</b> .....	<b>159</b>
<b>Conclusions and Future work</b> .....	<b>195</b>
<b>Appendix A</b> .....	<b>A1</b>
<b>Appendix B.</b> .....	<b>B1</b>
<b>Appendix C.</b> .....	<b>C1</b>
<b>Appendix D.</b> .....	<b>D1</b>

## Summary

The aim of the present thesis is to explore strategies for the improvement of cell-to-electrode electron transfer in bioanodes for their application in cellular-based biophotovoltaic (BPV) devices. Two strategies were approached: i) implementation of boronic acid derivatives as electrochemical connectors between the cell and the electrode ii) exposure of cells to stress to improve their exoelectrogenesis.

**Chapter 1** is a general introduction to the state of the art of the application of BPVs, with especial emphasis on the solutions focused on improving the efficiency of cell-to-electrode electron transfer. An overview of photosynthesis and the most common technique to assess photosynthetic efficiency and stress in photosynthetic microorganisms is also presented.

**Chapter 2** explores, for the first time, the use of poly(3-aminophenylboronic acid) (PAPBA) to improve the electron transfer from *Chlorella vulgaris* (*C. vulgaris*, green microalga) to nanostructured conductive surfaces. A biophotoelectrode was constructed by [REDACTED] 3-aminophenylboronic acid (3-APBA) on an oxidized carbon nanotube(oCNT)-modified electrode. Optimization of cell to polymer ratio was performed to achieve the highest possible performance, yielding some of the highest photocurrents reported for this strain ( $(2.0 \pm 0.6) \mu\text{A cm}^{-2}$ ). The mechanism proposed for the enhanced photocurrent is that boronic acid moieties bind to oligosaccharides of the cell surface promoting

intimate contact with the conducting polymer that ultimately acts as electrochemical wire towards the electrode. Microscopic characterisation showed the cells embedded within the conducting polymer, presumably establishing intimate contact with the electrode surface. The study of the electron transfer mechanism revealed the photoexcitation of photosystem II (PSII) as the electron source. Furthermore, the PAPBA-oCNT-modified electrode was tested with five more photosynthetic microorganisms outperforming electrodes without PAPBA in terms of photocurrent generation.

**Chapter 3** is a survey of homopolymers of unsubstituted and substituted anilines as a platform to construct bioanodes for their use in BPVs. The chemical and electronic structures of the polymers were studied by cyclic voltammetry (CV), X-Ray Photoelectron Spectroscopy (XPS) and Ultraviolet Photoelectron Spectroscopy (UPS). Different structures were obtained depending on the electronic effect and the position of the substituent in the aniline ring. Phenazine and phenoxazine-like polymers were obtained with amino and hydroxy groups as substituents and with carboxylic group in the *para*- position of the aniline ring. While polyaniline-like polymers were obtained with electron acceptor groups in *meta*- and *ortho*-position to amino. In all polymers with electron donor substituents, the photocurrent was ascribed to *their intrinsic photoactivity*. On the contrary, certain photocurrent generation was observed when *C. vulgaris* was attached on the surface of polyaniline (PANI) and polymers with electron withdrawing substituents. PAPBA-modified electrodes outperformed all the tested polymers in terms of photocurrent generation from *C. vulgaris*.

**Chapter 4** proposes a bioanode integrating boronic acid-modified *C. vulgaris* cells embedded in an Os complex-modified redox polymer (P-Os) hydrogel matrix. Prior to the integration of the cells in the hydrogel, the cell wall of *C. vulgaris* was functionalized with 3-APBA, improving the stability of the resulting film and promoting the electron transfer presumably due to an enhanced crosslinking between the redox polymer matrix and immobilized cells. The electron transfer mechanism was studied by analysing the action spectrum of the bioanode, the addition of a freely diffusing electron mediator, a photosynthetic inhibitor, and by scanning photoelectrochemical microscopy (SPECM), revealing that electrons in this configuration might originate from alternative electron pathways linked to the photoexcitation of photosystem I (PSI). Furthermore, the proposed bioanode was coupled to a bilirubin oxidase (BOD)-based biocathode to construct a proof-of-concept BPV.

**Chapter 5** evaluates [REDACTED] starvation and [REDACTED] as stressing agents to improve exoelectrogenesis of *C. vulgaris*-based biophotocathodes. The photocurrent generation, the photosynthetic efficiency and the stress induced to the cells under these conditions were analysed by simultaneously combining electrochemistry and pulse amplitude modulation (PAM) fluorometry. Photocurrent was only obtained when cells were immobilized by [REDACTED] on the PAPBA-oCNT-modified electrode. Transmission electron micrographs showed that [REDACTED] cells presented thinner cell wall than not [REDACTED] cells and certain degree of cell wall disruption, which might facilitate the extracellular electron transfer. PAM

fluorometry and transmission electron microscopy revealed that ██████████ *C. vulgaris* suffered photoinhibition, resulting in a compromised integrity of the photosynthetic apparatus.

Overall, this work has contributed to increasing the knowledge on the electron transfer mechanism of *C. vulgaris*-based-biophotoelectrodes for their application in cellular-based BPVs. The results presented here show boronic acid derivatives as promising element in tailoring bioanodes and encourage the optimization of electron-transfer pathways toward the development of advanced cellular-based BPVs.

# Chapter 1

## Introduction

According to the International Energy Agency, the world energy consumption in 2021 increased 4.6% [1] returning to pre-pandemic levels (14485 Mtoe (617 EJ) in 2019 [2]). About 80% of this energy was supplied by fossil fuels. The continuous increase of the world's population and the depletion of fossil fuels makes the current energy model unsustainable. Moreover, the burning of fossil fuels for energy production (i.e., electricity, heating, transport and industry) generates roughly three quarters of the greenhouse gas (GHG) emissions, 89% of it being CO<sub>2</sub> [2,3]. These GHG emissions are accountable for the climate change due to the increase in global temperature. Thus, considering the serious consequences of rising temperatures on our planet, the United Nations Framework Convention on Climate Change (UNFCCC) convened to pursue efforts to limit the increase in global temperature below 1.5 °C for this century to mitigate the climate change [4]. The forecast of reducing global CO<sub>2</sub> emissions to net zero by 2050 to fulfil the 2015 Paris Agreement [3], encourages governments and industry to completely transform the current “energy model” towards renewable energy (RE) sources.

From an engineering point of view, selecting a renewable primary energy source on which to focus innovation efforts requires an analysis of the technical potential of said source. As “technical potential” is defined the net energy that can reasonably reach the consumer based on best technologies available and considering, not



simply the total earth flux, but also land, geographical distribution, conversion, and ecosystem disturbance constraints. Such analysis shows that only solar energy (either directly through light conversion to energy or indirectly through its extraction from biomass) can satisfy humanity's growing energy needs [5,6]. In fact, at this moment, solar energy is accountable for 60% of the renewable capacity additions [7].

Nevertheless, the sustainable deployment of a RE source requires that economic, environmental and social factors be considered in addition to the technical potential of said source. Although photovoltaics (PV)s shows promising advances in light-to electricity conversion efficiency (above 40% at lab scale) [8,9] and helps job creation, it is not a carbon neutral RE source since the manufacturing, maintenance, transport and disposal of the PV cells contributes to GHG emissions. Furthermore, the scarcity of raw materials required for the manufacturing of PV systems, the necessity to implement devices for storage to alleviate the intermittency of energy generation (e.g., hours of less or lack of sun irradiance) and the mitigation of the albedo effect increase the investment costs and affect the sustainability of this technology, especially when its widespread implementation is considered. Hence, the productive model for the future will require that solutions be developed in parallel, including biorefineries that will also provide the raw materials that today are supplied by fossil hydrocarbons and coal, thus promoting the circular bioeconomy.

Among biorefineries, those based on microalgae, are promising in terms of sustainability since they would not compete for land and other resources with agriculture and furthermore, they would contribute to the removal of CO<sub>2</sub> from the atmosphere. However, overall sustainability can only be achieved if algae biorefineries are implemented in large scale, if all fractions of chemical compounds are exploited (without limiting exploitation to fatty acids and biofuels), and if the overall energy return on investment (EROI) is superior to 5-8. Current state of the art barely reaches this last requirement with cradle-to-factory-gate EROI estimates ranging from 1 to 4.1 for biodiesel production [10]. These low EROI values can be addressed by coupling bioreactors to biophotovoltaic (BPV) cells that allow the production of energy during algae growth avoiding second law limitations and downstream processes such as harvesting and digestion (Figure 1.1).

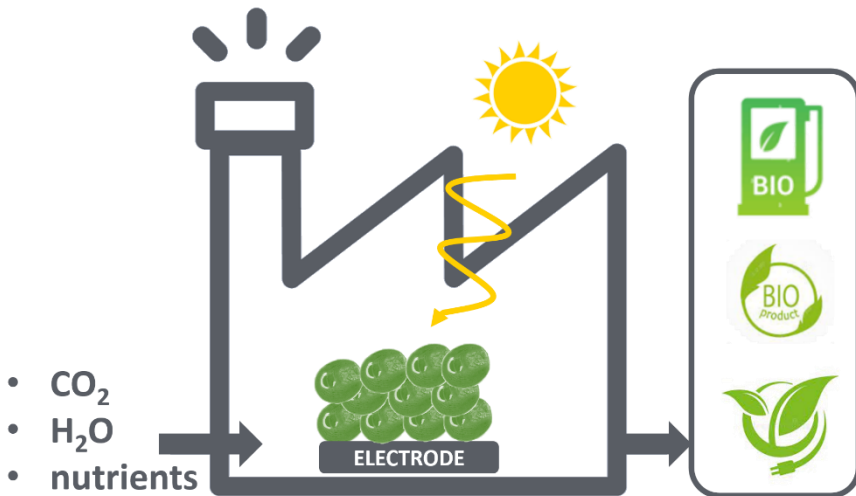


**Figure 1.1.** Schematic representation of an algal biorefinery coupled to biophotovoltaics

## 1.1 BPVs

BPVs are bioelectrochemical system (BES) that exploit the ability of oxygenic photosynthetic microorganisms or their subcellular photosynthetic parts to harness solar light and produce energy from the harvesting of electrons during the photosynthetic process. Current subcellular-based BPVs yield higher power efficiencies than cellular-based BPVs [11]. However, the stability of subcellular-based BPV is limited because they lack of the *in vivo* self-repair mechanisms [12,13], making this option less appealing for large scale applications than BPVs operated with the whole microorganism [14,15].

In cellular-based BPVs, the light absorbed by the photosystem II (PSII), located in the thylakoid membranes of photosynthetic microorganisms, is used to catalyse the splitting of water into oxygen, protons and electrons (Figure 1.2). These electrons are transferred through a series of electron carriers called the photosynthetic electron transport chain (PETC) to reduce nicotinamide adenine dinucleotide phosphate (NADP<sup>+</sup>) to NADPH, which is further used to reduce CO<sub>2</sub> to carbohydrates [16]. The principle of cellular-based BPVs relies on the possibility that some of these electrons can escape their natural pathway and be collected by an electrode, that can act as an anode in a fuel cell. The current is produced because electrons flow from the anode to the cathode through an external circuit. In the cathode, electrons are used to reduce oxygen to form water. The driving force for the electric current flow is the potential difference between the two electrodes.

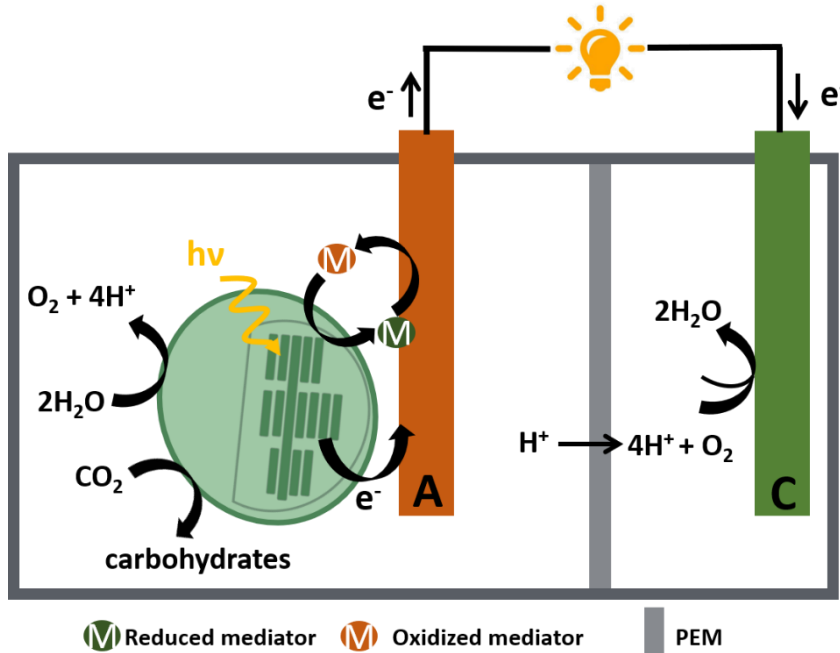


**Figure 1.2.** Schematic representation of a double-chamber microalgae-based BPV. PEM, proton exchange membrane.

There are other BESs that use heterotrophic microorganisms, such as microbial fuel cells (MFCs) [17] or anoxygenic photosynthetic microorganisms (i.e., photosynthetic microbial fuel cells (PMFCs)) [18] or a combination of oxygenic photosynthetic and heterotrophic microorganisms, namely complex PMFCs [19] (Figure 1.3). The former does not rely in the energy of the sun for electricity production while the two latter are sun-dependent. However, all of them generate electricity from the metabolism of an external organic source or electron reducing equivalents. On the contrary, BPVs only need water as the electron source to produce electricity. In addition, as a side reaction,  $\text{CO}_2$  is fixed and transformed to carbohydrates [16]. Furthermore, they are capable to produce electricity also in dark

conditions probably due to a breakdown of carbon intermediates during the light-phase of the photosynthesis [14,20].

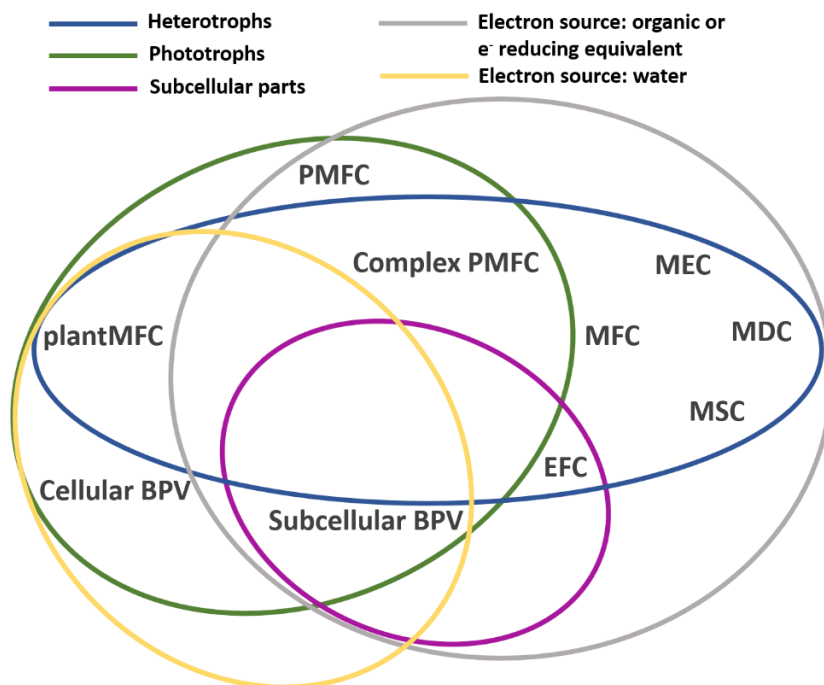


**Figure 1.3.** Classification of bioelectrochemical systems (BES). BPV, biophotovoltaic; EFC, enzymatic fuel cell; MEC, microbial electrosynthesis cell; MDC, microbial desalination cell; MFC, microbial fuel cell; MSC, microbial solar cell; PMFC, photosynthetic microbial fuel cell.

McCormick et al. estimated the maximum achievable power outputs of BPVs to range between 700 to 7000 mW m<sup>-2</sup> considering a potential at peak power of 213 mV or 315 mV and the worst and the best scenarios of power input and metabolic losses [21]. Nevertheless, these estimates are outdated since continuous advances in the design of BPVs have led to improved open circuit voltages (OCVs) and lower voltage drop. Thus, we recalculated the maximum potential power outputs of BPVs considering 0.4 V of potential at peak power obtained in a BPV assembled with a bioanode consisting

of *Synechococcus* sp.-iron oxide nanoparticles-neodymium iron boride magnet complexes, which attained the highest power output so far (806 mW m<sup>-2</sup>) [22]. The rest of variables were kept unchanged: two different solar radiation at the ground state level (SRG: 103000 and 263000 mW m<sup>-2</sup> for Oslo and Riyadh, respectively); 90% of photosynthetic efficiency conversion (i.e., 5 moles of photons generate 2 moles of electrons for the reduction of NADP<sup>+</sup> to NADPH) [23]; two different coulombic efficiencies (60% and 95% like in MFCs); and two different scenarios of metabolic losses (33% and 3%, for high and low, respectively). First, the photon flux ( $E_{QF}$ ,  $\mu\text{mol photons m}^{-2} \text{ s}^{-1}$ ) at the two different SRG was calculated using equation 1.1:

$$E_{QF} = SRG \times \frac{\lambda}{N_A \times h \times c} \times 10^{-5} \quad (1.1)$$

where  $\lambda$  is the midpoint wavelength at the photosynthetic active radiation (PAR),  $N_A$  is the Avogadro's number,  $h$  is the Planck constant ( $= 6.63 \times 10^{-34}$  J s) and  $c$  is the speed of light ( $= 2.998 \times 10^8$  m s<sup>-1</sup>). Then, the estimated theoretical achievable power output ( $P_T$ ) and the estimated theoretical power efficiency were calculated using equation 1.2 and 1.3, respectively:

$$P_T = \frac{E_{QF} \times 0.5 \times 0.9 \times 2 \text{ mol } e^- \times (100 - \% \text{ metabolic losses}) \times CE \times F \times OCV}{5 \text{ mol photons} \times 10^5} \quad (1.2)$$

$$\text{Power efficiency (\%)} = \frac{\text{Power output}}{\text{Power input}} \times 100 \quad (1.3)$$

where the factor 0.5 stands for the 50% of the  $E_{QF}$  that is used for light reactions (i.e., PAR),  $CE$  is the coulombic efficiency and  $F$  is the Faraday constant (96500C mol<sup>-1</sup>). The re-estimated maximum

achievable power output would range between 700 (the minimum achievable power output calculated by McCormick et al. [21]) and 9854 mW m<sup>-2</sup> and the maximum achievable power efficiencies would be between 0.7% and 3.7%. These theoretical achievable values are calculated considering the incident radiation and the aforementioned energy losses in the light-to-chemistry conversion, disregarding other important factors which are currently more complex to quantify (e.g., quantity of active photosystems units per cell, cyclic electron flow around photosystem I (PSI) and photosynthetic efficiency). These factors might affect the coulombic efficiency and shift the potential power outputs of BPVs up or down by several orders of magnitude.

Although the maximum achievable power efficiencies in BPVs are far lower than the achievable with PVs, BPVs still remain promising not only in algal biorefinery models, but also as alternative RE source in areas less suited for PVs. Furthermore, the estimated values indicate that there is still room for improvement with this emerging technology since the maximum power obtained so far (806 mW m<sup>-2</sup>) is roughly 12-fold less than the estimated achievable with the more optimistic exoelectrogenic scenario [22]. Improvement of BPVs' efficiency only can be addressed by overcoming the main current limitations on: the device architecture, the oxygen reduction efficiency of the cathode, the anode performance and the photosynthetic microorganism exoelectrogenicity (Figure 1.4).

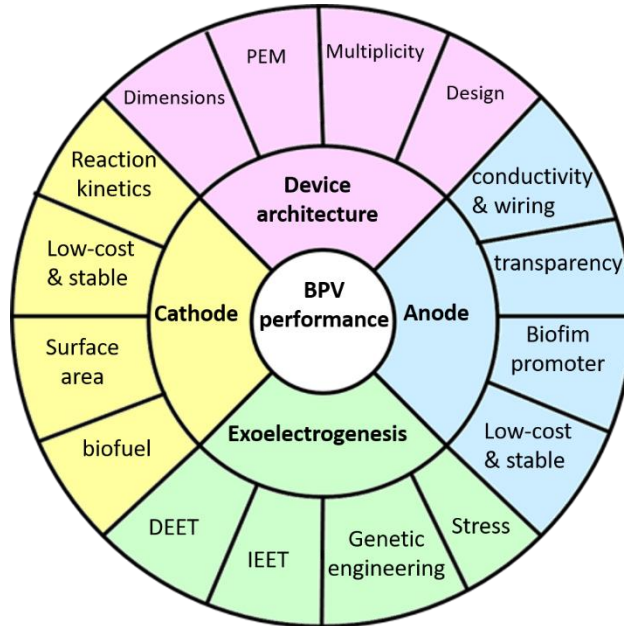


**Figure 1.4.** Main factors to consider in the construction of a BPV device.

Although the first cellular-based BPV was constructed nearly 40 years ago [20], this is an emerging technology given that it was not until 2010 that research on this topic delved into the fundamentals of the processes, assisted by advancements in characterisation techniques, genetic engineering, and materials technology [24]. Disregarding the differences on the microorganisms and the reductive processes that fuel the cell, the design of BPVs is based on the same features as their counterparts that use heterotrophs (MFCs), whose technological development is more established (ten times more publications in the last two decades than BPVs) [25]. In the next paragraphs, the state of the art in BPVs regarding the main contributors to the device performance is discussed, focusing especially on the architecture of the anode and in the exoelectrogenicity of the microorganisms.



## 1.2. BPVs' architecture

BPVs can be mounted in a two-chamber configuration, where anode and cathode are separated by a proton exchange membrane (PEM) [20,26,27] or in a single-chamber fashion, where both electrodes are placed in the same chamber without any membrane to isolate the microorganisms from the cathode [28–30]. Single-chamber configuration is preferable, whenever microorganisms are sessile on the anode surface, because reduces internal resistance and is cheaper. Since the distance between anode and cathode increases internal resistance, the miniaturization of BPV devices has led to improved power outputs [31–34]. In fact, some of the highest power outputs have been obtained with micro-BPVs ( $\mu$ -BPVs). 438 mW m<sup>-2</sup> were achieved by Liu et al. with a  $\mu$ -BPV fuelled by *Synechocystis* PCC6803 (*Synechocystis*) [32]. Saar et al. attained a maximum power output of 500 mW m<sup>-2</sup> using a mutant *Synechocystis* in a microfluidic BPV device that allowed to spatially decouple the operations of charging an electron carrier and power delivery [33]. Nevertheless, these  $\mu$ -BPVs are attractive for high-throughput studies but not for large-scale applications, unless the scale-up contemplates the parallelization of these devices [17,33,35].

## 1.3. The cathode

Another important contributor to the power output is the cathode. A highly efficient cathode should reduce oxidants at the most positive potential to increase the power efficiency of the device. Usually in BPVs, the electron acceptor of the cathode is O<sub>2</sub>, which is reduced to form water through a 4-electron pathway, or to form the less desired H<sub>2</sub>O<sub>2</sub> through a 2-electron pathway. The product of the oxygen

reduction reaction (ORR) will depend on the type of cathode material used. Of course, the cathode should be environmentally friendly, with high stability and cost-effective, but more importantly it should provide fast ORR kinetics. Therefore, good cathode materials should possess high active surface area and porosity to supply more reaction sites. Additionally, it should have great conductivity to enhance the electron transfer (ET) rate [36]. The most widely used cathodes in BPVs are platinum coated carbon-based [32,37], noble metal-based [14,34,38] and carbon-based electrodes [39,40]. However, limitations on the concentration of oxygen in catholytes led to the deployment of air-cathodes [22,30,32,41,42]. In recent years, biocathodes have gained attention. Electrode surfaces have been modified with multicopper oxidase enzymes that show high efficiency in reducing O<sub>2</sub>, such as laccase [43,44] or bilirubin oxidase (BOD) [45–47]. Furthermore, the use of biocathodes modified with other enzymes or proteins can be useful not only for power generation but also for biofuel production. For example, the use of biocathodes based on PSI coupled to hydrogenases have shown to be promising for hydrogen production [48,49].

#### **1.4. The anode**

The anode design is crucial for a good BPV performance since it is the collector of the electrons stemming from the photosynthetic microorganisms. Ideally, anodes should fulfil these three main requirements: high electrical conductivity, long-term electrochemical stability at the conditions of application and biocompatibility, especially if cells are expected to form a biofilm on the electrode. Moreover, the anode should be low-cost and sustainable. Table 1.1.

shows the maximum performance in BPVs of the different classes of anode configurations described below. The stability of the BPV and the method of immobilization of each configuration is also reported. However, the variability in the characterization methods used in different works, in the architecture of the BPVs, or in the microorganisms and the conditions used in the different studies makes difficult a reliable comparison between anode configurations.

#### **1.4.1. Metal-based anodes (MBA)**

Several anode materials have been used so far, being the metal-based the first ones chronologically, such as stainless-steel (SS) [42], indium tin bismuth (InSnBi) alloy [34] and platinum [38]. However, they are flat surfaces, which are less suitable for biofilm formation.

#### **1.4.2. Carbon-based anodes (CBA)**

Creation of biofilms on the electrode surface increases the microbe-electrode interaction enhancing the ET rate and reducing activation losses [50,51]. It is well known that the chemistry (e.g., hydrophilicity and charge density) and the surface area of the anode play a key role in the cell adhesion [52]. Thus, in the pursue of facilitating the cellular adhesion on the anode, carbon-based materials such as carbon paper [53], carbon cloth [54] and carbon fibre [55] substituted inorganic metal-based anodes (Figure 1.5). Carbon-based materials are cheaper, robust and their increased roughness enhances cell loading and biofilm stability. Pre-treatment of these materials not only increases active surface area but also introduces new functional groups that might favour biofilm development as has been observed in MFCs [56,57]. Moreover,

functional groups on the electrode surface can influence the ET process at the biofilm-electrode interface [52]. However, carbon-based electrodes present lower electrical conductivity than metals. For example, the electrical conductivity of graphite is  $3 \times 10^5 \text{ S m}^{-1}$ , whereas for Pt is  $9.43 \times 10^6 \text{ S m}^{-1}$  and for SS is  $1.39 \times 10^6 \text{ S m}^{-1}$  [58].

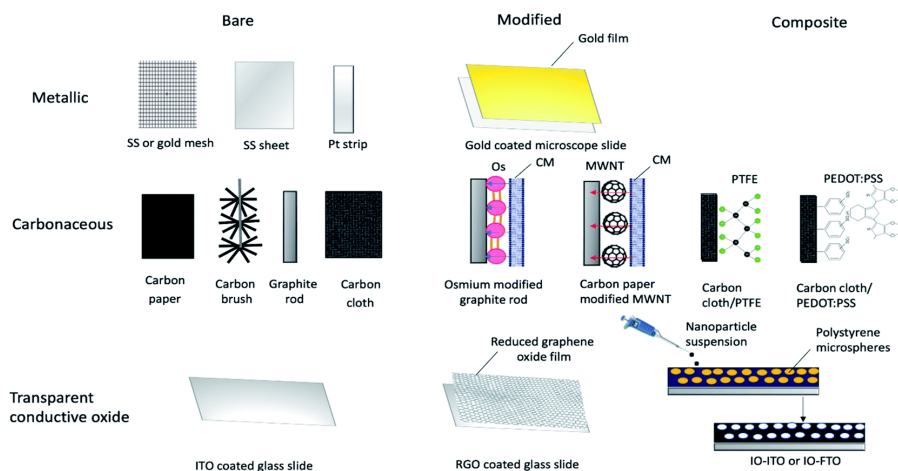


**Figure 1.5.** Summary of various anode architectures used in BPVs. CM, cytoplasmic membrane; IO-FTO, inverse opal fluorine doped tin oxide; IO-ITO, inverse opal indium tin oxide; ITO, indium tin oxide; MWNT, multiwalled nanotube; Os, osmium; Pt, platinum; PEDOT:PSS, poly(3,4-ethylenedioxythiophene):polystyrene sulfonate; PTFE, polytetrafluoroethylene; RGO, reduced graphene oxide; SS, stainless-steel. Reprinted from ref. [59].

Modification of carbon-based anodes with multiwalled carbon nanotubes (MWCNTs) improves electrical conductivity and enhances active surface area promoting cell adhesion [43,60,61]. High power outputs ( $35 \text{ mW m}^{-2}$ ) were achieved in a mediatorless BPV with cyanobacteria *Nostoc* sp. physiosorbed on carbon paper modified with MWCNTs [43]. However, these materials tend to hamper the light transfer to the photosynthetic biofilm due to their opacity.

### 1.4.3. Optically transparent anodes (OTA)

The opacity has been overcome by using transparent electrode materials, such as reduced graphene oxide (RGO) [62,63], fluorine-doped tin oxide (FTO)[30,39] and indium tin oxide (ITO)[14,41,42,62]. Moreover, recent advances in deposition techniques allow to modify porous substrates with these metal oxides and RGO to obtain nano and microstructured electrodes with good electrical conductivity ( $\approx 1 \times 10^4 \text{ S m}^{-1}$  for ITO films [64]), optical transparency and hydrophilicity. Moreover, highly porous structures improve mass transport and reduce nutrient starvation. Thorne et al. constructed a PMFC with *Chlorella vulgaris* (*C. vulgaris*) biofilms formed on a porous ceramic coated FTO electrode. This electrode offered a 3D-scaffold for biofilm formation that yielded 16-fold higher photocurrent than carbon-based anodes [39]. Wenzel *et al.* fabricated porous (at the nano and microscale length) inverse-opal ITO (IO-ITO) electrodes that enhanced the photocurrent generation of *Nostoc punctiforme* and *Synechocystis* ca. 300-fold compared to non-porous ITO electrodes [30]. However, the scarcity of indium limits the deployment of ITO anodes for large-scale applications.

**Table 1.1.** Anode performance of different anode configurations:

<i>Anode</i>	<i>Microorganism</i>	<i>BPV architecture</i>	<i>Stability</i>	<i>ET mechanism</i>	<i>Immobilization method</i>	<i>Power density (mW m<sup>-2</sup>)</i>	<i>Photocurrent density (mA m<sup>-2</sup>)</i>	<i>Ref.</i>
<b>MBA: InSnBi alloy</b>	<i>Synechocystis</i> sp PCC6803	μ-BPV	Not reported	Endogenous mediator	Physisorption	105	2840 <sup>a</sup>	[34]
<b>CBA: CP/MWCNT</b>	<i>Nostoc</i> sp ATCC 27893	Single chamber	5 days (photocurrent). Afterwards, required nutrient replenishment	Mediatorless	Physisorption	35	60	[43]
				Benzoquinone		100	2330 <sup>a</sup>	
<b>OTA: IO-ITO/FTO COATED GLASS</b>	<i>Synechocystis</i> sp PCC6803	Single chamber	3 days	Endogenous mediator	Physisorption		11.5	[30]
<b>CPA: CC/3D-PEDOT:PSS</b>	<i>Synechocystis</i> sp PCC6803	μ-BPV	> 20days at ≈18.6 mW m <sup>-2</sup>	Not reported	Physisorption	438	2270 <sup>a</sup>	[32]

CBA, carbon-based anode; CC, carbon cloth; CP, carbon paper; CPA, conducting polymer-based anode; InSnBi, indium tin bismuth; IO, inverse opal; ITO, indium tin oxide; FTO, fluorine-doped tin oxide; MBA, metal-based anode; MWCNT, multiwalled carbon nanotube; OTA, optically transparent anode; PEDOT:PSS, poly(3,4-ethylenedioxythiophene):polystyrene sulfonate. <sup>a</sup> Without dark current subtracted.

#### **1.4.4. Electron-conducting polymer-based anodes (CPA)**

The very extended wiring of photosynthetic components with redox polymers [65–67] has also been exploited in cellular-based BPVs. Gorton and coworkers electrochemically communicated green microalgae *Paulschulzia pseudovolvox* and cyanobacteria *Leptolyngbia* to graphite electrodes by electron hopping between osmium redox centers of an Os-complex modified redox polymer (P-Os) outperforming bare-graphite electrodes in terms of photocurrent [68,69]. The P-Os forms a 3D hydrogel with the cells by electrostatic interactions favouring the ET rate (since the cells are wrapped by Os-redox centres) and guaranteeing electrolyte diffusion.

Intrinsically conducting polymer (ICP)-modified anodes are widely used in MFCs due to their great conductivity (ranging between  $10^3$  to  $10^6$  S  $m^{-1}$ ) and relative low cost [70]. Polyaniline (PANI), polypyrrole (PP) and poly(3,4-ethylenedioxythiophene):polystyrene sulfonate (PEDOT:PSS) have demonstrated to improve BPV performance. PANI-coated glass electrodes have been used to immobilize cyanobacteria *Pseudanabaena limnetica* with enhanced power output compared to carbon paper electrodes [42]. *Synechocystis* biofilms on PP and PANI modified carbon anodes overperformed power outputs obtained with carbon cloth anodes ( $1.3$  mW  $m^{-2}$ ,  $0.95$  mW  $m^{-2}$  and  $0.35$  mW  $m^{-2}$  for PP-, PANI-modified and bare carbon cloth anodes, respectively) [28]. The improved power outputs were attributed to the favoured biofilm formation on the positively charged surface and to the enhanced ET efficiency through the conjugated systems of

ICPs. Liu et al. fabricated a microporous conductive anode by coating carbon cloth with PEDOT:PSS, with remarkable power outputs due to its conductive properties and its increased surface area for cell adhesion [32].

Electron-conducting polymers are promising materials in BPVs because they allow to coat almost any electrode surface even with complicated geometries like foams or sponges. Additionally, the plethora of functional moieties that can be introduced on these polymers permits to rationally tailor surfaces to improve biofilm formation. However, there is little knowledge about the long-term biocompatibility and stability of these polymer-based bioanodes.

#### **1.4.5. Cell immobilization on the anode surface**

Microalgal biofilm formation is a 4-step process that comprises aggregates of cells growing attached to a surface. These aggregates consist of cells embedded in extracellular polymeric substances (EPS), which are composed of polysaccharides, proteins, nucleic acids and phospholipids. The role of the EPS is to offer protection and stick cells together facilitating the inter and intracellular communication [71]. The physicochemical properties of the electrode (e.g., roughness, hydrophobicity and surface charge) are key in inducing biofilm formation.

Up to the present day, the immobilization of photosynthetic microorganisms in BPVs has been driven by electrostatic and hydrophobic interactions and Van der Waals forces between the cell and the electrode surface. This kind of interactions are relatively weak and cells can be easily detached from the electrode surface



under shear forces, hence compromising the stability of the bioanode. Stronger interactions such as covalent bond and supramolecular interactions can improve biofilm stability.

Surface modification of electrodes with molecules that can recognize cell structures through supramolecular interactions can increase the contact between the electrode and microorganisms. For example, lectins, which are proteins capable of binding to carbohydrates through supramolecular interactions, are widely used to identify and monitoring bacteria infestation [72,73]. However, lectins are very expensive making impractical their use for large-scale BPVs.

Boronic acid derivatives are a cheaper and not species-specific alternative to lectins. Covalent binding of cells with boronic acid residues have been widely used for cytosensor applications [74,75]. This approach has also been explored in MFCs but not yet in BPVs. Lapinsonnière et al. modified graphite electrodes with phenylboronic acid outperforming MFCs in terms of power output of bare graphite electrodes. Faster biofilm formation on the boronic acid modified anode was attributed to the covalent binding of boronic acid moieties to 1,2- or 1,3-diols present in saccharides of the bacteria's cell membrane [76]. Moreover, surface modification with boronic acids is relatively fast and cheap. Zhao et al. electropolymerized 3-aminophenylboronic acid (3-APBA) on carbon cloth electrodes. The resultant poly(3-aminophenylboronic acid) anode enhanced biofilm formation and facilitated the ET of *Shewanella putrefaciens* [77].

## **1.5. Exoelectrogenesis of oxygenic photosynthetic microorganisms**

### **1.5.1. Oxygenic photosynthetic microorganisms**

Oxygenic photosynthetic microorganisms are prokaryotic (cyanobacteria) and eukaryotic (microalgae) microbes that are capable to oxidize water and reduce CO<sub>2</sub> to form carbohydrates and oxygen. These types of cells are discriminated by the presence (microalgae) or lack (cyanobacteria) of membrane-bounded organelles (Figure 1.6). Microalgae are surrounded by a porous and rigid cell wall, whose composition might vary among classes, but generally it is composed by polysaccharides. On the contrary, the cell wall of cyanobacteria resembles that of Gram-negative bacteria. It consists of three layers: an inner layer (i.e., the peptidoglycan layer), a periplasmic space and an outer layer, namely S-layer, which is formed of glycoproteins and proteins. Extracellular appendages ascribed to motility and adhesion functions may traverse the cell wall and the plasma membrane of both prokaryotic and eukaryotic photoautotrophs. The plasma membrane, which is under the cell wall, controls the flux of molecules to the protoplasm. The photosynthetic apparatus is enclosed in the thylakoid membranes, which are located in the cytoplasm in cyanobacteria or inside the chloroplasts in the case of microalgae [78–80].

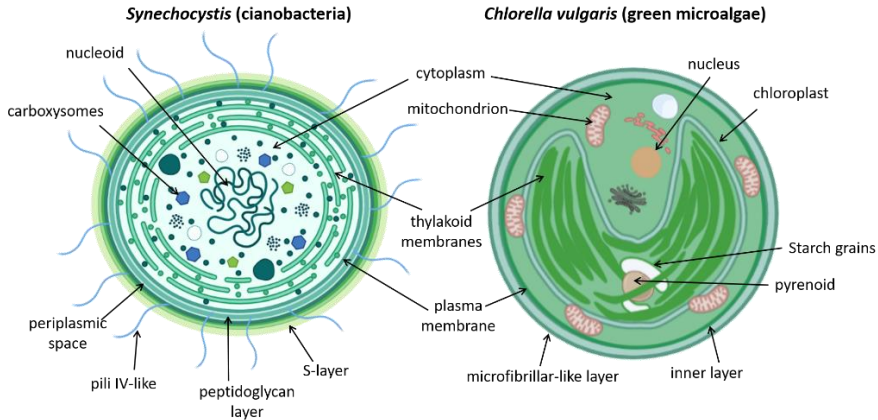


**Figure 1.6.** Schematic drawing of cyanobacteria *Synechocystis* and green microalgae *Chlorella vulgaris*. Created with BioRender.com.

### 1.5.2. Photosynthesis

Oxygenic photosynthesis begins with the light absorption by the light harvesting complexes I and II (LHCI and LHCII) associated to the multiprotein complexes PSI and PSII, respectively. These light harvesting complexes transfer the photons absorbed to the chlorophyll *a* (Chl *a*) present in both photosystems resulting in the excitation of an electron within the Chl *a* to a higher energy level. The excited Chl *a* in PSII oxidizes water by the oxygen evolving complex (OEC) and reduces the plastoquinone intermediate A ( $Q_A$ ), which in turn reduces plastoquinone (PQ) to plastoquinol ( $PQH_2$ ) at the plastoquinone intermediate B ( $Q_B$ ) site. Subsequently,  $PQH_2$  is oxidized by Cyt *b<sub>6</sub>f*, which successively reduces the soluble electron carrier plastocyanin (PC). The excited Chl *a* in PSI oxidizes PC and reduces the soluble protein ferredoxin (Fd). Afterwards, Fd is used by the ferredoxin-NADP<sup>+</sup> reductase (FNR) to reduce NADP<sup>+</sup> to NADPH, which is ultimately used to reduce CO<sub>2</sub> to carbohydrates in the Calvin-Benson-Bassham (CBB) cycle (Figure 1.7). Throughout

all these electron transfer reactions a proton gradient is formed between the inner (lumen) and outer (stroma) sides of the thylakoid membrane, which results in the generation of adenosine triphosphate (ATP) via the transmembrane protein ATP synthase.

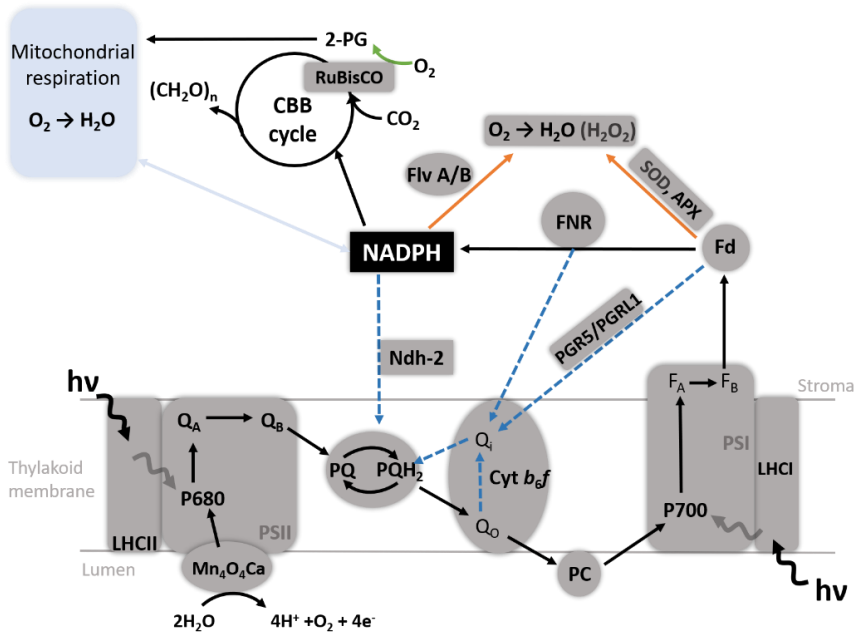


**Figure 1.7.** Schematic of the photosynthetic electron transport chain of microalgae. Solid black lines indicate the linear electron transport (LET) from the oxidation of water by photosystem II (PSII) to the reduction of NADPH by Fd-NADP<sup>+</sup> reductase (FNR). Putative electron pathways to decrease the over-reduction of the LET during the light phase of the photosynthesis are represented with different colours: cyclic electron transport around photosystem I (PSI) (blue dashed lines), pseudocyclic electron transport or water-water cycle for the photoreduction of O<sub>2</sub> (orange solid lines), photorespiration catalysed by RuBisCO (green solid line), NAD(P)<sup>+</sup>/NAD(P)H interchange between mitochondria and chloroplast (light blue solid line). APX, ascorbate peroxidase; CBB, Calvin-Benson-Bassham cycle; LHCII/LHCI, light harvesting complexes II and I; Nhd-2, type II NADH dehydrogenase; Fd, ferredoxin; Flv A/B, flavodiiron proteins; P680, PSII reaction center Chl; P700, PSI reaction center chlorophyll; PC, plastocyanin; PGR5 and PGRL1, proton gradient regulation 5 and proton gradient regulation like 1; PQ, plastoquinone; SOD, superoxide dismutase.

This process is known as the linear electron transport (LET) pathway. There are also alternative electron pathways that compete with the



### **1.5.2.1. Measurement of photosynthesis by pulse-amplitude modulation fluorometry (PAM)**

Photosynthesis can be monitored in real time by several non-invasive methods: gas exchange measurements of CO<sub>2</sub> uptake and O<sub>2</sub> production [84,85]; polarographic oxygen evolution detection with the Clark electrode [86,87]; and chlorophyll fluorescence measurement methods [23,88,89]. Among them, the fluorescence method is the fastest, and easiest tool to obtain detailed information regarding the state of PSII and the induction of photoprotective mechanisms under different environmental conditions [90,91]. PAM fluorometry is the most popular fluorescence technique due to its selectivity and ability to discern between fluorescence and ambient light, thus allowing its use for in situ studies [92]. The first PAM fluorometer was constructed by Schreiber and coworkers in 1986 [93,94] and since then, several models have been developed with different features to embrace the variety of samples and to adapt to new applications.

PAM fluorometry relies on the principle of chlorophyll fluorescence. The light energy absorbed by Chl *a* can be used for photochemical reactions (photosynthesis) or can be dissipated as heat and fluorescence. These three processes are complementary (Figure 1.9). Therefore, by determining the yield of chlorophyll fluorescence one can assess the portion of radiation that is used in photosynthesis and the portion that is non-radiatively emitted [95,96].

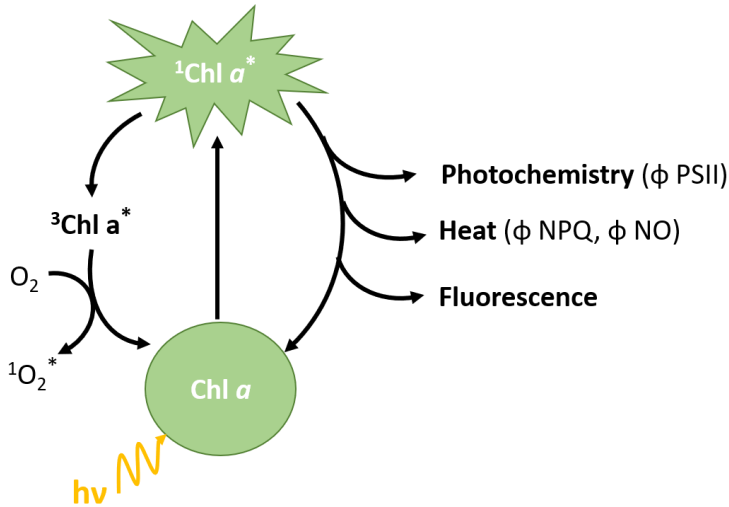


**Figure 1.9.** Light absorbed energy dissipation of Chl *a*.  $^1\text{Chl } a^*$ , singlet excited state;  $^3\text{Chl } a^*$ , triplet excited state.

Upon light, Chl *a* experiences a sharp transient fluorescence rise (generally of 1 s), known as the Kautsky effect [97], which is due to the reduction of the electron acceptors of the PETC, especially  $\text{Q}_A$  (Figure 1.10). In this moment, reaction centres of PSII (RCII) are considered to be closed because  $\text{Q}_A$  cannot accept another electron until it is oxidized by  $\text{Q}_B$ . As a result, there is a decline in the photosynthetic efficiency with the consequent increase in the fluorescence yield. After this short period, fluorescence starts to decrease (namely fluorescence quenching) basically due to the light activation of the photosynthetic process (i.e., activation of CBB) that enables the oxidation of the primary electron acceptor  $\text{Q}_A$  and the subsequent electron carriers on the PETC. At this time, there is a proportion of open RCII resulting in the increase in the photosynthetic efficiency and the decline in the fluorescence yield. This phenomenon is known as photochemical quenching [95].

Another contributor to the decline in fluorescence yield is the development of the non-photochemical quenching, which includes the processes of dissipation of excess energy as heat. These processes are classified in two groups: light-induced non-photochemical quenching (NPQ) and non-regulated non-photochemical quenching (NO), this latter is supposed to be constitutive heat dissipation [98]. The mechanisms involved in the NO are still not well understood. Conversely, the mechanisms underlying NPQ are known to be related with the rapid and reversible thermal dissipation of excess energy by LHCII induced by: the acidification of thylakoid lumen with the consequent formation of zeaxanthin [99,100]; and the phosphorylation of LHCII followed by its detachment from PSII and its binding to PSI [101]. Another component of the NPQ is the photoinhibition of PSII, which is related to the sustained conversion of zeaxanthin (independent of pH) and to an inactivation/degradation of D1 protein of PSII. These three mechanisms are activated when light absorbed exceeds the capacity for its use in photochemical reactions [101–105].

PAM fluorometry can determine fluorescence quenching and calculate the quantum yields of photochemical and non-photochemical processes. The system records the fluorescence derived from applying saturation pulses during dark and light to calculate several fluorescence parameters that give information about the photosynthetic efficiency and the induction of photoprotection mechanisms.



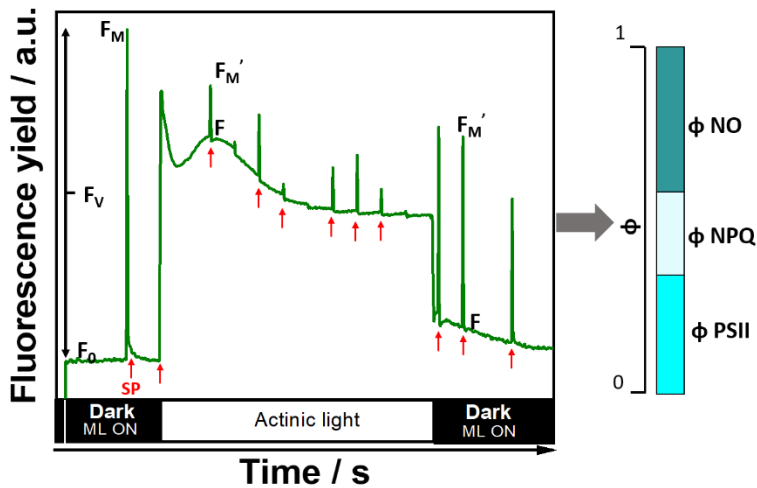


**Figure 1.10.** Typical fluorescence induction curve by means of a MICRO-PAM fluorometer without far-red light (the  $F_0$  is calculated instead of measured). Red arrows indicate saturation pulse (SP). ML indicates measuring light.  $F_0$  and  $F_M$  stand for minimal and maximal fluorescence level for the dark-adapted states, respectively.  $F_V$  is the difference between  $F_M$  and  $F_0$ .  $F$  is the fluorescence level immediately before the SP is performed.  $F_M'$  is the maximal fluorescence level in the light.  $\Phi$  NO, quantum yield of non-regulated non-photochemical quenching;  $\Phi$  NPQ, quantum yield of light-induced non-photochemical quenching;  $\Phi$  PSII, effective photochemical quantum yield of PSII.

Here, only the fluorescence parameters derived from fluorescence induction curves required to understand the research discussed in *Chapter 5* are described. A more thorough description and analysis of said and other Chl *a* fluorescence parameters can be found in references [95,96,101,106,107]. Other fluorescence techniques besides fluorescence induction curves can be performed with some PAM fluorometers (e.g., rapid light curves to determine the electron transfer rate, OJIP fluorescence rise and determination of quantum yield of PSI) [108–110]. However, these are beyond the scope of this thesis and hence, they are not discussed here and we only focus on the parameters derived from the fluorescence induction curves.

---

Generally, prior to start the fluorescence induction curve (Figure 1.10), the sample is dark-acclimated to allow all the RCIIIs to be fully open (i.e., all  $Q_A$  are oxidized). In this manner, all the fluorescence parameters can be unbiasedly determined. The measurement begins by switching on the measuring light (ML), which is a very low intensity light that allows the assessment of the minimum fluorescence in the dark ( $F_0$ ) without inducing a significant rise in the fluorescence yield [92]. Then, a saturation pulse (SP) is performed, whose intensity is high enough to ensure the full closure of RCIIIs resulting in the rise of the fluorescence up to the maximum level ( $F_M$ ). From these two fluorescence levels, the maximum photochemical quantum yield of PSII ( $F_V/F_M$ ) can be calculated. Subsequently, an actinic light is switched on and SPs are applied at appropriate intervals to assess the steady state fluorescence ( $F$ ) and the maximum fluorescence of the illuminated sample ( $F_M'$ ) measured immediately before and after each given SP, respectively. These measurements upon actinic light allow to assess the effective photochemical quantum yield of PSII ( $\Phi_{PSII}$ ). Afterwards, the minimum fluorescence level upon light ( $F_0'$ ) can be assessed by a SP after removing the actinic light if far red light can be applied. Otherwise, the software calculates the  $F_0'$  according to Oxborough and Baker [111]. From these measured fluorescence levels, photochemical and non-photochemical quantum yields ( $\Phi_{NPQ}$  and  $\Phi_{NO}$ ) and other parameters such as the coefficient of photochemical fluorescence quenching ( $q_p$ ), which gives information about the proportion of open RCII, can be derived using the equations described in Table 1.2. Since the quantum yields of photochemical and non-photochemical

processes are calculated from the fluorescence quenching and, as it is mentioned above, these processes are competitive, the sum of the three quantum yields is unity ( $\Phi_{PSII} + \Phi_{NPQ} + \Phi_{NO} = 1$ ) (Figure 1.10).

**Table 1.2.** List of the basic fluorescence parameters measured and calculated from a fluorescence induction curve by PAM fluorometry:

<i>Parameter</i>	<i>Measurement</i>	<i>Equation</i>	<i>Ref.</i>
$F_0'$	Minimum fluorescence level upon light	$F_0' = \frac{1}{\frac{1}{F_0} - \frac{1}{F_M} + \frac{1}{F_M'}}$	[111]
$F_V/F_M$	Maximum photochemical quantum yield of PSII	$\frac{F_V}{F_M} = \frac{F_M - F_0}{F_M}$	[112]
$\Phi_{PSII}$	Effective photochemical quantum yield of PSII	$\Phi_{PSII} = \frac{F_M' - F}{F_M'}$	[89]
$\Phi_{NPQ}$	Light-induced non-photochemical quantum yield	$\Phi_{NPQ} = \frac{F}{F_M'} - \frac{F}{F_M}$	[98,107]
$\Phi_{NO}$	Non-regulated non-photochemical quantum yield	$\Phi_{NO} = \frac{F}{F_M}$	[98,107]
$q_p$	Coefficient of photochemical fluorescence quenching	$q_p = \frac{F_M' - F}{F_M' - F_0'}$	[94,113]

In suspensions of healthy photosynthetic microorganisms, the values of  $F_V/F_M$  usually range between 0.6-0.75 [114–116]. The  $\Phi_{PSII}$  decreases upon light due to the partially closure of RCII and increases after the light is switched off, reaching after 30 minutes in darkness, similar levels to  $F_V/F_M$ . The  $\Phi_{NPQ}$  increases after several seconds of the onset of illumination as a photoprotective mechanism and sharply declines in darkness.  $\Phi_{NO}$  keeps constant upon light and declines in darkness. Thus, the alteration of these quantum yields

gives information of the stress and photoinhibition undergone by photosynthetic microorganisms under certain conditions [90,117–120].

### **1.5.3. Exoelectrogenesis**

Exoelectrogenesis is the ability of microorganisms to transfer electrons or reducing equivalents from their internal metabolism to the extracellular space. In bacteria used in MFCs, exoelectrogenesis to electrodes occurs either through direct or indirect extracellular electron transfer (DEET and IEET, respectively). DEET depends on the direct contact between the electrode surface and conductive structures of the cell membrane (i.e., outer membrane cytochromes (OMCs) [121,122], type IV pili [123] and nanowires [124,125]). IEET relies on the secretion of electron shuttles such as phenazines [126], flavines [127] and quinones [128] to transfer electrons to the external acceptor. IEET can also be facilitated by the use of exogenous electron mediators (e.g., quinones [26,43,129] and ferricyanide [29,69,130]). However, the use of these mediators for large-scale BPVs seems unfeasible due to their toxicity to the cell, their low stability that requires their continuous feeding to the system and the loss of potential [131].

Exoelectrogenesis of photosynthetic microorganisms is poorly understood. Unlike bacteria, oxygenic photosynthetic microorganisms lack the extracellular electron transfer structures on their cell surface. Although several studies have claimed the presence of nanowires and pili IV-like structures in cyanobacteria [37,132,133], recent investigations with *Synechocystis* demonstrate

that neither these structures nor the S-layer contribute to the exoelectrogenesis [134,135].

Nonetheless, there is evidence of IEET from some cyanobacteria to the electrode surface. Saper et al. discovered that the photocurrent produced by *Synechocystis* was mediated by the excretion of an endogenous electron mediator that interplays both in the photosynthetic and respiratory systems. The release of this electron shuttle was improved when cells were subdued to a mild pressure causing a slight disruption of the cell wall [136]. Furthermore, Shlosberg et al. identified NADPH and NADH as the endogenous electron mediators in three cyanobacteria: *Synechocystis*, *Synechococcus elongatus* PCC7942 and *Acaryochloris marina* MBIC 11017 [137]. The mechanism proposed involves the crosstalk between respiration and photosynthesis [138,139], suggesting that the production of NAD(P)H involves the activation of CET around PSI fuelled by a substrate from the respiratory pathway.

Genetic engineering of proteins and complexes involved in the extracellular electron transfer has proved to enhance exoelectrogenesis of photosynthetic microorganisms. 9-fold higher photocurrent generation was obtained by genetically engineering *Synechococcus elongatus* PCC7942 to express the outer membrane cytochrome S (OmcS) from *Geobacter sulfurreducens* [140]. Bradley et al. inactivated three terminal oxidases in *Synechocystis* resulting in up to 24-fold increase in photoreduction of ferricyanide compared to the wild-type. The mechanism suggested for the photocurrent improvement was the increased production of

NAD(P)H resulting from a highly more reduced PQ pool in the terminal oxidase mutants [29]. Although the introduction of electrogenic structures of well-known exoelectrogens or the genetically induction of exoelectrogenesis seems promising, ethical issues are a major drawback to their deployment for large-scale applications.

Exoelectrogenic activity has also been improved both in cyanobacteria and green microalgae grown in iron limited conditions. Gonzalez-Aravena et al. observed a 24-fold and 2.2-fold improved photoreduction of ferricyanide from *Synechococcus elongatus* PCC7942 and *C. vulgaris*, respectively, grown in iron deficient medium compared to cultures grown in replete medium [130]. Photoreduction of ferricyanide was also enhanced in green microalgae *Chlamydomonas reinhardtii* that was iron-starved [141]. These studies propose the interplay between NAD(P)H produced both by photosynthesis and respiration with ferric reductase enzymes located in the plasma membrane, which ultimately reduce the external electron mediator.

### **1.7. Thesis objective**

Considering the stated along this chapter, BPV is a promising green technology in contributing to the palliation of the energy crisis aroused by global warming and fossil fuel depletion. PV panels can supply  $260 \text{ W m}^{-2}$  (Sunpower Maxeon 3<sup>®</sup>, 400W, solar panel of  $1.6 \text{ m}^2$ ). The average sunpeak hours in Tarragona (Spain) are  $4.34 \pm 1.76$ . Thus, PV panels supply  $(1.13 \pm 0.46) \text{ kWh m}^{-2}$ , which corresponds to  $(410.5 \pm 166.6) \text{ kWh m}^{-2}\text{year}^{-1}$ . Therefore, at least 28

---

$\text{m}^2$  of solar panels are required to fulfil the energy demand of a regular household (the average power and energy consumption of a household in Spain is  $4.6\text{kW}$  and  $11528.5\text{ kWh year}^{-1}$ , respectively, according to the users and consumers organization (OCU) of Spain [142]). In contrast, assuming that the maximum achievable power estimated of a BPV can be obtained ( $9854\text{ mW m}^{-2}$ ) and the sunlight hours in Tarragona (Spain) are  $12.01 \pm 2.21.$ , this BPV could yield a light-dependent power output of  $(43.2 \pm 7.9)\text{ kWh m}^{-2}\text{year}^{-1}$ . Thus, the architecture of the BPV would require an anode of  $267\text{ m}^2$  to supply the energy demand of a regular home in Tarragona. Therefore, this technology would be less practical for private home application than PVs. However, its coupling to algal biorefinery would favour circular economy allowing to produce biofuel and raw materials whilst generating electricity directly without the need of downstream processes. According to Dasan et al. [143], the electricity consumption of all the unit operations of a *C. vulgaris* biorefinery cultivated in an open raceway pond (OPR) of  $1000\text{ m}^2$  would be of  $1329.84\text{ MWh year}^{-1}$ . Thus, if a BPV with the estimated maximum achievable power output could be coupled to the *C. vulgaris* biorefinery (with an anode covering the whole area of the OPR), the BPV would directly power  $((43.2 \pm 7.9)\text{ MWh year}^{-1})$  the 3% of the algal biorefinery without the necessity of an external power supply. It is worth to mention that these estimates are calculated regarding only the light-dependent power output of BPVs without accounting for the dark power. Alternatively, if this BPV could be coupled to large microalgal biorefineries, such as the one located in California (Earthrise,USA), which accounts of  $43.7\text{ ha}$  of OPR dedicated to the

culture and processing of *Spirulina* sp. [144], the power directly generated with the BPV (assuming light hours of Tarragona) would be  $18.9 \pm 3.5$  GWh year<sup>-1</sup>. Considering that the energy model of the future will be decentralized and will rely on energetic communities, this BPV coupled to large microalgal biorefineries could supply enough energy to power 1637 homes.

Nevertheless, this emerging technology is lagging behind its potential mainly due to a limited cell-to-electrode electron transfer: from the previous discussion, it appears that only 10% of the possible potential of this technology has been reached. The aim of this thesis is to improve the cell-to-electrode electron transfer by tackling both the features of the electrode to enhance the electron transfer from the cell and the ability of the cell to release electrons to the extracellular space.

**Hypothesis:**

- Modification of electrode surfaces with molecules that can interact with structures of the cell surface through covalent bonds leads not only to more stable biofilms but also to improved electron transfer to the electrode.
- Stressing phototrophs (i.e., high light, nutrient starvation and desiccation) induces the activation of alternative electron transport pathways that facilitate the exoelectrogenesis.



To achieve our goal, we have set the following objectives:

- To improve cell immobilization and to promote intimate contact of photosynthetic microorganisms with electrodes modified with boronic acid derivatives.
- To enhance electron transfer from cells to electrodes modified with boronic acid derivatives.
- To evaluate the electronic properties of a boronic acid-based conducting polymer and compare its ability to assist in the electron transfer from microalgae with other related conducting polymers.
- To construct a proof-of-concept biophotovoltaic cell with a boronic acid-based bioanode.
- To improve the exoelectrogenesis of a green microalga by exposing cells to diverse stressing factors.

## References

- [1] IEA, Global energy review: CO2 emissions in 2021, Paris, 2022. <https://www.iea.org/reports/global-energy-review-co2-emissions-in-2021-2>.
- [2] IEA, World energy balances: overview, Paris, 2021. <https://www.iea.org/reports/world-energy-balances-overview>.
- [3] IEA, Net zero by 2050, Paris, 2021. <https://www.iea.org/reports/net-zero-by-2050>.
- [4] United Nations Framework Convention on Climate Change, Paris Agreement, (2015). <https://unfccc.int/process-and-meetings/the-paris-agreement/the-paris-agreement> (accessed April 22, 2020).
- [5] P. Moriarty, D. Honnery, Can renewable energy power the future?, *Energy Policy*. 93 (2016) 3–7. <https://doi.org/10.1016/j.enpol.2016.02.051>.
- [6] P. Moriarty, D. Honnery, What is the global potential for renewable energy?, *Renew. Sustain. Energy Rev.* 16 (2012) 244–252. <https://doi.org/10.1016/j.rser.2011.07.151>.
- [7] IEA, Renewables 2021, Paris, 2021. <https://www.iea.org/reports/renewables-2021>.
- [8] M.H. Mohamed Hariri, M.K. Mat Desa, S. Masri, M.A.A. Mohd Zainuri, Grid-connected PV generation system-components and challenges: a review, *Energies*. 13 (2020) 4279. <https://doi.org/10.3390/en13174279>.
- [9] J.A. Luceño-Sánchez, A.M. Díez-Pascual, R.P. Capilla, Materials for photovoltaics: State of art and recent developments, *Int. J. Mol. Sci.* 20 (2019) 976. <https://doi.org/10.3390/ijms20040976>.
- [10] L. Reijnders, Life cycle assessment of microalgae-based processes and products, in: E. Jacob-Lopes, M. Manzoni Maroneze, M.I. Queiroz, L. Queiroz Zepka (Eds.), *Handb. Microalgae-Based Process. Prod. Fundam. Adv. Energy, Food, Feed. Fertil. Bioact. Compd.*, Academic Press, 2020: pp. 823–840. <https://doi.org/10.1016/B978-0-12-818536->

0.00030-0.

- [11] Y.J. Kim, H. Hong, J. Yun, S. Il Kim, H.Y. Jung, W. Ryu, Photosynthetic nanomaterial hybrids for bioelectricity and renewable energy systems, *Adv. Mater.* 33 (2021) 2005919. <https://doi.org/10.1002/adma.202005919>.
- [12] K.D. Wolfe, D. Dervishogullari, J.M. Passantino, C.D. Stachurski, G.K. Jennings, D.E. Cliffel, Improving the stability of photosystem I-based bioelectrodes for solar energy conversion, *Curr. Opin. Electrochem.* 19 (2020) 27–34. <https://doi.org/10.1016/j.coelec.2019.09.009>.
- [13] D. Pankratov, G. Pankratova, L. Gorton, Thylakoid membrane-based photobioelectrochemical systems: Achievements, limitations, and perspectives, *Curr. Opin. Electrochem.* 19 (2020) 49–54. <https://doi.org/10.1016/j.coelec.2019.09.005>.
- [14] A.J. McCormick, P. Bombelli, A.M. Scott, A.J. Philips, A.G. Smith, A.C. Fisher, C.J. Howe, Photosynthetic biofilms in pure culture harness solar energy in a mediatorless biophotovoltaic cell (BPV) system., *Energy Environ. Sci.* 4 (2011) 4699–4709. <https://doi.org/10.1039/c1ee01965a>.
- [15] P. Bateson, J.E.H. Fleet, A.S. Riseley, E. Janeva, A.S. Marcella, C. Farinea, M. Kuptsova, N. Conde Pueyo, C.J. Howe, P. Bombelli, B.M. Parker, Electrochemical characterisation of bio-bottle-voltaic (BBV) systems operated with algae and built with recycled materials, *Biology (Basel)*. 7 (2018) 26. <https://doi.org/10.3390/biology7020026>.
- [16] M.P. Johnson, Photosynthesis, *Essays Biochem.* 60 (2016) 255–273. <https://doi.org/10.1042/EBC20160016>.
- [17] A. Nawaz, I. ul Haq, K. Qaisar, B. Gunes, S.I. Raja, K. Mohyuddin, H. Amin, Microbial fuel cells: Insight into simultaneous wastewater treatment and bioelectricity generation, *Process Saf. Environ. Prot.* 161 (2022) 357–373. <https://doi.org/10.1016/j.psep.2022.03.039>.
- [18] X. Qi, Y. Ren, P. Liang, X. Wang, New insights in photosynthetic microbial fuel cell using anoxygenic phototrophic bacteria, *Bioresour. Technol.* 258 (2018) 310–

317. <https://doi.org/10.1016/j.biortech.2018.03.058>.
- [19] C.N. Reddy, H.T.H. Nguyen, T. Noori, B. Min, Potential applications of algae in the cathode of microbial fuel cells for enhanced electricity generation with simultaneous nutrient removal and algae biorefinery: Current status and future perspectives, *Bioresour. Technol.* 292 (2019) 122010. <https://doi.org/10.1016/j.biortech.2019.122010>.
- [20] K. Tanaka, R. Tamamushib, T. Ogawac, Bioelectrochemical fuel-cells operated by the cyanobacterium , *Anabaena variabilis*, *J. Chem. Technol. Biotechnol.* 35 (1985) 191–197. <https://doi.org/10.1002/jctb.280350304>.
- [21] A.J. McCormick, P. Bombelli, R.W. Bradley, R. Thorne, T. Wenzel, C.J. Howe, Biophotovoltaics: oxigenic photosynthetic organisms in the world of bioelectrochemical systems, *Energy Environ. Sci.* 8 (2015) 1092–1109. <https://doi.org/10.1039/C4EE03875D>.
- [22] M.J. Kim, S. Jai Bai, J.R. Youn, Y.S. Song, Anomalous power enhancement of biophotovoltaic cell, *J. Power Sources.* 412 (2019) 301–310. <https://doi.org/10.1016/j.jpowsour.2018.11.056>.
- [23] O. Björkman, B. Demmig, Photon yield of O<sub>2</sub> evolution and chlorophyll fluorescence characteristics at 77 K among vascular plants of diverse origins, *Planta.* 170 (1987) 489–504. <https://doi.org/10.1007/BF00402983>.
- [24] C.J. Howe, P. Bombelli, Electricity production by photosynthetic microorganisms, *Joule.* 4 (2020) 2065–2069. <https://doi.org/10.1016/j.joule.2020.09.003>.
- [25] M.N. Naseer, A.A. Zaidi, H. Khan, S. Kumar, M.T. bin Owais, J. Jaafar, N.S. Suhaimin, Y.A. Wahab, K. Dutta, M. Asif, S.F.W.M. Hatta, Mapping the field of microbial fuel cell : A quantitative literature review (1970-2020), *Energy Reports.* 7 (2021) 4126–4138. <https://doi.org/10.1016/j.egyr.2021.06.082>.
- [26] K. Tanaka, N. Kashiwagi, T. Ogawac, Effects of light on the electrical output of bioelectrochemical fuel-cells containing *Anabaena variabilis* M-2: mechanism of the post-illumination

- burst, J. Chem. Technol. Biotechnol. 42 (1988) 235–240. <https://doi.org/10.1002/jctb.280420307>.
- [27] T. Yagishita, T. Horigome, Effects of light, CO<sub>2</sub> and inhibitors on the current output of biofuel cells containing the photosynthetic organism *Synechococcus* sp., J. Chem. Technol. Biotechnol. 56 (1993) 393–399. <https://doi.org/10.1002/jctb.280560411>.
- [28] Z. Yongjin, J. Pisciotta, R.B. Billmyre, I. V. Baskakov, Photosynthetic microbial fuel cells with positive light response, Biotechnol. Bioeng. 104 (2009) 939–946. <https://doi.org/10.1002/bit.22466>.
- [29] R.W. Bradley, P. Bombelli, D.J. Lea-Smith, C.J. Howe, Terminal oxidase mutants of the cyanobacterium *Synechocystis* sp. PCC 6803 show increased electrogenic activity in biological photo-voltaic systems, Phys. Chem. Chem. Phys. 15 (2013) 13611–13618. <https://doi.org/10.1039/c3cp52438h>.
- [30] T. Wenzel, D. Härtter, P. Bombelli, C.J. Howe, U. Steiner, Porous translucent electrodes enhance current generation from photosynthetic biofilms, Nat. Commun. 9 (2018) 1299. <https://doi.org/10.1038/s41467-018-03320-x>.
- [31] X. Wei, M. Mohammadifar, W. Yang, S. Choi, A microscale biophotovoltaic device, in: IEEE Sensors, IEEE, 2016: pp. 1–3. <https://doi.org/10.1109/ICSENS.2016.7808944>.
- [32] L. Liu, S. Choi, Self-sustainable, high-power-density bio-solar cells for lab-on-a-chip applications, Lab Chip. 17 (2017) 3817. <https://doi.org/10.1039/c7lc00941k>.
- [33] K.L. Saar, P. Bombelli, D.J. Lea-Smith, T. Call, E.M. Aro, T. Müller, C.J. Howe, T.P.J. Knowles, Enhancing power density of biophotovoltaics by decoupling storage and power delivery, Nat. Energy. 3 (2018) 75–81. <https://doi.org/10.1038/s41560-017-0073-0>.
- [34] P. Bombelli, T. Müller, T.W. Herling, C.J. Howe, T.P.J. Knowles, A high power-density, mediator-free, microfluidic biophotovoltaic device for cyanobacterial cells, Adv. Energy Mater. 5 (2015) 1401299.

<https://doi.org/10.1002/aenm.201401299>.

- [35] P. Aelterman, K. Rabaey, H.T. Pham, N. Boon, W. Verstraete, Continuous electricity generation at high voltages and currents using stacked microbial fuel cells, *Environ. Sci. Technol.* 40 (2006) 3388–3394. <https://doi.org/10.1021/es0525511>.
- [36] M.A. Costa De Oliveira, A. D’Epifanio, H. Ohnuki, B. Mecheri, Platinum group metal-free catalysts for oxygen reduction reaction: applications in microbial fuel cells, *Catalysts*. 10 (2020) 1–22. <https://doi.org/10.3390/catal10050475>.
- [37] Y.A. Gorby, S. Yanina, J.S. McLean, K.M. Rosso, D. Moyles, A. Dohnalkova, T.J. Beveridge, I. Seop Chang, B. Hong Kim, K. Shik Kim, D.E. Culley, S.B. Reed, M.F. Romine, D.A. Saffarini, E.A. Hill, L. Shi, D.A. Elias, D.W. Kennedy, G. Pinchuk, K. Watanabe, I. Ishii, B. Logan, K.H. Nealson, J.K. Fredrickson, Electrically conductive bacterial nanowires produced by *Shewanella oneidensis* strain MR-1 and other microorganisms, *Proc. Natl. Acad. Sci.* 103 (2006) 11358–11363. <https://doi.org/10.1073/pnas.0604517103>.
- [38] W. Haehnel, H.J. Hochheimer, On the current generated by a galvanic cell driven by photosynthetic electron transport, *J. Electroanal. Chem.* 104 (1979) 563–574. [https://doi.org/10.1016/S0022-0728\(79\)81069-4](https://doi.org/10.1016/S0022-0728(79)81069-4).
- [39] R. Thorne, H. Hu, K. Schneider, P. Bombelli, A. Fisher, L.M. Peter, A. Dent, P.J. Cameron, Porous ceramic anode materials for photo-microbial fuel cells, *J. Mater. Chem.* 21 (2011) 18055–18060. <https://doi.org/10.1039/c1jm13058g>.
- [40] C.-C. Lin, C.-H. Wei, C.-I. Chen, C.-J. Shieh, Y.-C. Liu, Characteristics of the photosynthesis microbial fuel cell with a *Spirulina platensis* biofilm, *Bioresour. Technol.* 135 (2013) 640–643. <https://doi.org/10.1016/j.biortech.2012.09.138>.
- [41] P. Bombelli, R.W. Bradley, A.M. Scott, A.J. Philips, A.J. McCormick, S.M. Cruz, A. Anderson, K. Yunus, D.S. Bendall, P.J. Cameron, J.M. Davies, A.G. Smith, C.J. Howe, A.C. Fisher, Quantitative analysis of the factors limiting solar power transduction by *Synechocystis* sp. PCC 6803 in biological photovoltaic devices, *Energy Environ. Sci.* 4 (2011)

4690. <https://doi.org/10.1039/c1ee02531g>.
- [42] P. Bombelli, M. Zarrouati, R.J. Thorne, K. Schneider, S.J.L. Rowden, A. Ali, K. Yunus, P.J. Cameron, A.C. Fisher, D. Ian Wilson, C.J. Howe, A.J. McCormick, Surface morphology and surface energy of anode materials influence power outputs in a multi-channel mediatorless bio-photovoltaic (BPV) system, *Phys. Chem. Chem. Phys.* 14 (2012) 12221. <https://doi.org/10.1039/c2cp42526b>.
- [43] N. Sekar, Y. Umasankar, R.P. Ramasamy, Photocurrent generation by immobilized cyanobacteria via direct electron transport in photo-bioelectrochemical cells, *Phys. Chem. Chem. Phys.* 16 (2014) 7862–7871. <https://doi.org/10.1039/c4cp00494a>.
- [44] N.D. Kirchhofer, M.A. Rasmussen, F.W. Dahlquist, S.D. Minteer, G.C. Bazan, The photobioelectrochemical activity of thylakoid bioanodes is increased via photocurrent generation and improved contacts by membrane-intercalating conjugated oligoelectrolytes, *Energy Environ. Sci.* 8 (2015) 2698–2706. <https://doi.org/10.1039/c5ee01707f>.
- [45] S. Tsujimura, A. Wadano, K. Kano, T. Ikeda, Photosynthetic bioelectrochemical cell utilizing cyanobacteria and water-generating oxidase, *Enzyme Microb. Technol.* 29 (2001) 225–231. [https://doi.org/10.1016/S0141-0229\(01\)00374-X](https://doi.org/10.1016/S0141-0229(01)00374-X).
- [46] N. Marković, F. Conzuelo, J. Szczesny, M.B. González García, D. Hernández Santos, A. Ruff, W. Schuhmann, An air-breathing carbon cloth -based screen-printed electrode for applications in enzymatic biofuel cells, *Electroanalysis.* 31 (2019) 217–221. <https://doi.org/10.1002/elan.201800462>.
- [47] L. Dos Santos, V. Climent, C.F. Blanford, F.A. Armstrong, Mechanistic studies of the “blue” Cu enzyme, bilirubin oxidase, as a highly efficient electrocatalyst for the oxygen reduction reaction, *Phys. Chem. Chem. Phys.* 12 (2010) 13962–13974. <https://doi.org/10.1039/c0cp00018c>.
- [48] F. Zhao, P. Wang, A. Ruff, V. Hartmann, S. Zacarias, I.A.C. Pereira, M.M. Nowaczyk, M. Rögner, F. Conzuelo, W. Schuhmann, A photosystem I monolayer with anisotropic electron flow enables Z-scheme like photosynthetic water

- splitting, *Energy Environ. Sci.* 12 (2019) 3133–3143.  
<https://doi.org/10.1039/c9ee01901d>.
- [49] L.M. Utschig, S.R. Soltau, D.M. Tiede, Light-driven hydrogen production from photosystem I-catalyst hybrids, *Curr. Opin. Chem. Biol.* 25 (2015) 1–8.  
<https://doi.org/10.1016/j.cbpa.2014.11.019>.
- [50] Y. Qiao, S. Bao, C.M. Li, Electrocatalysis in microbial fuel cells—from electrode material to direct electrochemistry, *Energy Environ. Sci.* 3 (2010) 544–553.  
<https://doi.org/10.1039/b923503e>.
- [51] B.E. Logan, B. Hamelers, R. Rozendal, U. Schröder, J. Keller, S. Freguia, P. Aelterman, W. Verstraete, K. Rabaey, Microbial fuel cells: Methodology and technology, *Environ. Sci. Technol.* 40 (2006) 5181–5192.  
<https://doi.org/10.1021/es0605016>.
- [52] A. Kumar, L.H.-H. Hsu, P. Kavanagh, F. Barrière, P.N.L. Lens, L. Lapinonnière, J.H. Lienhard V, U. Schröder, X. Jiang, D. Leech, The ins and outs of microorganism–electrode electron transfer reactions, *Nat. Rev. Chem.* 1 (2017) 0024.  
<https://doi.org/10.1038/s41570-017-0024>.
- [53] C. Xu, K. Poon, M.M.F. Choi, R. Wang, Using live algae at the anode of a microbial fuel cell to generate electricity, *Environ. Sci. Pollut. Res.* 22 (2015) 15621–15635.  
<https://doi.org/10.1007/s11356-015-4744-8>.
- [54] A. Cereda, A. Hitchcock, M.D. Symes, L. Cronin, T.S. Bibby, A.K. Jones, A bioelectrochemical approach to characterize extracellular electron transfer by *Synechocystis* sp. PCC6803, *PLoS One.* 9 (2014) e91484.  
<https://doi.org/10.1371/journal.pone.0091484>.
- [55] K.S. Madiraju, D. Lyew, R. Kok, V. Raghavan, Carbon neutral electricity production by *Synechocystis* sp. PCC6803 in a microbial fuel cell, *Bioresour. Technol.* 110 (2012) 214–218.  
<https://doi.org/10.1016/j.biortech.2012.01.065>.
- [56] J.L. Liu, D.A. Lowy, R.G. Baumann, L.M. Tender, Influence of anode pretreatment on its microbial colonization, *J. Appl. Microbiol.* 102 (2007) 177–183.



<https://doi.org/10.1111/j.1365-2672.2006.03051.x>.

- [57] M. Picot, L. Lapinsoinière, M. Rothballer, F. Barrière, Graphite anode surface modification with controlled reduction of specific aryl diazonium salts for improved microbial fuel cells power output, *Biosens. Bioelectron.* 28 (2011) 181–188. <https://doi.org/10.1016/j.bios.2011.07.017>.
- [58] D.R. Lide, W.M.M. Haynes, G. Baysinger, L.I. Berger, H. V Kehiaian, D.L. Roth, D. Zwillinger, M. Frenkel, R.N. Goldberg, *CRC Handbook of Chemistry and Physics*, 90th ed., CRC Press, 2010.
- [59] M. Anam, H.I. Gomes, G. Rivers, R.L. Gomes, R. Wildman, Evaluation of photoanode materials used in biophotovoltaic systems for renewable energy generation, *Sustain. Energy Fuels.* 5 (2021) 4209–4232. <https://doi.org/10.1039/d1se00396h>.
- [60] M. Sawa, A. Fantuzzi, P. Bombelli, C.J. Howe, K. Hellgardt, P.J. Nixon, Electricity generation from digitally printed cyanobacteria, *Nat. Commun.* 8 (2017) 1327. <https://doi.org/10.1038/s41467-017-01084-4>.
- [61] N. Sekar, R. Jain, Y. Yan, R.P. Ramasamy, Enhanced photo-bioelectrochemical energy conversion by genetically engineered cyanobacteria, *Biotechnol. Bioeng.* 113 (2016) 675–679. <https://doi.org/10.1002/bit.25829>.
- [62] F.-L. Ng, M.M. Jaafar, S.-M. Phang, Z. Chan, N.A. Salleh, S.Z. Azmi, K. Yunus, A.C. Fisher, V. Periasamy, Reduced graphene oxide anodes for potential application in algae biophotovoltaic platforms, *Sci. Rep.* 4 (2014) 7562. <https://doi.org/10.1038/srep07562>.
- [63] F.-L. Ng, S.-M. Phang, V. Periasamy, J. Beardall, K. Yunus, A.C. Fisher, Algal biophotovoltaic (BPV) device for generation of bioelectricity using *Synechococcus elongatus* (Cyanophyta), *J. Appl. Phycol.* 30 (2018) 2981–2988. <https://doi.org/10.1007/s10811-018-1515-1>.
- [64] C.G. Granqvist, A. Hultåker, Transparent and conducting ITO films: new developments and applications, *Thin Solid Films.* 411 (2002) 1–5. <https://doi.org/10.1016/S0040->

6090(02)00163-3.

- [65] V. Hartmann, T. Kothe, S. Pö, E. El-Mohsnawy, M.M. Nowaczyk, N. Plumeré, W. Schuhmann, M. Rö, Redox hydrogels with adjusted redox potential for improved efficiency in Z-scheme inspired biophotovoltaic cells, *Phys. Chem. Chem. Phys.* 16 (2014) 11936. <https://doi.org/10.1039/c4cp00380b>.
- [66] H. Hamidi, K. Hasan, S.C. Emek, Y. Dilgin, H.E. Åkerlund, P.Å. Albertsson, D. Leech, Gorton, Photocurrent generation from thylakoid membranes on osmium-redox-polymer-modified electrodes, *ChemSusChem.* 8 (2015) 990–993. <https://doi.org/10.1002/cssc.201403200>.
- [67] K.P. Sokol, D. Mersch, V. Hartmann, J.Z. Zhang, M.M. Nowaczyk, M. Rögner, A. Ruff, W. Schuhmann, N. Plumeré, E. Reisner, Rational wiring of photosystem II to hierarchical indium tin oxide electrodes using redox polymers, *Energy Environ. Sci.* 9 (2016) 3698–3709. <https://doi.org/10.1039/c6ee01363e>.
- [68] K. Hasan, E. Çevik, E. Sperling, M.A. Packer, D. Leech, L. Gorton, Photoelectrochemical wiring of *Paulschulzia pseudovolvox* (algae) to osmium polymer modified electrodes for harnessing solar energy, *Adv. Energy Mater.* 5 (2015) 1501100. <https://doi.org/10.1002/aenm.201501100>.
- [69] K. Hasan, H. Bekir Yildiz, E. Sperling, P.Ó. Conghaile, M.A. Packer, D. Leech, C. Hägerhäll, L. Gorton, Photoelectrochemical communication between cyanobacteria (*Leptolyngbia* sp.) and osmium redox polymer modified electrodes, *Phys. Chem. Chem. Phys.* 16 (2014) 24676–24680. <https://doi.org/10.1039/c4cp04307c>.
- [70] R. Rudra, P. Pattanayak, P.P. Kundu, Conducting polymer-based microbial fuel cells, in: Inamuddin, M.F. Ahmer, M.I. Ahamed, A.M. Asiri (Eds.), *Enzym. Fuel Cells Mater. Applications*, Materials Research Foundations, 2019. <https://doi.org/10.21741/9781644900079>.
- [71] J.H.M. Osorio, A. Pollio, L. Frunzo, P.N.L. Lens, G. Esposito, A review of microalgal biofilm technologies: definition, applications, settings and analysis, *Front. Chem. Eng.* 3 (2021)

737710. <https://doi.org/10.3389/fceng.2021.737710>.
- [72] Y. Wang, Z. Ye, C. Si, Y. Ying, Monitoring of *Escherichia coli* O157:H7 in food samples using lectin based surface plasmon resonance biosensor, *Food Chem.* 136 (2013) 1303–1308. <https://doi.org/10.1016/j.foodchem.2012.09.069>.
- [73] N. Bodenberger, D. Kubiczek, D. Halbgebauer, V. Rimola, S. Wiese, D. Mayer, A.A. Rodriguez Alfonso, L. Ständker, S. Stenger, F. Rosenau, Lectin-functionalized composite hydrogels for “capture-and-killing” of carbapenem-resistant *Pseudomonas aeruginosa*, *Biomacromolecules.* 19 (2018) 2472–2482. <https://doi.org/10.1021/acs.biomac.8b00089>.
- [74] Q.-W. Zhang, J. Ouyang, Y. Wang, T.-T. Zhai, C. Wang, Z.-Q. Wu, T.-Q. Zhang, K. Wang, X.-H. Xia, Specific cell capture and noninvasive release via moderate electrochemical oxidation of boronic ester linkage, *Biosens. Bioelectron.* 138 (2019) 111316. <https://doi.org/10.1016/j.bios.2019.111316>.
- [75] A. Stephenson-Brown, S. Yong, M.H. Mansor, Z. Hussein, N.-C. Yip, P.M. Mendes, J.S. Fossey, F.J. Rawson, Electronic communication of cells with a surface mediated by boronic acid saccharide interactions, *Chem. Commun.* 51 (2015) 17213–17216. <https://doi.org/10.1039/C5CC04311E>.
- [76] L. Lapinsonnière, M. Picot, C. Poriel, F. Barrière, Phenylboronic acid modified anodes promote faster biofilm adhesion and increase microbial fuel cell performances., *Electroanalysis.* 25 (2013) 601–605. <https://doi.org/10.1002/elan.201200351>.
- [77] X. Zhao, W. Deng, Y. Tan, Q. Xie, Promoting electricity generation of *Shewanella putrefaciens* in a microbial fuel cell by modification of porous poly(3-aminophenylboronic acid) film on carbon anode, *Electrochim. Acta.* 354 (2020) 136715. <https://doi.org/10.1016/j.electacta.2020.136715>.
- [78] I. Moro, N. La Rocca, N. Rascio, Photosynthetic apparatus in cyanobacteria and microalgae, in: M. Pessaraki (Ed.), *Handb. Photosynth.*, 3rd ed., CRC Press, 2016: pp. 349–367.
- [79] R.E. Lee, *Phycology*, 5th ed., Cambridge University Press, 2018.

- [80] J. Šmarda, D. Šmajš, J. Komrska, V. Krzyžánek, S-layers on cell walls of cyanobacteria, *Micron*. 33 (2002) 257–277. [https://doi.org/10.1016/S0968-4328\(01\)00031-2](https://doi.org/10.1016/S0968-4328(01)00031-2).
- [81] P. Cardol, G. Forti, G. Finazzi, Regulation of electron transport in microalgae, *Biochim. Biophys. Acta*. 1807 (2011) 912–918. <https://doi.org/10.1016/j.bbabi.2010.12.004>.
- [82] M.R. Badger, S. Von Caemmerer, S. Ruuska, H. Nakano, Electron flow to oxygen in higher plants and algae: rates and control of direct photoreduction (Mehler reaction) and rubisco oxygenase, *Philos. Trans. R. Soc. London. B, Biol. Sci.* 355 (2000) 1433–1446. <https://doi.org/10.1098/rstb.2000.0704>.
- [83] J. Tschörtner, B. Lai, J.O. Krömer, Biophotovoltaics: green power generation from sunlight and water, *Front. Microbiol.* 10 (2019) 866. <https://doi.org/10.3389/fmicb.2019.00866>.
- [84] C.A. Oakley, B.M. Hopkinson, G.W. Schmidt, A modular system for the measurement of CO<sub>2</sub> and O<sub>2</sub> gas flux and photosynthetic electron transport in microalgae, *Limnol. Oceanogr. Methods*. 10 (2012) 968–977. <https://doi.org/10.4319/lom.2012.10.968>.
- [85] D. Schories, U. Mehlig, CO<sub>2</sub> gas exchange of benthic microalgae during exposure to air: a technique for the rapid assessment of primary production, *Wetl. Ecol. Manag.* 8 (2000) 273–280. <https://doi.org/10.1023/A:1008448729277>.
- [86] M. Cuaresma, I. Garbayo, J.M. Vega, C. Vílchez, Growth and photosynthetic utilization of inorganic carbon of the microalga *Chlamydomonas acidophila* isolated from Tinto river, *Enzyme Microb. Technol.* 40 (2006) 158–162. <https://doi.org/10.1016/j.enzmictec.2005.10.049>.
- [87] T. Delieu, D.A. Walker, An improved cathode for the measurement of photosynthetic oxygen evolution by isolated chloroplasts, *New Phytol.* 71 (1972) 201–225. <https://doi.org/10.1111/J.1469-8137.1972.TB04068.X>.
- [88] Z. Kolber, J. Zehr, P. Falkowski, Effects of growth irradiance and nitrogen limitation on photosynthetic energy conversion in photosystem II, *Plant Physiol.* 88 (1988) 923–929. <https://doi.org/10.1104/pp.88.3.923>.

- [89] B. Genty, J.M. Briantais, N.R. Baker, The relationship between the quantum yield of photosynthetic electron transport and quenching of chlorophyll fluorescence, *Biochim. Biophys. Acta - Gen. Subj.* 990 (1989) 87–92. [https://doi.org/10.1016/S0304-4165\(89\)80016-9](https://doi.org/10.1016/S0304-4165(89)80016-9).
- [90] S. White, A. Anandraj, F. Bux, PAM fluorometry as a tool to assess microalgal nutrient stress and monitor cellular neutral lipids, *Bioresour. Technol.* 102 (2011) 1675–1682. <https://doi.org/10.1016/j.biortech.2010.09.097>.
- [91] A. Solovchenko, A. Lukyanov, S. Vasilieva, E. Lobakova, Chlorophyll fluorescence as a valuable multitool for microalgal biotechnology, *Biophys. Rev.* (2022) 1–11. <https://doi.org/10.1007/s12551-022-00951-9>.
- [92] U. Schreiber, Pulse-amplitude-modulation (PAM) fluorometry and saturation pulse method: an overview., in: G. Papageorgiou G.C. (Ed.), *Chlorophyll a Fluoresc. Adv. Photosynth. Respir.* Vol 19, 1st ed., Springer Netherlands, Dordrecht, 2004: pp. 279–319. [https://doi.org/10.1007/978-1-4020-3218-9\\_11](https://doi.org/10.1007/978-1-4020-3218-9_11).
- [93] U. Schreiber, Detection of rapid induction kinetics with a new type of high-frequency modulated chlorophyll fluorometer, *Photosynth. Res.* 9 (1986) 261–272. <https://doi.org/10.1007/BF00029749>.
- [94] U. Schreiber, U. Schliwa, W. Bilger, Continuous recording of photochemical and non-photochemical chlorophyll fluorescence quenching with a new type of modulation fluorometer, *Photosynth. Res.* 10 (1986) 51–62. <https://doi.org/10.1007/BF00024185>.
- [95] K. Maxwell, G.N. Johnson, Chlorophyll fluorescence-a practical guide, *J. Exp. Bot.* 51 (2000) 659–668. <https://doi.org/10.1016/j.rsci.2018.02.001>.
- [96] B. Demmig-Adams, W.W. Adams, D.H. Barker, B.A. Logan, D.R. Bowling, A.S. Verhoeven, Using chlorophyll fluorescence to assess the fraction of absorbed light allocated to thermal dissipation of excess excitation, *Physiol. Plant.* 98 (1996) 253–264. <https://doi.org/10.1034/j.1399-3054.1996.980206.x>.

- [97] H. Kautsky, A. Hirsch, Neue versuche zur kohlen säureassimilation, *Naturwissenschaften*. 19 (1931) 964. <https://doi.org/10.1007/BF01516164>.
- [98] B. Genty, J. Harbinson, A. Cailly, F. Rizza, Fate of excitation at PS II in leaves: the non-photochemical side, Present. Third BBSRC Robert Hill Symp. Photosynth. March 31 to April 3, 1996, Univ. Sheffield, Dep. Mol. Biol. Biotechnol. West. Bank, Sheffield, UK, Abstr. No. P28. (1996).
- [99] B. Demmig-Adams, Carotenoids and photoprotection in plants: A role for the xanthophyll zeaxanthin, *Biochim. Biophys. Acta - Bioenerg.* 1020 (1990) 1–24. [https://doi.org/10.1016/0005-2728\(90\)90088-L](https://doi.org/10.1016/0005-2728(90)90088-L).
- [100] P. Horton, A. V Ruban, M. Wentworth, Allosteric regulation of the light-harvesting system of photosystem II, *Philos. Trans. R. Soc. London. B, Biol. Sci.* 355 (2000) 1361–1370. <https://doi.org/10.1098/rstb.2000.0698>.
- [101] G.H. Krause, E. Weis, Chlorophyll fluorescence and photosynthesis: the basics, *Annu. Rev. Plant Physiol. Plant Mol. Biol.* 42 (1991) 313–349. <https://doi.org/10.1146/annurev.pp.42.060191.001525>.
- [102] M. Hodges, G. Cornic, J.M. Briantais, Chlorophyll fluorescence from spinach leaves: resolution of non-photochemical quenching, *Biochim. Biophys. Acta - Bioenerg.* 974 (1989) 289–293. [https://doi.org/10.1016/S0005-2728\(89\)80246-4](https://doi.org/10.1016/S0005-2728(89)80246-4).
- [103] P. Horton, A. Hague, Studies on the induction of chlorophyll fluorescence in isolated barley protoplasts. IV. Resolution of non-photochemical quenching, *Biochim. Biophys. Acta - Bioenerg.* 932 (1988) 107–115. [https://doi.org/10.1016/0005-2728\(88\)90144-2](https://doi.org/10.1016/0005-2728(88)90144-2).
- [104] W.P. Quick, M. Stitt, An examination of factors contributing to non-photochemical quenching of chlorophyll fluorescence in barley leaves, *Biochim. Biophys. Acta - Bioenerg.* 977 (1989) 287–296. [https://doi.org/10.1016/S0005-2728\(89\)80082-9](https://doi.org/10.1016/S0005-2728(89)80082-9).
- [105] R.G. Waiters, P. Horton, M. Biology, P.O. Box, F. Court, W.

- Bank, Theoretical assessment of alternative mechanisms for non-photochemical quenching of PS II fluorescence in barley leaves, *Photosynth. Res.* 36 (1993) 119–139. <https://doi.org/10.1007/BF00016277>.
- [106] D. Lazár, Parameters of photosynthetic energy partitioning, *J. Plant Physiol.* 175 (2015) 131–147. <https://doi.org/10.1016/j.jplph.2014.10.021>.
- [107] C. Klughammer, U. Schreiber, Complementary PS II quantum yields calculated from simple fluorescence parameters measured by PAM fluorometry and the Saturation Pulse method, *PAM Appl. Notes.* 1 (2008) 27–35.
- [108] R.J. Strasser, Govindjee, The Fo and the O-J-I-P fluorescence rise in higher plants and algae, in: J.. Argyroudi-Akoyunoglou (Ed.), *Regul. Chloroplast Biog.*, Springer, Boston, MA, 1992: pp. 423–426. [https://doi.org/10.1007/978-1-4615-3366-5\\_60](https://doi.org/10.1007/978-1-4615-3366-5_60).
- [109] P.J. Ralph, R. Gademann, Rapid light curves: a powerful tool to assess photosynthetic activity, *Aquat. Bot.* 82 (2005) 222–237. <https://doi.org/10.1016/j.aquabot.2005.02.006>.
- [110] C. Klughammer, U. Schreiber, Saturation Pulse method for assessment of energy conversion in PS I, 2008. <https://www.walz.com/files/downloads/pan/PAN07002.pdf>.
- [111] K. Oxborough, N.R. Baker, Resolving chlorophyll a fluorescence images of photosynthetic efficiency into photochemical and non-photochemical components—calculation of qP and Fv'/Fm' without measuring Fo', *Photosynth. Res.* 54 (1997) 135–142. <https://doi.org/10.1023/A:1005936823310>.
- [112] M. Kitajima, W.L. Butler, Quenching of chlorophyll fluorescence and primary photochemistry in chloroplasts by dibromothymoquinone, *Biochim. Biophys. Acta.* 376 (1975) 105–115. [https://doi.org/10.1016/0005-2728\(75\)90209-1](https://doi.org/10.1016/0005-2728(75)90209-1).
- [113] O. Van Kooten, J.F.H. Snel, The use of fluorescence nomenclature in plant stress physiology, *Photosynth. Res.* 25 (1990) 147–150. <https://doi.org/10.1007/BF00033156>.
- [114] H.V. Perales-Vela, R. Velasco García, E.A. Gómez-Juárez,

- M.O. Salcedo-Álvarez, R.O. Cañizares-Villanueva, Streptomycin affects the growth and photochemical activity of the alga *Chlorella vulgaris*, *Ecotoxicol. Environ. Saf.* 132 (2016) 311–317. <https://doi.org/10.1016/j.ecoenv.2016.06.019>.
- [115] P. Juneau, P.J. Harrison, Comparison by PAM fluorometry of photosynthetic activity of nine marine phytoplankton grown under identical conditions, *Photochem. Photobiol.* 81 (2005) 649–653. <https://doi.org/10.1111/j.1751-1097.2005.tb00239.x>.
- [116] S.M. Rincon, N.F. Urrego, K.J. Avila, H.M. Romero, H. Beyenal, Photosynthetic activity assessment in mixotrophically cultured *Chlorella vulgaris* biofilms at various developmental stages, *Algal Res.* 38 (2019) 101408. <https://doi.org/10.1016/j.algal.2019.101408>.
- [117] O. Herlory, J. Bonzom, R. Gilbin, Sensitivity evaluation of the green alga *Chlamydomonas reinhardtii* to uranium by pulse amplitude modulated ( PAM ) fluorometry, *Aquat. Toxicol.* 140–141 (2013) 288–294. <https://doi.org/10.1016/j.aquatox.2013.06.007>.
- [118] A.T. Lombardi, M.T. Maldonado, The effects of copper on the photosynthetic response of *Phaeocystis cordata*, *Photosynth. Res.* 108 (2011) 77–87. <https://doi.org/10.1007/s11120-011-9655-z>.
- [119] A. Nikolaou, A. Bernardi, A. Meneghesso, F. Bezzo, T. Morosinotto, B. Chachuat, A model of chlorophyll fluorescence in microalgae integrating photoproduction, photoinhibition and photoregulation, *J. Biotechnol.* 194 (2015) 91–99. <https://doi.org/10.1016/j.jbiotec.2014.12.001>.
- [120] E.D. Fleming, B.M. Bebout, R.W. Castenholz, Effect of salinity and light intensity on the resumption of photosynthesis in rehydrated cyanobacterial mats from Baja California Sur, Mexico, *J. Phycol.* 43 (2007) 15–24. <https://doi.org/10.1111/j.1529-8817.2006.00297.x>.
- [121] H. Richter, K.P. Nevin, H. Jia, D.A. Lowy, R. Lovley, L.M. Tender, Cyclic voltammetry of biofilms of wild type and mutant *Geobacter sulfurreducens* on fuel cell anodes indicates



- possible roles of OmcB, OmcZ, type IV pili, and protons in extracellular electron transfer, *Energy Environ. Sci.* 2 (2009) 506–516. <https://doi.org/10.1039/b816647a>.
- [122] M. Breuer, K.M. Rosso, J. Blumberger, J.N. Butt, Multi-haem cytochromes in *Shewanella oneidensis* MR-1: structures, functions and opportunities, *J. R. Soc. Interface.* 12 (2015) 20141117. <https://doi.org/10.1098/rsif.2014.1117>.
- [123] D.E. Holmes, Y. Dang, D.J.F. Walker, D.R. Lovley, The electrically conductive pili of *Geobacter* species are a recently evolved feature for extracellular electron transfer, *Microb. Genomics.* 2 (2016) e000072. <https://doi.org/10.1099/mgen.0.000072>.
- [124] M.Y. El-Naggar, G. Wanger, K. Man Leung, T.D. Yuzvinsky, G. Southam, J. Yang, W. Ming Lau, K.H. Nealson, Y.A. Gorby, Electrical transport along bacterial nanowires from *Shewanella oneidensis* MR-1, *Proc. Natl. Acad. Sci.* 107 (2010) 18127–18131. <https://doi.org/10.1073/pnas.1004880107>.
- [125] S. Pirbadian, S.E. Barchinger, K.M. Leung, H.S. Byun, Y. Jangir, R.A. Bouhenni, S.B. Reed, M.F. Romine, D.A. Saffarini, L. Shi, Y.A. Gorby, J.H. Golbeck, M.Y. El-Naggar, *Shewanella oneidensis* MR-1 nanowires are outer membrane and periplasmic extensions of the extracellular electron transport components, *Proc. Natl. Acad. Sci.* 111 (2014) 12883–12888. <https://doi.org/10.1073/pnas.1410551111>.
- [126] T.H. Pham, N. Boon, K. De Maeyer, M. Höfte, K. Rabaey, W. Verstraete, Use of *Pseudomonas* species producing phenazine-based metabolites in the anodes of microbial fuel cells to improve electricity generation, *Appl. Microbiol. Biotechnol.* 80 (2008) 985–993. <https://doi.org/10.1007/s00253-008-1619-7>.
- [127] E. Marsili, D.B. Baron, I.D. Shikhare, D. Coursolle, J.A. Gralnick, D.R. Bond, *Shewanella* secretes flavins that mediate extracellular electron transfer, *Proc Natl Acad Sci.* 105 (2008) 3968–3973. <https://doi.org/10.1073/pnas.0710525105>.
- [128] D.K. Newman, R. Kolter, A role for excreted quinones in extracellular electron transfer, *Nature.* 405 (2000) 94–97.

<https://doi.org/10.1038/35011098>.

- [129] J.Z. Zhang, P. Bombelli, K.P. Sokol, A. Fantuzzi, A.W. Rutherford, C.J. Howe, E. Reisner, Photoelectrochemistry of photosystem II in vitro vs in vivo, *J. Am. Chem. Soc.* 140 (2018) 6–9. <https://doi.org/10.1021/jacs.7b08563>.
- [130] A.C. Gonzalez-Aravena, K. Yunus, L. Zhang, B. Norling, A.C. Fisher, Tapping into cyanobacteria electron transfer for higher exoelectrogenic activity by imposing iron limited growth, *RSC Adv.* 8 (2018) 20263–20274. <https://doi.org/10.1039/c8ra00951a>.
- [131] E.R. Cli, R.W. Bradley, L.T. Wey, J.M. Lawrence, X. Chen, C.J. Howe, J.Z. Zhang, Phenazines as model low-midpoint potential electron shuttles for photosynthetic bioelectrochemical systems, *Chem. Sci.* 12 (2021) 3328–3338. <https://doi.org/10.1039/d0sc05655c>.
- [132] S. Sure, A.A.J. Torriero, A. Gaur, L.H. Li, Y. Chen, C. Tripathi, A. Adholeya, M.L. Ackland, M. Kochar, Inquisition of *Microcystis aeruginosa* and *Synechocystis* nanowires: characterization and modelling, *Antonie Van Leeuwenhoek.* 108 (2015) 1213–1225. <https://doi.org/10.1007/s10482-015-0576-2>.
- [133] S. Sure, A.A.J. Torriero, A. Gaur, L. Hua, Y. Chen, C. Tripathi, A. Adholeya, M.L. Ackland, M. Kochar, Identification and topographical characterisation of microbial nanowires in *Nostoc punctiforme*, *Antonie Van Leeuwenhoek.* 109 (2016) 475–480. <https://doi.org/10.1007/s10482-015-0644-7>.
- [134] L.T. Wey, J.M. Lawrence, X. Chen, R. Clark, D.J. Lea-smith, J.Z. Zhang, C.J. Howe, A biophotoelectrochemical approach to unravelling the role of cyanobacterial cell structures in exoelectrogenesis, *Electrochim. Acta.* 395 (2021) 139214. <https://doi.org/10.1016/j.electacta.2021.139214>.
- [135] M.A. Thirumurthy, A. Hitchcock, A. Cereda, J. Liu, M.S. Chavez, B.L. Doss, R. Ros, M.Y. El-naggar, J.T. Heap, T.S. Bibby, A.K. Jones, Type IV pili-independent photocurrent production by the cyanobacterium *Synechocystis* sp. PCC6803, *Front. Microbiol.* 11 (2020) 1344.

<https://doi.org/10.3389/fmicb.2020.01344>.

- [136] G. Saper, D. Kallmann, F. Conzuelo, F. Zhao, T.N. Tóth, V. Liveanu, S. Meir, J. Szymanski, A. Aharoni, W. Schuhmann, A. Rothschild, G. Schuster, N. Adir, Live cyanobacteria produce photocurrent and hydrogen using both the respiratory and photosynthetic systems, *Nat. Commun.* 9 (2018) 2168. <https://doi.org/10.1038/s41467-018-04613-x>.
- [137] Y. Shlosberg, B. Eichenbaum, T.N. Tóth, G. Levin, V. Liveanu, G. Schuster, N. Adir, NADPH performs mediated electron transfer in cyanobacterial-driven biophotocatalytic cells, *IScience.* 24 (2021) 101892. <https://doi.org/10.1016/j.isci.2020.101892>.
- [138] C.W. Mullineaux, Co-existence of photosynthetic and respiratory activities in cyanobacterial thylakoid membranes, *BBA - Bioenerg.* 1837 (2014) 503–511. <https://doi.org/10.1016/j.bbabi.2013.11.017>.
- [139] T. Ogawa, K. Suzuki, K. Sonoike, Respiration interacts with photosynthesis through the acceptor side of photosystem I, reflected in the dark-to-light induction kinetics of chlorophyll fluorescence in the cyanobacterium *Synechocystis* sp. PCC6803, *Front. Plant Sci.* 12 (2021) 717968. <https://doi.org/10.3389/fpls.2021.717968>.
- [140] N. Sekar, R. Jain, Y. Yan, R.P. Ramasamy, Enhanced photobioelectrochemical energy conversion by genetically engineered cyanobacteria, *Biotechnol. Bioeng.* 113 (2016) 675–679. <https://doi.org/10.1002/bit.25829>.
- [141] H.G. Weger, G.S. Espie, Ferric reduction by iron-limited *Chlamydomonas* cells interacts with both photosynthesis and respiration, *Planta.* 210 (2000) 775–781. <https://doi.org/10.1007/s004250050679>.
- [142] OCU, ¿Cuánta energía consume una casa?, (2016). <https://www.ocu.org/vivienda-y-energia/gas-luz/noticias/cuanta-energia-consume-una-casa-571584> (accessed June 9, 2022).
- [143] Y.K. Dasan, M.K. Lam, S. Yusup, J.-W. Lim, K.T. Lee, Life cycle evaluation of microalgae biofuels production: Effect of

cultivation system on energy, carbon emission and cost balance analysis, *Sci. Total Environ.* 688 (2019) 112–128. <https://doi.org/10.1016/j.scitotenv.2019.06.181>.

- [144] Earthrise Nutritionals, Eco-friendly farm, (n.d.). <https://www.earthrise.com/ecofriendly-farm> (accessed June 9, 2022).



## Chapter 2

### **Boronic acid modified electrodes for electrochemical communication with *Chlorella vulgaris***

#### **2.1. Introduction**

*C. vulgaris* is a green microalgae widely used in pharmaceutical and nutraceutical industries [1–4] with great potential as a renewable energy source as feedstock for biofuel cells [5–7] or through direct light-to-energy conversion in BPV devices [8–11]. One of the main drawbacks of BPVs is their low power efficiency, which is mainly due to the poor exoelectrogenesis of the photosynthetic microorganisms. Therefore, this system usually requires the use of either exogenous or auto excreted electron mediators (endogenous mediators) [12,13] to transfer electrons from the microorganism to the electrode (i.e., IEET) leading to limitations of mass transport and also algae viability (if exogenous mediators are required) [14]. Notwithstanding, DEET with the electrode, either through direct contact of redox surface proteins on the cell wall or through pili-like structures, as observed in bacteria used in MFCs [15–17], would reduce not only the internal resistance, but also the toxicity resulting in an improved efficiency. Although many studies have claimed DEET using photosynthetic microorganisms [10,18–21], latest investigations contradict these hypothesis suggesting that endogenous mediators are responsible of the electron transfer to the electrode [22–24].

Rational design of electrode surfaces that promotes biofilm formation and helps in the electron transfer process has become essential to boost the power efficiency of BPVs. Among the approaches for electrode design, carbon nanostructures and ICPs are widely used in their counterpart MFCs [25]. In this sense, poly-(3-aminophenylboronic acid) (PAPBA) is an increasingly used ICP in biosensors[26–28] and cytosensors [29,30] due to its ability to covalently bind 1,2 or 1,3-cis diols. Nonetheless, to the best of our knowledge, boronic acid derivatives have not yet been explored for the immobilization of photosynthetic microorganisms for their application in BPVs. In this chapter, we successfully combine the excellent electrical conductivity and surface chemistry of oxidized multi-walled carbon nanotubes (oCNT) with the great electrical conductivity and ability of PAPBA to bind to saccharides present in the cell wall [31] to improve the photocurrent generation from *C. vulgaris* and other photosynthetic microorganisms.

## 2.2. Materials and methods

### 2.2.1. Algal and cyanobacterial cultures:

*C. vulgaris* [redacted] was purchased [redacted] [redacted], *Chlamydomonas reinhardtii* (*C. reinhardtii*) [redacted] was purchased [redacted] [redacted]. *Synechocystis* [redacted] [redacted], *Synechococcus* [redacted] and *Nostoc* [redacted] [redacted] were purchased from [redacted] [redacted]. *Scenedesmus* sp. was purchased from [redacted] [redacted]. *C. reinhardtii* and *C. vulgaris* cultures were grown in 100 mL of [redacted] [redacted] [32]. *Synechocystis*

---

PCC6803, *Synechococcus* PCC7942 and *Scenedesmus* sp. [REDACTED]  
[REDACTED]  
[REDACTED] and *Nostoc* PCC7120 in  
[REDACTED] [33]. All cultures were grown  
in 250 mL Corning polycarbonate Erlenmeyer flasks (Fisher  
Scientific S.L) at  $(20 \pm 2)$  °C and shaken at 150 rpm with the  
[REDACTED].

### 2.2.2. Concentration of culture supernatant:

Eighty milliliters of *C. vulgaris* culture were centrifuged at 15000 rpm and 4 °C. The pellet was discarded and the supernatant was lyophilized at -50 °C and 1.5 mbar. Afterwards, the lyophilized was resuspended in 4 mL of ultrapure water (Milli-Q, Millipore, Spain).

### 2.2.3. Oxidation of MWCNTs:

[REDACTED]  
[REDACTED]  
[REDACTED]. [REDACTED]  
[REDACTED] the oxidized MWCNT (thereafter called oCNT) were purified by extracting through a series of cycles of washing with ultrapure water (Milli-Q, Millipore, Spain) and centrifuging. The oCNT were dried overnight in an oven under vacuum. Afterwards, they were [REDACTED] to a final concentration of  $1 \text{ mg mL}^{-1}$ .

### 2.2.4. Electrochemical measurement:

All electrochemical measurements were performed by triplicate unless otherwise stated with a multi-channel PalmSens3 potentiostat



and analyzed with PStrace 5 software (PalmSens BV) in a three-electrode electrochemical cell. Bare and modified glassy carbon electrodes (GCE) were used as working electrodes, Ag/AgCl/sat KCl and platinum wire as reference and counter electrodes, respectively. All potentials in this chapter are referred vs. Ag/AgCl/sat KCl. For experiments with bare and modified electrodes with and without immobilized algae and cyanobacteria, the electrochemical cell was kept in a dark box and light was provided by cold white LED strips of 12 V DC, 4.8 W m<sup>-1</sup> (Silver Sanz S.A.) [REDACTED]. The irradiance was measured with an ULM-500 light meter (Heinz Walz GmbH). Chronoamperometries (CAs) were carried out at 0.2 V in 0.1 M phosphate buffer (PB) pH 7 [REDACTED] under several cycles of 2 min light ON/OFF, [REDACTED]. Characterization of the electropolymerization was accomplished by performing cyclic voltammetries (CVs) at 0.1 V s<sup>-1</sup> in 0.2 M HCl monomer-free solution. Square-wave voltammetries (SWVs) were conducted in 0.1 M PB pH 7 from -0.5 V to 0.5 V at 1 Hz, 5 mV of step potential and an amplitude of 0.3 V.

### **2.2.5. Surface modification of electrodes:**

GCE of 3 mm diameter, model CHI104 (CH Instruments, Inc.), were polished with aqueous slurries of 0.3 μm alumina on nylon polishing pads. Subsequently, electrodes were ultrasonicated in Milli-Q water and blow dried with N<sub>2</sub>. [REDACTED] oCNT dispersion was drop-cast on the GCE surface and left to dry [REDACTED]. The resulting electrodes (denoted as GCE/oCNT) were further modified with a film of poly-(3-aminophenylboronic

---

acid) [REDACTED]

[REDACTED]

[REDACTED]

[REDACTED]

[REDACTED]

[REDACTED]

[REDACTED]

[REDACTED]

(GCE/oCNT/PAPBA) were washed for 20 minutes in 0.1 M PB pH 7 and preserved under N<sub>2</sub> atmosphere until further use.

#### **2.2.6. Immobilization of algae and cyanobacteria on electrodes:**

When cultures reached an optical density at 680 nm (OD<sub>680</sub>) of c.a. 0.8 (i.e., at the beginning of the exponential growth phase) were centrifuged at 4 °C and 4000 rpm for 10 minutes, washed in 0.1 M PB pH 7 and centrifuged. [REDACTED]

[REDACTED]

[REDACTED] Controls were performed by drop-casting 5 μL of supernatant of algae on electrodes. The OD<sub>680</sub> of the cultures was calculated from the absorbance divided by the optical path length, following the Beer-Lambert's law. The absorbance was measured in triplicate with the Spectramax microplate reader (Molecular Devices, LLC) by placing 100 μL of sample (optical path length of ≈ 0.25 cm) in MaxiSorp nunc 96 microwell plates (Thermo Fisher Scientific Inc.).

#### **2.2.7. Microscopy characterization:**

Surface of modified electrodes with and without immobilized *C. vulgaris* were analyzed by environmental scanning electron

microscopy (ESEM) with a Quanta 600 microscope (FEI Company, Inc.) at low vacuum without any pretreatment. Fluorescence microscopy of electrodes incubated with algae and cyanobacteria were examined after the electrochemical analysis with a NIKON TE2000-E microscope under red excitation light since chlorophyll pigments present autofluorescence with an excitation/emission wavelengths of 630/(650-700) nm [34]. Cell densities were calculated from fluorescence microscope images with the free image processing software ImageJ (National Institutes of Health, USA).

#### **2.2.8. Determination of the surface area coverage of PAPBA ( $\Gamma_{\text{PAPBA}}$ ):**

The cyclic voltammograms of the electropolymerization characterization in 0.2 M HCl monomer-free solution were used to determine the amount of PAPBA electrodeposited on the electrode.  $\Gamma_{\text{PAPBA}}$  was calculated from the charge of the first cathodic peak using the Faraday's law electrolysis equation (equation 2.1) [35] and considering 2 electrons involved in the redox process [36]:

$$\Gamma = \frac{Q}{nFA} \quad (2.1)$$

where  $\Gamma$  is the surface area coverage ( $\text{mol cm}^{-2}$ ),  $Q$  is the charge (C),  $F$  is the Faraday constant ( $96485 \text{ C mol}^{-1}$ ),  $A$  is the geometrical surface area of the electrode ( $0.07 \text{ cm}^2$ ) and  $n$  is the stoichiometric number of electrons consumed in the electrodeposition.

#### **2.2.9. DCMU experiments:**

CAs at 0.2 V in 0.1 M PB pH 7 of GCE/oCNT/PAPBA incubated with *C. vulgaris* were performed by adding deoxygenated 3-(3,4-

dichlorophenyl)-1,1-dimethylurea (DCMU, Sigma-Aldrich) in 0.1 M PB pH 7 to [REDACTED]. The addition was executed after 4 cycles of light ON/OFF. The decrease in photocurrent was calculated comparing the last and the first cycle of light before and after the addition of DCMU, respectively.

## 2.3. Results and discussion

### 2.3.1. Preparation and characterization of *C. vulgaris*-based biophotocathode:

To construct the *C. vulgaris*-based biophotocathode (GCE/oCNT/PAPBA\_*C. vulgaris*), the surface of glassy carbon electrodes was modified with oCNT [REDACTED]

[REDACTED] (Figure 2.1).

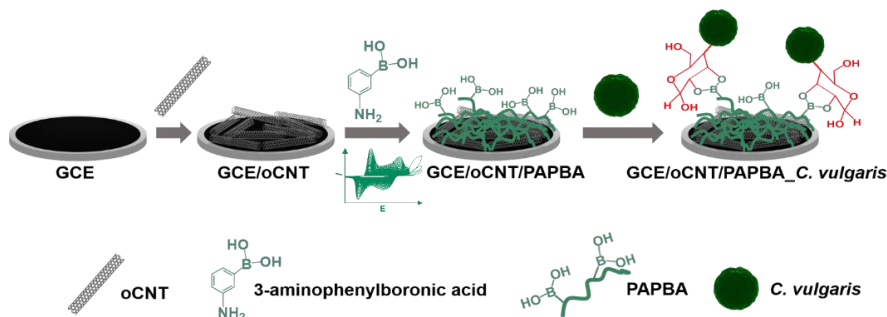


**Figure 2.1.** Schematic representation of the steps involved in the preparation of the *C. vulgaris*-based biophotocathode.

Successive voltammograms [REDACTED]

[REDACTED] are shown in Figure

Appendix A.1a. [REDACTED]

[REDACTED]

[REDACTED]. [REDACTED]

[REDACTED]

The [REDACTED]  
[REDACTED]. The cyclic voltammogram (Figure 2.2a) shows well defined redox peaks at  $E_{pa1} = 159$  mV,  $E_{pc1} = 10$  mV,  $E_{pa2} = 489$  mV and  $E_{pc2} = 479$  mV which correspond to the characteristic redox processes of boronic acid substituted polyaniline [27,37]. When electrodes were modified with oCNT, the amount of polymer deposited ( $(49 \pm 6)$  nmol  $\text{cm}^{-2}$ ) on the electrode was 4 times higher than in the absence of oCNT ( $(12 \pm 5)$  nmol  $\text{cm}^{-2}$ ) for the same number of cycles of electropolymerization (Figure 2.2b).

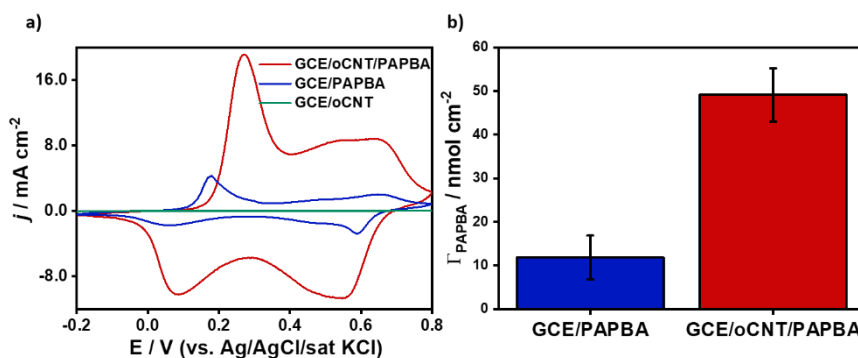


**Figure 2.2.** (a) Cyclic voltammogram recorded in 0.2 M HCl monomer free solution of oCNT-modified electrode (GCE/oCNT), PAPBA-modified electrode (GCE/PAPBA) and electrodes modified with both oCNT and PAPBA (GCE/oCNT/PAPBA). Scan rate.  $0.1 \text{ V s}^{-1}$ . (b) Surface area coverage of the electrodeposited PAPBA on oCNT-modified and unmodified glassy carbon electrodes calculated from a) ( $n = 3$ ). Error bars represent the standard deviation.

The increment in the amount of PAPBA deposited on GCE/oCNT surface could be a result of an increase of the adsorption of monomer on the GCE/oCNT surface mainly because of:  $\pi$ -  $\pi$  interactions

between the  $\pi$ -system of oCNT surfaces and the aromatic rings of 3-APBA, H-bond and electrostatic interaction between carboxylic groups of oCNT and amino groups of 3-APBA [38].

Subsequently, the GCE/oCNT/PAPBA electrodes were used as platform to construct a *C. vulgaris*-based bioanode. The rationale behind using boronic acid modified surfaces to anchor the algae cells is the ability of boronic acid moieties to bind 1,2 or 1,3-cis diols of saccharides found on the cell wall (Figure 2.1). [REDACTED]

[REDACTED]. Thus, *C. vulgaris* suspension in 0.1 M PB pH 7 was drop-casted on GCE/oCNT/PAPBA electrodes and left to dry for 2 h at  $(23 \pm 2)$  °C to ensure the formation of covalent bonds between the boronic acid moieties on the electrode surface and the saccharide units on the cell wall of *C. vulgaris*. It is important to note, that the ester bond formation between the boronic acid and saccharides is pH dependent, being favored near or above the  $pK_a$  of the boronic acid derivative. However, depending on the saccharide structure, the ester bond can also occur at pH values lower than the  $pK_a$  [39–43]. In the case of 3-APBA, its  $pK_a$  value is 8.8 [44], thus it would be expected more favored boron-saccharide interactions at pH values higher than 9. Nevertheless, the conductivity of polyaniline derivatives decreases at basic pH [45–47], therefore pH 7 was chosen for the incubation of

the cells with PAPBA as a compromise between favoring the ester bond formation and a good conductivity of the polymer.

The different steps involved on the surface modifications of the biophotocathode were examined by ESEM. The ESEM images show [REDACTED], the oCNT layer on the GCE was fully covered with a film of PAPBA (Figure 2.3a and b).

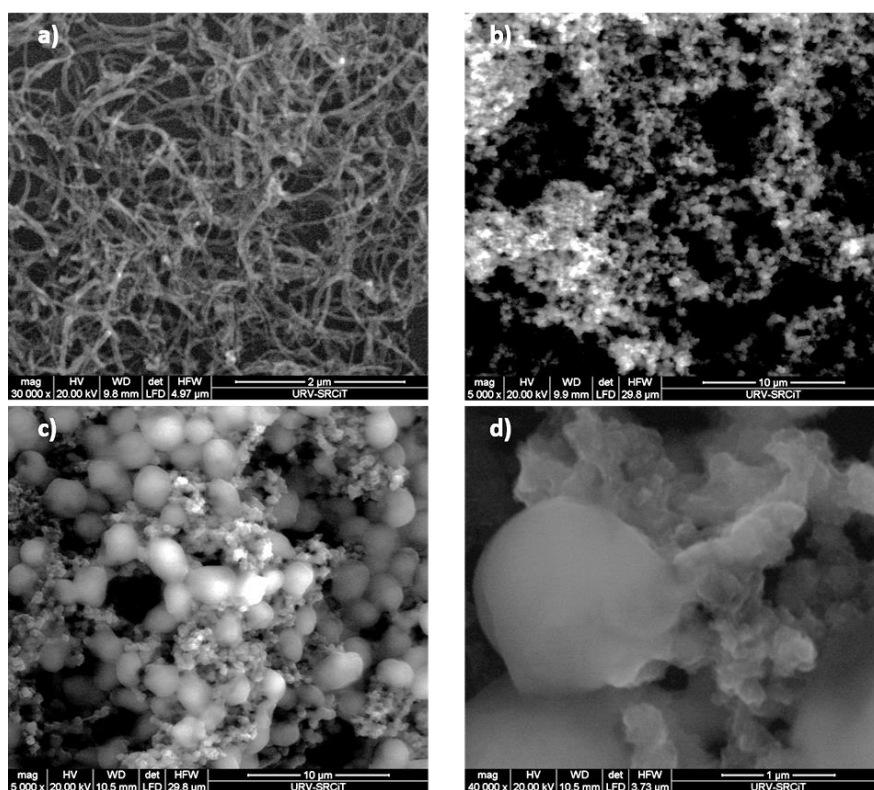


**Figure 2.3.** ESEM images of GCE modified with (a) oCNT, (b) oCNT and PAPBA, (c) *C. vulgaris* attached to GCE/oCNT/PAPBA electrodes, and (d) magnification image of c).

The polymer was not evenly distributed and seemed to grow vertically forming agglomerates of irregular shape with sizes in the order of micrometers. The grainy structure of the electropolymerized

---

PAPBA resembles that obtained for PANI and it is a result of the chaotic agglomeration of nucleates and formation of phenazine-like clusters [48]. This self-organization process seems to proceed probably according to the diffusion-limited aggregation mechanism [49]. After incubation of modified electrodes with *C. vulgaris*, cells were entrapped within the polymeric aggregates, which appeared to establish intimate contact with the cell surface (Figure 2.3c and d). This is probably because of the formation of ester bonds between saccharides on the cell wall of *C. vulgaris* and the boronic acid moieties on the electrode surface.

### 2.3.2. Optimization of cell loading and amount of polymer:

Prior to further evaluation, the effects of cell loading and the number of cycles of electropolymerization on the generation of photocurrent was investigated by photochronoamperometry. Figure 2.4a presents the increase in photocurrent density with the increase [REDACTED] [REDACTED] [REDACTED], though with significant variability ( $1.98 \pm 0.65 \mu\text{A cm}^{-2}$ ).

The variability of photocurrent at high concentration of cells might be due to the polymer, since differences in amount of electrodeposited polymer among electrodes were observed (Figure 2.2b), and due to the variability in cell immobilization, as it will be discussed further. The photocurrent decreased at OD<sub>680</sub> higher than [REDACTED], probably due to more cells hindering the physical contact with the conducting polymer and the increased cell' self-shading of the



multilayered biofilm hampering the light transmission to the bottom layers[50].

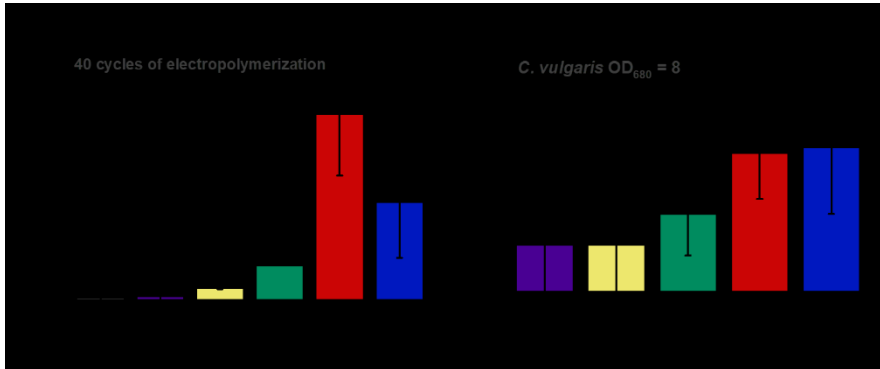


**Figure 2.4.** Comparison of the average photocurrent generation of *C. vulgaris*-based biophotocathode (GCE/oCNT/PAPBA-*C. vulgaris*) with (a) different cell loading for electrodes with 40 cycles of electropolymerization of 3-APBA ( $n = 2$ ) and (b) with same cell loading ( $OD_{680}$  of 8) and different cycles of electropolymerization of 3-APBA ( $n = 3$ ). Error bars represent the standard deviation.

Figure 2.4b shows the average photocurrent response with increasing the number of cycles of electropolymerization of 3-APBA for electrodes incubated with [REDACTED]. The increase in the number of cycles of electropolymerization led to more polymer on the surface of the electrode (see Figure Appendix A.1b). [REDACTED]

[REDACTED]. However, at [REDACTED] of electropolymerization, the standard deviation was relatively higher than the increase in photocurrent c [REDACTED]

[REDACTED]. Thus, [REDACTED]. The high inter-variability among electrodes might be a consequence of three factors:

i) the reproducibility of the oCNT coating by drop-casting due to the

occurrence of the coffee-ring effect [51,52]; ii) the difficulty to control the formation of the polymeric film because of the deposition-dissolution equilibrium of the electropolymerization products at the electrode-solution interface; and iii) the arrangement of the cells on the polymer since at higher cell loading the standard deviation of the photocurrent increases (see Figure 2.4a).

### **2.3.3. Assessment of the photocurrent generation of GCE/oCNT/PAPBA\_ *C. vulgaris*:**

To investigate the role of PAPBA in the photocurrent generation of *C. vulgaris*, photochronoamperometries were performed in 0.1 M PB pH 7 comparing the proposed *C. vulgaris*-based biophotoelectrode with *C. vulgaris* immobilized on bare GCE, GCE modified with oCNT and GCE modified with PAPBA (Figure 2.5a and b). For sake of comparison, the same XXXXXXXXXX and cycles of electrodeposition of PAPBA, when necessary, were used. As a control, modified electrodes were incubated with the media where the cells were growing (namely supernatant) (Figure Appendix A.2) and their photocurrent response was subtracted from the photocurrent obtained with cells.

Algae attached directly on bare GCE (GCE\_ *C. vulgaris*) generated an increase in current density of  $(0.048 \pm 0.015) \mu\text{A cm}^{-2}$  upon illumination. When *C. vulgaris* was immobilized on electrodes modified with PAPBA (GCE/PAPBA\_ *C. vulgaris*), the photocurrent only increased 2.3-fold ( $(0.11 \pm 0.02) \mu\text{A cm}^{-2}$ ). In contrast, the attachment of *C. vulgaris* on electrodes modified with both oCNT and PAPBA (GCE/oCNT/PAPBA\_ *C. vulgaris*) yielded a maximum

photocurrent of  $(1.98 \pm 0.65) \mu\text{A cm}^{-2}$ . This is more than 40 and 17-fold increase in photocurrent generation compared to those obtained with algae attached to unmodified and PAPBA modified GCE, respectively. This significant difference in photocurrent generation might be related with the amount of PAPBA deposited on the electrode surface, which was 4 times higher in the case of modified electrodes with oCNT (see Figure 2.2b). On the other hand, it is important to note that oCNT *per se* did not improve the electron transfer of algae, on the contrary, the photocurrent obtained ( $(0.030 \pm 0.008) \mu\text{A cm}^{-2}$ ) was slightly lower than that of GCE\_ *C. vulgaris* system.

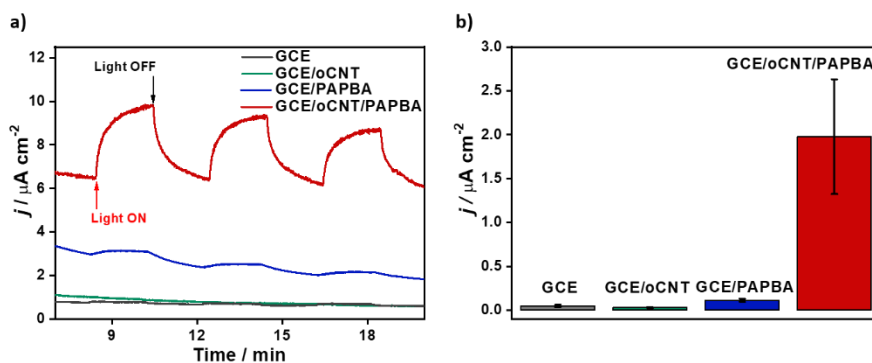


**Figure 2.5.** (a) Chronoamperograms recorded in 0.1 M PB pH 7 at 0.2 V vs Ag/AgCl/sat KCl of *C. vulgaris* ( $\text{OD}_{680} = 2$ ) immobilized on bare GCE, GCE/oCNT, GCE/PAPBA and GCE/oCNT/PAPBA electrodes. Irradiation of  $90 \mu\text{mol photons m}^{-2} \text{s}^{-1}$  incident white light. Red and black arrows indicate light ON and OFF, respectively. (b) Average photocurrent generation calculated from a) subtracting the photocurrent in the absence of *C. vulgaris* ( $n = 3$ ). Error bars indicate the standard deviation.

Moreover, the immobilization degree of *C. vulgaris* on each surface modification was assessed by fluorescence microscopy (Figure Appendix A.3) on account of the chlorophyll's autofluorescence.

Cell densities were quite similar among all the electrodes tested with significative intra-variability (Figure 2.6a).

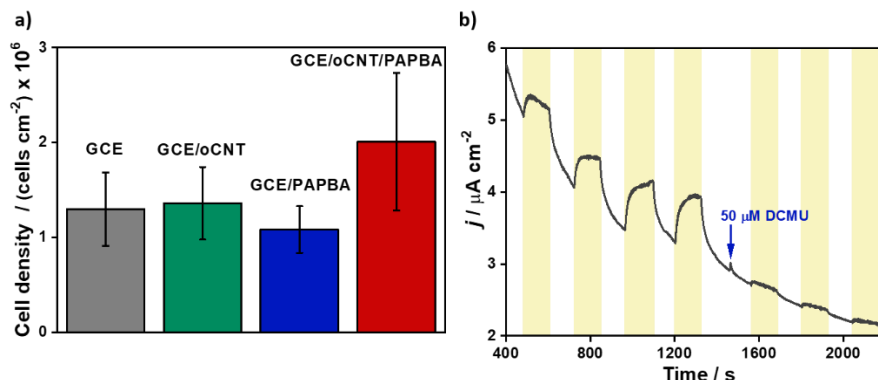


**Figure 2.6.** (a) Comparison of average cell density of *C. vulgaris* immobilized on unmodified GCE, oCNT-modified GCE, PAPBA-modified GCE and GCE modified with both oCNT and PAPBA. Cell densities were calculated from fluorescence micrographs. Error bars represent the standard deviation ( $n = 3$ ). (b) Chronoamperogram of *C. vulgaris* immobilized on GCE/oCNT/PAPBA electrode recorded in 0.1 M PB pH 7 at 0.2 V vs. Ag/AgCl/sat KCl in the presence of 50 μM DCMU. Irradiation of 90 μmol photons m<sup>-2</sup> s<sup>-1</sup> incident white light (yellow shadows).

GCE/oCNT/PAPBA electrodes showed a 50% improvement of immobilization degree of *C. vulgaris* ( $2.0 \pm 0.7$ )  $\times 10^6$  cell cm<sup>-2</sup>) compared to unmodified GCE ( $(1.3 \pm 0.4) \times 10^6$  cell cm<sup>-2</sup>). However, the photocurrent generation was remarkably greater (40-fold higher than unmodified electrodes). The improved cell immobilization on GCE/oCNT/PAPBA electrodes might be due to higher surface area rather than just to the presence of boronic acid moieties, since electrodes modified only with PAPBA yield the lowest cell density ( $(1.1 \pm 0.2) \times 10^6$  cell cm<sup>-2</sup>) but a greater photocurrent response than with unmodified or oCNT-modified electrodes. These facts provide strong evidence of the key role of PAPBA on facilitating the electron transfer from the algae to the electrode. It is worth to mention that

previous works from other groups have demonstrated that boronic acid modified surfaces are also capable of mediating charge transfer with other cell types such as macrophages, erythrocytes and bacteria [43,53,54]. It has been also suggested that these cells seem to communicate with the surface through sialic acid moieties found on the saccharide chains of the cell surface.

#### **2.3.4. Origin of the photocurrent:**

Although, the exact mechanism of the electron transfer is not clearly understood, the light dependence of the electron transfer between the *C. vulgaris* cells and the GCE/oCNT/PAPBA electrodes points to the photosynthetic metabolism of the algae as the source of the electrons being transferred. To test this hypothesis, photochronoamperometries of GCE/oCNT/PAPBA\_ *C. vulgaris* electrodes were performed by adding DCMU at a final concentration of 50  $\mu\text{M}$ . DCMU is a widely used photosynthetic inhibitor that binds at the  $\text{Q}_\text{B}$  site of the PSII blocking the electron transfer from plastoquinone intermediate A ( $\text{Q}_\text{A}$ ) to plastoquinone intermediate B ( $\text{Q}_\text{B}$ ) [55,56]. Figure 2.6b shows that after the addition of DCMU the photocurrent immediately dropped to values like the achieved without cells, proving that electrons stem from the photoexcitation of PSII.

From the results discussed above, it is difficult to elucidate the pathways involved in the transfer of electrons from the photosynthetic machinery to the electrode. Since it is unlikely that the polymeric chains of PAPBA penetrate the cell wall, the cell membrane, and the chloroplast membrane to wire the PSII, electrons should be transferred from the interior of the chloroplast to the cell

wall through electron shuttles or transmembrane redox proteins (as observed for cyanobacteria) [13,57,58] and from there to the electrode surface probably through a surface–surface saccharide redox chemistry which is facilitated by the presence of boronic acid moieties on the electrode surface.

The excretion of endogenous electron mediators was discarded by SWV of the electrode modified with both oCNT and PAPBA in the absence of cells (GCE/oCNT/PAPBA) recorded in 0.1 M PB pH 7 with and without the addition of 20 times concentrated supernatant (SN\*). SWV is a very sensitive technique frequently used for quantitative analysis of low concentrations of heavy metals in water and redox compounds for the pharmaceutical and nutraceutical industry [59]. The redox peak at -0.04 V vs. Ag/AgCl/sat KCl observed for both samples (Figure 2.7a) is due to the interconversion of the different oxidation states of PAPBA at neutral pH. No discernible extra redox peaks were observed after the addition of the 600  $\mu$ L of concentrated supernatant.

Additionally, photochronoamperometries of GCE/oCNT/PAPBA with and without *C. vulgaris* were performed in 0.1 M PB pH 7 with successive additions of concentrated supernatant (Figure 2.7b) to discard the photo-catalysis by *C. vulgaris* of potential excreted redox mediators. No photocurrent increase was observed upon successive additions of the concentrated supernatant even under illumination. The spikes in photocurrent observed after the addition of the concentrated supernatant are due to the difference in salt concentration rather than to some redox species present in the

supernatant. Therefore, these findings suggest that the interaction between PAPBA and the cell surface of *C. vulgaris* leads to DEET since endogenous electron mediators were undetectable under these experimental conditions.

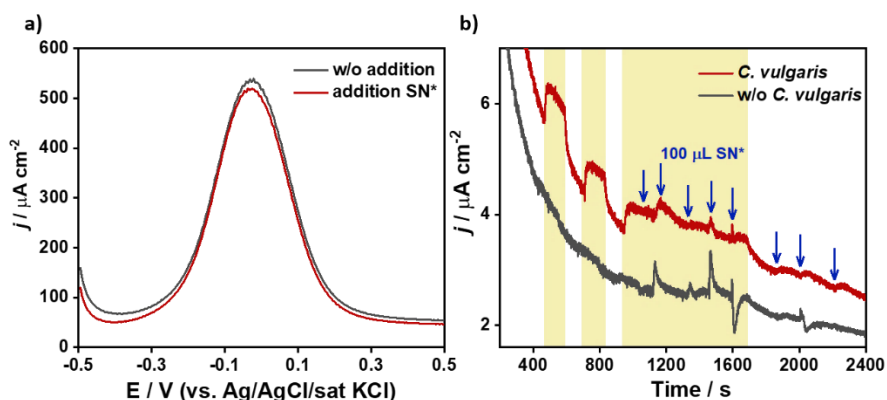


**Figure 2.7.** (a) Square-wave voltammograms of GCE/oCNT/PABPA electrodes recorded in 4 mL of 0.1 M PB pH 7 with and without the addition of 600  $\mu\text{L}$  of concentrated supernatant (SN\*). Frequency = 1 Hz,  $E_{\text{step}} = 5$  mV. (b) Chronoamperograms of GCE/oCNT/PABPA electrodes with and without immobilized *C. vulgaris* recorded in 0.1 M PB pH 7 with successive additions of SN\*.  $E_{\text{app}} = 0.2$  V vs Ag/AgCl/sat KCl. Irradiation of  $90 \mu\text{mol photons m}^{-2} \text{ s}^{-1}$  incident white light (yellow shadows).

Our observations are in fairly agreement with the findings of the aforementioned study of Stephenson-Brown et al. [53]. They found that boronic acid self-assembled monolayers were able to communicate electrochemically with macrophages through the formation of an ester bond between boronic acid residues and diols of glycoproteins present on the cell surface. Although DEET from *C. vulgaris* has been previously reported [9,19,60], these studies did not perform a rigorous investigation of the electron transfer mechanism that could discard the excretion of endogenous mediators. To the best of our knowledge, this is the highest photocurrent density obtained

for this strain in a mediator-less system (Table Appendix A.1). These higher values of photocurrent might be a result of the combination of the excellent conductive properties of the polyaniline-like backbone of PAPBA and the formation of multiple boronic ester linkages that brings together the cell wall of *C. vulgaris* to close proximity with the electrode surface favoring the DEET process.

### **2.3.5. Stability of the GCE/oCNT/PAPBA\_ *C. vulgaris*:**

The stability of the photocurrent generation of GCE/oCNT/PAPBA\_ *C. vulgaris* electrodes was assessed by performing photochronoamperometries for 1 hour both in PB pH 7 and in the optimum growing medium for *C. vulgaris* strain, BBM (Figure Appendix A.4). Figure 2.8a summarizes the results of these experiments. It is observed that GCE/oCNT/PAPBA\_ *C. vulgaris* electrode shows similar trend of loss of photocurrent in time for both electrolytes tested. When PB was used as electrolyte, a sharply dropped in photocurrent (89%) after 1h was observed. Nevertheless, the drop in photocurrent generation was more moderated (65%) when CAs were recorded in fresh BBM, which might be due to the presence of nutrients necessary for the well-being of the photosynthetic machinery. Thus, the decrease of the photocurrent in time might be due to i) the loss of photosynthetic efficiency of the immobilized *C. vulgaris*, ii) the loss of conductivity of the polymer at neutral pH [42,61] and iii) the irreversible oxidation of arylboronic acids to phenol in the presence of reactive oxygen species (ROS) produced during the photosynthesis[62–64].



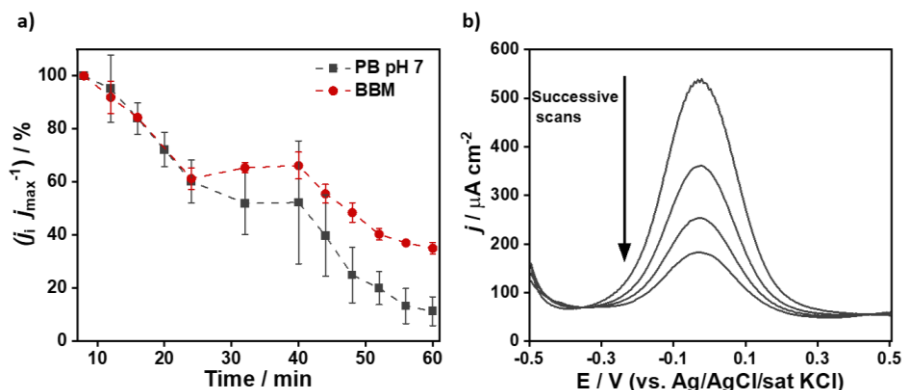


**Figure 2.8.** (a) Average percentage of photocurrent at each illumination cycle of *C. vulgaris* immobilized on GCE/oCNT/PAPBA calculated from photochronoamperometries (shown in Figure S4) in 0.1 M PB pH 7 and BBM. Error bars represent the standard deviation ( $n = 2$ ). (b) Successive square wave voltammograms of GCE/oCNT/PAPBA electrode in the absence of *C. vulgaris* recorded in 0.1 M PB pH 7. Frequency = 1 Hz,  $E_{\text{step}} = 5$  mV.

In addition, the stability of PAPBA at neutral pH was evaluated by successively scanning the GCE/oCNT/PAPBA electrode in the absence of *C. vulgaris* in PB pH 7. Square-wave voltammograms show that the redox peak of PAPBA decreases with scanning (Figure 2.8b). This phenomenon is consistent with previous works with polyaniline derivatives [65–67], where the conductivity of the polymer decreases due to low concentration of protons that results in the loss of polymer doping. However, further experiments on the detection of ROS species and photosynthetic efficiency of *C. vulgaris* are aim of future research to have a wider comprehension of the instability of the *C. vulgaris*-based biophotocathode.

### 2.3.6. Survey of GCE/oCNT/PAPBA as anode for other photosynthetic species:

Furthermore, a survey of photocurrent generation of other species immobilized on PAPBA-modified electrodes (GCE/oCNT/PAPBA)

was performed. The species tested were *C. reinhardtii* and *Scenedesmus* sp., both green microalgae, and cyanobacteria such as *Synechocystis* [REDACTED], *Synechococcus* [REDACTED] and *Nostoc* [REDACTED]. The photocurrent generation of these species was evaluated by photochronoamperometry in PB pH 7 and compared to the photocurrent obtained with these strains immobilized on electrodes in the absence of PAPBA. Figure 2.9 shows that the presence of PAPBA increases substantially the photocurrent generation for all the species. Some of the strains yielded negative photocurrents on oCNT modified electrodes because the photocurrent of these electrodes in the absence of cells was higher.

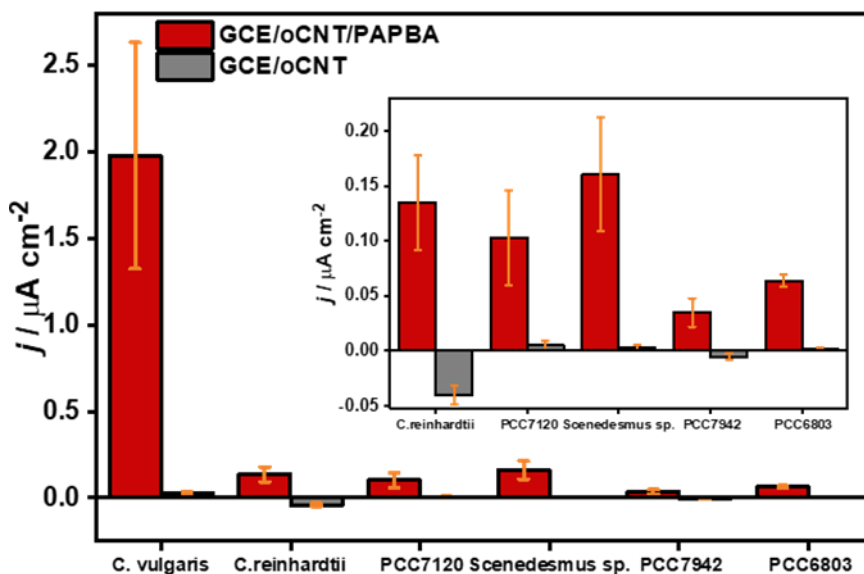


**Figure 2.9.** Comparison of average photocurrent generation of *C. vulgaris*, *C. reinhardtii*, *Scenedesmus* sp., *Nostoc* [REDACTED], *Synechocystis* [REDACTED] and *Synechococcus* [REDACTED] immobilized on oCNT-modified and oCNT-PAPBA-modified GCE electrodes (n = 3). Error bars represent the standard deviation.

Photocurrents were higher for all green microalgae ( $(0.16 \pm 0.05) \mu\text{A cm}^{-2}$  for *Scenedesmus* sp. and  $(0.14 \pm 0.04) \mu\text{A cm}^{-2}$  for *C. reinhardtii*)

---

followed by *Nostoc* [REDACTED] ( $(0.10 \pm 0.04) \mu\text{A cm}^{-2}$ ), *Synechocystis* [REDACTED] ( $(0.064 \pm 0.006) \mu\text{A cm}^{-2}$ ) and  $(0.04 \pm 0.01) \mu\text{A cm}^{-2}$  for *Synechococcus* [REDACTED]. Although the highest photocurrent was obtained for *C. vulgaris*, it should be noted that all the strains were tested at the conditions optimized for *C. vulgaris*. Therefore, further optimization of cell loading, incubation time and applied potential should be considered for each species for further improvement of their photocurrent generation.

## 2.4. Conclusions

A novel biophotocatalytic architecture based on *C. vulgaris* immobilized on GCE modified with both oCNT and PAPBA has been constructed. To achieve the highest possible performance, the effects of the cell loading and the number of electropolymerization cycles of 3-APBA on the photocurrent generation were assessed. ESEM images show the cells enclosed within the conducting polymer, which appeared to establish intimate contact with the cell surface. Experiments in the presence of DCMU confirmed the photoexcitation of PSII as the electron source. The absence of extra redox peaks to the polymer in the square-wave voltammogram and the invariance of the photocurrent response with the addition of concentrated supernatant suggest that there are no excreted electron mediators. These results support our hypothesis that PAPBA acts as a molecular wire that electrochemically communicates *C. vulgaris* with the electrode surface. This architecture yields the highest photocurrent density obtained so far with this alga in a mediator-less system. Moreover, the presence of PAPBA also increased the photocurrent generation of another two green microalgae and three

cyanobacteria species. Although the stability of the bioanode should be improved, boronic acid-nanostructured electrodes open new avenues to develop novel bioanode architectures to enhance the efficiency of actual BPVs.

## References

- [1] T.L. Chacón-Lee, G.E. González-Mariño, Microalgae for “healthy” foods-possibilities and challenges, *Compr. Rev. Food Sci. Food Saf.* 9 (2010) 655–675. <https://doi.org/10.1111/j.1541-4337.2010.00132.x>.
- [2] R. Dineshlumar, R. Narendran, P. Jayasingam, Sampathkumar P, Cultivation and chemical composition of microalgae *Chlorella vulgaris* and its antibacterial activity against human pathogens, *J. Aquac. Mar. Biol.* 5 (2017) 00119. <https://doi.org/10.15406/jamb.2017.05.00119>.
- [3] R.G. de Melo, A.F. de Andrade, R.P. Bezerra, D. de A. Viana Marques, V.A. da Silva, S.T. Paz, J.L. de Lima Filho, A.L.F. Porto, Hydrogel-based *Chlorella vulgaris* extracts: a new topical formulation for wound healing treatment, *J. Appl. Phycol.* 31 (2019) 3653–3663. <https://doi.org/10.1007/s10811-019-01837-2>.
- [4] I.T.K. Ru, Y.Y. Sung, M. Jusoh, M.E.A. Wahid, T. Nagappan, *Chlorella vulgaris*: a perspective on its potential for combining high biomass with high value bioproducts, *Appl. Phycol.* 1 (2020) 2–11. <https://doi.org/10.1080/26388081.2020.1715256>.
- [5] B. Ievina, F. Romagnoli, Potential of *Chlorella* species as feedstock for bioenergy production: a review, *Environ. Clim. Technol.* 24 (2020) 203–220. <https://doi.org/10.2478/rtuct-2020-0067>.
- [6] P. Moradi, M. Saidi, Biodiesel production from *Chlorella vulgaris* microalgal-derived oil via electrochemical and thermal processes, *Fuel Process. Technol.* 228 (2022) 107158. <https://doi.org/10.1016/j.fuproc.2021.107158>.
- [7] E.S. Salama, J.H. Hwang, M.M. El-Dalatony, M.B. Kurade, A.N. Kabra, R.A.I. Abou-Shanab, K.H. Kim, I.S. Yang, S.P. Govindwar, S. Kim, B.H. Jeon, Enhancement of microalgal growth and biocomponent-based transformations for improved biofuel recovery: A review, *Bioresour. Technol.* 258 (2018) 365–375. <https://doi.org/10.1016/j.biortech.2018.02.006>.

- [8] F.-L. Ng, S.-M. Phang, V. Periasamy, K. Yunus, A.C. Fisher, Enhancement of power output by using alginate immobilized algae in biophotovoltaic devices, *Sci. Rep.* 7 (2017) 16237. <https://doi.org/10.1038/s41598-017-16530-y>.
- [9] R. Thorne, H. Hu, K. Schneider, P. Bombelli, A. Fisher, L.M. Peter, A. Dent, P.J. Cameron, Porous ceramic anode materials for photo-microbial fuel cells, *J. Mater. Chem.* 21 (2011) 18055–18060. <https://doi.org/10.1039/c1jm13058g>.
- [10] C. Thong, S. Phang, F. Ng, V. Periasamy, T. Ling, K. Yunus, A.C. Fisher, Effect of different irradiance levels on bioelectricity generation from algal biophotovoltaic (BPV) devices, *Energy Sci. Eng.* 7 (2019) 2086–2097. <https://doi.org/10.1002/ese3.414>.
- [11] F.L. Ng, S.M. Phang, B.L. Lan, V. Kalavally, C.H. Thong, K.T. Chong, V. Periasamy, K. Chandrasekaran, G.G. Kumar, K. Yunus, A.C. Fisher, Optimised spectral effects of programmable LED arrays (PLA)s on bioelectricity generation from algal-biophotovoltaic devices, *Sci. Rep.* 10 (2020) 16105. <https://doi.org/10.1038/s41598-020-72823-9>.
- [12] E. Marsili, D.B. Baron, I.D. Shikhare, D. Coursolle, J.A. Gralnick, D.R. Bond, *Shewanella* secretes flavins that mediate extracellular electron transfer, *Proc Natl Acad Sci.* 105 (2008) 3968–3973. <https://doi.org/10.1073/pnas.0710525105>.
- [13] G. Saper, D. Kallmann, F. Conzuelo, F. Zhao, T.N. Tóth, V. Liveanu, S. Meir, J. Szymanski, A. Aharoni, W. Schuhmann, A. Rothschild, G. Schuster, N. Adir, Live cyanobacteria produce photocurrent and hydrogen using both the respiratory and photosynthetic systems, *Nat. Commun.* 9 (2018) 2168. <https://doi.org/10.1038/s41467-018-04613-x>.
- [14] A.J. McCormick, P. Bombelli, R.W. Bradley, R. Thorne, T. Wenzel, C.J. Howe, Biophotovoltaics: oxigenic photosynthetic organisms in the world of bioelectrochemical systems, *Energy Environ. Sci.* 8 (2015) 1092–1109. <https://doi.org/10.1039/C4EE03875D>.
- [15] J.K.F. Y. A. Gorby, S. Yanina, J. S. McLean, K. M. Rosso, D. Moyles, A. Dohnalkova, T. J. Beveridge, I. S. Chang, B. H. Kim, K. S. Kim, D. E. Culley, S. B. Reed, M. F. Romine, D.

- A. Saffarini, E. A. Hill, Electrically conductive bacterial nanowires produced by *Shewanella oneidensis* strain MR-1 and other microorganisms, *Proc Natl Acad Sci.* 103 (2006) 11358–11363. <https://doi.org/10.1073/pnas.0900028106>.
- [16] L. V Richter, S.J. Sandler, R.M. Weis, Two isoforms of *Geobacter sulfurreducens* pilA have distinct roles in pilus biogenesis, cytochrome localization, extracellular electron transfer, and biofilm formation, *J. Bacteriol.* 194 (2012) 2551–2563. <https://doi.org/10.1128/JB.06366-11>.
- [17] R.A. Bouhenni, G.J. Vora, J.C. Biffinger, S. Shirodkar, K. Brockman, R. Ray, P. Wu, B.J. Johnson, E.M. Biddle, M.J. Marshall, L.A. Fitzgerald, B.J. Little, J.K. Fredrickson, A.S. Beliaev, B.R. Ringeisen, D.A. Saffarini, The role of *Shewanella oneidensis* MR-1 outer surface structures in extracellular electron transfer, *Electroanalysis.* 22 (2010) 856–864. <https://doi.org/10.1002/elan.200880006>.
- [18] F.-L. Ng, S.-M. Phang, V. Periasamy, J. Beardall, K. Yunus, A.C. Fisher, Algal biophotovoltaic (BPV) device for generation of bioelectricity using *Synechococcus elongatus* (Cyanophyta), *J. Appl. Phycol.* 30 (2018) 2981–2988. <https://doi.org/10.1007/s10811-018-1515-1>.
- [19] F.-L. Ng, M.M. Jaafar, S.-M. Phang, Z. Chan, N.A. Salleh, S.Z. Azmi, K. Yunus, A.C. Fisher, V. Periasamy, Reduced graphene oxide anodes for potential application in algae biophotovoltaic platforms, *Sci. Rep.* 4 (2014) 7562. <https://doi.org/10.1038/srep07562>.
- [20] A. Cereda, A. Hitchcock, M.D. Symes, L. Cronin, T.S. Bibby, A.K. Jones, A bioelectrochemical approach to characterize extracellular electron transfer by *Synechocystis* sp. PCC6803, *PLoS One.* 9 (2014) e91484. <https://doi.org/10.1371/journal.pone.0091484>.
- [21] P. Bombelli, T. Müller, T.W. Herling, C.J. Howe, T.P.J. Knowles, A high power-density, mediator-free, microfluidic biophotovoltaic device for cyanobacterial cells, *Adv. Energy Mater.* 5 (2015) 1401299. <https://doi.org/10.1002/aenm.201401299>.
- [22] M.A. Thirumurthy, A. Hitchcock, A. Cereda, J. Liu, M.S.

- Chavez, B.L. Doss, R. Ros, M.Y. El-naggar, J.T. Heap, T.S. Bibby, A.K. Jones, Type IV pili-independent photocurrent production by the cyanobacterium *Synechocystis* sp. PCC6803, *Front. Microbiol.* 11 (2020) 1344. <https://doi.org/10.3389/fmicb.2020.01344>.
- [23] Y. Shlosberg, B. Eichenbaum, T.N. Tóth, G. Levin, V. Liveanu, G. Schuster, N. Adir, NADPH performs mediated electron transfer in cyanobacterial-driven biophotocatalytic cells, *IScience.* 24 (2021) 101892. <https://doi.org/10.1016/j.isci.2020.101892>.
- [24] L.T. Wey, J.M. Lawrence, X. Chen, R. Clark, D.J. Lea-smith, J.Z. Zhang, C.J. Howe, A biophotocatalytic approach to unravelling the role of cyanobacterial cell structures in exoelectrogenesis, *Electrochim. Acta.* 395 (2021) 139214. <https://doi.org/10.1016/j.electacta.2021.139214>.
- [25] Y. Hindatu, M. Annuar, A.M. Gumel, Mini-review: Anode modification for improved performance of microbial fuel cell, *Renew. Sustain. Energy Rev.* 73 (2017) 236–248. <https://doi.org/10.1016/j.rser.2017.01.138>.
- [26] S. Liu, L. Bakovic, A. Chen, Specific binding of glycoproteins with poly(aniline boronic acid) thin film, *J. Electroanal. Chem.* 591 (2006) 210–216. <https://doi.org/10.1016/j.jelechem.2006.04.021>.
- [27] S.R. Ali, R.R. Parajuli, Y. Balogun, Y. Ma, H. He, A nonoxidative electrochemical sensor based on a self-doped polyaniline/carbon nanotube composite for sensitive and selective detection of the neurotransmitter dopamine: A review, *Sensors.* 8 (2008) 8423–8452. <https://doi.org/10.3390/s8128423>.
- [28] Y. Zhou, H. Dong, L. Liu, J. Liu, M. Xu, A novel potentiometric sensor based on a poly(anilineboronic acid)/graphene modified electrode for probing sialic acid through boronic acid-diol recognition, *Biosens. Bioelectron.* 60 (2014) 231–236. <https://doi.org/10.1016/j.bios.2014.04.012>.
- [29] Q.-W. Zhang, J. Ouyang, Y. Wang, T.-T. Zhai, C. Wang, Z.-Q. Wu, T.-Q. Zhang, K. Wang, X.-H. Xia, Specific cell



- capture and noninvasive release via moderate electrochemical oxidation of boronic ester linkage, *Biosens. Bioelectron.* 138 (2019) 111316. <https://doi.org/10.1016/j.bios.2019.111316>.
- [30] G. Pankratova, L. Hederstedt, L. Gorton, Extracellular electron transfer features of Gram-positive bacteria, *Anal. Chim. Acta.* 1076 (2019) 32–47. <https://doi.org/10.1016/J.ACA.2019.05.007>.
- [31] S. Hadjoudja, V. Deluchat, M. Baudu, Cell surface characterisation of *Microcystis aeruginosa* and *Chlorella vulgaris*, *J. Colloid Interface Sci.* 342 (2010) 293–299. <https://doi.org/10.1016/j.jcis.2009.10.078>.
- [32] J. Pruvost, G. Van Vooren, G. Cogne, J. Legrand, Investigation of biomass and lipids production with *Neochloris oleoabundans* in photobioreactor, *Bioresour. Technol.* 100 (2009) 5988–5995. <https://doi.org/10.1016/j.biortech.2009.06.004>.
- [33] R.A. Andersen, *Algal culturing techniques*, Phycological Society of America Elsevier Academic Press, 2005.
- [34] Y. Kodama, Time gating of chloroplast autofluorescence allows clearer fluorescence imaging in planta, *PLoS One.* 11 (2016) e0152484. <https://doi.org/10.1371/journal.pone.0152484>.
- [35] A.J. Bard, L.R. Faulkner, *Electrochemical methods: fundamentals and applications*, 2nd ed., John Wiley & Sons, Inc., 2002.
- [36] G.E. Wnek, A proposal for the mechanism of conduction in polyaniline, *Synth. Met.* 15 (1986) 213–218. [https://doi.org/https://doi.org/10.1016/0379-6779\(86\)90026-3](https://doi.org/https://doi.org/10.1016/0379-6779(86)90026-3).
- [37] B.A. Deore, I. Yu, M.S. Freund, A switchable self-doped polyaniline: interconversion between self-doped and non-self-doped forms, *J. Am. Chem. Soc.* 126 (2004) 52–53. <https://doi.org/10.1021/ja038499v>.
- [38] B. Pan, B. Xing, Adsorption mechanisms of organic chemicals on carbon nanotubes, *Environ. Sci. Technol.* 42 (2008) 9005–

9013. <https://doi.org/10.1021/es801777n>.
- [39] B.A. Deore, M.D. Braun, M.S. Freund, pH dependent equilibria of poly(anilineboronic acid)-saccharide complexation in thin films, *Macromol. Chem. Phys.* 207 (2006) 660–664. <https://doi.org/10.1002/macp.200500560>.
- [40] H. Liu, Y. Li, K. Sun, J. Fan, P. Zhang, J. Meng, S. Wang, L. Jiang, Dual-responsive surfaces modified with phenylboronic acid-containing polymer brush to reversibly capture and release cancer cells, *J. Am. Chem. Soc.* 135 (2013) 7603–7609. <https://doi.org/10.1021/ja401000m>.
- [41] T. Figueiredo, V. Cosenza, Y. Ogawa, I. Jeacomine, A. Vallet, S. Ortega, R. Michel, J.D.M. Olsson, T. Gerfaud, J.G. Boiteau, J. Jing, C. Harris, R. Auzély-Velty, Boronic acid and diol-containing polymers: how to choose the correct couple to form “strong” hydrogels at physiological pH, *Soft Matter*. 16 (2020) 3628–3641. <https://doi.org/10.1039/d0sm00178c>.
- [42] E. Shoji, M.S. Freund, Potentiometric saccharide detection based on the  $pK_a$  changes of poly(aniline boronic acid), *J. Am. Chem. Soc.* 124 (2002) 12486–12493. <https://doi.org/10.1021/ja0267371>.
- [43] L. Lapinsonnière, M. Picot, C. Poriel, F. Barrière, Phenylboronic acid modified anodes promote faster biofilm adhesion and increase microbial fuel cell performances, *Electroanalysis*. 25 (2012) 601–605. <https://doi.org/10.1002/elan.201200351>.
- [44] X. Qin, Z. Zhang, H. Shao, R. Zhang, L. Chen, X. Yang, Boronate affinity material-based sensors for recognition and detection of glycoproteins, *Analyst*. 145 (2020) 7511–7527. <https://doi.org/10.1039/d0an01410a>.
- [45] E.M. Genies, E. Vieil, Theoretical charge and conductivity “state-diagrams” for polyaniline versus potential and pH, *Synth. Met.* 20 (1987) 97–108. [https://doi.org/10.1016/0379-6779\(87\)90549-2](https://doi.org/10.1016/0379-6779(87)90549-2).
- [46] J.C. Chiang, A.G. MacDiarmid, “Polyaniline”: protonic acid doping of the emeraldine form to the metallic regime, *Synth. Met.* 13 (1986) 193–205. [87](https://doi.org/10.1016/0379-</a></p></div><div data-bbox=)

6779(86)90070-6.

- [47] E. Ortega, F. Armijo, I. Jessop, M.A. Del Valle, F.R. Diaz, Chemical synthesis and characterization of polyaniline derivatives. Substituent effect on solubility and conductivity, *J. Chil. Chem. Soc.* 58 (2013) 1959–1962. <https://doi.org/10.4067/S0717-97072013000400010>.
- [48] M.A. Shishov, V.A. Moshnikov, I.Y. Sapurina, Self-organization of polyaniline during oxidative polymerization: formation of granular structure, *Chem. Pap.* 67 (2013) 909–918. <https://doi.org/10.2478/s11696-012-0284-6>.
- [49] W.R. Heinson, C.M. Sorensen, A. Chakrabarti, A three parameter description of the structure of diffusion limited cluster fractal aggregates, *J. Colloid Interface Sci.* 375 (2012) 65–69. <https://doi.org/10.1016/j.jcis.2012.01.062>.
- [50] N. Sekar, Y. Umasankar, R.P. Ramasamy, Photocurrent generation by immobilized cyanobacteria via direct electron transport in photo-bioelectrochemical cells, *Phys. Chem. Chem. Phys.* 16 (2014) 7862–7871. <https://doi.org/10.1039/c4cp00494a>.
- [51] S.K. Arkana Kaliyaraj, Y. Zhang, D. Li, R.G. Compton, A mini-review: How reliable is the drop casting technique?, *Electrochem. Commun.* 121 (2020) 106867. <https://doi.org/10.1016/j.elecom.2020.106867>.
- [52] R.G. Larson, Twenty years of drying droplets, *Nature.* 550 (2017) 466–467. <https://doi.org/10.1038/550466a>.
- [53] A. Stephenson-Brown, S. Yong, M.H. Mansor, Z. Hussein, N.-C. Yip, P.M. Mendes, J.S. Fossey, F.J. Rawson, Electronic communication of cells with a surface mediated by boronic acid saccharide interactions, *Chem. Commun.* 51 (2015) 17213–17216. <https://doi.org/10.1039/C5CC04311E>.
- [54] A. Matsumoto, N. Sato, K. Kataoka, Y. Miyahara, Noninvasive sialic acid detection at cell membrane by using phenylboronic acid modified self-assembled monolayer gold electrode, *J. Am. Chem. Soc.* 131 (2009) 12022–12023. <https://doi.org/10.1021/ja902964m>.

- [55] W. Oettmeier, H.J. Soll, Competition between plastoquinone and 3-(3,4-dichlorophenyl)-1,1-dimethylurea at the acceptor side of Photosystem II, *Biochim. Biophys. Acta - Bioenerg.* 724 (1983) 287–290. [https://doi.org/10.1016/0005-2728\(83\)90147-0](https://doi.org/10.1016/0005-2728(83)90147-0).
- [56] A. Trebst, Inhibitors in the functional dissection of the photosynthetic electron transport system, *Photosynth. Res.* 92 (2007) 217–224. <https://doi.org/10.1007/s11120-007-9213-x>.
- [57] D.J. Lea-Smith, P. Bombelli, R. Vasudevan, C.J. Howe, Photosynthetic, respiratory and extracellular electron transport pathways in cyanobacteria, *Biochim. Biophys. Acta.* 1857 (2016) 247–255. <https://doi.org/10.1016/j.bbabi.2015.10.007>.
- [58] A.C. Gonzalez-Aravena, K. Yunus, L. Zhang, B. Norling, A.C. Fisher, Tapping into cyanobacteria electron transfer for higher exoelectrogenic activity by imposing iron limited growth, *RSC Adv.* 8 (2018) 20263–20274. <https://doi.org/10.1039/c8ra00951a>.
- [59] V. Mirceski, S. Komorsky-Lovric, M. Lovric, Square-wave voltammetry: theory and application, Springer Berlin Heidelberg, 2007.
- [60] F.L. Ng, S.M. Phang, V. Periasamy, K. Yunus, A.C. Fisher, Enhancement of power output by using alginate immobilized algae in biophotovoltaic Devices, *Sci. Rep.* 7 (2017) 16237. <https://doi.org/10.1038/s41598-017-16530-y>.
- [61] W.W. Focke, G.E. Wnek, Y. Wei, Influence of oxidation state, pH, and counterion on the conductivity of polyaniline, *J. Phys. Chem.* 91 (1987) 173. <https://doi.org/https://doi.org/10.1021/j100306a059>.
- [62] K. Hasan, E. Çevik, E. Sperling, M.A. Packer, D. Leech, L. Gorton, Photoelectrochemical wiring of *Paulschulzia pseudovolvox* (algae) to osmium polymer modified electrodes for harnessing solar energy, *Adv. Energy Mater.* 5 (2015) 1501100. <https://doi.org/10.1002/aenm.201501100>.
- [63] J. Zielonka, A. Sikora, M. Hardy, J. Joseph, B.P. Dranka, B. Kalyanaraman, Boronate Probes as Diagnostic Tools for Real

- Time Monitoring of Peroxynitrite and Hydroperoxides, *Chem. Res. Toxicol.* 25 (2012) 1793–1799. <https://doi.org/10.1021/tx300164j>.
- [64] T. Roach, A. Krieger-Liszkay, Regulation of photosynthetic electron transport and photoinhibition, *Curr. Protein Pept. Sci.* 15 (2014) 351–362. <https://doi.org/10.2174/1389203715666140327105143>.
- [65] T. Lindfors, A. Ivaska, pH sensitivity of polyaniline and its substituted derivatives, *J. Electroanal. Chem.* 531 (2002) 43–52. [https://doi.org/10.1016/S0022-0728\(02\)01005-7](https://doi.org/10.1016/S0022-0728(02)01005-7).
- [66] C. Li, S. Mu, The electrochemical activity of sulfonic acid ring-substituted polyaniline in the wide pH range, *Synth. Met.* 149 (2005) 143–149. <https://doi.org/10.1016/j.synthmet.2004.12.015>.
- [67] Z. Chen, H. Lv, X. Zhu, D. Li, S. Zhang, X. Chen, Y. Song, Electropolymerization of aniline onto anodic WO<sub>3</sub> film: an approach to extend polyaniline electroactivity beyond pH 7, *J. Phys. Chem. C.* 118 (2014) 27449–27458. <https://doi.org/10.1021/jp509268t>.

## Chapter 3

### Derivatives of polyanilines as platforms to construct biophotoelectrodes

#### 3.1. Introduction

The bottleneck of cellular-BPVs' performance is the low cell-to-electrode transfer, mainly due to high interfacial charge transfer resistance and poor exoelectrogenesis of photosynthetic microorganisms [1]. Limitations in the interfacial electron transfer can be overcome by promoting intimate contact between cells and the electrode surface and by tailoring electrode surfaces with highly conductive materials. In this sense, ICPs are attractive materials in BES owing to their high electronic conductivity, ease synthesis and great environmental stability [2]. ICPs are hyperconjugated systems with delocalized electrons that allow the electron transfer along their backbone [3].

Enhanced electron transfer rates from microbes to anodes in MFCs have been reported by means of several ICPs [4]. The widest used ICP in MFCs is PANI and its composites with other materials [5–9]. It has been demonstrated that PANI increased bacterial cell adhesion at neutral pH due to electrostatic interactions and acted as a nanowire to *Shewanella oneidensis* MR-1 by enhancing the intimate contact with OMCs [8,10]. PANI has also demonstrated to increase power outputs in BPVs [11]. However, the meagre conductivity of PANI at neutral pH limits its large-scale application [12].

Enhanced electroactivity of polyaniline at neutral pH can be achieved by incorporating substituents in the aromatic ring of aniline, changing the acidity constant of the amino group [13,14]. [REDACTED] [REDACTED] [REDACTED] [15]. Moreover, the ability of boronic acid moieties to covalently bind to 1,2- or 1,3-diols makes them versatile functionalities for biosensors [16,17], cytosensors [18,19] and MFCs applications [20,21].

In *Chapter 2* we reported a 40-fold increased photocurrent from *C. vulgaris* immobilized on PAPBA-modified electrodes compared to unmodified electrodes. Nevertheless, to the best of our knowledge, the use of other polymers of substituted anilines in BPVs has not yet been explored.

In this chapter, a survey of several homopolymers of un- and substituted anilines for their use in *C. vulgaris*-based bioanodes is reported. Furthermore, a systematic analysis [REDACTED] [REDACTED] on the electron transfer from *C. vulgaris* is presented.

## **3.2. Materials and methods**

### **3.2.1. Algal culture:**

The *C. vulgaris* [REDACTED] was purchased from [REDACTED] [REDACTED]. Cultures were grown in [REDACTED] [22] in 250 mL Corning polycarbonate Erlenmeyer flasks (Fisher Scientific) at  $(20 \pm 2)$  °C and shaken at 150

rpm under a photosynthetic photon flux density (PPFD) of [REDACTED]  
[REDACTED]

### 3.2.2. Surface modification of electrodes:

[REDACTED] *polymerization of unsubstituted and substituted anilines:*

The surface of GCE of 3 mm Ø, model CHI104 (CH Instruments, Inc.) were polished with aqueous slurries of 0.3 µm alumina on nylon polishing pads. Subsequently, electrodes were ultrasonicated in Milli-Q water and blow dried with N<sub>2</sub>. One microliter of oCNT dispersion, prepared as in *Chapter 2*, was drop-cast on the GCE surface and [REDACTED]. The resulting electrodes (denoted as GCE/oCNT) were used as substrate for the [REDACTED] synthesis of homopolymers of aniline (ANI) and substituted aniline monomers: 3-aminophenylboronic acid (3-APBA), [REDACTED] (2-ABA), [REDACTED] (4-ABA), [REDACTED] (3-AP), [REDACTED] (2-PDA) and [REDACTED] (3-PDA). All monomers were [REDACTED]  
[REDACTED]. [REDACTED]  
[REDACTED]  
[REDACTED]  
[REDACTED]  
[REDACTED]  
[REDACTED]  
[REDACTED].



**Table 3.1.** [REDACTED] of polyaniline derivatives:

[REDACTED]	[REDACTED]	[REDACTED]	[REDACTED]	[REDACTED]	[REDACTED]
[REDACTED]	[REDACTED]	[REDACTED]	[REDACTED]	[REDACTED]	[REDACTED]
[REDACTED]	[REDACTED]	[REDACTED]	[REDACTED]	[REDACTED]	[REDACTED]
[REDACTED]	[REDACTED]	[REDACTED]	[REDACTED]	[REDACTED]	[REDACTED]
[REDACTED]	[REDACTED]	[REDACTED]	[REDACTED]	[REDACTED]	[REDACTED]
[REDACTED]	[REDACTED]	[REDACTED]	[REDACTED]	[REDACTED]	[REDACTED]
[REDACTED]	[REDACTED]	[REDACTED]	[REDACTED]	[REDACTED]	[REDACTED]
[REDACTED]	[REDACTED]	[REDACTED]	[REDACTED]	[REDACTED]	[REDACTED]

██████████ *polymerization of sulfonic acid substituted aniline:*

GCE/oCNT electrodes were also modified with chemically synthesized homopolymers of ██████████ (AHSA) and ██████████ (AMSA). ██████████ (PAHSA) ██████████ were synthesized following an adapted procedure described elsewhere [23,24]. Briefly, a solution of 10 mL of 0.5 M of the specific sulfonic acid substituted aniline in 0.5 M NH<sub>4</sub>OH was prepared and 5 mL of 1.25 M ammonium persulfate (APS) were dropwise while stirring the monomer solution at 18 °C. The solution was stirred overnight and further dialysed in cellulose dialysis tubes of 12 KDa molecular weight cut off (MWCO) from Sigma-Aldrich. Dialysis was performed against Milli-Q water changing the water trice every 2 h and finally allowed to dialysed for 24 h. Afterwards, the polymer was converted to its protonated form by passing the dialysed through an ██████████ (Fisher Scientific). Subsequently, the solvent of the protonated polymer was evaporated by means of a Büchi rotavapor R-200 (Afora, S.A.-Spain) in half isopropanol solution at 70 °C. The solid was collected and allowed to dry under vacuum at 50 °C. Eventually, two microliters of aqueous solution of polymer (██████████) were drop-cast on the GCE/oCNT electrodes and left to dry at RT.

### **3.2.3. Electrochemical characterization of polymer-modified electrodes and determination of the surface area coverage ( $\Gamma$ ) of each polymer:**

Characterization of polymer-modified electrodes was accomplished by performing CVs either in 0.2 M HCl and in 0.1 M PB pH 7 at 0.1 V s<sup>-1</sup>.

The  $\Gamma$  of each polymer was determined from the cyclic voltammograms in acidic solution. The charge of the first cathodic peak was measured to calculate  $\Gamma$  using the Faraday's law electrolysis equation (equation 2.1 in *Chapter 2*) [25] and assuming that 2 electrons are involved in the redox process of all synthesized polymers, as in the case of polyaniline [26].

### **3.2.4. Characterization of polymer-modified electrodes by X-Ray Photoelectron Spectroscopy (XPS) and Ultraviolet Photoelectron Spectroscopy (UPS):**

XPS and UPS were conducted at the Catalan Institute of Nanoscience and Nanotechnology (ICN2) facilities in Barcelona, Spain. XPS and UPS analysis were performed using a Specs PHOIBOS 150 (SPECS Surface Nano Analysis GmbH, Berlin, Germany spectrometer) with a monochromate Al K $\alpha$  source at a power of 400 W and a hemispherical analyzer operating in the fixed analyzer transmission mode. [REDACTED]

[REDACTED] [REDACTED]. To obtain more detailed information about chemical structure and oxidation states of the surfaces, high-resolution spectra were recorded from individual

peaks at 20 eV pass energy and 0.05 eV step size. Each specimen was analyzed at an emission angle of 0° as measured from the surface normal. Assuming typical values for the electron attenuation length of relevant photoelectrons, the XPS analysis depth (from which 95% of the detected signal originates) ranges between 5 and 10 nm for a flat surface. Quantification Data processing was performed using CASAXPS processing software version 2.3.24 (Casa Software Ltd., Teignmouth, UK). All elements present in the samples were identified from survey spectra. The atomic concentrations (atm %) of the detected elements were calculated using integral peak intensities and the sensitivity factors supplied by the manufacturer. Binding energies were referenced to the C 1s peak at 284.8 eV as it is recommended in specialized literature [27–29].

a layer of oCNT.

### **3.2.5. Immobilization of *C. vulgaris* on polymer-modified electrodes:**

*C. vulgaris* cultures at the beginning of the exponential growth phase were centrifuged at 4 °C and 4000 rpm for 10 minutes, washed in 0.1 M PB pH 7 and centrifuged. Pellets were resuspended in 0.1 M PB pH 7 to obtain an [REDACTED]. Then, [REDACTED] cells were [REDACTED] on electrodes and [REDACTED]. The OD<sub>680</sub> of the cultures was calculated from the absorbance divided by the optical path length, following the Beer-Lambert's law. The absorbance was measured at 680 nm in triplicate with the Spectramax microplate reader (Molecular Devices, LLC) by placing 100 µL of

sample (optical path length of  $\approx 0.25$  cm) in MaxiSorp nunc 96 microwell plates (Thermo Fisher Scientific Inc.).

### **3.2.6. Microscopy characterization:**

Autofluorescence of Chl *a* from GCE/oCNT/PAPBA\_ *C.vulgaris* was observed with a NIKON TE2000-E fluorescence microscope at excitation/emission wavelengths of 630/(650-700) nm [30]. Cell densities were calculated from fluorescence micrographs with the free image processing software ImageJ (National Institutes of Health, USA).

### **3.2.7. Electrochemical analysis of biophotoelectrodes:**

CAs were performed in triplicate in a 3-electrode electrochemical cell to scrutinize the ability of each conducting polymers to electronically communicate *C. vulgaris* with the electrode. The electrochemical cell was placed in a dark box and light was supplied by cold white LED strips of 12 V DC, 4.8 W m<sup>-1</sup> (Silver Sanz S.A.) [REDACTED]

[REDACTED] The irradiance was measured with an ULM-500 light meter (Heinz Walz GmbH). CAs were carried out at 0.2 V in 0.1 M PB pH 7 under several cycles of 2 min light ON/OFF, which [REDACTED]. [REDACTED]

[REDACTED]

[REDACTED]

[REDACTED].

### 3.3. Results and discussion

#### 3.3.1. Electrochemical characterization:

[REDACTED]

[REDACTED]

[REDACTED]. The chemical structures of selected anilines are represented in Figure 3.1a. All these commercially available anilines were chosen considering the electron donor/acceptor characteristics of the substituents. Anilines with the same substituent but in different position were also considered to assess the influence of their relative position in the aromatic ring on the [REDACTED] and the electron transfer with the cells. Additionally, the substituents were selected according to their possible interactions with the chemical species on the surface of the cell wall of *C. vulgaris* cells. The cell wall of *C. vulgaris* consists of a three-layer structure mainly composed of polysaccharides, chitin-like polysaccharides and 10 % of protein [31]. Boronic acid substituents can covalently bind to 1,2- or 1,3-diols present in polysaccharides of the cell surface. Carboxylic, amino, hydroxyl and sulfonic groups can form hydrogen bonds with sugars of the cell surface. Sulfonic acid groups can also react with glucosamines via acid-base reaction.

Prior to the deposition of polymeric films, the surface of GCE was modified with a layer of oCNT (Figure 3.1b) to enhance the amount of deposited polymers. oCNT might increase several times (> 4x) the deposition of polymers respect to bare surfaces as have been observed in *Chapter 2* for PAPBA. Such enhancement resulted from an increased adsorption of monomers on the electrode surface mainly

because of various attractive intermolecular interactions between the monomers and nanotubes [32].

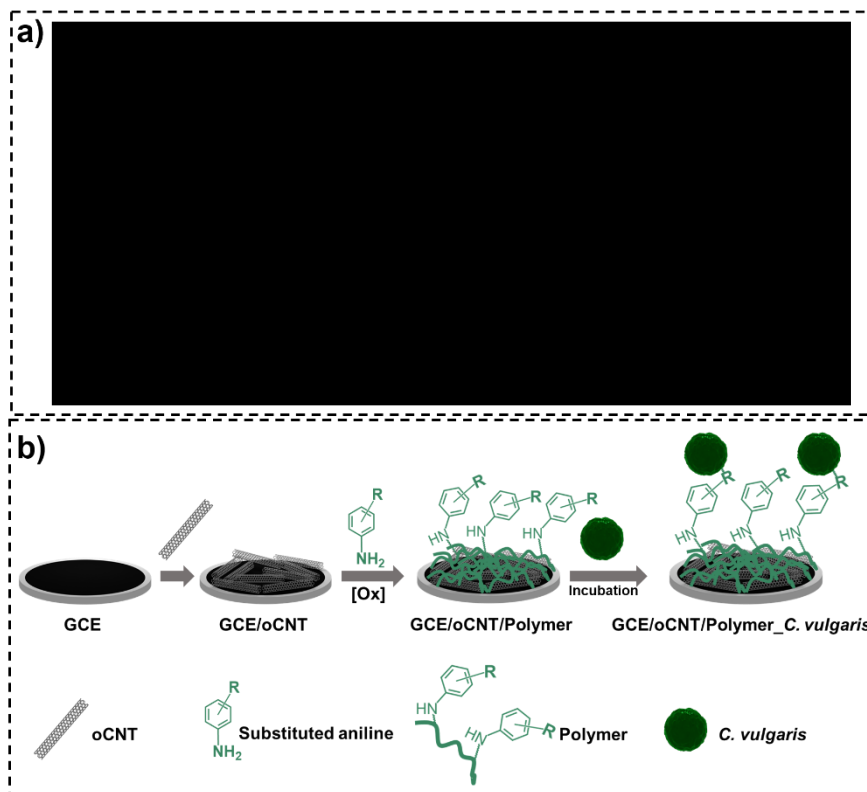


**Figure 3.1.** (a) Schematic representation of the steps involved in the preparation of *C. vulgaris*-based biophotoelectrodes (b) Chemical structure of the monomers used in this study to prepare the different polyaniline derivatives.

3-APBA: [redacted]  
 4-ABA: [redacted], 2-ABA: [redacted]  
 AHSA: [redacted], AMSA: [redacted]  
 3-AP: [redacted], 2-PDA: [redacted], 1,2-  
 d 3-PDA: [redacted].

Most of the substituted aniline represented in Figure 3.1a [redacted]  
 [redacted] polymerized on the surface of GCE/oCNT  
 electrodes by means [redacted]. [redacted]  
 [redacted]  
 [redacted] Previous reports showed that oxidation of substituted

anilines by APS yields products which are indistinguishable from those prepared by electrochemical methods [33–35].

Successive voltammograms obtained in acidic solution of relevant monomers 3-APBA, ANI, 4-ABA, 2-ABA, 3-AP, 2-PDA and 3-PDA at GCE/oCNT electrodes are shown in Figure Appendix B.1. All voltammograms showed an irreversible oxidation peak in the first forward scan attributed to the oxidation of the monomer. On the reverse and subsequent scans different redox processes were observed at lower potentials which may be attributed to the formation of polymeric surface-bound products. In general, continuous cycling produces a progressive increase of the reversible systems with filming of the electrode surface. However, [REDACTED]

[REDACTED]. These results are in line with a previous report that have demonstrated that substituted anilines are more difficult to electropolymerize than aniline [35].

The observed trend on the [REDACTED]  
[REDACTED]  
[REDACTED]  
[REDACTED] Polyaniline grows through an electrophilic aromatic



substitution in the *para*- position relative to the amino group [36,37].

Thus, this process in substituted anilines

[35].

The coating of electrode surfaces with chemically and electrochemically polymerized substituted anilines was investigated by CV in acidic and neutral solutions. Cyclic voltammograms recorded in 0.2 M HCl and 0.1 M PB pH 7 for all polymer-modified

electrodes are presented in Figure 3.2. All polymers showed well-defined anodic and cathodic peaks in acidic solutions. The voltammograms of electrodes modified with PAPBA and P2ABA display two well-defined sets of peaks which are similar in shape and position to those of PANI and other substituted anilines [35,37,40,41]. PAMSA also displays two sets of peaks but with some degree of overlap. In addition, the potential difference between these two subsequent redox processes is progressively reduced from PANI (0.52 V) to PAPBA (0.36 V) and P2ABA (0.27 V) until overlapping in PAMSA. This trend is paralleled by the increase of electron withdrawing effect of the substituent, where the sulphonic group has the most accentuated impact. Such behavior is characteristic of polyaniline derivatives and it has been explained as a result of the destabilization of the emeraldine state caused by electronic and steric effects of the substituent in the aniline derivative [40]. Hence, the observed redox pattern of PAPBA, P2ABA and PAMSA can be attributed to the emeraldine-to-leucoemeraldine and pernigraniline-to-emeraldine redox processes in analogy to those observed in PANI [35,36]. All together suggests structural similarities of PAPBA, P2ABA and PAMSA with PANI and also with other alkyl substituted anilines [42].

In contrast to previous polymers, P4ABA, PAHSA, P3AP, P2PDA and P3PDA display voltammograms with single redox pair located at different potentials depending on the substituent nature. These polymers appear to be switchable between two redox states without an intermediate oxidation state like emeraldine. The redox signature indicates that the electropolymerization of 4-ABA, AHSA, 3-AP, 2-

PDA and 3-PDA yields polymers that differ in structure to PANI derivatives [43–46]. Incorporation of amino and hydroxy groups as substituent in the aniline ring forms ladder-type polymers [43–45]. It has been established that they consist in phenazine or phenoxazine rings (for amino and hydroxy substituent, respectively) which are partially ring-opened and oxidized structures of the quinone-imine type [46–48] (see Figure 3.3a). Accordingly, the chemical structure of PAHSA, P3AP, P2PDA and P3PDA would be expected to be similar. In the case of 4-ABA the *ortho*- position to the amino should be the most susceptible to electrophilic aromatic substitution. This might favor the formation of 1,4-diazine moieties like in the case of 2-PDA and 3-PDA. Thus, it might be expected that the polymerization of 4-ABA also resulted in a ladder-type polymer with phenazine as redox moiety.

The voltammograms in neutral solution for all polymers presented anodic and cathodic peaks shifted to more negative potentials, as it is expected. In all these polymers, the electron transfer steps are coupled with protonation-deprotonation reactions. Thus, redox peaks shift to more negative potentials as pH is increased accordingly to the transferred protons to electrons ratio. This kind of pH-dependent redox behavior has been applied for potentiometric determinations of pH using electrodeposited PANI and other conducting polymers [49–52]. On the other hand, PAPBA and P4ABA presented redox peaks with a lower current than in acidic media while P2ABA and PANI lost completely their electroactivity in neutral media. It is well documented that PANI and some of its derivatives are undoped by increasing the pH of the media and being converted to insulators at

pH >4 [35]. Since sulphonate polyanilines are more prompt to retain their electroactivity in neutral media than PANI [13,33,37], it seems that the disappearance of the redox peaks of PAMSA and PAHSA was due to the leaching of the polymers to the media rather than the dedoping process. The other polymers (P3AP and P2PDA) retained their redox activity in neutral media or even it was improved as for P3PDA.

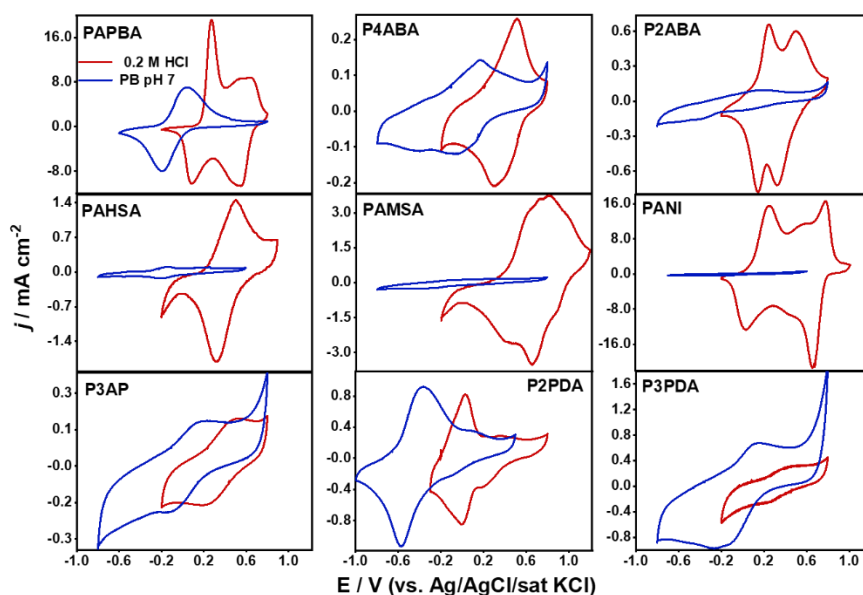


**Figure 3.2.** CVs of GCE/oCNT electrodes modified with different polyaniline derivatives recorded in 0.2 M HCl (red lines) and in 0.1 M PB pH 7 (blue lines). Scan rate: 100 mV s<sup>-1</sup>. PAPBA: [redacted], P4ABA: [redacted], P2ABA: [redacted], PAHSA: [redacted], PAMSA: [redacted], PANI: [redacted], P3AP: [redacted], P2PDA: [redacted] and P3PDA: [redacted].

### 3.3.2. XPS and UPS characterization:

XPS analysis was performed for further supporting the formation of the polymeric films on GCE/oCNT electrodes and for determining

the surface chemical composition of the films. XPS is a reliable technique to characterize polymers both qualitatively and quantitatively [28]. Survey spectra for each polymer are presented in Figures Appendix B.2-B.10. In general, the XPS survey spectra of all polymeric films show the presence of carbon (C 1s ~ 285 eV), nitrogen (N 1s ~ 400 eV) and oxygen (O 1s ~ 532 eV). The presence of sulfur (S 2p ~ 168 eV) was observed in the survey spectra of PAHSA and PAMSA and the signature of boron (B 1s ~ 190 eV) was detected in case of PAPBA. Chlorine (Cl 2p ~ 198 eV) was detected in the case of PANI, P3AP, P2PDA and P3PDA samples, that might be coming from the electrolyte (HCl) for the electrochemical characterization of these surfaces. The relative chemical composition (as atm %) for all polymeric films under study in this work are listed in Table 3.2.

**Table 3.2.** Relative surface composition (as atm %) in the polymeric films determined by XPS analysis.

<i>Atomic composition (atm %)</i>							
<i>Polymer</i>	<b>C</b>	<b>N</b>	<b>O</b>	<b>Cl</b>	<b>B</b>	<b>S</b>	<b>Empirical Formula</b>
<b>PAPBA</b>	76.7	5.3	13.2	-	4.7	-	C <sub>14.3</sub> N <sub>1</sub> O <sub>2.5</sub> B <sub>0.9</sub>
<b>P4ABA</b>	78.5	6.2	15.2	-	-	-	C <sub>12.6</sub> N <sub>1</sub> O <sub>2.4</sub>
<b>P2ABA</b>	75.2	6.9	17.9	-	-	-	C <sub>10.9</sub> N <sub>1</sub> O <sub>2.6</sub>
<b>PAHSA</b>	61.6	5.9	25.6	-	-	6.9	C <sub>10.4</sub> N <sub>1</sub> O <sub>4.3</sub> S <sub>1.1</sub>
<b>PAMSA</b>	56.5	8.8	26.3	-	-	8.4	C <sub>6.5</sub> N <sub>1</sub> O <sub>3</sub> S <sub>1</sub>
<b>PANI</b>	84.9	9.5	4.9	0.7	-	-	C <sub>8.9</sub> N <sub>1</sub> O <sub>0.5</sub> Cl <sub>0.07</sub>
<b>P3AP</b>	77.8	6.1	15.3	0.8	-	-	C <sub>12.7</sub> N <sub>1</sub> O <sub>2.5</sub> Cl <sub>0.1</sub>
<b>P2PDA</b>	80.7	11.0	7.9	0.4	-	-	C <sub>7.3</sub> N <sub>1</sub> O <sub>0.7</sub> Cl <sub>0.04</sub>
<b>P3PDA</b>	77.1	13.4	8.7	0.8	-	-	C <sub>5.8</sub> N <sub>1</sub> O <sub>0.6</sub> Cl <sub>0.06</sub>

It may be noted that remarkable amounts of oxygen were found in PANI, P2PDA and P3PDA when the contrary would be expected.

According to previous works, oxygen in the polymerization products of substituted anilines can be originated from partial oxidation of the film's surface or due to the degradation of the polymer via hydrolysis to benzoquinone [53–55].

XPS analysis of the C, N, O, S and B core levels was further performed to identify and quantify the chemical/oxidation states of these elements in the polymeric films. Chemical/oxidation state information was obtained from chemical shifts in the binding energies, which are the result of different chemical/binding environments for an element [56]. The core level spectra for all polymers prepared in the present study are provided in Figures Appendix B.2-B.10. All core-level spectra of all samples clearly resolved multiple features associated with the corresponding atom environment. These features were decomposed into different components using Voigt functions which are the best representation of a photoelectron peak [57]. The binding energies of the synthetic fit components, their line shapes, full width at half maximum (FWHM), relative percentage areas and corresponding assignation of all components are reported in Tables Appendix B.2-B.10. The assignment of each component to a particular chemical environment was made based on a comparison of their binding energy values with those reported in the literature [58,59].

The main carbon components of C 1s core level spectra for all polymers correspond to carbon atoms in C-C and C-H bonds (C-C/C-H at ~ 284-285 eV), in carbon-nitrogen single or double bonds (C-N/C=N at ~ 285-286 eV) and carbon atoms bonded to positive charge

nitrogen (C-N<sup>+</sup>/C=N<sup>+</sup> at ~ 285-286 eV). These features are consistent with polymers derived from un- and substituted anilines [53,55,60–63]. Components attributed to carbon atoms in C-O and C=O bonds were also found at about 286 and 288 eV, respectively. This is indicative of some level of oxidation of the polymeric surfaces. Moreover, these species can also arise from the incorporation of benzoquinone and hydroquinone units within the polymer chains as a result of the hydrolysis of imine moieties [60,64]. Components at ~ 288-289 eV attributed to carbon atoms in carboxylic or carboxylate group were found in the case of P2ABA and P4ABA samples. Satellites arising from  $\pi \rightarrow \pi^*$  shake-up processes were also observed in some polymers at high binding energies (> 289 eV). These satellites appear in polymers containing aromatic groups and are absent in analogous saturated systems [65]. Additionally, the absence or presence of shake-up satellites can provide a qualitative means to judge the thickness and homogeneity of polymer thin films. If the shake-up structure cannot be observed, the polymer film would be continuous and thicker than the XPS sampling depth (5 to 10 nm) [28].

The oxygen 1s core level spectra of each polymer were also fitted using different components. All of them reflected the variety of chemical environments of oxygen atoms in the polymers. Accordingly, components attributed to oxygen atoms in hydroxyl, carbonyl, carboxylic, sulphonic and boronic acid groups were identified. It is worth to mention that the binding energies for these groups are very similar in the oxygen 1s core level and overlapping

---

might occur. Thus, conclusions from these spectra should be done with caution.

The B 1s core level spectrum of PAPBA confirms the presence of boronic acid moieties within the polymer backbone. Interestingly, the experimental spectrum can be fitted to two main components at 191.2 and 192.6 eV. This means that boron is surrounded by two different chemical environments in PAPBA. The B 1s binding energies correlate linearly with the atomic charges: the greater the positive charge of B atoms, the higher the binding energy is [66]. Given that a tetrahedral geometry gives rise to a net negative formal charge on boron, it may be concluded that the low binding energy component arises from the tetrahedral boron moieties in the polymer while the component at higher binding energy is attributed to trigonal boron moieties as it is represented in Figure 3.3b. Based on the above assignment, it is found that  $\sim 82\%$  of boron in PAPBA has a tetrahedral geometry as  $-\text{[B(OH)}_3\text{]}^-$  moieties and  $\sim 18\%$  in trigonal geometry as  $-\text{B(OH)}_2$  groups. Similar observations have been reported for self-assembled monolayers containing boronic acid groups [67].

The S 2p core level spectra of PAMSA and PAHSA were fitted using a doublet per component to reflect the S 2p spin-orbit interaction. The energy separation between them was assumed to be 1.16 eV and the relative intensity of spin-up state,  $j = 3/2$ , and spin-down state,  $j = 1/2$ , was equal to 2 [28,68]. Two and three set of doublets were used to fit the S 2p spectra of PAMSA and PAHSA, respectively. The two main doublets are attributed to sulfur atoms from the sulphonic



groups in two different environments. The doublet at lower binding energy corresponds to sulfur atoms in neutral sulfonic acid groups. The doublet at higher binding energy is attributed to sulfur in sulfonate groups. These assignments are based on considering that sulfur in the sulfonate group has lower electron density than sulfur in the neutral sulfonic acid because of the electrostatic interactions between the oxygen of sulfonate anions and positively charged nitrogen atoms [69,70] (see Figure 3.3b). A third doublet was necessary to be added to satisfactory fit the S 2p spectra of PAHSA. This doublet might rise from sulfur atoms in sulphate anions or due to a satellite signal [71–73].

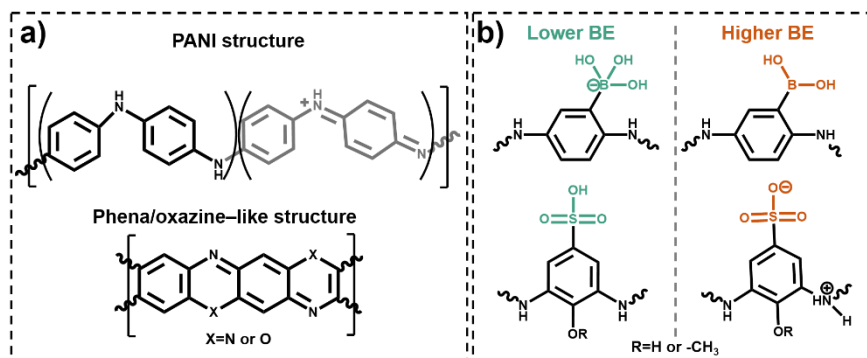


**Figure 3.3** (a) Chemical structures of PANI and phena/oxazine-like polymers that are commonly accepted in the literature. (b) Possible chemical structures of the low and high binding energy components observed in the B 1s region of PAPBA and in the S 2p region of PAMSA and PAHSA.

The analysis of the nitrogen 1s core level spectra of polymers derived from un- and substituted anilines permits to quantify their oxidation level and doping degree. Both characteristics are responsible of the conductive properties of polyanilines and related systems [40]. The oxidation level is quantified as the imine-to-amine (-N=/-NH-) ratio while the doping degree is estimated as the positively charged

nitrogen species-to-total nitrogen ( $\sum N^+/N$ ) ratio [74]. The imine, amine and positively charged nitrogen species are quantitatively differentiated in curve-fitted N 1s core-level spectrum. They correspond to peak component with binding energy at about 398, 399 and  $> 400$  eV, respectively [53,54,75]. Figure 3.4 presents the N 1s core level spectra of all polymers examined here. From the fitted curves, it is possible to confirm the presence of imine and amine groups in most of the samples

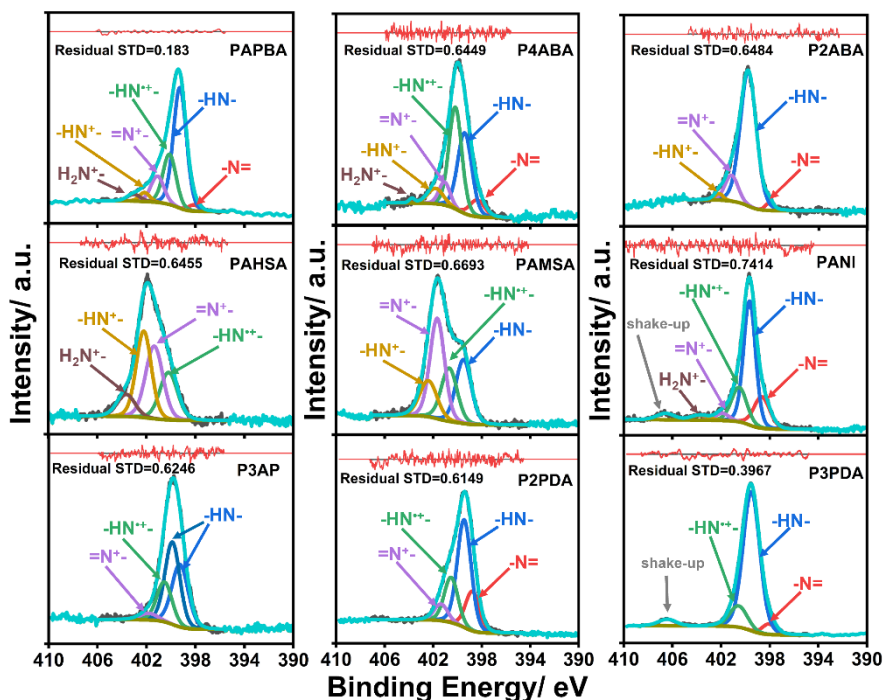


**Figure 3.4.** High resolution XPS spectra in the N 1s region of GCE/oCNT electrodes modified with the different polyaniline derivatives.

Additionally, more than one synthetic fit component was used to fit the regions at binding energies greater than 400 eV. Such components have been attributed to nitrogen atoms with delocalized radical cations ( $-N^{+•}$ ), positively charged imine cation ( $-N^{+=}$ ), positively

charged di-substituted amine ( $-N^+H-$ ) and positively charged mono-substituted amine ( $-N^+H_2$ ). Their corresponding binding energies are about 400, 401, 402 and 403 eV, respectively [76–79]. Moreover, some polymers showed a signal at about 405 eV corresponding to shake-up satellite characteristic in conjugated molecular skeletons [76,80,81].

The binding energies of the synthetic fit components, their relative percentage areas, the level of oxidation and degree of doping for all the polymers are reported in Table 3.3. It is observed that the lowest oxidation degree was obtained for PAPBA, P2ABA, PAHSA and PAMSA. On the other hand, the highest doping level was observed for PAHSA and PAMSA samples. The higher doping degree of these polymers might be explained as a self-doping process resulting from the protonation of the imine and amine groups withing the backbone of the polymer by the sulfonic acid moieties [62,82]. Similar interactions may occur with polyaniline derivatives containing boronic and carboxylic acid moieties which might explain the higher doping degree of PAPBA and P4ABA in comparison to P3AP, P2PDA and P3PDA [37,64].

**Table 3.3.** Contribution (in %) of nitrogen components, oxidation level and doping degree resulting from the fitting of high resolution XPS spectra in the N 1s region of all polymer films:

<i>Component</i>		<i>Binding Energy (eV)</i>								
		398 -N=	399 -HN-	400 -HN <sup>+</sup> -	401 =N <sup>+</sup> -	402 -HN <sup>+</sup> -	403 -H <sub>2</sub> N <sup>+</sup> -	405 s.u.*	OL* -N=-/HN-	DG* $\sum(N^+)/N$
<i>Polymers</i>	<b>PAPBA</b>	2.4	55.7	23.3	12.2	3.3	3.1	-	0.04	38.7
	<b>P4ABA</b>	7.8	35.5	40.6	8.0	7.5	0.7	-	0.22	56.1
	<b>P2ABA</b>	2.1	82.8	13.0	2.1	-	-	-	0.03	15.1
	<b>PAHSA</b>	-	-	22.1	33.1	34.5	10.3	-	-	89.7
	<b>PAMSA</b>	-	25.1	21.6	37.2	16.1	-	-	0	74.9
	<b>PANI</b>	15.6	61.9	19.2	3.4	-	-	-	0.25	22.6
	<b>P3AP</b>	34.4	41.2	20.5	4.0	-	-	-	0.83	24.4
	<b>P2PDA</b>	19.1	51.5	21.5	7.9	-	-	-	0.37	29.4
	<b>P3PDA</b>	4.7	78.8	12.7	-	-	-	3.8	0.06	12.7

\*OL, DG and s.u. stand for oxidation level, doping degree, and shake-up, respectively

UPS analysis was performed to all polymer thin films for further characterization. UPS spectra provide information about the valence band of a material. Figure 3.5 shows the UPS spectra of all polymers prepared in the present work. The intensity of the spectra is related with the density of states (DOS) of the samples. In region between 0 to 12 eV, the intensity arises from electronic states involving benzenoid rings, imine and amine moieties within the backbone of the polymers [77,83]. The inset in Figure 3.5 shows the valence band spectra near the Fermi level ( $E_F$  at  $E=0$  since it is used as energy reference level in UPS experiments) for all the polymers. It is noteworthy that the DOS near  $E_F$  of PAMSA and PAHSA is not zero. A non-zero DOS near  $E_F$  indicates that both polymers have an electronic structure with semi-metallic characteristics. These results are in line with the high doping degree of both polymers that was found from the XPS analysis of the N 1s core level spectra. On the contrary, the UPS spectra of the other polymers revealed no electronic states near  $E_F$ . This corresponds to the electronic characteristics of semiconductor materials, with valence bands located at less than one eV below the  $E_F$  [84].

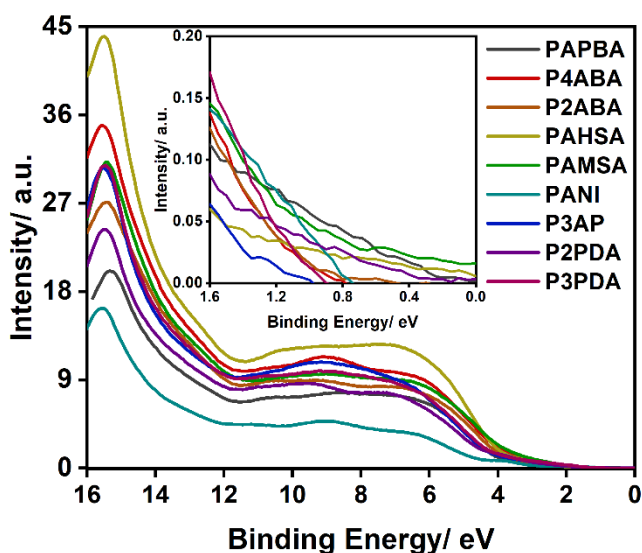


**Figure 3.5.** UPS spectra of the different polymers deposited on GCE/oCNT electrodes. Inset: close-up of the UPS spectra in the 0 to 1.6 eV region.

### 3.3.3. Assessment of the photocurrent generation of *C. vulgaris* immobilized on polymers of un-and substituted aniline:

GCE/oCNT electrodes modified with the polymers described above were used as platforms to construct bioanodes. *Chlorella vulgaris* cells were selected as the photosynthetic microorganism to be attached on the electrode surface. To investigate the role of the chemical structure of synthesized polymers in the photocurrent generation of *C. vulgaris*, photochronoamperometries were performed in 0.1 M PB pH 7 using the aforementioned polymer-modified electrodes. As a control, modified electrodes were incubated with the supernatant (the media where the cells were growing), and their photocurrent response was subtracted from the photocurrent obtained with cells immobilized on the electrodes.

Figures 3.6a and b show photochronoamperograms obtained with different polymers in the presence and in the absence of *C. vulgaris*.

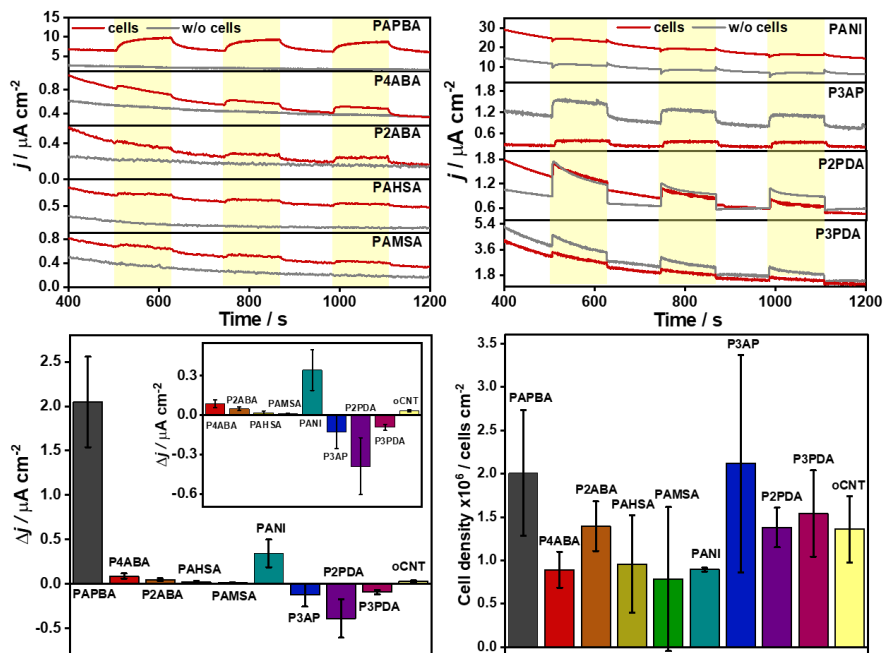


**Figure 3.6.** Chronoamperograms recorded under successive cycles (yellow boxes) of incident white-light ( $90 \mu\text{mol photons m}^{-2} \text{s}^{-1}$ ) for GCE/oCNT electrodes modified with polyaniline derivatives containing (a) electron withdrawing and (b) electron donor substituents. Red and grey lines correspond to electrodes with and without immobilized *Chlorella vulgaris* cells, respectively. Electrolyte: 0.1 M PB pH 7 and  $E_{\text{app}} = 0.2 \text{ V}$  vs Ag/AgCl/sat KCl. (c) Average photocurrent generation calculated from (a) and (b) subtracting the photocurrent in the absence of *C. vulgaris* ( $n = 3$ ). (d) cell density of *Chlorella vulgaris* immobilized on each polymer-modified electrode ( $n = 3$ ). Error bars indicate the standard deviation.

It is observed that algae attached to PAPBA, P4ABA, P2ABA, PAMSA, PAHSA and PANI modified electrodes generated an immediate increase in current density upon illumination. The same electrodes without cells presented negligible responses upon light. The light dependence of the current only in presence of *C. vulgaris* points to the photosynthetic metabolism of the algae as the source of

electrons, as it was discussed in *Chapter 2*. Additionally, results from *Chapter 2* with DCMU proved that electrons stem from the photoexcitation of PSII in the case of PAPBA.

On the contrary, electrodes modified with P3AP, P2PDA and P3PDA responded to light indistinctly whether *C. vulgaris* cells were or not attached on the electrode surface. The photoresponse of these electrodes was even higher when cells were absent. This means that P3AP, P2PDA and P3PDA are photoactive polymers with cells hindering the amount of light that hits the polymer layer. Thus, the photocurrent observed for these polymer-modified electrodes in presence of *C. vulgaris* was due to the polymer photoactivity rather than to a cell-to-electrode electron transfer process. Figure 3.6c summarizes the average photocurrent response obtained with *C. vulgaris* immobilized on each polymer. Among them, PAPBA resulted in the highest photocurrent generation from *C. vulgaris*. The average net photocurrent for *C. vulgaris* immobilized on PAPBA modified surfaces was  $(2.0 \pm 0.6) \mu\text{A cm}^{-2}$  which is almost three times higher than that obtained  $(0.64 \mu\text{A cm}^{-2})$  with *C. vulgaris* immobilized within an alginate matrix [86], and about the half of those using Osmium-redox polymers  $(5 \pm 1) \mu\text{A cm}^{-2}$  [87].

The outperforming of PAPBA in terms of photocurrent generation of *C. vulgaris* respect to other polymers examined here might be a combination of different factors. First, PAPBA is easily electropolymerized on conductive surfaces. A surface area coverage of  $(49 \pm 6) \text{ nmol cm}^{-2}$  was obtained with 40 cycles of electropolymerization. This is almost 20-fold greater than that



---

obtained for P4ABA ( $(2.4 \pm 0.6) \text{ nmol cm}^{-2}$ ) in 100 cycles and 50-fold greater than that obtained for P3PDA ( $(0.93 \pm 0.07) \text{ nmol cm}^{-2}$ ) in 50 cycles (see Figure Appendix B.11). Second, the polyaniline-like backbone of PAPBA confers good conductivities ( $\sim 0.03 \text{ S cm}^{-1}$ ) to the polymer [88]. Third, PAPBA presents good redox behavior even at neutral pH because of the self-doping process in the polymer. This self-doping results from the interactions between boronic acid moieties and the imine or amine moieties in the polymer backbone as it was discussed previously. And last but most important, the chemical properties of boronic acid moieties. Boronic acids are able to reversibly bind to 1,2 or 1,3-cis diols which are ubiquitous as oligosaccharides on the cell wall of most microorganism [31,89–92]. The possible formation of multiple boronic ester linkages with saccharide-like structures in the cell wall of *C. vulgaris* may lead a favorable cell-to-electrode surface electron transfer process. Thus, higher photocurrent generation is obtained. Previous works from other groups have demonstrated that boronic acid modified surfaces are also capable of mediating charge transfer with macrophages, erythrocytes and cyanobacteria [18,21,93].

To discard the effect of cell loading in the photocurrent generation, the immobilization degree of *C. vulgaris* on each polymer modified surface was assessed by fluorescence microscopy. Cells can be counted on account of the autofluorescence upon excitation with red light of chlorophyll present inside the cell. Figure 3.6d shows the average cell density obtained after the immobilization of *C. vulgaris* on each polymer-modified surface. The number of cells attached to the electrode surface was fairly similar among PAPBA, P2ABA,

P3AP, P2PDA and P3PDA. The cell density on PAPBA electrodes was about twice that of P4ABA, PAHSA, PAMSA and PANI. However, this difference in cell density would not explain by itself the huge difference in photocurrent generation. Hence, the differences in photocurrent generation of *C. vulgaris* among polymers might be due to their intrinsic properties (i.e., interactions with the cell surface and electronic wiring capacity) rather than the number of cells attached on each electrode surface.

### 3.4. Conclusion

Substituted anilines containing electron withdrawing and electron donating groups were polymerized on the surface of electrodes modified with oxidized carbon nanotubes. The resulting polymers were characterized by electrochemical (CVs) and spectroscopic techniques (XPS and UPS). Results indicate that the polymerization yields polymers with different structures depending on the position and electronic properties of the substituent in the aniline ring. Furthermore, polymer modified electrodes were used as platforms to construct a *C. vulgaris*-based biophotoelectrodes. Photoelectrochemical experiments with the prepared biophotoelectrodes indicate that polymers containing electron withdrawing groups facilitated the electronic communication between algae and electrode. Conversely, the photoresponse of polymers containing electron donating groups was due to the polymer photoactivity rather than from a cell-to-electrode electron transfer process. Among all the polymers examined in the present Chapter, poly(3-aminophenyl boronic acid) outperformed the photocurrent generation of *C. vulgaris*. The results presented here

provide strong evidences that boronic acid containing molecules are interesting materials to modified surfaces to improve the electronic communication between biological entities and conducting surfaces.

## References

- [1] M. Anam, H.I. Gomes, G. Rivers, R.L. Gomes, R. Wildman, Evaluation of photoanode materials used in biophotovoltaic systems for renewable energy generation, *Sustain. Energy Fuels*. 5 (2021) 4209–4232. <https://doi.org/10.1039/d1se00396h>.
- [2] K. Namsheer, C.S. Rout, Conducting polymers: a comprehensive review on recent advances in synthesis, properties and applications, *RSC Adv*. 11 (2021) 5659–5697. <https://doi.org/10.1039/D0RA07800J>.
- [3] M. Jaiswal, R. Menon, Polymer electronic materials: a review of charge transport, *Polym. Int*. 55 (2006) 1371–1384. <https://doi.org/10.1002/pi.2111>.
- [4] Q. Zhu, J. Hu, B. Liu, S. Hu, S. Liang, K. Xiao, J. Yang, H. Hou, Recent advances on the development of functional materials in microbial fuel cells: from fundamentals to challenges and outlooks, *Energy Environ. Mater*. 5 (2021) 401–426. <https://doi.org/10.1002/eem2.12173>.
- [5] Y. Hindatu, M.S.M. Annuar, A.M. Gumel, Mini-review: Anode modification for improved performance of microbial fuel cell, *Renew. Sustain. Energy Rev*. 73 (2017) 236–248. <https://doi.org/10.1016/j.rser.2017.01.138>.
- [6] R. Kandpal, M. Shahadat, S.W. Ali, S.Z. Ahmmad, Alternating current based electrochemically polymerized polyaniline modified flexible conducting paper as an exoelectrogenic biofilm platform for a microbial fuel cell, *J. Water Process Eng*. 46 (2022) 102459. <https://doi.org/10.1016/j.jwpe.2021.102459>.
- [7] H. Xu, Y. Du, Y. Chen, Q. Wen, C. Lin, J. Zheng, Z. Qiu, Electricity generation in simulated benthic microbial fuel cell with conductive polyaniline-polypyrrole composite hydrogel anode, *Renew. Energy*. 183 (2022) 242–250. <https://doi.org/10.1016/j.renene.2021.10.098>.
- [8] Y.-C. Yong, X.-C. Dong, M.B. Chan-Park, H. Song, P. Chen, Macroporous and monolithic anode based on polyaniline hybridized three-dimensional graphene for high-performance

- microbial fuel cells, *ACS Nano*. 6 (2012) 2394–2400. <https://doi.org/10.1021/nn204656d>.
- [9] C. Zhao, P. Gai, C. Liu, X. Wang, H. Xu, J. Zhang, J. Zhu, Polyaniline networks grown on graphene nanoribbons-coated carbon paper with a synergistic effect for high-performance microbial fuel cells, *J. Mater. Chem. A*. 1 (2013) 12587–12594. <https://doi.org/10.1039/c3ta12947k>.
- [10] L. Zou, Y. Qiao, C. Zhong, C. Ming Li, Enabling fast electron transfer through both bacterial outer-membrane redox centers and endogenous electron mediators by polyaniline hybridized large-mesoporous carbon anode for high-performance microbial fuel cells, *Electrochim. Acta*. 229 (2017) 31–38. <https://doi.org/10.1016/j.electacta.2017.01.081>.
- [11] P. Bombelli, M. Zarrouati, R.J. Thorne, K. Schneider, S.J.L. Rowden, A. Ali, K. Yunus, P.J. Cameron, A.C. Fisher, D. Ian Wilson, C.J. Howe, A.J. McCormick, Surface morphology and surface energy of anode materials influence power outputs in a multi-channel mediatorless bio-photovoltaic (BPV) system, *Phys. Chem. Chem. Phys.* 14 (2012) 12221. <https://doi.org/10.1039/c2cp42526b>.
- [12] W.W. Focke, G.E. Wnek, Y. Wei, Influence of oxidation state, pH, and counterion on the conductivity of polyaniline, *J. Phys. Chem.* 91 (1987) 173. <https://doi.org/https://doi.org/10.1021/j100306a059>.
- [13] A.A. Karyakin, A.K. Strakhova, A.K. Yatsimirsky, Self-doped polyanilines electrochemically active in neutral and basic aqueous solutions., *J. Electroanal. Chem.* 371 (1994) 259–265. [https://doi.org/10.1016/0022-0728\(93\)03244-J](https://doi.org/10.1016/0022-0728(93)03244-J).
- [14] C.M. Brett, C. Thiemann, Conducting polymers from aminobenzoic acids and aminobenzenesulphonic acids: influence of pH on electrochemical behaviour, *J. Electroanal. Chem.* 538–539 (2002) 215–222. [https://doi.org/10.1016/S0022-0728\(02\)01215-9](https://doi.org/10.1016/S0022-0728(02)01215-9).
- [15] B.A. Deore, S. Hachey, M.S. Freund, Electroactivity of electrochemically synthesized poly(aniline boronic acid) as a function of pH: role of self-doping, *Chem. Mater.* 16 (2004) 1427–1432. <https://doi.org/10.1021/cm035296x>.

- [16] M. Şenel, C. Nergiz, M. Dervisevic, E. Çevik, Development of amperometric glucose biosensor based on reconstitution of glucose on polymeric 3-aminophenyl boronic acid monolayer, *Electroanalysis*. 25 (2013) 1194–1200. <https://doi.org/10.1002/elan.201200535>.
- [17] X. Wang, N. Xia, L. Liu, Boronic acid-based approach for separation and immobilization of glycoproteins and its application in sensing, *Int. J. Mol. Sci.* 14 (2013) 20890–20912. <https://doi.org/10.3390/ijms141020890>.
- [18] A. Stephenson-Brown, S. Yong, M.H. Mansor, Z. Hussein, N.-C. Yip, P.M. Mendes, J.S. Fossey, F.J. Rawson, Electronic communication of cells with a surface mediated by boronic acid saccharide interactions, *Chem. Commun.* 51 (2015) 17213–17216. <https://doi.org/10.1039/C5CC04311E>.
- [19] Q.-W. Zhang, J. Ouyang, Y. Wang, T.-T. Zhai, C. Wang, Z.-Q. Wu, T.-Q. Zhang, K. Wang, X.-H. Xia, Specific cell capture and noninvasive release via moderate electrochemical oxidation of boronic ester linkage, *Biosens. Bioelectron.* 138 (2019) 111316. <https://doi.org/10.1016/j.bios.2019.111316>.
- [20] X. Zhao, W. Deng, Y. Tan, Q. Xie, Promoting electricity generation of *Shewanella putrefaciens* in a microbial fuel cell by modification of porous poly(3-aminophenylboronic acid) film on carbon anode, *Electrochim. Acta.* 354 (2020) 136715. <https://doi.org/10.1016/j.electacta.2020.136715>.
- [21] L. Lapinsonnière, M. Picot, C. Poriel, F. Barrière, Phenylboronic acid modified anodes promote faster biofilm adhesion and increase microbial fuel cell performances., *Electroanalysis*. 25 (2013) 601–605. <https://doi.org/10.1002/elan.201200351>.
- [22] J. Pruvost, G. Van Vooren, G. Cogne, J. Legrand, Investigation of biomass and lipids production with *Neochloris oleoabundans* in photobioreactor, *Bioresour. Technol.* 100 (2009) 5988–5995. <https://doi.org/10.1016/j.biortech.2009.06.004>.
- [23] F. Masdarolomoor, P.C. Innis, S. Ashraf, G.G. Wallace, Purification and characterisation of poly(2-methoxyaniline-5-sulfonic acid), *Synth. Met.* 153 (2005) 181–184.

<https://doi.org/10.1016/j.synthmet.2005.07.249>.

- [24] F. Masdarolomoor, P.C. Innis, G.G. Wallace, Electrochemical synthesis and characterisation of polyaniline/ poly(2-methoxyaniline-5-sulfonic acid) composites, *Electrochim. Acta.* 53 (2008) 4146–4155. <https://doi.org/10.1016/j.electacta.2007.12.055>.
- [25] A.J. Bard, L.R. Faulkner, *Electrochemical methods: fundamentals and applications*, 2nd ed., John Wiley & Sons, Inc., 2002.
- [26] G.E. Wnek, A proposal for the mechanism of conduction in polyaniline, *Synth. Met.* 15 (1986) 213–218. [https://doi.org/https://doi.org/10.1016/0379-6779\(86\)90026-3](https://doi.org/https://doi.org/10.1016/0379-6779(86)90026-3).
- [27] D.R. Baer, K. Artyushkova, C.R. Brundle, J.E. Castle, M.H. Engelhard, K.J. Gaskell, J.T. Grant, R.T. Haasch, M.R. Linford, C.J. Powell, A.G. Shard, P.M.A. Sherwood, V.S. Smentkowski, Practical guides for x-ray photoelectron spectroscopy: First steps in planning, conducting, and reporting XPS measurements, *J. Vac. Sci. Technol. A Vacuum, Surfaces, Film.* 37 (2019) 031401. <https://doi.org/10.1116/1.5065501>.
- [28] C.D. Easton, C. Kinnear, S.L. McArthur, T.R. Gengenbach, Practical guides for x-ray photoelectron spectroscopy: Analysis of polymers, *J. Vac. Sci. Technol. A.* 38 (2020) 023207. <https://doi.org/10.1116/1.5140587>.
- [29] A.G. Shard, Practical guides for x-ray photoelectron spectroscopy: Quantitative XPS, *J. Vac. Sci. Technol. A Vacuum, Surfaces, Film.* 38 (2020) 041201. <https://doi.org/10.1116/1.5141395>.
- [30] Y. Kodama, Time gating of chloroplast autofluorescence allows clearer fluorescence imaging in planta, *PLoS One.* 11 (2016) e0152484. <https://doi.org/10.1371/journal.pone.0152484>.
- [31] E. Kapaun, W. Reisser, A chitin-like glycan in the cell wall of a *Chlorella* sp. (Chlorococcales, Chlorophyceae), *Planta.* 197 (1995) 577–582. <https://doi.org/10.1007/BF00191563>.

- [32] B. Pan, B. Xing, Adsorption Mechanisms of Organic Chemicals on Carbon Nanotubes, *Environ. Sci. Technol.* 42 (2008) 9005–9013. <https://doi.org/10.1021/es801777n>.
- [33] J. Yue, A.J. Epstein, A.G. Macdiarmid, Sulfonic Acid Ring-Substituted Polyaniline, A Self-Doped Conducting Polymer, *Mol. Cryst. Liq. Cryst. Inc. Nonlinear Opt.* 189 (1990) 255–261. <https://doi.org/10.1080/00268949008037237>.
- [34] Y. Wei, W.W. Focke, G.E. Wnek, A. Ray, A.G. MacDiarmid, Synthesis and electrochemistry of alkyl ring-substituted polyanilines, *J. Phys. Chem.* 93 (1989) 495–499. <https://doi.org/10.1021/j100338a095>.
- [35] S. Cattarin, L. Doubova, G. Mengoli, G. Zotti, Electrosynthesis and properties of ring-substituted polyanilines, *Electrochim. Acta.* 33 (1988) 1077–1084. [https://doi.org/10.1016/0013-4686\(88\)80198-1](https://doi.org/10.1016/0013-4686(88)80198-1).
- [36] W.-S. Huang, B.D. Humphrey, A.G. MacDiarmid, Polyaniline, a novel conducting polymer. Morphology and chemistry of its oxidation and reduction in aqueous electrolytes, *J. Chem. Soc. Faraday Trans. 1 Phys. Chem. Condens. Phases.* 82 (1986) 2385. <https://doi.org/10.1039/f19868202385>.
- [37] V.N. Nikitina, I.R. Kochetkov, E.E. Karyakina, A.K. Yatsimirsky, A.A. Karyakin, Tuning electropolymerization of boronate-substituted anilines: Fluoride-free synthesis of the advanced affinity transducer, *Electrochem. Commun.* 51 (2015) 121–124. <https://doi.org/10.1016/j.elecom.2014.12.021>.
- [38] G. Berionni, V. Morozova, M. Heininger, P. Mayer, P. Knochel, H. Mayr, Electrophilic aromatic substitutions of aryltrifluoroborates with retention of the  $\text{BF}_3^-$  group: Quantification of the activating and directing effects of the trifluoroborate group, *J. Am. Chem. Soc.* 135 (2013) 6317–6324. <https://doi.org/10.1021/ja4017655>.
- [39] M. Nicolas, B. Fabre, G. Marchand, J. Simonet, New Boronic-Acid- and Boronate-Substituted Aromatic Compounds as Precursors of Fluoride-Responsive Conjugated Polymer Films, *European J. Org. Chem.* 2000 (2000) 1703–1710.



[https://doi.org/10.1002/\(SICI\)1099-0690\(200005\)2000:9<1703::AID-EJOC1703>3.0.CO;2-S](https://doi.org/10.1002/(SICI)1099-0690(200005)2000:9<1703::AID-EJOC1703>3.0.CO;2-S).

- [40] A.N. Andriianova, Y.N. Biglova, A.G. Mustafin, Effect of structural factors on the physicochemical properties of functionalized polyanilines, *RSC Adv.* 10 (2020) 7468–7491. <https://doi.org/10.1039/c9ra08644g>.
- [41] B.A. Deore, I. Yu, M.S. Freund, A switchable self-doped polyaniline: Interconversion between self-doped and non-self-doped forms, *J. Am. Chem. Soc.* 126 (2004) 52–53. <https://doi.org/10.1021/ja038499v>.
- [42] K. Chiba, T. Ohsaka, N. Oyama, Electrode kinetics of electroactive electropolymerized polymers deposited on graphite electrode surfaces, *J. Electroanal. Chem. Interfacial Electrochem.* 217 (1987) 239–251. [https://doi.org/10.1016/0022-0728\(87\)80221-8](https://doi.org/10.1016/0022-0728(87)80221-8).
- [43] S. Samanta, P. Roy, P. Kar, Synthesis of poly(o-phenylenediamine) nanofiber with novel structure and properties, *Polym. Adv. Technol.* 28 (2017) 797–804. <https://doi.org/10.1002/pat.3981>.
- [44] S. Samanta, P. Roy, P. Kar, Structure and properties of conducting poly(o-phenylenediamine) synthesized in different inorganic acid medium, *Macromol. Res.* 24 (2016) 342–349. <https://doi.org/10.1007/s13233-016-4054-0>.
- [45] A.K. Behera, B. Adhikari, P. Kar, Synthesis of processable conducting poly(m-aminophenol) having structure like keto derivative of polyaniline, *Polym. Sci. Ser. B.* 57 (2015) 159–166. <https://doi.org/10.1134/S1560090415020025>.
- [46] K. Martinusz, E. Cziráok, G. Inzelt, Studies of the formation and redox transformation of poly(o-phenylenediamine) films using a quartz crystal microbalance, *J. Electroanal. Chem.* 379 (1994) 437–444. [https://doi.org/10.1016/0022-0728\(94\)87168-X](https://doi.org/10.1016/0022-0728(94)87168-X).
- [47] K. Chiba, T. Ohsaka, Y. Ohnuki, N. Oyama, Electrochemical preparation of a ladder polymer containing phenazine rings, *J. Electroanal. Chem. Interfacial Electrochem.* 219 (1987) 117–124. [https://doi.org/10.1016/0022-0728\(87\)85034-9](https://doi.org/10.1016/0022-0728(87)85034-9).

- 
- [48] O. Haas, J. Rudnicki, F.R. McLarnon, E.J. Cairns, Mechanistic investigations of redox polymer-coated electrodes using probe-beam deflection and cyclic voltammetry, *J. Chem. Soc. Faraday Trans.* 87 (1991) 939. <https://doi.org/10.1039/ft9918700939>.
- [49] A.J. Bandothkar, V.W.S. Hung, W. Jia, G. Valdés-Ramírez, J.R. Windmiller, A.G. Martinez, J. Ramírez, G. Chan, K. Kerman, J. Wang, Tattoo-based potentiometric ion-selective sensors for epidermal pH monitoring, *Analyst*. 138 (2013) 123–128. <https://doi.org/10.1039/c2an36422k>.
- [50] X. Zhang, B. Ogorevc, J. Wang, Solid-state pH nanoelectrode based on polyaniline thin film electrodeposited onto ion-beam etched carbon fiber, *Anal. Chim. Acta*. 452 (2002) 1–10. [https://doi.org/10.1016/S0003-2670\(01\)01435-0](https://doi.org/10.1016/S0003-2670(01)01435-0).
- [51] G.D. Sulka, K. Hnida, A. Brzózka, pH sensors based on polypyrrole nanowire arrays, *Electrochim. Acta*. 104 (2013) 536–541. <https://doi.org/10.1016/j.electacta.2012.12.064>.
- [52] T. Guinovart, G. Valdés-Ramírez, J.R. Windmiller, F.J. Andrade, J. Wang, Bandage-based wearable potentiometric sensor for monitoring wound pH, *Electroanalysis*. 26 (2014) 1345–1353. <https://doi.org/10.1002/elan.201300558>.
- [53] E.T. Kang, K.G. Neoh, K.L. Tan, Polyaniline: A polymer with many interesting intrinsic redox states, *Prog. Polym. Sci.* 23 (1998) 277–324. [https://doi.org/10.1016/S0079-6700\(97\)00030-0](https://doi.org/10.1016/S0079-6700(97)00030-0).
- [54] E.T. Kang, K.G. Neoh, K.L. Tan, Protonation and deprotonation of polyaniline films and powders revisited, *Synth. Met.* 68 (1995) 141–144. [https://doi.org/10.1016/0379-6779\(94\)02279-8](https://doi.org/10.1016/0379-6779(94)02279-8).
- [55] S. Golczak, A. Kancierzewska, M. Fahlman, K. Langer, J.J. Langer, Comparative XPS surface study of polyaniline thin films, *Solid State Ionics*. 179 (2008) 2234–2239. <https://doi.org/10.1016/j.ssi.2008.08.004>.
- [56] G.H. Major, V. Fernandez, N. Fairley, M.R. Linford, A detailed view of the Gaussian–Lorentzian sum and product functions and their comparison with the Voigt function, *Surf.*

- 
- Interface Anal. 54 (2022) 262–269.  
<https://doi.org/10.1002/sia.7050>.
- [57] G.H. Major, T.G. Avval, D.I. Patel, D. Shah, T. Roychowdhury, A.J. Barlow, P.J. Pigram, M. Greiner, V. Fernandez, A. Herrera-Gomez, M.R. Linford, A discussion of approaches for fitting asymmetric signals in X-ray photoelectron spectroscopy (XPS), noting the importance of Voigt-like peak shapes, *Surf. Interface Anal.* 53 (2021) 689–707. <https://doi.org/10.1002/sia.6958>.
- [58] NIST X-ray Photoelectron Spectroscopy (XPS) Database, (n.d.). <https://doi.org/10.18434/T4T88K>.
- [59] D. Beamson, G. Briggs, *High resolution XPS of organic polymers: The Scienta ESCA300 database*, 1st ed., John Wiley and Sons, New York, 1992.
- [60] H.R. Tantawy, B.F. Kengne, D.N. McIlroy, T. Nguyen, D. Heo, Y. Qiang, D.E. Aston, X-ray photoelectron spectroscopy analysis for the chemical impact of solvent addition rate on electromagnetic shielding effectiveness of HCl-doped polyaniline nanopowders, *J. Appl. Phys.* 118 (2015) 175501. <https://doi.org/10.1063/1.4934851>.
- [61] H. Sariarslan, E. Karaca, M. Şahin, N.Ö. Pekmez, Electrochemical synthesis and corrosion protection of poly(3-aminophenylboronic acid-co-pyrrole) on mild steel, *RSC Adv.* 10 (2020) 38548–38560. <https://doi.org/10.1039/D0RA07311C>.
- [62] J. Yue, A.J. Epstein, XPS study of self-doped conducting polyaniline and parent systems, *Macromolecules.* 24 (1991) 4441–4445. <https://doi.org/10.1021/ma00015a030>.
- [63] P. Snauwaert, R. Lazzaroni, J. Riga, J.J. Verbist, Electronic structure of polyanilines: An XPS study of electrochemically prepared compounds, *Synth. Met.* 16 (1986) 245–255. [https://doi.org/10.1016/0379-6779\(86\)90117-7](https://doi.org/10.1016/0379-6779(86)90117-7).
- [64] H.S.O. Chan, S.C. Ng, W.S. Sim, K.L. Tan, B.T.G. Tan, Preparation and characterization of electrically conducting copolymers of aniline and anthranilic acid: evidence for self-doping by X-ray photoelectron spectroscopy,

- Macromolecules. 25 (1992) 6029–6034.  
<https://doi.org/10.1021/ma00048a026>.
- [65] D.T. Clark, D.B. Adams, A. Dilks, J. Peeling, H.R. Thomas, Some aspects of shake-up phenomena in some simple polymer systems, *J. Electron Spectros. Relat. Phenomena*. 8 (1976) 51–60. [https://doi.org/10.1016/0368-2048\(76\)80006-0](https://doi.org/10.1016/0368-2048(76)80006-0).
- [66] D.N. Hendrickson, J.M. Hollander, W.L. Jolly, Core-electron binding energies for compounds of boron, carbon, and chromium, *Inorg. Chem.* 9 (1970) 612–615. <https://doi.org/10.1021/ic50085a035>.
- [67] D. Barriet, C.M. Yam, O.E. Shmakova, A.C. Jamison, T.R. Lee, 4-Mercaptophenylboronic Acid SAMs on Gold: Comparison with SAMs Derived from Thiophenol, 4-Mercaptophenol, and 4-Mercaptobenzoic Acid, *Langmuir*. 23 (2007) 8866–8875. <https://doi.org/10.1021/la7007733>.
- [68] G.H. Major, N. Fairley, P.M.A. Sherwood, M.R. Linford, J. Terry, V. Fernandez, K. Artyushkova, Practical guide for curve fitting in x-ray photoelectron spectroscopy, *J. Vac. Sci. Technol. A*. 38 (2020) 061203. <https://doi.org/10.1116/6.0000377>.
- [69] B.. Lindberg, K. Hamrin, G. Johansson, U. Gelius, A. Fahlman, C. Nordling, K. Siegbahn, Molecular spectroscopy by means of ESCA, *Phys. Scr.* 1 (1970) 286–298. <https://doi.org/10.1088/0031-8949/1/5-6/020>.
- [70] H. Harker, P.M.A. Sherwood, X-ray photoelectron studies of sulphur in carbon, *Philos. Mag. A J. Theor. Exp. Appl. Phys.* 27 (1972) 1241–1244. <https://doi.org/10.1080/14786437308225832>.
- [71] Z. Lv, Q. Zhong, Z. Zhao, Y. Bu, Facile synthesis of hierarchical nickel–cobalt sulfide quadrangular microtubes and its application in hybrid supercapacitors, *J. Mater. Sci. Mater. Electron.* 28 (2017) 18064–18074. <https://doi.org/10.1007/s10854-017-7750-4>.
- [72] D. Escalera-López, Y. Niu, S.J. Park, M. Isaacs, K. Wilson, R.E. Palmer, N. V. Rees, Hydrogen evolution enhancement of ultra-low loading, size-selected molybdenum sulfide

- nanoclusters by sulfur enrichment, *Appl. Catal. B Environ.* 235 (2018) 84–91. <https://doi.org/10.1016/j.apcatb.2018.04.068>.
- [73] A.A. Audi, P.M.A. Sherwood, X-ray photoelectron spectroscopic studies of sulfates and bisulfates interpreted by  $X\alpha$  and band structure calculations, *Surf. Interface Anal.* 29 (2000) 265–275. [https://doi.org/10.1002/\(SICI\)1096-9918\(200004\)29:4<265::AID-SIA739>3.0.CO;2-3](https://doi.org/10.1002/(SICI)1096-9918(200004)29:4<265::AID-SIA739>3.0.CO;2-3).
- [74] Y. Chen, E.T. Kang, K.G. Neoh, S.L. Lim, Z.H. Ma, K.L. Tan, Intrinsic redox states of polyaniline studied by high-resolution X-ray photoelectron spectroscopy, *Colloid Polym. Sci.* 279 (2001) 73–76. <https://doi.org/10.1007/s003960000418>.
- [75] E.T. Kang, K.G. Neoh, K.L. Tan, X-ray photoelectron spectroscopic studies of electroactive polymers, in: *Polym. Charact.*, Springer-Verlag, Berlin/Heidelberg, 1993: pp. 135–190. <https://doi.org/10.1007/BFb0025863>.
- [76] X.-R. Zeng, T.-M. Ko, Structures and properties of chemically reduced polyanilines, *Polymer.* 39 (1998) 1187–1195. [https://doi.org/10.1016/S0032-3861\(97\)00381-9](https://doi.org/10.1016/S0032-3861(97)00381-9).
- [77] A.P. Monkman, G.C. Stevens, D. Bloor, X-ray photoelectron spectroscopic investigations of the chain structure and doping mechanisms in polyaniline, *J. Phys. D. Appl. Phys.* 24 (1991) 738. <https://doi.org/10.1088/0022-3727/24/5/017>.
- [78] K.L. Tan, B.T.G. Tan, E.T. Kang, K.G. Neoh, X-ray photoelectron spectroscopy studies of the chemical structure of polyaniline, *Phys. Rev. B.* 39 (1989) 8070–8073. <https://doi.org/10.1103/PhysRevB.39.8070>.
- [79] H.R. Tantawy, B.A.F. Kengne, D.N. McIlroy, T. Nguyen, D. Heo, Y. Qiang, D.E. Aston, X-ray photoelectron spectroscopy analysis for the chemical impact of solvent addition rate on electromagnetic shielding effectiveness of HCl-doped polyaniline nanopowders, *J. Appl. Phys.* 118 (2015) 175501. <https://doi.org/10.1063/1.4934851>.
- [80] B. Sjögren, W.R. Salaneck, S. Stafström, Core X-ray photoelectron shake-up states of model molecules for polyaniline, *J. Chem. Phys.* 97 (1998) 137.

<https://doi.org/10.1063/1.463612>.

- [81] S. Wen, G. Huang, S. Wu, J. Li, A. Qu, Determinant factors of photocatalytic hydrogen evolution activity for Schiff-base conjugated polymers, *Chem. Eng. J.* 374 (2019) 1055–1063. <https://doi.org/10.1016/j.cej.2019.06.003>.
- [82] X.-L. Wei, M. Fahlman, A.J. Epstein, XPS Study of Highly Sulfonated Polyaniline, *Macromolecules.* 32 (1999) 3114–3117. <https://doi.org/10.1021/ma981386p>.
- [83] T. Nakajima, M. Harada, R. Osawa, T. Kawagoe, Y. Furukawa, I. Harada, Study on the interconversion of unit structures in polyaniline by x-ray photoelectron spectroscopy, *Macromolecules.* 22 (1989) 2644–2648. <https://doi.org/10.1021/ma00196a018>.
- [84] Y. Xu, M.A.A. Schoonen, The absolute energy positions of conduction and valence bands of selected semiconducting minerals, *Am. Mineral.* 85 (2000) 543–556. <https://doi.org/10.2138/am-2000-0416>.
- [85] F.-L. Ng, S.-M. Phang, V. Periasamy, K. Yunus, A.C. Fisher, Enhancement of power output by using alginate immobilized algae in biophotovoltaic devices, *Sci. Rep.* 7 (2017) 16237. <https://doi.org/10.1038/s41598-017-16530-y>.
- [86] C. Thong, S. Phang, F. Ng, V. Periasamy, T. Ling, K. Yunus, A.C. Fisher, Effect of different irradiance levels on bioelectricity generation from algal biophotovoltaic (BPV) devices, *Energy Sci. Eng.* 7 (2019) 2086–2097. <https://doi.org/10.1002/ese3.414>.
- [87] Z. Herrero-Medina, P. Wang, A. Lielpetere, A.S. Bashammakh, A.O. Alyoubi, I. Katakis, F. Conzuelo, W. Schuhmann, A biophotoelectrode based on boronic acid-modified *Chlorella vulgaris* cells integrated within a redox polymer, *Bioelectrochemistry.* 146 (2022) 108128. <https://doi.org/10.1016/j.bioelechem.2022.108128>.
- [88] B.A. Deore, M.S. Freund, Self-doped polyaniline nanoparticle dispersions based on boronic acid-phosphate complexation, *Macromolecules.* 42 (2009) 164–168. <https://doi.org/10.1021/ma8020344>.

- [89] H. Liu, Y. Li, K. Sun, J. Fan, P. Zhang, J. Meng, S. Wang, L. Jiang, Dual-responsive surfaces modified with phenylboronic acid-containing polymer brush to reversibly capture and release cancer cells, *J. Am. Chem. Soc.* 135 (2013) 7603–7609. <https://doi.org/10.1021/ja401000m>.
- [90] B.A. Deore, M.D. Braun, M.S. Freund, pH dependent equilibria of poly(anilineboronic acid)-saccharide complexation in thin films, *Macromol. Chem. Phys.* 207 (2006) 660–664. <https://doi.org/10.1002/macp.200500560>.
- [91] T. Figueiredo, V. Cosenza, Y. Ogawa, I. Jeacomine, A. Vallet, S. Ortega, R. Michel, J.D.M. Olsson, T. Gerfaud, J.-G. Boiteau, J. Jing, C. Harris, R. Auzély-Velty, Boronic acid and diol-containing polymers: how to choose the correct couple to form “strong” hydrogels at physiological pH, *Soft Matter*. 16 (2020) 3628–3641. <https://doi.org/10.1039/D0SM00178C>.
- [92] E. Shoji, M.S. Freund, Potentiometric saccharide detection based on the pK<sub>a</sub> changes of poly(aniline boronic acid), *J. Am. Chem. Soc.* 124 (2002) 12486–12493. <https://doi.org/10.1021/JA0267371>
- [93] A. Matsumoto, N. Sato, K. Kataoka, Y. Miyahara, Noninvasive sialic acid detection at cell membrane by using phenylboronic acid modified self-assembled monolayer gold electrode, *J. Am. Chem. Soc.* 131 (2009) 12022–12023. <https://doi.org/10.1021/ja902964m>.

## Chapter 4

### **A biophotocathode based on boronic acid-modified *Chlorella vulgaris* cells integrated within a redox polymer<sup>1</sup>**

#### **4.1. Introduction**

One of the most important factors limiting the performance of microorganism-based BPVs is the cell-to-electrode electron transfer. Ideally, more environmentally friendly, cost-effective and long-lasting BPV devices could be achieved based on DEET [1,2] between cells and the electrode. However, DEET remains elusive for a great majority of microorganisms. Thus, the use of electron mediators that boost the ET kinetics has become necessary [3]. Among these, surface-confined redox mediators such as P-Os have shown to be promising materials to electronically communicate with photosynthetic microorganisms [4–6]. P-Os forms a 3D-hydrogel that can integrate the microorganisms, facilitating their immobilization and the electron transfer to the electrode by electron hopping between adjacent Os-complexes [7,8]. Higher and faster ET rates can be achieved if stronger interactions that direct the redox centres to be in proximity with phototrophs immobilized within the hydrogel matrix can be attained.

---

<sup>1</sup> Part of his chapter was published in Z. Herrero-Medina et al., *Bioelectrochemistry*. 146 (2022) 108128



In this chapter, we report an improved electronic communication between an Os-complex modified redox polymer and boronic acid modified *C. vulgaris* cells. 3-APBA is incorporated to increase the intimate contact between the redox polymer and the immobilized cells, thus improving the integration of *C. vulgaris* with the polymer redox centers and enhancing the stability of the resulting biofilm. Furthermore, as a proof of concept, the proposed bioanode is coupled to a bilirubin oxidase biocathode to build a BPV cell.

## **4.2. Materials and methods**

### **4.2.1. Algal culture:**

The *C. vulgaris* strain 211-11b was purchased from Sammlung von Algenkulturen der Universität Göttingen (SAG). Cultures were grown in 100 mL of BBM [9] in 250 mL Corning polycarbonate Erlenmeyer flasks (Fisher Scientific) at  $(20 \pm 2)$  °C and 150 rpm with an irradiance of  $\approx 50 \mu\text{mol photons m}^{-2} \text{ s}^{-1}$  on a 12:12 h light:dark regime.

### **4.2.2. Anode modification:**

When cultures reached the exponential phase, they were centrifuged at 4 °C and 4000 rpm for 10 min, washed in 0.1 M PB pH 7, centrifuged again and concentrated in a fresh solution of 2 mg mL<sup>-1</sup> 3-APBA in 0.1 M PB pH 7 until an OD<sub>680</sub> of 5 was achieved. The resuspended culture with 3-APBA was kept under agitation at 200 rpm for 2 h at RT. Afterwards, it was ultra-filtrated with Vivaspin 500, 10000 MWCO (Sartorius) tubes to remove the loosely bound 3-APBA and resuspended in 0.1 M PB pH 7 to a final OD<sub>680</sub> of 10. Prior to modification, gold disk electrodes of 2 mm Ø (CH Instru-

ments) were polished with diamond slurries of 0.1  $\mu\text{m}$  (LECO) and subsequently ultrasonicated in ethanol and deionized water for 5 min. Afterwards, the electrodes were electrochemically cleaned in 0.5 M  $\text{H}_2\text{SO}_4$  for 10 cycles at 0.1  $\text{V s}^{-1}$  from -0.2 V to 1.6 V vs. Ag/AgCl/3 M KCl. Au-coated wafers prepared as reported in [10] were cleaned with Piranha solution and rinsed with deionized water prior to modification. Afterwards, 3  $\mu\text{L}$  of a freshly prepared solution consisting of 1.7  $\text{mg mL}^{-1}$  of the redox polymer poly(1-vinylimidazole-*co*-allylamine)-[Os(bpy) $_2$ Cl]Cl (P-Os G43, synthesized as described in [11]), 0.033  $\text{mg mL}^{-1}$  of poly(ethylene glycol) diglycidyl ether (PEGDGE,  $\text{Mn} = 400 \text{ g mol}^{-1}$ , Polysciences), and 6.25 OD  $\text{mL}^{-1}$  of *C. vulgaris* were drop-cast on the electrode and desiccated for 3 h at 21  $^\circ\text{C}$  and 10% relative humidity (RH). Next, the hydrogel was collapsed by dipping the electrode for 30 min in Tris-HCl buffer (AppliChem) pH 9 containing 10 mM  $\text{CaCl}_2$ , 10 mM  $\text{MgCl}_2$  and 100 mM KCl, and was left to dry.

#### 4.2.3. Electrochemical analysis of the anode:

All electrochemical measurements were performed in a three-electrode electrochemical cell with the modified gold electrode, Pt wire and Ag/AgCl/3 M KCl as the working, counter, and reference electrodes, respectively. All potentials are referred vs. Ag/AgCl/3 M KCl. To assess the anode performance, CVs at a scan rate of 10  $\text{mV s}^{-1}$  and CAs were performed using a PalmSens2 potentiostat (PalmSens) in 0.1 M PB, pH 7 and at an irradiation of 50  $\text{mW cm}^{-2}$  of white light supplied by a He-Xe lamp (LC8 type 03, Hamamatsu photonics). The applied potential for the CA was 350 mV, which

ensures the oxidation of the P-Os G43, allowing the collection of electrons coming from the immobilized cells.

To evaluate the action spectrum, the modified Au-electrodes with and without *C. vulgaris* cells were polarized to 350 mV with an Autolab PGSTAT302N (Metrohm Autolab) under irradiation cycles of 20 s. Each irradiation cycle was performed at different wavelengths ranging from 297 nm to 797 nm selected by a monochromator setup (Instytut Fotonowy) placed immediately in front of a 150 W Xe lamp (Ushio) used as light source. The photocurrent at each wavelength was normalized to the photon flux at each wavelength.

#### **4.2.4. Chlorophyll *a* UV-Vis spectroscopy:**

Extraction of Chl *a* from *C. vulgaris* was performed following a method adapted from [12] under subdued light. Briefly, cultures were centrifuged at 4 °C and 5000 rpm for 10 min, washed with 0.1 M PB pH 7 and the pellet was resuspended in the same buffer. Then, pellets were lyophilized and resuspended in pure methanol (Sigma-Aldrich) (pretreated with magnesium carbonate to remove any acid) and kept at 4 °C for 4 h. Then 0.1 mm zirconia beads were added, and the cells were disrupted by means of a MiniBead Beater-8 (Biospec) for 1 min. Afterwards, the cultures were centrifuged, the pellet was discarded and the spectrum of the supernatant (Chl *a*) was measured from 350 nm to 800 nm in quartz cuvettes with an UV-Vis spectrophotometer Cary 100 Bio (Varian).

#### **4.2.5. DCMU and DCBQ experiments:**

Solutions of 10 mM of the photosynthetic inhibitor DCMU (Sigma-Aldrich) and 10 mM of the redox mediator 2,6-dichloro-1,4-benzo-

quinone (DCBQ, Sigma-Aldrich) dissolved in pure ethanol (Sigma-Aldrich) were prepared for being used at the final concentrations as further specified in the *Results and discussion* section.

#### **4.2.6. Scanning photoelectrochemical microscopy (SPECM):**

SPECM measurements were performed with the *C. vulgaris*-based bioanode as the sample interrogated by the SPECM tip. The electrochemical cell was filled with 0.1 M PB, pH 7, and the bioanode, a Pt mesh and a Ag/AgCl/ 3 M KCl were the working (sample electrode), the counter and reference electrodes, respectively. The tip was a Pt disk microelectrode (25  $\mu\text{m}$   $\varnothing$  Pt wire, Goodfellow). Full details of the SPECM setup are described elsewhere [13]. Local illumination of the sample with white light was attained by coupling the lamp with the top glass of the tip microelectrode by means of a light fiber (HITRONIC POF Simplex PE). Photochronoamperometry was performed with the tip microelectrode positioned at one tip radius distance above the sample surface. The sample was polarized to 350 mV and the tip microelectrode was poised to -600 mV for the reduction of O<sub>2</sub>.

#### **4.2.7. Preparation and characterization of the biocathode:**

Prior to modification, graphite electrodes of 3 mm  $\varnothing$  (SGL Carbon) were polished with sandpaper and then rinsed with deionized water. Then, the electrodes were modified by oxidation of 2-aminobenzoic acid (2-ABA) (Sigma-Aldrich) in 0.1 M KCl solution at 0.8 V for 60 s as described elsewhere [14]. Subsequently, the modified electrodes were rinsed with deionized water to remove loosely bound 2-ABA and shortly dried at RT. 20  $\mu\text{L}$  of a solution of 5 mg mL<sup>-1</sup> of

*Myrothecium verrucaria* bilirubin oxidase (*Mv*-BOD) (Sigma-Aldrich) in 0.1 M phosphate buffer saline (PBS) (Sigma-Aldrich) pH 7 were drop-cast on the electrode surface and allowed to dry at RT. Afterwards, the electrodes were washed with deionized water to remove loosely bound enzyme. *Mv*-BOD-modified electrodes were characterized by CV from 0.6 V to 0 V at a scan rate of 10 mV s<sup>-1</sup> in 0.1 M PBS pH 7 in both air and Ar atmosphere.

#### **4.2.8. Biophotovoltaic measurements:**

A single chamber BPV cell was constructed by coupling the *C. vulgaris*-modified photoanode with the *Mv*-BOD biocathode. The electrolyte solution was 0.1 M PB pH 7. The bioanode surface with an area of 0.636 cm<sup>2</sup> was exposed to white light with an incident power of  $\approx 200$  mW cm<sup>-2</sup>. Polarization and power curves were calculated by measuring the steady-state current in dark and light conditions at different applied cell voltages using a PGU-BI 100 potentiostat (IPS Jaissle).

### **4.3. Results and discussion**

#### **4.3.1. Preparation and characterization of *C. vulgaris*-based bioanode:**

*C. vulgaris*-based bioanodes were constructed by modifying a gold electrode surface with *C. vulgaris* cells embedded within a P-Os hydrogel matrix crosslinked with PEGDGE. Prior to the integration of the microalgae in the hydrogel, *C. vulgaris* cells were functionalized with 3-APBA, which covalently binds to 1,2 and 1,3 cis-diols of saccharides present in the cell wall, in order to improve the crosslinking between the P-Os and the cells. Although it is not

expected to be a quantitative reaction, the ring-opening of the epoxide by the substituted aniline without catalyst in water is expected [15–17] (Figure 4.1). In a similar way to previously reported enzyme and photosystem-modified bioelectrodes, the use of PEGDGE during electrode modification assists in the formation of a more stable film over the electrode as a highly cross-linked matrix can be obtained [11,18].

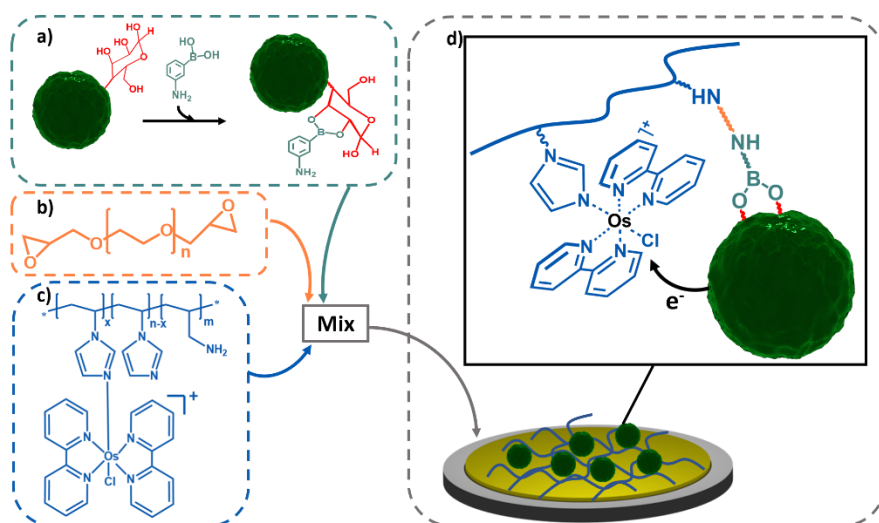


**Figure 4.1.** (a) Schematic of covalent binding of 3-APBA with polysaccharides on the cell wall of *Chlorella vulgaris* during the preincubation step. Chemical structures of (b) poly(ethylene glycol) diglycidyl ether (PEGDGE) and (c) poly(1-vinylimidazole-co-allylamine)-[Os(2,2'-bipyridine)<sub>2</sub>Cl]Cl (P-Os G43). (d) Schematic of the bioanode: gold electrode modified with *C. vulgaris* with covalently bound 3-APBA embedded within a P-Os hydrogel matrix crosslinked with PEGDGE. Inset: proposed crosslinking of amino groups of both P-Os and 3-APBA bound to cells.

The maximum photocurrent ( $(6.0 \pm 0.7) \mu\text{A cm}^{-2}$ ) was obtained for this bioanode during the first illumination cycle and it decayed to almost half after the fifth cycle of illumination (Figure 4.2a). To investigate the role of 3-APBA in enhancing the intimate contact and

thus contributing to an improved electronic communication between microalgae and the redox polymer, the photochronoamperometric performance of the *C. vulgaris*-based bioanode was compared with P-Os modified electrodes in the absence of *C. vulgaris*. After subtracting the photocurrent arising from photoexcitation of the redox polymer alone (Figure 4.2b), the average net photocurrent for *C. vulgaris* was  $(5 \pm 1) \mu\text{A cm}^{-2}$  (Figure 4.2c). This photocurrent is almost 10 times higher than that obtained in previous reports ( $0.64 \mu\text{A cm}^{-2}$ ) with *C. vulgaris* immobilized within an alginate matrix [20] and more than two times higher than the obtained with the approach described in Chapter 2 ( $2.0 \pm 0.6 \mu\text{A cm}^{-2}$ ), where *C. vulgaris* was immobilized on poly(3-aminophenylboronic acid)-modified electrodes. However, the normalized current to the incident light was greater with the PAPBA-modified biophotocathode ( $160 \pm 48 \mu\text{A } \mu\text{mol photons}^{-1} \text{ s}^{-1}$ ) than this approach with redox polymer hydrogel integrating cells functionalized with 3-APBA ( $21.4 \pm 4.3 \mu\text{A } \mu\text{mol photons}^{-1} \text{ s}^{-1}$ ).

In addition, control experiments were performed by fabricating biophotocathodes with a mixture of cells and 3-APBA but without a preincubation step and without 3-APBA (Figure 4.2a). In contrast to the optimized bioanode, lower photocurrents (about 33% lower) were obtained when the cells were directly mixed with P-Os and 3-APBA before drop-casting (i.e., without preincubation with 3-APBA). These lower photocurrents might be due to a shorter time for interaction preventing the formation of covalent bonds between the boronic acid moiety in 3-APBA and polysaccharides of the cell wall than in the situation when cells are preincubated with 3-APBA.

Moreover, when the cells were immobilized in the absence of boronic acid, the photocurrent response was also lower and less stable (see Table Appendix C.1).

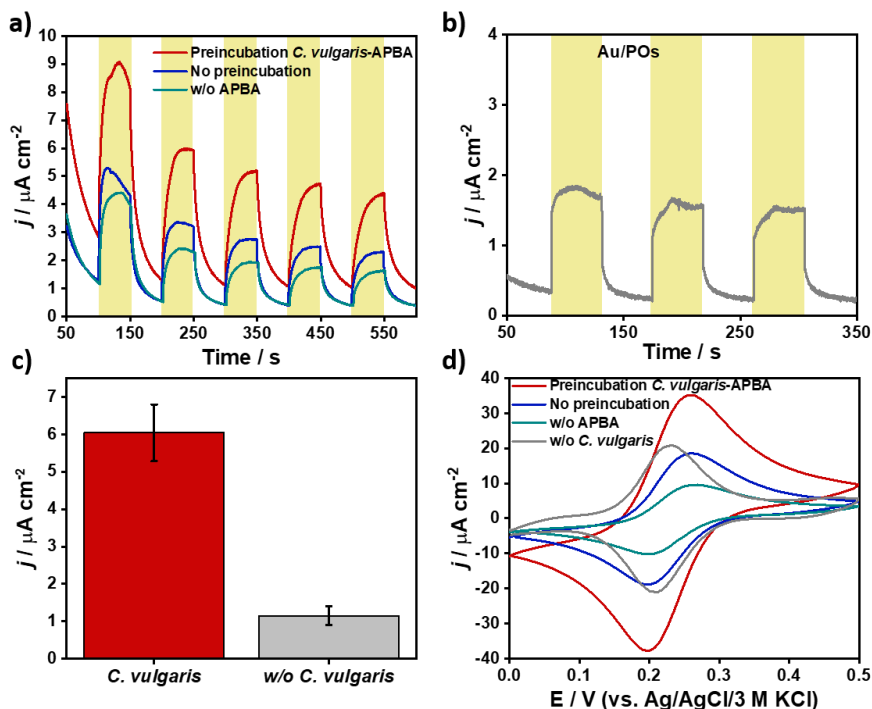


**Figure 4.2.** (a) CA of electrodes modified with P-Os integrating *Chlorella vulgaris* cells preincubated with 3-APBA (red line), P-Os with *C. vulgaris* and 3-APBA directly mixed without preincubation (blue line), and P-Os integrating *C. vulgaris* in the absence of 3-APBA (green line). (b) CA of P-Os modified electrode without *C. vulgaris* (grey line).  $E_{\text{app}} = 350 \text{ mV}$  vs.  $\text{Ag}/\text{AgCl}/3 \text{ M KCl}$ . Irradiation with  $50 \text{ mW cm}^{-2}$  incident white light (yellow shadows). (c) Comparison of the average responses for P-Os modified electrodes in the absence and presence of *C. vulgaris* ( $n = 3$ ). Error bars represent the standard deviation. (d) CV recorded for electrodes after CA as shown in (a) and (b). Scan rate:  $10 \text{ mV s}^{-1}$ . Electrolyte:  $0.1 \text{ M PB buffer}$ , pH 7.

CVs in dark conditions recorded after photochronoamperometry for electrodes integrating *C. vulgaris* within the redox hydrogel showed larger peak-to-peak separations for the redox peaks associated with the  $\text{Os}^{2+/3+}$  interconversion than those for electrodes without the



microalgae (see Fig. 4.2d and Table Appendix C.2). This indicated the successful incorporation of *C. vulgaris* into the hydrogel matrix, with the cells hampering to some extent the electron-transfer kinetics between the Os-centers within the polymer deposited over the electrode. In addition, higher anodic and cathodic peak currents were also obtained when the cells were preincubated with 3-APBA while the controls using cells without preincubation and without 3-APBA delivered similar or lower peak currents in comparison with P-Os alone (Table Appendix C.2). These results support our hypothesis that 3-APBA favours the covalent attachment of amino moieties of P-Os *via* PEGDGE crosslinking [21] to the amino groups of 3-APBA at the cell wall. Supposedly, this crosslinking is contributing to bringing the Os centers in close proximity to the cell wall of *C. vulgaris*, which facilitates the electron transfer from the microalgae via P-Os to the electrode causing increased photocurrent generation (Figure 4.2a and c).

#### **4.3.2. Study of the ET mechanism:**

To demonstrate that the origin of the photocurrent is due to the presence of *C. vulgaris* and that the Os complex-modified polymer is responsible for the electron transfer to the electrode, the action spectrum of the bioelectrode was assessed by polarizing the electrode at a constant potential while varying the wavelength at each illumination cycle in the wavelength range from 300 nm to 800 nm. As a control, an electrode with bovine serum albumin (BSA) replacing *C. vulgaris* was used (Figure Appendix C.1). BSA is a non-redox active protein able to stabilize the polymer matrix after

crosslinking and prevents hydrogel over-swelling leading to a more comparable electron transfer in contrast to electrodes based on P-Os alone [22,23]. Figure 4.3 shows that the action spectra profile of redox polymer-modified electrodes with and without *C. vulgaris* are substantially different.

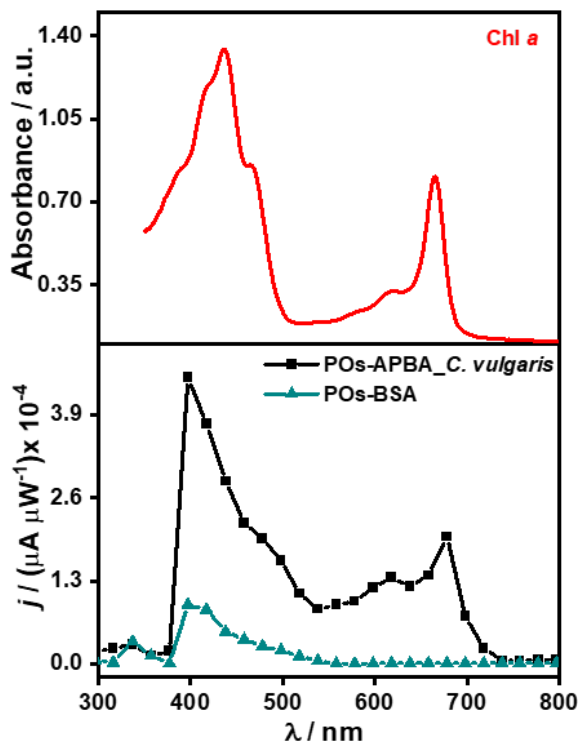


**Figure 4.3.** Comparison of the absorption spectrum of chlorophyll a (Chl *a*) extracted from *Chlorella vulgaris* (top) and the action spectra of P-Os modified electrodes (bottom) integrating either BSA (green) or *C. vulgaris* (black).  $E_{\text{app}} = 350$  mV vs. Ag/AgCl/3 M KCl. Electrolyte: 0.1 M PB buffer, pH 7.

In the absence of *C. vulgaris* cells, P-Os only exhibits a small photoactivity in the violet to blue wavelength range (from 390 to 520 nm) with a maximum of  $0.9 \times 10^{-4} \mu\text{A } \mu\text{W}^{-1}$  at 400 nm. In contrast, when cells are present inside the P-Os film, the photocurrent is up to four times higher than in the absence of cells and the photoresponse

persists throughout a longer wavelength range (from 390 to 720 nm), with two local maxima of  $4.5 \times 10^{-4}$  and  $2.0 \times 10^{-4} \mu\text{A} \mu\text{W}^{-1}$  at 400 and 680 nm, respectively. The profile of this action spectrum concurs almost perfectly with the electronic transitions of Chl *a* pigments present in the chloroplasts of *C. vulgaris* as it can be seen in the absorption spectrum of Chl *a*. This strongly supports our hypothesis that photocurrent generation is related with the photosynthetic machinery of *C. vulgaris* and productive electron-transfer communication between the polymer-integrated cells and the electrode via P-Os is established.

To further investigate the source of electrons, the photosynthetic inhibitor DCMU was added to the electrolyte to a final concentration of 50  $\mu\text{M}$  during the third cycle of illumination. DCMU blocks the reduction of the  $\text{Q}_\text{B}$  by  $\text{Q}_\text{A}$  (both located in the RCII, preventing further electron transfer to redox proteins of the photosynthetic electron transport chain [24] (Figure 4.4). After the addition of DCMU no significant decrease in photocurrent was observed even after 10 min of illumination, compared to a sample where only the solvent (ethanol) was added (Figure 4.5a).

In order to discard the possible impact of 3-APBA and P-Os on the diffusion of DCMU to the immobilized polymer-integrated *C. vulgaris* cells, a culture of free cells was treated with 150  $\mu\text{M}$  DCMU in 0.1 M PB pH 7 for 30 min prior incubation with 3-APBA and further immobilization with P-Os. Figure 4.5b shows that the photocurrent responses were very similar when the cells were exposed to DCMU or using unexposed *C. vulgaris* cells.

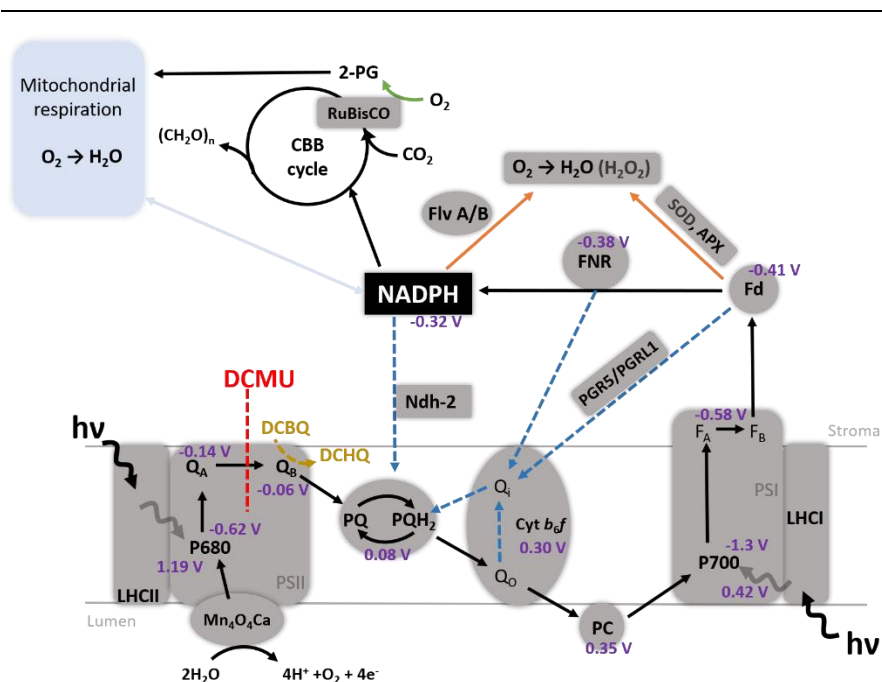


**Figure 4.4.** Schematic of the photosynthetic electron transport chain with the relevant midpoint potentials (V vs. SHE as indicated in [25]). Solid black lines indicate the linear electron transport (LET) from the oxidation of water by photosystem II (PSII) to the reduction of NADPH by Fd-NADP<sup>+</sup> reductase (FNR). Putative electron pathways to decrease the over-reduction of the LET during the light phase of the photosynthesis are represented with different colours: cyclic electron transport around photosystem I (PSI) (blue dashed lines), pseudocyclic electron transport or water-water cycle for the photoreduction of O<sub>2</sub> (orange solid lines), photorespiration catalysed by RuBisCO (green solid line), NAD(P)<sup>+</sup>/NAD(P)H interchange between mitochondria and chloroplast (light blue solid line). APX, ascorbate peroxidase; CBB, Calvin-Benson-Bassham cycle; DCBQ/DCHQ, 2,6-dichloro-1,4-benzoquinone/hydroquinone; DCMU, 3-(3,4-dichlorophenyl)-1,1-dimethylurea; LHCII/LHCI, light harvesting complexes II and I; Ndh-2, type II NADH dehydrogenase; Fd, ferredoxin; Flv A/B, flavodiiron proteins; PC, plastocyanin; PGR5 and PGRL1, proton gradient regulation 5 and proton gradient regulation like 1; PQ, plastoquinone; SOD, superoxide dismutase.

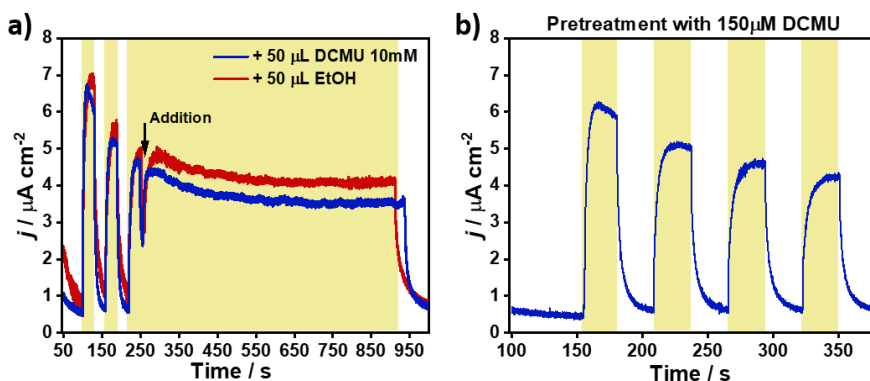


**Figure 4.5.** (a) CA of a *C. vulgaris*-based bioanode in presence and absence of DCMU (50  $\mu\text{M}$ ) and (b) with pre-treatment of *C. vulgaris* cultures with 150  $\mu\text{M}$  DCMU for 30 min.  $E_{\text{app}} = 350$  mV vs. Ag/AgCl/3 M KCl. Electrolyte: 0.1 M PB buffer pH 7. Irradiation with 50 mW  $\text{cm}^{-2}$  incident white light (yellow shadows).

Moreover, a photochronoamperometric measurement of a *C. vulgaris*-based bioanode was performed in presence of the free-diffusing redox mediator DCBQ after a few irradiation cycles. As shown in Figure 4.6a, the addition of DCBQ did not result in an increased photocurrent response meaning that the redox mediator was not reduced to 2,6-dichloro-1,4-hydroquinone (DCHQ) by PSII inside the cells [26] (Figure 4.4). The prevention of the DCBQ electron transfer within the hydrogel could be discarded since an additional pair of redox peaks with a formal potential of 0.11 V vs. Ag/AgCl/3 M KCl for the DCBQ/DCHQ interconversion was observed in the CV of the bioanode (Figure 4.6b). All these findings confirm that  $Q_B$  is not implicated in photocurrent generation by communication with the redox polymer, and thus, an alternative electron pathway should be involved. As it is unlikely that the redox polymer is able to cross the cell wall and wire the  $Q_A$  site at PSII to the electrode as it has been reported for biophotoelectrodes integrating isolated PSII [10,27], the obtained results suggest that

there is a source of electrons that interplays downstream of  $Q_B$  to eventually be excited by PSI [28].

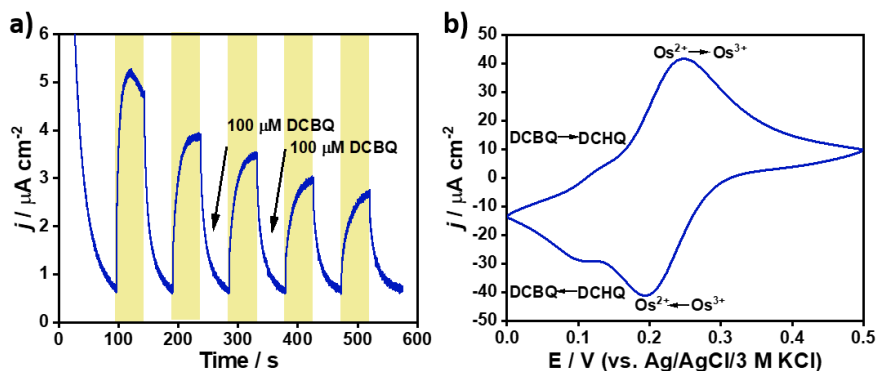


**Figure 4.6.** (a) Chronoamperogram of a *C. vulgaris*-based bioanode with the addition of DCBQ.  $E_{app} = 350$  mV vs. Ag/AgCl/3 M KCl. Irradiation with  $50 \text{ mW cm}^{-2}$  incident white light (yellow shadows). (b) Cyclic voltammogram after (a) showing the redox peaks for the DCBQ/DCHQ and  $\text{Os}^{2+/3+}$  interconversions. Electrolyte: 0.1 M PB buffer pH 7.

A closer examination of the mechanism related to the photocurrent generation was performed using SPECM to locally evaluate the oxygen evolution of the system. SPECM has been shown to be a valuable tool for analysing light-reactions at a specific location of the sample, such as oxygen evolution and generation of ROS by means of microelectrodes polarized at specific potentials [10,29]. In the improbable case of P-Os wiring to  $Q_A$ , the OEC would be functional, and thus an increase in  $\text{O}_2$  collection efficiency associated with the generated photocurrent response would be expected under illumination. Conversely, the obtained SPECM results (Figure 4.7) show a considerable decrease in the tip current for  $\text{O}_2$  reduction when the sample with immobilized *C. vulgaris* is irradiated, meaning that there is  $\text{O}_2$  consumption instead of its production at the analyzed sample under illumination. When the experiment was repeated with

a control electrode fabricated with BSA instead of *C. vulgaris*, only a minor (5 times lower) O<sub>2</sub> consumption was observed under illumination, confirming that the observed consumption of O<sub>2</sub> is correlated with the generation of photocurrent.

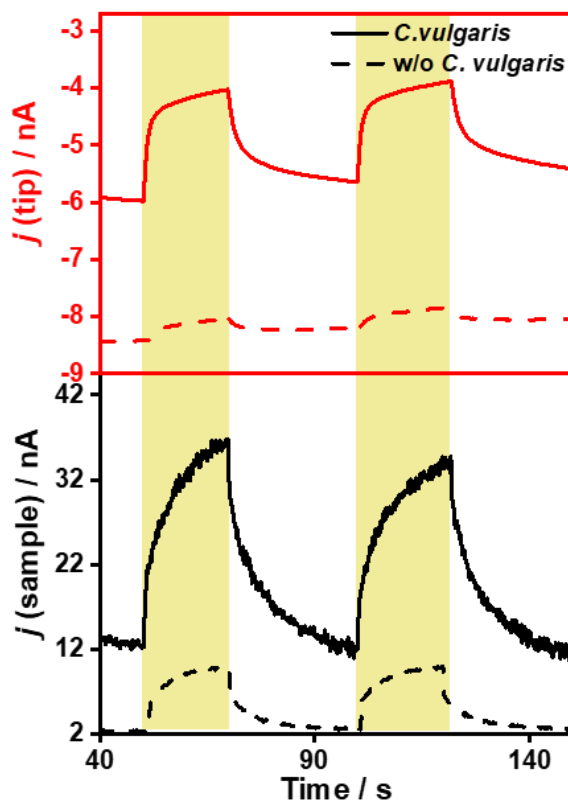


**Figure 4.7.** SPECM analysis of P-Os modified electrodes integrating either BSA (dashed lines) or *Chlorella vulgaris* preincubated with 3-APBA (solid lines). Black: sample photocurrent. Red: tip current for the reduction of O<sub>2</sub>. The sample and tip were polarized at 350 mV and -600 mV vs. Ag/AgCl/3 M KCl, respectively. Electrolyte: 0.1 M PB buffer, pH 7. The sample was locally irradiated with  $\approx 200$  mW cm<sup>-2</sup>. Tip-to-sample distance: 13  $\mu$ m.

It is important to note that despite the fact that the photosynthetic and respiratory systems in *Chlorella* are located in separated organelles, there is evidence of cross-talk between them [30–32]. Not only oxygen is consumed by respiration in the mitochondria, but it is also

consumed in the chloroplast during the light and dark phases of photosynthesis (chlororespiration, photorespiration, Mehler and Mehler-like reactions) [30,33] as a mechanism to avoid the over-reduction of the photosynthetic machinery under stress conditions (i.e., high light intensity, low concentrations of CO<sub>2</sub> and nutrient starvation) [34,35]. Thus, the oxygen uptake observed in the SPECM might indicate that alternative electron pathways are activated to avoid light photodamage. These results together with the observations from the action spectra (Figure 4.3) and the experiments with DCMU and DCBQ (Figure 4.5 and 4.6) strongly support our hypothesis that electrons stem from processes downstream of Q<sub>B</sub> that involve PSI, whether oxygen is directly involved or not, i.e., CET (Figure 4.4). To elucidate the exact electron transfer mechanism, further investigation with other inhibitors, mediators and knockout cells should be performed, which is the aim of future research to confirm this hypothesis.

#### **4.3.3. Assembly of a BPV cell with the *C. vulgaris*-based bioanode (Au/POs-APBA-*C. vulgaris*):**

As a proof of concept for a functioning BPV cell, the *C. vulgaris*-based bioanode was coupled to a *Mv*-BOD biocathode. The BPV cell performance was assessed under light and dark regimes (Figure 4.8). CVs of the *Mv*-BOD cathode under argon and air were conducted to ensure that the cathode was not limiting the BPV performance (Figure Appendix C.2). The OCV of the BPV cell was around 270 mV. After subtracting the background outputs in darkness, a



maximum current density of  $13.66 \mu\text{A cm}^{-2}$  and a power output of  $1.48 \mu\text{W cm}^{-2}$  at 130 mV were obtained.

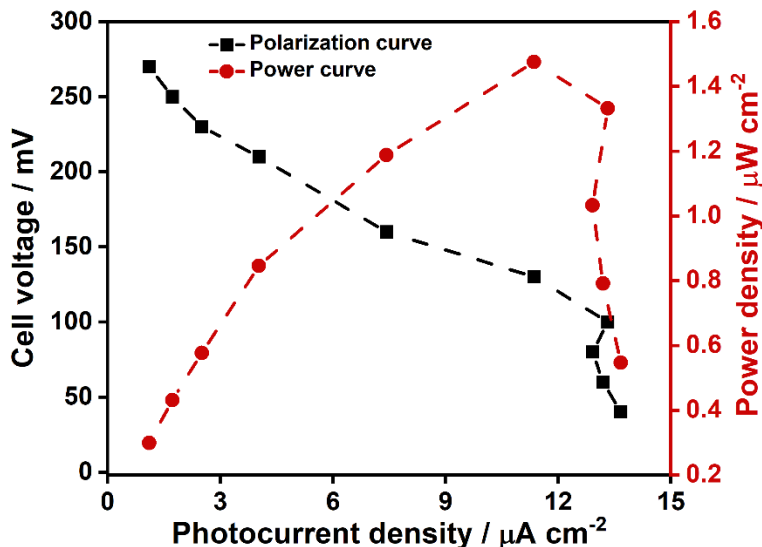


**Figure 4.8.** Polarization (black) and power (red) curves for the assembled BPV cell with a P-Os modified electrode integrating *Chlorella vulgaris* functionalized with 3-APBA as photoanode and a *Mv*-BOD modified electrode as biocathode. The photoanode was irradiated with white light at a power of  $\approx 200 \text{ mW cm}^{-2}$ . Electrolyte: 0.1 M PB buffer pH 7.

The quantum yield (QY) of the BPV cell was calculated dividing the power output by the power input (light supply) and compared to quantum yields for previous works of biophotovoltaic cells. The quantum yield attained ( $7.4 \times 10^{-4} \%$ ) was lower than the obtained with devices using subcellular elements or cyanobacteria as a bioanode (Table 4.1), since the electron transfer is hampered due to the presence of biological barriers to surpass. Nevertheless, the quantum yield obtained with our system was greater than other configurations using *C. vulgaris* as a bioanode.

**Table 4.1.** Comparison of quantum yields calculated with the power reported using photosynthetic elements (subcellular and cellular) as bioanode in biophotovoltaic cells:

<i>Photosynth. element</i>	<i>Anode</i>	<i>Cathode</i>	<i>Power output</i> ( $\mu\text{W cm}^{-2}$ )	<i>Power input</i> ( $\text{mW cm}^{-2}$ )	<i>QY (%)</i>	<i>Ref.</i>
<b>PSI</b>	Au/P-vio	CC/GOX	3.7	100	$3.7 \times 10^{-3}$	[36]
<b>PSII</b>	IO-TiO <sub>2</sub> /PbS/ P-Os	IO-ATO/ PCA/ BOD	45	100	$45 \times 10^{-2}$	[37]
<b>Thylakoid</b>	CP/PFP	MWCN T/ PBSE/ BOD	0.33	100	$3.3 \times 10^{-4}$	[38]
<b>Thylakoid</b>	ITO/Au/CNT <sup>a</sup>	BOD/KB /WPCC	50	434	$1.2 \times 10^{-2}$ <sub>c</sub>	[39]
<i>Nostoc sp.</i>	CNT/CP <sup>b</sup>	<i>Laccase</i> / CNT/CP	10	76	$1.3 \times 10^{-2}$	[40]
<i>C. vulgaris</i>	ITO/alginate	ITO	$2.6 \times 10^{-3}$	2.6	$1.1 \times 10^{-4}$ <sub>c, d</sub>	[20]
<i>C. vulgaris</i>	Au/P-Os	BOD/ Graphite	1.5	200	$7.4 \times 10^{-4}$	*

ATO, antimony-tin oxide; GOX, glucose oxidase; IO, inverse opal; ITO, indium-tin oxide; KB/WPCC, ketjen Black-modified waterproof carbon cloth; MWCNT, multiwalled carbon nanotube; PBSE, 1-pyrenebutyric acid N-hydroxysuccinimide ester; PCA, pyrenecarboxylic acid; PFP, poly(fluorene-*alt*-phenylene); P-vio, viologen modified polymer; QY, quantum yield. <sup>a</sup>and <sup>b</sup> used diffusive mediators ruthenium hexaamine trichloride and 1,4-benzoquinone, respectively. <sup>c</sup> calculated from the stated photon flux on the reports converted to power density using equation Appendix C.2. <sup>d</sup> subtracting power output in dark. \* stands for "this work"

#### 4.4. Conclusions

A bioanode comprised of *Chlorella vulgaris* cells functionalized with 3-APBA embedded in an Os complex-modified polymer matrix has been developed. The binding of 3-APBA with the cells increases the

stability of the resulting film as well as promotes the photocurrent presumably due to an improved crosslinking between the redox polymer matrix and immobilized cells. Furthermore, the overlap between the absorbance spectrum of Chl *a* and the action spectrum of the bioanode, indicates that the photocurrent is mainly due to the photoexcitation of the photosynthetic machinery of the immobilized *C. vulgaris* cells. The addition of DCMU and DCBQ demonstrated that  $Q_B$  was not involved in photocurrent generation. Moreover, SPECM results indicate that electrons might originate from alternative electron pathways linked to PSI. A BPV device was assembled by coupling the proposed bioanode to a BOD-based biocathode which resulted in a considerable current density and power output for such microalgae-based devices. These results show boronic acid derivatives as promising element in tailoring bioanodes for microorganism-based BPV cells.

---

**References**

- [1] M. Anam, H.I. Gomes, G. Rivers, R.L. Gomes, R. Wildman, Evaluation of photoanode materials used in biophotovoltaic systems for renewable energy generation, *Sustain. Energy Fuels*. 5 (2021) 4209–4232. <https://doi.org/10.1039/d1se00396h>.
- [2] A.J. McCormick, P. Bombelli, R.W. Bradley, R. Thorne, T. Wenzel, C.J. Howe, Biophotovoltaics: oxigenic photosynthetic organisms in the world of bioelectrochemical systems, *Energy Environ. Sci.* 8 (2015) 1092–1109. <https://doi.org/10.1039/C4EE03875D>.
- [3] J.Z. Zhang, P. Bombelli, K.P. Sokol, A. Fantuzzi, A.W. Rutherford, C.J. Howe, E. Reisner, Photoelectrochemistry of photosystem II in vitro vs in vivo, *J. Am. Chem. Soc.* 140 (2018) 6–9. <https://doi.org/10.1021/jacs.7b08563>.
- [4] K. Hasan, H. Bekir Yildiz, E. Sperling, P.Ó. Conghaile, M.A. Packer, D. Leech, C. Hägerhäll, L. Gorton, Photoelectrochemical communication between cyanobacteria (*Leptolyngbia* sp.) and osmium redox polymer modified electrodes, *Phys. Chem. Chem. Phys.* 16 (2014) 24676–24680. <https://doi.org/10.1039/c4cp04307c>.
- [5] K. Hasan, E. Çevik, E. Sperling, M.A. Packer, D. Leech, L. Gorton, Photoelectrochemical wiring of *Paulschulzia pseudovolvox* (algae) to osmium polymer modified electrodes for harnessing solar energy, *Adv. Energy Mater.* 5 (2015) 1501100. <https://doi.org/10.1002/aenm.201501100>.
- [6] L. Darus, T. Sadakane, P. Ledezma, S. Tsujimura, I. Osadebe, D. Leech, L. Gorton, S. Freguia, Redox-polymers enable uninterrupted day/night photo-driven electricity generation in biophotovoltaic devices, *J. Electrochem. Soc.* 164 (2017) H3037–H3040. <https://doi.org/10.1149/2.0091703jes>.
- [7] H. Shkil, A. Schulte, D.A. Guschin, W. Schuhmann, Electron transfer between genetically modified *Hansenula polymorpha* yeast cells and electrode surfaces via Os-complex modified redox polymers, *ChemPhysChem*. 12 (2011) 806–813. <https://doi.org/10.1002/cphc.201000889>.

- [8] G. Pankratova, L. Hederstedt, L. Gorton, Extracellular electron transfer features of Gram-positive bacteria, *Anal. Chim. Acta.* 1076 (2019) 32–47. <https://doi.org/10.1016/j.aca.2019.05.007>.
- [9] J. Pruvost, G. Van Vooren, G. Cogne, J. Legrand, Investigation of biomass and lipids production with *Neochloris oleoabundans* in photobioreactor, *Bioresour. Technol.* 100 (2009) 5988–5995. <https://doi.org/10.1016/j.biortech.2009.06.004>.
- [10] F. Zhao, V. Hartmann, A. Ruff, M.M. Nowaczyk, W. Schuhmann, F. Conzuelo, Unravelling electron transfer processes at photosystem 2 embedded in an Os-complex modified redox polymer, *Electrochim. Acta.* 290 (2018) 451–456. <https://doi.org/10.1016/j.electacta.2018.09.093>.
- [11] F. Conzuelo, N. Markovic, A. Ruff, W. Schuhmann, The open circuit voltage in biofuel cells: nernstian shift in pseudocapacitive electrodes, *Angew. Chemie Int. Ed.* 57 (2018) 13681–13685. <https://doi.org/10.1002/anie.201808450>.
- [12] R.J. Ritchie, Consistent sets of spectrophotometric chlorophyll equations for acetone, methanol and ethanol solvents, *Photosynth. Res.* 89 (2006) 27–41. <https://doi.org/10.1007/s11120-006-9065-9>.
- [13] F. Conzuelo, K. Sliozberg, R. Gutkowski, S. Gru, M. Nebel, W. Schuhmann, High-resolution analysis of photoanodes for water splitting by means of scanning photoelectrochemical microscopy, *Anal. Chem.* 89 (2017) 1222–1228. <https://doi.org/10.1021/acs.analchem.6b03706>.
- [14] J. Szczesny, N. Marković, F. Conzuelo, S. Zacarias, I.A.C. Pereira, W. Lubitz, N. Plumeré, W. Schuhmann, A. Ruff, A gas breathing hydrogen/air biofuel cell comprising a redox polymer/hydrogenase-based bioanode, *Nat. Commun.* 9 (2018) 4715. <https://doi.org/10.1038/s41467-018-07137-6>.
- [15] N. Azizi, M.R. Saidi, Highly chemoselective addition of amines to epoxides in water, *Org. Lett.* 7 (2005) 3649–3651. <https://doi.org/10.1021/ol051220q>.

- [16] S. Bonollo, F. Fringuelli, F. Pizzo, L. Vaccaro, A green route to  $\beta$ -amino alcohols via the uncatalyzed aminolysis of 1,2-epoxides by alkyl- and arylamines, *Green Chem.* 8 (2006) 960–964. <https://doi.org/10.1039/b607620c>.
- [17] S. Bonollo, D. Lanari, L. Vaccaro, Ring-opening of epoxides in water, *European J. Org. Chem.* 2011 (2011) 2587–2598. <https://doi.org/10.1002/ejoc.201001693>.
- [18] T. Kothe, S. Pöller, F. Zhao, P. Fortgang, M. Rögner, W. Schuhmann, N. Plumeré, Engineered electron-transfer chain in photosystem 1 based photocathodes outperforms electron-transfer rates in natural photosynthesis, *Chem. - A Eur. J.* 20 (2014) 11029–11034. <https://doi.org/10.1002/chem.201402585>.
- [19] F.-L. Ng, S.-M. Phang, V. Periasamy, K. Yunus, A.C. Fisher, Enhancement of power output by using alginate immobilized algae in biophotovoltaic devices, *Sci. Rep.* 7 (2017) 16237. <https://doi.org/10.1038/s41598-017-16530-y>.
- [20] C. Thong, S. Phang, F. Ng, V. Periasamy, T. Ling, K. Yunus, A.C. Fisher, Effect of different irradiance levels on bioelectricity generation from algal biophotovoltaic (BPV) devices, *Energy Sci. Eng.* 7 (2019) 2086–2097. <https://doi.org/10.1002/ese3.414>.
- [21] A. Stephenson-Brown, S. Yong, M.H. Mansor, Z. Hussein, N.-C. Yip, P.M. Mendes, J.S. Fossey, F.J. Rawson, Electronic communication of cells with a surface mediated by boronic acid saccharide interactions, *Chem. Commun.* 51 (2015) 17213–17216. <https://doi.org/10.1039/c5cc04311e>.
- [22] K. Yokoyama, T. Shibasaki, Y. Murakami, Electrochemical characterization of enzyme electrodes mediated by ferrocene-containing acrylamide-acrylic acid copolymers, *Denki Kagaku Oyobi Kogyo Butsuri Kagaku.* 64 (1996) 1221–1227. <https://doi.org/10.5796/kogyobutsurikagaku.64.1221>.
- [23] S. Koide, K. Yokoyama, Electrochemical characterization of an enzyme electrode based on a ferrocene-containing redox polymer, *J. Electroanal. Chem.* 468 (1999) 193–201. [https://doi.org/10.1016/S0022-0728\(99\)00174-6](https://doi.org/10.1016/S0022-0728(99)00174-6).

- [24] A. Trebst, Inhibitors in the functional dissection of the photosynthetic electron transport system, *Photosynth. Res.* 92 (2007) 217–224. <https://doi.org/10.1007/s11120-007-9213-x>.
- [25] J. Tschörtner, B. Lai, J.O. Krömer, Biophotovoltaics: green power generation from sunlight and water, *Front. Microbiol.* 10 (2019) 866. <https://doi.org/10.3389/fmicb.2019.00866>.
- [26] Y. Kashino, M. Yamashite, Y. Okamoto, H. Koike, K. Satoh, Mechanism of electron flow through the QB site in photosystem II. 3. Effects of the presence of membrane structure on the redox reactions at the QB site, *Plant Cell Physiol.* 37 (1996) 976–982. <https://doi.org/10.1093/oxfordjournals.pcp.a029047>.
- [27] U. Gözde, G.W. Brudvig, Redirecting electron transfer in photosystem II from water to redox-active metal complexes, *J. Am. Chem. Soc.* 133 (2011) 13260–13263. <https://doi.org/10.1021/ja2049226>.
- [28] G. Saper, D. Kallmann, F. Conzuelo, F. Zhao, T.N. Tóth, V. Liveanu, S. Meir, J. Szymanski, A. Aharoni, W. Schuhmann, A. Rothschild, G. Schuster, N. Adir, Live cyanobacteria produce photocurrent and hydrogen using both the respiratory and photosynthetic systems, *Nat. Commun.* 9 (2018) 2168. <https://doi.org/10.1038/s41467-018-04613-x>.
- [29] F. Zhao, S. Hardt, V. Hartmann, H. Zhang, M.M. Nowaczyk, M. Rögner, N. Plumeré, W. Schuhmann, F. Conzuelo, Light-induced formation of partially reduced oxygen species limits the lifetime of photosystem 1-based biocathodes, *Nat. Commun.* 9 (2018) 1973. <https://doi.org/10.1038/s41467-018-04433-z>.
- [30] P. Cardol, G. Forti, G. Finazzi, Regulation of electron transport in microalgae, *Biochim. Biophys. Acta.* 1807 (2011) 912–918. <https://doi.org/10.1016/j.bbabi.2010.12.004>.
- [31] B. Bailleul, N. Berne, O. Murik, D. Petroustos, J. Prihoda, A. Tanaka, V. Villanova, R. Bligny, S. Flori, D. Falconet, A. Krieger-liszkay, S. Santabarbara, F. Rappaport, P. Joliot, L. Tirichine, P.G. Falkowski, P. Cardol, C. Bowler, G. Finazzi, Energetic coupling between plastids and mitochondria drives CO<sub>2</sub> assimilation in diatoms, *Nature.* 524 (2015) 366–369.

<https://doi.org/10.1038/nature14599>.

- [32] V. Larosa, A. Meneghesso, N. La Rocca, J. Steinbeck, M. Hippler, I. Szabò, T. Morosinotto, Mitochondria affect photosynthetic electron transport and photosensitivity in a green alga, *Plant Physiol.* 176 (2018) 2305–2314. <https://doi.org/10.1104/pp.17.01249>.
- [33] M.R. Badger, S. Von Caemmerer, S. Ruuska, H. Nakano, Electron flow to oxygen in higher plants and algae: rates and control of direct photoreduction (Mehler reaction) and rubisco oxygenase, *Philos. Trans. R. Soc. London. B, Biol. Sci.* 355 (2000) 1433–1446. <https://doi.org/10.1098/rstb.2000.0704>.
- [34] D.F. Sueltemeyer, K. Klug, H.P. Fock, Effect of photon fluence rate on oxygen evolution and uptake by *Chlamydomonas reinhardtii* suspensions grown in ambient and CO<sub>2</sub>-enriched air, *Plant Physiol.* 81 (1986) 372–375. <https://doi.org/10.1104/pp.81.2.372>.
- [35] S. Upadhyaya, B.J. Rao, Reciprocal regulation of photosynthesis and mitochondrial respiration by TOR kinase in *Chlamydomonas reinhardtii*, *Plant Direct.* 3 (2019) e00184. <https://doi.org/10.1002/pld3.184>.
- [36] P. Wang, F. Zhao, A. Frank, S. Zerria, A. Lielpetere, A. Ruff, M.M. Nowaczyk, W. Schuhmann, F. Conzuelo, Rational design of a photosystem I photoanode for the fabrication of biophotovoltaic devices, *Adv. Energy Mater.* 11 (2021) 2102858. <https://doi.org/10.1002/aenm.202102858>.
- [37] M. Riedel, J. Wersig, A. Ruff, W. Schuhmann, A. Zouni, F. Lisdat, A Z-scheme-inspired photobioelectrochemical H<sub>2</sub>O/O<sub>2</sub> cell with a 1 V open-circuit voltage combining photosystem II and PbS quantum dots, *Angew. Chemie. Int. Ed.* 58 (2019) 801–805. <https://doi.org/10.1002/anie.201811172>.
- [38] X. Zhou, P. Gai, P. Zhang, H. Sun, F. Lv, L. Liu, S. Wang, Conjugated polymer enhanced photoelectric response of self-circulating photosynthetic bioelectrochemical cell, *ACS Appl. Mater. Interfaces* 11 (2019) 38993–39000. <https://doi.org/10.1021/acsami.9b12560>.
- [39] T. Adachi, K. Kataoka, Y. Kitazumi, O. Shirai, K. Kano, A



bio-solar cell with thylakoid membranes and bilirubin oxidase, *Chem. Lett.* 48 (2019) 686–689. <https://doi.org/10.1246/cl.190176>.

- [40] N. Sekar, Y. Umasankar, R.P. Ramasamy, Photocurrent generation by immobilized cyanobacteria via direct electron transport in photo-bioelectrochemical cells, *Phys. Chem. Chem. Phys.* 16 (2014) 7862–7871. <https://doi.org/10.1039/c4cp00494a>.

## Chapter 5

### Exoelectrogenesis of *C. vulgaris*-based biophotocatalytic electrodes due to stress

#### 5.1. Introduction

A milestone in BPVs performance has been the formation of photosynthetic biofilms on the electrode surface [1–4]. Although biofilm formation has led to improved power efficiencies ascribed to lower internal resistance [5], they are still very low mainly due to the poor exoelectrogenesis of photosynthetic microorganisms [4]. Unlike bacteria, oxygenic photosynthetic microorganisms lack the extracellular electron transfer structures on their cell surface. Although several studies have claimed the presence of nanowires and pili IV-like structures in cyanobacteria [6–8], recent investigations with *Synechocystis* demonstrate that neither these structures nor the S-layer contribute to the exoelectrogenesis [9,10]. Nonetheless, there is evidence of IEET from some cyanobacteria to the electrode surface through the excretion of NAD(P)H [11–14]. The photosynthetic machinery in cyanobacteria and microalgae is wrapped and protected by a cell membrane or even isolated in chloroplasts [15]. Therefore, electrons or electron reducing equivalents have to surpass these biological barriers to eventually be collected by the electrode to generate electricity. The disruption of these biological membranes would facilitate the electron transfer process from the microorganism to the electrode leading to an enhanced photocurrent. In this sense, photocurrent enhancement has been reported in the cyanobacteria

strain *Synechocystis* PCC6803 after being exposed to a mild pressure, which slightly disrupted the cell wall and hence facilitated the release of electron mediators to the electrode. [12]. Following similar assumptions, throughout all this thesis, *C. vulgaris* cells have been exposed to desiccation during the preparation of the biophotoelectrodes resulting in an outstanding photocurrent generation for this strain (see *Chapter 2 and 4*).

Exoelectrogenesis can also be improved by forcing the diversion of electrons from the PETC towards alternative electron sinks, which are less competitive, facilitating the electron transfer to the electrode. In this regard, iron-starved *C. reinhardtii* showed increased ferricyanide photoreduction related to photosynthesis that resulted in a reduced photosynthetic CO<sub>2</sub> fixation compared to cells grown in iron replete medium [16]. Gonzalez-Aravena et al. also reported increased ferricyanide photoreduction for iron-starved cyanobacteria *Synechococcus elongatus* PCC7942 and *C. vulgaris* [17]. Both studies pointed out to NAD(P)H as the intracellular substrate for exoelectrogenesis through a ferric reductase located in the plasma membrane.

Previous works have demonstrated that desiccation not only causes disruption of cell membranes, but also the suppression of photosynthesis, photoinhibition due to a decreased repair of D1 protein in PSII and increased formation of ROS [18,19]. Iron-starvation has also been related to reduced photosynthetic efficiency in microalgae [16,20–22]. Most of these works have been focused on the physiological status of microalgae after exposure to different

stress regimes without addressing their impact on the exoelectrogenesis of the microorganisms under study.

In this chapter, for the first time, we evaluate the impact of the photosynthetic stress on the exoelectrogenesis in *C. vulgaris* by combining PAM fluorometry and electrochemistry. PAM fluorometry has proved to be an extremely useful, rapid and non-invasive tool to measure the photosynthetic efficiency and consequently the stress undergone by photosynthetic microorganisms [23–27]. We hypothesize that [REDACTED] [REDACTED] [REDACTED] facilitating the electron transfer from *C. vulgaris* to the electrode. We also formulate that [REDACTED] starvation induce activation of alternative electron pathways to prevent PSII photodamage, which results in increased exoelectrogenesis.

## 5.2. Materials and methods

### 5.2.1. Algal culture:

The *C. vulgaris* strain [REDACTED] was purchased from [REDACTED] [REDACTED]. Cultures were grown in [REDACTED] [28] in 250 mL Corning polycarbonate Erlenmeyer flasks (Fisher Scientific) at  $(20 \pm 2)$  °C and shaken at 150 rpm under a PPFD of  $\approx$  [REDACTED] [REDACTED]

[REDACTED] starved cultures were obtained by transferring exponentially growing cells of a nutrient replete culture to [REDACTED] [REDACTED] deficient [REDACTED] media. [REDACTED] in the nutrient deficient medium, they were subcultured to new fresh

nutrient deficient medium to ensure the specific nutrient starvation, since Chl *a* content in nitrogen-deprived cells has proven to be significantly reduced after several days (> 7) of growth [29].

### 5.2.2. Determination of Chl *a*:

The determination of Chl *a* was performed on cultures prior to the cell immobilization on the electrode. Extraction of Chl *a* from *C. vulgaris* was performed following a method adapted from [30] under subdued light. Briefly, cultures were centrifuged at 4 °C and 5000 rpm for 10 min, washed with 0.1 M PB pH 7, centrifuged again and the resulting pellet lyophilized. Chl *a* was extracted [REDACTED] [REDACTED] At 4 °C for 4 h. Then [REDACTED] [REDACTED] cells were disrupted [REDACTED] [REDACTED] These two latter steps were repeated until the bleaching of the pellet. Afterwards, the solutions were centrifuged, the pellet was discarded and the spectrum of the supernatant (Chl *a*) was measured from 350 nm to 800 nm in quartz cuvettes with an UV-Vis spectrophotometer Cary 100 Bio (Varian). The Chl *a* concentration was calculated from the measured absorbance using the equation described by Wellburn [31]

### 5.2.3. Electrode modification:

GCEs of 3 mm diameter, (cod. CHI104, CH Instruments, Inc.), were polished with aqueous slurries of 0.3 µm alumina on nylon polishing pads. Subsequently, electrodes were ultrasonicated in ultrapure water (Milli-Q, Millipore, Spain) and blow dried with N<sub>2</sub>. Then electrodes were modified as described in *Chapter 2*. Briefly, one microliter of

oCNT dispersion was drop-cast on the GCE surface and [REDACTED]. Then electrodes were further modified [REDACTED] 3-APBA (Sigma-Aldrich) [REDACTED] a three-electrode configuration with oCNT modified GCE, the platinum and the Ag/AgCl/sat KCl as working, counter and reference electrodes, respectively. All potentials are referred vs. Ag/AgCl/sat KCl. [REDACTED]  
[REDACTED]  
[REDACTED] After the electropolymerization, the PAPBA-modified electrodes (GCE/oCNT/PAPBA) were washed for 20 minutes in 0.1 M PB pH 7 and preserved under N<sub>2</sub> atmosphere until further use.

#### **5.2.4. Immobilization of *C. vulgaris* on GCE/oCNT/PAPBA:**

Absorbance of cultures was measured at 680 nm of wavelength in triplicate with a Spectramax microplate reader (Molecular Devices, LLC) by placing 100  $\mu$ L of sample (optical path length of  $\approx$  0.25 cm) in MaxiSorp nunc 96 microwell plates (Thermo Fisher Scientific Inc.). The absorbance was converted to OD<sub>680</sub> by dividing the optical path length following Beer-Lambert's law. When cultures reached an [REDACTED], they were centrifuged at 4 °C and 4000 rpm for 10 minutes, washed in 0.1 M PB pH 7 and centrifuged. The pellet was resuspended in 0.1 M PB pH 7 to obtain [REDACTED]. Then [REDACTED] of cells were drop-cast on the modified electrode and immobilized by [REDACTED]  
[REDACTED]  
[REDACTED]  
[REDACTED].

### **5.2.5. Electrochemical analysis of the *C. vulgaris*-based biophotocathode (GCE/oCNT/PAPBA\_*C. vulgaris*):**

All electrochemical measurements were performed in triplicate unless otherwise stated, with a multi-channel PalmSens3 potentiostat and analyzed with PStrace 5 software (PalmSens BV) in a three-electrode electrochemical cell. GCE/oCNT/PAPBA\_*C. vulgaris* were used as working electrodes, Ag/AgCl/sat KCl and platinum wire as reference and counter electrodes, respectively. CAs were carried out at 0.2 V in 0.1 M PB pH 7.

### **5.2.6. DCMU experiments:**

A solution of 10 mM of the photosynthetic inhibitor DCMU (Sigma-Aldrich) dissolved in pure ethanol (Sigma-Aldrich) was prepared for being added at a 50  $\mu$ M final concentration in the electrolyte 0.1 M PB pH 7 during the CAs.

### **5.2.7. Modulated Chl *a* fluorescence measurements:**

Chl *a* fluorescence was simultaneously measured with CA by means of a [REDACTED] fluorometer [REDACTED]. The electrochemical cell was placed in a dark box with a hole in the bottom that allowed the light guide of the micro measuring head to pass. [REDACTED]

[REDACTED]  
[REDACTED]  
[REDACTED]  
[REDACTED] blue power LED with maximum emission at 465 nm. Samples were dark-adapted for 15 min to allow complete oxidation of RCII. The irradiance reported is

the irradiance impinging on the surface of the sample measured with an ULM-500 light meter (Heinz Walz GmbH). Fluorescence induction curves were performed with the measuring light [REDACTED]. [REDACTED] The  $F_0$  and  $F_M$  levels in the dark were recorded before and after the first SP [REDACTED]. [REDACTED] the actinic light ([REDACTED]) was switched on and  $F$  and  $F_M'$  were measured before and after a given SP of the same intensity and duration as in dark conditions. A total of [REDACTED]. [REDACTED]. The  $F_0'$  was calculated according to Oxborough and Baker (see Table 1.2 in *Chapter 1*) [32]. After switching off the actinic light, further SPs were performed in dark to assess the recovery of the photosynthetic efficiency. Then, the photochemical and non-photochemical quantum yields and fluorescence quenching were calculated as described in Table 1.2 in *Chapter 1*.

#### **5.2.8. Fluorescence microscopy:**

Autofluorescence of Chl *a* from GCE/oCNT/PAPBA\_ *C.vulgaris* was observed with a NIKON TE2000-E fluorescence microscope at excitation/emission wavelengths of 630/(650-700) nm [33]. Cell densities were calculated from fluorescence micrographs with the free image processing software ImageJ (National Institutes of Health, USA).

#### **5.2.9. Transmission electron microscopy (TEM):**

Cells exposed and unexposed to desiccation were prepared following a modified protocol described elsewhere [34]. [REDACTED]







was a reduced growth rate during the first subculturing in [REDACTED] (Figure 5.2a). Additionally, a strong reduction in the Chl *a* content was detected in the cultures harvested for electrode experimentation, i.e., after the second subculturing in nutrient deficient media (and when all cultures had OD<sub>680</sub> [REDACTED]) (Figure 5.2b). Chl *a* under [REDACTED] starvation was lower ( $(1.75 \pm 0.07) \mu\text{g mL}^{-1}$ ) and even lower under [REDACTED] deprivation ( $(0.87 \pm 0.02) \mu\text{g mL}^{-1}$ ) than compared to cells grown in replete medium ( $(4.5 \pm 0.6) \mu\text{g mL}^{-1}$ ). That is a 61 and 81% reduction in the amount of Chl *a* in cells grown in [REDACTED], respectively. These results are in agreement with that previously reported for green microalgae [29,39–41].

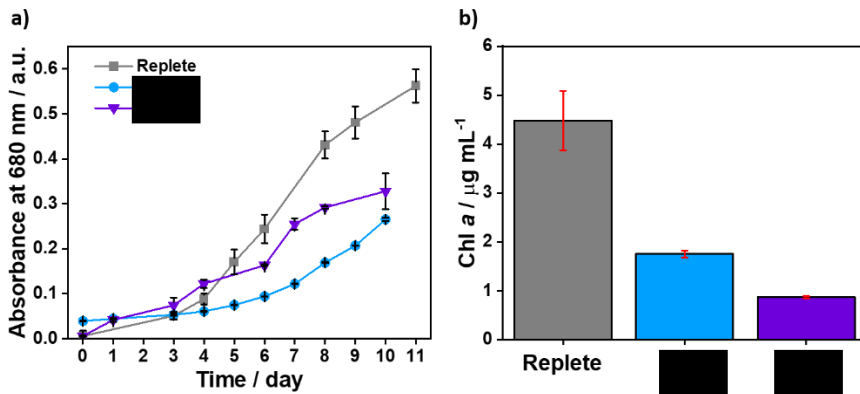


**Figure 5.2.** Growth curves of *C. vulgaris* in (a) replete medium, medium [REDACTED] and (b) medium [REDACTED]. Error bars stand for standard deviation ( $n = 2$ ). (c) concentration of Chl *a* of cultures grown in replete, [REDACTED] media at the time harvested for their immobilization on the electrodes (when OD<sub>680</sub> reached values around 0.8). Error bars stand for standard deviation ( $n = 3$ ).

### 5.3.2. Photosynthetic stress and exoelectrogenesis assessment:

PAM fluorometry of Chl *a* was used to evaluate the stress of *C. vulgaris* grown in nutrient deprived conditions and further attached to the surface of GCE/oCNT/PAPBA electrodes [REDACTED]

[REDACTED] Chl *a* fluorescence induction curves give information about the portion of absorbed light energy that is used for photosynthesis (i.e.,  $F_V/F_M$  and  $\Phi$  PSII) and the portion that is re-emitted as heat (i.e.,  $\Phi$  NPQ and  $\Phi$  NO).

To ensure that all the RCII were in their open state (i.e., the  $Q_A$  is oxidized), all Chl *a* fluorescence induction curves were performed on biophotoelectrodes dark-adapted for 15 min. At the same time, chronoamperometries were performed to assess the photocurrent generation in each condition (Figures Appendix D.1 and Appendix D.2). Figure 5.3 and 5.4 show the  $F_V/F_M$  and the percentage of  $\Phi$  PSII recovered after 30 min post-illumination, respectively, for *C. vulgaris* grown in replete and nutrient deplete media and attached to GCE/oCNT/PAPBA electrodes [REDACTED]

[REDACTED] approach. The  $F_V/F_M$  and  $\Phi$  PSII values of cell suspensions grown in replete media (S) are also shown for comparison. One-way ANOVA and post-hoc Tukey HSD test were executed to assess whether or not the  $F_V/F_M$  and  $\Phi$  PSII recoveries obtained in each case were significantly different within a 95% confidence interval.

#### 5.3.2.1. Evaluation of photosynthetic stress:

The  $F_V/F_M$  of nutrient replete *C. vulgaris* cell suspensions ( $F_V/F_{M(S)}$ ) was  $0.67 \pm 0.01$  (Figure 5.3a), which is in agreement with that

reported in literature for *C. vulgaris* and green microalgae in good physiological state [42–44]. After 30 min from the switch off of the actinic light, a 98%  $\Phi$  PSII<sub>(S)</sub> recovery was observed ( $0.65 \pm 0.01$ , Figure 5.4), confirming the wellness of the photosynthetic machinery of cell suspensions of *C. vulgaris*.

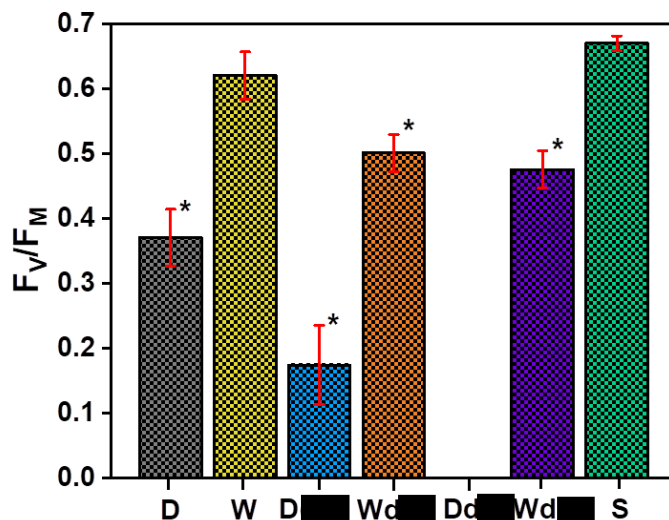


**Figure 5.3.** Average of maximum photochemical quantum yield ( $F_V/F_M$ ) of *C. vulgaris* attached to GCE/oCNT/PAPBA electrodes by [redacted], in [redacted] and cell suspensions (S). \* indicates statistical significance. Error bars stand for standard deviation ( $n = 3$ ). Actinic light ([redacted]).

On the contrary, the  $F_V/F_M$  for cells attached to electrodes [redacted] and grown in [redacted] deficient medium (Wd [redacted]) was  $0.50 \pm 0.03$  and in [redacted] deficient medium (Wd [redacted]) was  $0.47 \pm 0.03$ . That is, both [redacted] starvation unfavorably influenced the photosynthetic efficiency of *C. vulgaris*, with a 20% and a 24% reduction of  $F_V/F_M$  compared to their homologue grown in replete medium ( $p < 0.5$ , Tables Appendix D.1 and Appendix D.2

and Figure 5.3). Furthermore, the decline in  $F_V/F_M$  ( $0.17 \pm 0.06$ ) was even more drastic when cells grown in [REDACTED]-deficient medium were [REDACTED] (Dd [REDACTED]) on the electrode surface. In fact, [REDACTED] samples showed the highest decline in  $F_V/F_M$  among all the growth and immobilization conditions under study. The effects of [REDACTED] in the photosynthetic efficiency will be discussed in detail in next paragraphs. It is noteworthy that fluorescence measurements with *C. vulgaris* grown under [REDACTED] deprivation and immobilized by [REDACTED] (Dd [REDACTED]) were unworkable, probably due to low capacity for protein reparation after [REDACTED] [45,46]. The reduction in the photosynthetic efficiency in [REDACTED] and [REDACTED]-deprived cells might be a consequence of reduced Chl *a* content and a decreased capacity of PSII turnover [40,47]. Hence, the reduction on the  $F_V/F_M$  of *C. vulgaris* under [REDACTED] and [REDACTED] starvation confirms that cells grown deprived of these macronutrients have their photosynthetic capacity compromised and suffer nutrient stress, which is consistent with that reported in literature for algae [20,21,38,40,48].

### 5.3.2.2. Evaluation of photodamage:

The recoveries of  $\Phi$  PSII after 30 min in darkness post-illumination for cells grown in nutrient starvation and immobilized in [REDACTED] [REDACTED] were not significantly lower than that of *C. vulgaris* grown in replete medium ( $84 \pm 6\%$  and  $90 \pm 6\%$  for WdFe and WdN, respectively) (Figure 5.4). It has been reported that [REDACTED] [REDACTED] increases CET as a mechanism to prevent photodamage [20,22,37]. Increased CET has also been observed in [REDACTED] deprived microalgae [40]. Noteworthy, the  $\Phi$  NPQ

in Wd $\square$  was strongly increased upon actinic light (Figure Annex-5.2a-left) showing a highly photoinduced protective energy dissipation to prevent *C. vulgaris* from photodamage.

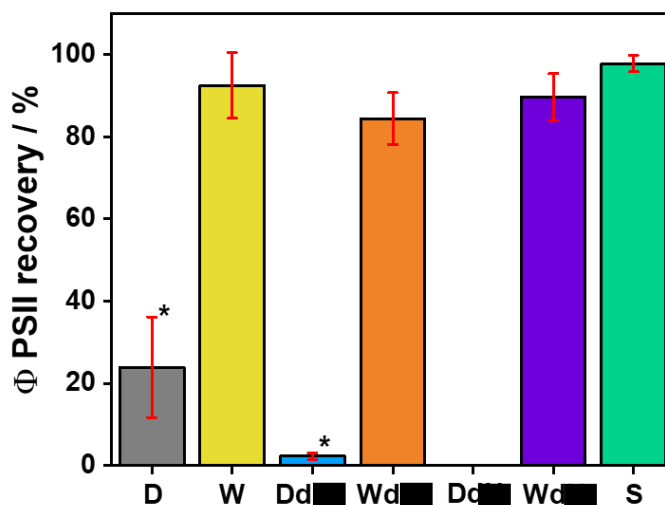


**Figure 5.4.** Average of recovery of the photochemical quantum yield ( $\Phi$  PSII) after 30 min post-illumination of *C. vulgaris* attached to GCE/oCNT/PAPBA electrodes by  $\square$  and by  $\square$  immobilization and grown in: replete medium (D and W, respectively), in  $\square$  deficient medium (Dd $\square$  and Wd $\square$ , respectively), in  $\square$ -deficient medium (Dd $\square$  and Wd $\square$ , respectively) and cell suspensions (S). \* indicates statistical significance. Error bars stand for standard deviation (n = 3). Actinic light ( $\square$ ).

However, in the case of  $\square$  *C. vulgaris*, only a  $23.9 \pm 0.5\%$  (replete, D) and a  $2.3 \pm 0.8\%$  (Dd $\square$ ) of the initial photosynthetic capacity was recovered, manifesting severe photoinhibition ( $p < 0.5$ , Table Appendix D.3). Unequivocally, the results from the recovery of  $\Phi$  PSII revealed that nutrient deprivation did not entail photodamage per se, instead photodamage was clearly consequence of  $\square$  stress (Table Appendix D.4). A deeper insight on the photodamage induced by  $\square$  will be further discussed.

### 5.3.2.3. Evaluation of exoelectrogenesis:

Regarding photocurrent generation (Figure 5.5), no photocurrent was observed with cells grown in replete media and immobilized  $\square$  conditions ( $0.15 \pm 0.03$ )  $\mu\text{A cm}^{-2}$ ). These photocurrents were considered negligible since they were similar to that of the modified electrode without *C. vulgaris* ( $0.15 \pm 0.03$ )  $\mu\text{A cm}^{-2}$ , Figure Appendix D.3), which results from the blue light photoexcitation of PAPBA.

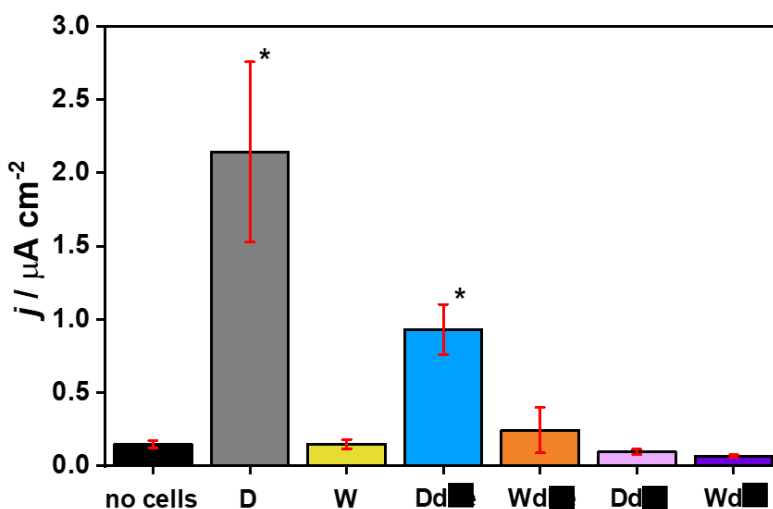


**Figure 5.5.** Average of photocurrent obtained for *C. vulgaris* attached to GCE/oCNT/PAPBA electrodes by  $\square$  and by  $\square$  immobilization and grown in: replete medium (D and W, respectively), in  $\square$ -deficient medium (Dd and Wd, respectively), in  $\square$ -deficient medium (Dd and Wd, respectively) and cell suspensions (S). \* indicates statistical significance. Error bars stand for standard deviation ( $n = 3$ ).  $E_{\text{app}} = 0.2$  V vs. Ag/AgCl/sat KCl. Electrolyte: PB pH 7. Actinic light ( $\square$ ).

*C. vulgaris* exposed to nutrient deprivation and immobilized in  $\square$  conditions did not yield any significant photocurrent ( $(0.24 \pm 0.15)$   $\mu\text{A cm}^{-2}$  and  $(0.07 \pm 0.01)$   $\mu\text{A cm}^{-2}$  for Wd and Wd, respectively). The statistical analysis of photochronoamperometry experiments indicates that photocurrent was only significant ( $p <$



0.05, Tables Appendix D.5 and Appendix D.6) for samples with cells immobilized by [REDACTED] and previously grown in replete ( $(2.1 \pm 0.6) \mu\text{A cm}^{-2}$ ) or [REDACTED] deprived ( $(0.93 \pm 0.17) \mu\text{A cm}^{-2}$ ) media. [REDACTED] deprived cells attached to electrodes by desiccation did not produce significant photocurrent. The absence of photocurrent in [REDACTED] starved [REDACTED] cells might be due to severe photodamage since no fluorescence was observed in these samples, as mentioned above. The lower photocurrent obtained from cells deprived of [REDACTED], might be related with lower photosynthetic efficiency, higher photoinhibition (Figure 5.3 and 5.4) and decreased Chl *a* content (about a 61% lower) than that of cells grown in replete medium.

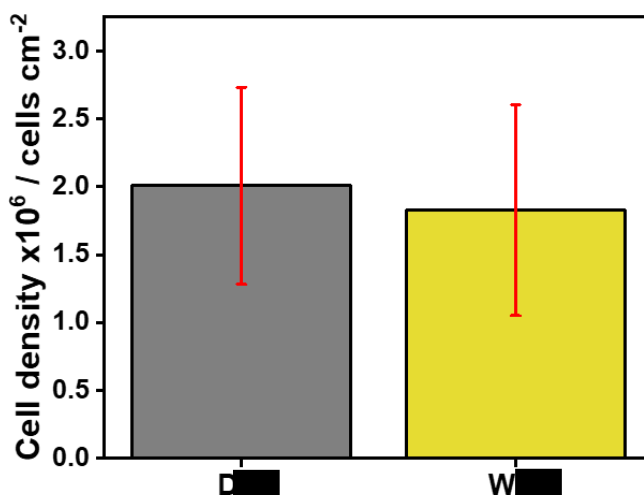


**Figure 5.6.** Comparison of average cell density for *C. vulgaris* immobilized by [REDACTED] (D) and by [REDACTED] immobilization (W) on GCE/oCNT/PAPBA electrodes. Cell densities were calculated from fluorescence micrographs using red excitation light. Error bands indicate standard deviation ( $n=3$ ).

To discard the effect of the immobilization efficiency on the photocurrent, the algal coating on the electrodes surface was

examined by fluorescence microscopy, on account of Chl *a* autofluorescence (Figure Appendix D.4). These observations were performed only for cells grown in replete medium. The degree of immobilization was similar for [REDACTED] immobilization, yielding cell densities on the electron surface of  $(2.0 \pm 0.7) \times 10^6$  cell  $\text{cm}^{-2}$  and  $(1.8 \pm 0.8) \times 10^6$  cell  $\text{cm}^{-2}$ , respectively (Figure 5.6). Therefore, the higher photocurrent in [REDACTED] electrodes was not related to a higher immobilization efficiency.

#### 5.3.2.4. Assessment of [REDACTED] stress and photodamage:

A deeper analysis of the fluorescence induction curves of cells grown in replete media was conducted to evaluate the effect of [REDACTED] on the photosynthetic efficiency and to assess photodamage. Although the  $\Phi$  PSII,  $\Phi$  NPQ and  $\Phi$  NO are competing processes, i.e., the sum of the three quantum yields is unity ( $\Phi$  PSII +  $\Phi$  NPQ +  $\Phi$  NO = 1), this work especially focuses on the changes in  $\Phi$  PSII and  $\Phi$  NPQ when cells are exposed to harsh conditions, since the processes underlying the non-regulated non-photochemical fluorescence quenching are still not completely understood.

For sake of comparison, the photochemical and non-photochemical quantum yields were estimated for cells attached to the electrodes by the two immobilization approaches and for cell suspensions (Figure 5.7a-c). As stated above, *C. vulgaris* cell suspensions showed good physiological state and were used as control. The quantum yield profile upon actinic light and in the recovery time in the dark for cells immobilized in [REDACTED] conditions ( $\Phi$  PSII<sub>(w)</sub>,  $\Phi$  NPQ<sub>(w)</sub> and  $\Phi$  NO<sub>(w)</sub>, Figure 5.7b) was comparable to that of cell suspensions (Figure 5.7a).

As expected, the  $\Phi$  PSII decreased upon actinic light in all cases due to the partial closure of RCII as a consequence of the accumulation of reduced plastoquinone intermediate A ( $Q_A^-$ ) and due to the light induction of various types of non-photochemical energy losses [49]. Despite that the light-induced energy dissipation upon actinic light increased when cells were immobilized under [REDACTED] conditions compared to cell suspensions ( $\Phi$  NPQ<sub>(w)</sub> >  $\Phi$  NPQ<sub>(s)</sub>), the  $\Phi$  PSII<sub>(w)</sub> was almost fully recovered (92%) after 30 minutes in darkness, revealing that this immobilization approach keeps the cells with good photosynthetic performance and discarding a harmful effect of the applied potential on the cells. The slight effect of the applied voltage on the photosynthetic efficiency has also been observed by Cinciato et al. with biofilms of *Chlorella* sp [50].

Conversely, the photosynthetic efficiency was acutely reduced when *C. vulgaris* cells were immobilized by [REDACTED] ( $F_v/F_{M(D)} = 0.37 \pm 0.04$ ) (Figure 5.7c), which was a 45% less than that of cell suspensions. This value is consistent with that reported by Gray et al. [19] for *Chlorella* sp. subdued to [REDACTED]. It should be noted that although the [REDACTED]. [REDACTED] The  $\Phi$  PSII<sub>(D)</sub> after 30 min post-illumination was  $0.09 \pm 0.04$  ( $\approx 23\%$  recovery). The low  $\Phi$  PSII<sub>(D)</sub> could be due to photodamage of RCII or due to a highly induced photoprotective energy dissipation processes that prevent PSII from photodamage [51,52].

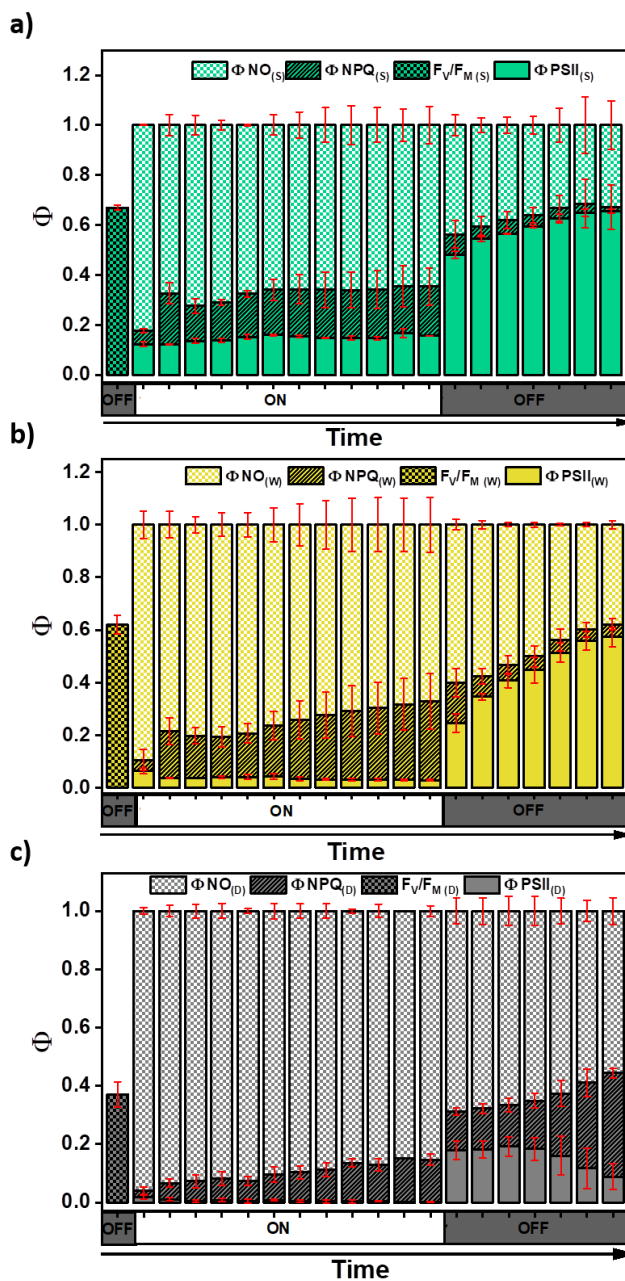


**Figure 5.7.** Average of photochemical, light-regulated non-photochemical and non-regulated non-photochemical quantum yields ( $F_v/F_M$ ,  $\Phi PSII$ ,  $\Phi NPQ$  and  $\Phi NO$ , respectively) of *C. vulgaris* (a) in suspension (S) and attached to GCE/oCNT/PAPBA by (b) ■ immobilization (W) and (c) ■ (D). Error bars indicate standard deviation ( $n = 3$ ).

---

Photodamage can be evaluated by monitoring the relaxation of  $\Phi$  NPQ during a recovery time in darkness post-illumination. The  $\Phi$  NPQ is the sum of three components: i) high-energy-state quenching (qE), which is induced by an acidification of the thylakoid lumen that activates the xanthophyll cycle towards the conversion of zeaxanthin; ii) state transition quenching (qT) that involves the phosphorylation of LHCII followed by binding of the LHCII to PSI; and iii) photoinhibitory quenching (qI), which is related both to an inactivation and/or degradation of D1 protein and to a sustained photoprotective energy dissipation. These NPQ components can be discriminated by their relaxation time, with qE relaxing in about 30 s to 1 min, qT having a half-time relaxation of 5 to 8 min and qI with a half-time relaxation of 20 min to more [53–56]. Therefore, at 30 min of recovery, we can assume that the  $\Phi$  NPQ is mainly qI, since qE and qT are completely relaxed.

$\Phi$  NPQ<sub>(s)</sub> (Figure 5.7a) and  $\Phi$  NPQ<sub>(w)</sub> (Figure 5.7b) at the end of the recovery time were very low ( $0.015 \pm 0.09$  and  $0.05 \pm 0.02$ , respectively). Conversely, the persistence of high  $\Phi$  NPQ<sub>(D)</sub> after 30 min in darkness post-illumination (Figure 5.7c) confirmed photoinhibition in [REDACTED] cells, which suggests either an inactivation or damage of RCII [57] or an exacerbated slow and sustained activation of the xanthophyll cycle conversion of violaxanthin to zeaxanthin [58–60].

To corroborate the permanent closure of RCII for cells immobilized by [REDACTED], the  $q_p$ , which estimates the fraction of open RCII, was measured after illumination [61,62]. Figure 5.8a shows  $q_p$  during the

recovery time in darkness for cell suspensions and for cells immobilized onto electrodes by the two approaches. The  $q_p$  after 30 min in darkness post-illumination for cell suspensions ( $1.0 \pm 0.9$ ) and wet immobilization ( $0.97 \pm 0.01$ ) indicated that almost all the RCII were open, thus corroborating that there was no photoinhibition. On the contrary, the  $q_p$  of cells immobilized by [redacted] increased just after switching off the light but sharply decayed after 30 min in dark ( $0.33 \pm 0.12$ ), implying severe photodamage with 67% of the RCII permanently closed [54,63]. Thus, the results of  $F_v/F_M(D)$ ,  $\Phi$  PSII(D),  $q_{p(D)}$  and  $\Phi$ NPQ(D) confirm that [redacted] stress causes severe photodamage in *C. vulgaris*.

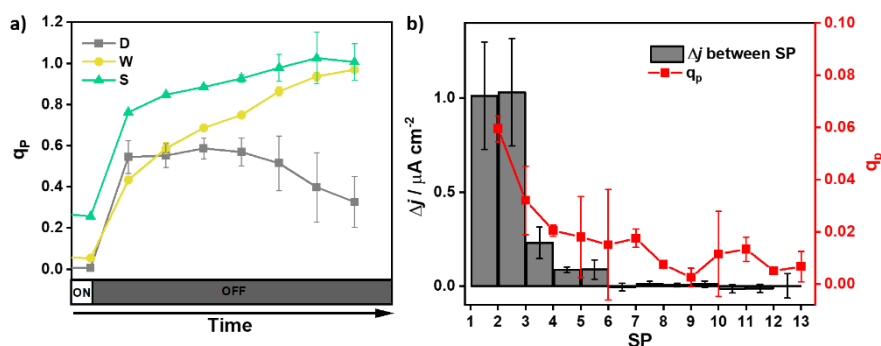


**Figure 5.8.** (a) Coefficient of photochemical fluorescence quenching ( $q_p$ ) upon actinic light and in the recovery time (dark) of *C. vulgaris* in suspension (S) and attached to GCCE/oCNT/PAPBA electrodes by [redacted] immobilization (W) and by [redacted] (D). (b) Increase in photocurrent between saturation pulses (SPs) ( $\Delta j$ , bars) and  $q_p$  (red squares) calculated from the simultaneous chronoamperometry and PAM-fluorometry measurements of *C. vulgaris* immobilized by [redacted] on GCE/oCNT/PAPBA electrodes. Error bars stand for standard deviation ( $n = 3$ ).  $E_{app} = 0.2 \text{ V}$  vs. Ag/AgCl/sat KCl. Electrolyte: PB pH 7. Actinic light ([redacted]).

### 5.3.3. Origin of the photocurrent:

The photocurrent was proved to be originated from the photosynthetic machinery since the addition of 50  $\mu\text{M}$  of DCMU

decreased the photocurrent to zero (Figure Appendix D.5). DCMU blocks the reduction of the quinolone intermediate  $Q_B$  by the  $Q_A$ , therefore, prevents the electron transfer downstream of the PSII in the PETC [64,65].

Moreover, a closer examination of the correlation between photocurrent and the fraction of open RCII revealed that PSII was involved in the photocurrent generation. Figure 5.8b shows the increase in photocurrent between successive SPs ( $\Delta j$ ) and the  $q_p$  at each SP during a fluorescence induction curve for *C. vulgaris* immobilized by XXXXXXXXXX on GCE/oCNT/PAPBA electrode. The first SP was performed in the dark, where all the RCII are supposed to be open, and the rest of SP were executed upon continuous illumination.

At the onset of illumination, the photocurrent sharply increased coinciding with higher fraction of open RCII. Next, there was an expected decrease of  $q_p$  with time upon actinic light due to the reduction of the PETC. When the fraction of open RCII was below 0.02, the photocurrent kept constant at its maximum ( $(2.1 \pm 0.6) \mu\text{A cm}^{-2}$ ), with just small fluctuations. These results confirm that the overreduction of PSII limited the photocurrent generation. However, the collection of electrons by the electrode translated into a reduced pressure over the PETC since not only higher maximum photosynthetic efficiencies were attained compared to *C. vulgaris*-based bioelectrode without applied potential ( $F_V/F_M = 0.19 \pm 0.08$ ) but also higher immediate post-illumination  $\Phi_{PSII}$  were observed

( $0.18 \pm 0.03$  and  $0.08 \pm 0.05$ , for with and without applied potential, respectively) (Figure 5.7c compared to Figure Appendix D.6).

#### 5.3.4. Analysis of the ultrastructure of *C. vulgaris* [REDACTED]

Furthermore, the ultrastructure of *C. vulgaris* cells exposed and unexposed to [REDACTED] was analyzed by TEM (Figure 5.9). In both conditions, cells showed the typical globular-ellipsoidal shape and the characteristic pyrenoid of *C. vulgaris* (embedded between two starch plates with a double-layered thylakoid crossing the pyrenoid matrix) [66,67]. Cells [REDACTED] did not show cytoplasm retraction. Although the majority of the [REDACTED] cells presented a thinner cell wall (Figure 5.9e and f) than that of the unexposed cells, whose inner layer (lower electron density [68]) appeared to be thicker (Figure 5.9d), they preserved the typical chitosan-like microfibrillar structure composed of glucosamine (Figure 5.9d-f) [67,69]. Furthermore, cell wall remnants and some degree of cell wall disruption were appreciable only in [REDACTED] cells, especially if they had thinner cell wall (Figure 5.9f). That supports our hypothesis that [REDACTED] causes cell wall and membrane disruption facilitating the electron transfer from the cell to the electrode.

In [REDACTED] cells, thylakoids appeared well ordered and occurred in stacks of three to six (Figure 5.9d), indicating good physiological state. On the contrary, thylakoids appeared to be unstacked and disordered in most of the [REDACTED] cells (Figure 5.9e and f). Unstacking of thylakoids has been related to reduced photosynthetic capacity [70,71]. Thylakoid membranes contain the photosynthetic apparatus (PSII, electron carriers and PSI). PSII complexes are



located along the stacked region of the thylakoid and PSI are positioned in the stroma. The photosynthetic efficiency not only depends on the intramembrane thylakoid interactions, i.e., linear electron transport from PSII to PSI, but also depends on the intermembrane thylakoid interactions in the stacked region. Thus, the unstacking of thylakoids might explain the low photosynthetic efficiencies and high photoinhibition observed in our work for [REDACTED] cells. Our results are in agreement with that of Petrova et al. [70], which reported that the unstacking of thylakoids leads to higher degree of state transitions, where LHCII disassembled from PSII to attach PSI, resulting in higher non-photochemical heat dissipation and lower photochemical use of excitation energy.

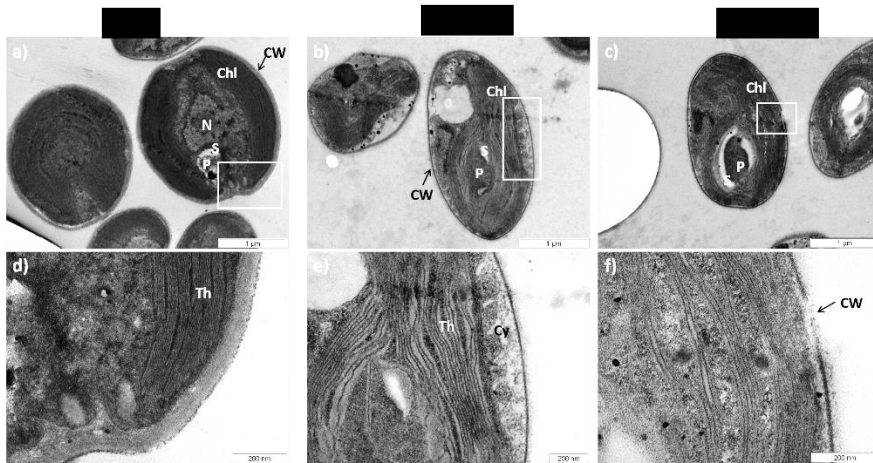


**Figure 5.9.** TEM micrographs of *C. vulgaris* unexposed (a, d) and exposed to [REDACTED] (b, c, e, f). Bottom row are the magnifications of the regions marked by the white rectangles in the upper micrographs. Chl, chloroplast; CW, cell wall; Cy, cytoplasm; N, nucleus; P, pyrenoid; S, starch; Th, thylakoid.

#### 5.4. Conclusions

The effect of different [REDACTED] stresses on the exoelectrogenesis of *C. vulgaris* has been evaluated by combining chronoamperometry and PAM fluorometry. *C. vulgaris*-based biophotoelectrodes were constructed by [REDACTED] immobilization of cells on the electrode surface. Although both immobilization approaches resulted in similar degree of cell immobilization, photocurrent was only obtained when cells were immobilized by [REDACTED] starved cells did not produce fluorescence, reflecting severe photodamage, and consequently no photocurrent could be retrieved from them.

PAM fluorometry measurements revealed that [REDACTED] and [REDACTED] starvation led to reduced photosynthetic capacity but not to photodamage, unless cells were [REDACTED]. The addition of DCMU demonstrated that the PSII is involved in the photocurrent generation. Moreover, the correlation of the increase in photocurrent with the fraction of open RCII and the further stagnation of the photocurrent coinciding with the highest fraction of closed RCII confirmed the overreduction of PSII as the bottleneck in the photocurrent generation.

Furthermore, disruption and reduction of the thickness of the cell wall were observed in the TEM micrographs of cells subdued to [REDACTED], supporting our hypothesis that [REDACTED] enhances the cell-to-electrode electron transfer process due to the disruption of biological barriers. Further analysis of potential electron shuttles released upon slight disruption of cell wall and membranes is aim of

future work. Additionally, cells exposed to [REDACTED] presented unstacked thylakoids, which correlated with the decline of photosynthetic efficiency and photoinhibition observed for these cells. The absence of photocurrent in cells immobilized in [REDACTED] conditions even under nutrient deprivation, suggests that exoelectrogenesis was improved by [REDACTED] stress and not by nutrient starvation. These findings encourage the exposure of photosynthetic microorganisms to [REDACTED] in order to improve the power efficiency of BPV devices whenever it does not compromise the integrity of their photosynthetic apparatus. Thus, [REDACTED]-tolerant species, which keep their physiological photosynthetic capacity while their cell walls are mildly disrupted [REDACTED], are promising target species of future research in BPVs.

## References

- [1] A.J. McCormick, P. Bombelli, A.M. Scott, A.J. Philips, A.G. Smith, A.C. Fisher, C.J. Howe, Photosynthetic biofilms in pure culture harness solar energy in a mediatorless biophotovoltaic cell (BPV) system., *Energy Environ. Sci.* 4 (2011) 4699–4709. <https://doi.org/10.1039/c1ee01965a>.
- [2] F.-L. Ng, S.-M. Phang, V. Periasamy, J. Beardall, K. Yunus, A.C. Fisher, Algal biophotovoltaic (BPV) device for generation of bioelectricity using *Synechococcus elongatus* (Cyanophyta), *J. Appl. Phycol.* 30 (2018) 2981–2988. <https://doi.org/10.1007/s10811-018-1515-1>.
- [3] N. Sekar, Y. Umasankar, R.P. Ramasamy, Photocurrent generation by immobilized cyanobacteria via direct electron transport in photo-bioelectrochemical cells, *Phys. Chem. Chem. Phys.* 16 (2014) 7862–7871. <https://doi.org/10.1039/c4cp00494a>.
- [4] J. Tschörtner, B. Lai, J.O. Krömer, Biophotovoltaics: green power generation from sunlight and water, *Front. Microbiol.* 10 (2019) 866. <https://doi.org/10.3389/fmicb.2019.00866>.
- [5] L.T. Wey, P. Bombelli, X. Chen, J.M. Lawrence, C.M. Rabideau, S.J.L. Rowden, J.Z. Zhang, C.J. Howe, The development of biophotovoltaic systems for power generation and biological analysis, *ChemElectroChem.* 6 (2019) 5375–5386. <https://doi.org/10.1002/celec.201900997>.
- [6] Y.A. Gorby, S. Yanina, J.S. McLean, K.M. Rosso, D. Moyles, A. Dohnalkova, T.J. Beveridge, I. Seop Chang, B. Hong Kim, K. Shik Kim, D.E. Culley, S.B. Reed, M.F. Romine, D.A. Saffarini, E.A. Hill, L. Shi, D.A. Elias, D.W. Kennedy, G. Pinchuk, K. Watanabe, I. Ishii, B. Logan, K.H. Nealson, J.K. Fredrickson, Electrically conductive bacterial nanowires produced by *Shewanella oneidensis* strain MR-1 and other microorganisms, *Proc. Natl. Acad. Sci.* 103 (2006) 11358–11363. <https://doi.org/10.1073/pnas.0604517103>.
- [7] S. Sure, A.A.J. Torriero, A. Gaur, L.H. Li, Y. Chen, C. Tripathi, A. Adholeya, M.L. Ackland, M. Kochar, Inquisition of *Microcystis aeruginosa* and *Synechocystis* nanowires:

- characterization and modelling, *Antonie Van Leeuwenhoek*. 108 (2015) 1213–1225. <https://doi.org/10.1007/s10482-015-0576-2>.
- [8] S. Sure, A.A.J. Torriero, A. Gaur, L. Hua, Y. Chen, C. Tripathi, A. Adholeya, M.L. Ackland, M. Kochar, Identification and topographical characterisation of microbial nanowires in *Nostoc punctiforme*, *Antonie Van Leeuwenhoek*. 109 (2016) 475–480. <https://doi.org/10.1007/s10482-015-0644-7>.
- [9] L.T. Wey, J.M. Lawrence, X. Chen, R. Clark, D.J. Lea-smith, J.Z. Zhang, C.J. Howe, A biophotoelectrochemical approach to unravelling the role of cyanobacterial cell structures in exoelectrogenesis, *Electrochim. Acta*. 395 (2021) 139214. <https://doi.org/10.1016/j.electacta.2021.139214>.
- [10] M.A. Thirumurthy, A. Hitchcock, A. Cereda, J. Liu, M.S. Chavez, B.L. Doss, R. Ros, M.Y. El-naggar, J.T. Heap, T.S. Bibby, A.K. Jones, Type IV pili-independent photocurrent production by the cyanobacterium *Synechocystis* sp. PCC6803, *Front. Microbiol.* 11 (2020) 1344. <https://doi.org/10.3389/fmicb.2020.01344>.
- [11] Y. Shlosberg, B. Eichenbaum, T.N. Tóth, G. Levin, V. Liveanu, G. Schuster, N. Adir, NADPH performs mediated electron transfer in cyanobacterial-driven biophotoelectrochemical cells, *IScienc.* 24 (2021) 101892. <https://doi.org/10.1016/j.isci.2020.101892>.
- [12] G. Saper, D. Kallmann, F. Conzuelo, F. Zhao, T.N. Tóth, V. Liveanu, S. Meir, J. Szymanski, A. Aharoni, W. Schuhmann, A. Rothschild, G. Schuster, N. Adir, Live cyanobacteria produce photocurrent and hydrogen using both the respiratory and photosynthetic systems, *Nat. Commun.* 9 (2018) 2168. <https://doi.org/10.1038/s41467-018-04613-x>.
- [13] C.W. Mullineaux, Co-existence of photosynthetic and respiratory activities in cyanobacterial thylakoid membranes, *BBA - Bioenerg.* 1837 (2014) 503–511. <https://doi.org/10.1016/j.bbabi.2013.11.017>.
- [14] T. Ogawa, K. Suzuki, K. Sonoike, Respiration interacts with photosynthesis through the acceptor side of photosystem I,

- reflected in the dark-to-light induction kinetics of chlorophyll fluorescence in the cyanobacterium *Synechocystis* sp. PCC6803, *Front. Plant Sci.* 12 (2021) 717968. <https://doi.org/10.3389/fpls.2021.717968>.
- [15] I. Moro, N. La Rocca, N. Rascio, Photosynthetic apparatus in cyanobacteria and microalgae, in: M. Pessaraki (Ed.), *Handb. Photosynth.*, 3rd ed., CRC Press, 2016: pp. 349–367.
- [16] H.G. Weger, G.S. Espie, Ferric reduction by iron-limited *Chlamydomonas* cells interacts with both photosynthesis and respiration, *Planta.* 210 (2000) 775–781. <https://doi.org/10.1007/s004250050679>.
- [17] A.C. Gonzalez-Aravena, K. Yunus, L. Zhang, B. Norling, A.C. Fisher, Tapping into cyanobacteria electron transfer for higher exoelectrogenic activity by imposing iron limited growth, *RSC Adv.* 8 (2018) 20263–20274. <https://doi.org/10.1039/c8ra00951a>.
- [18] A. Holzinger, U. Karsten, Desiccation stress and tolerance in green algae: Consequences for ultrastructure, physiological, and molecular mechanisms, *Front. Plant Sci.* 4 (2013) 1–18. <https://doi.org/10.3389/fpls.2013.00327>.
- [19] D.W. Gray, L.A. Lewis, Z.G. Cardon, Photosynthetic recovery following desiccation of desert green algae (Chlorophyta) and their aquatic relatives, *Plant, Cell Environ.* 30 (2007) 1240–1255. <https://doi.org/10.1111/j.1365-3040.2007.01704.x>.
- [20] N. Schuback, C. Schallenberg, C. Duckham, M.T. Maldonado, P.D. Tortell, Interacting effects of light and iron availability on the coupling of photosynthetic electron transport and CO<sub>2</sub>-assimilation in marine phytoplankton, *PLoS One.* 10 (2015) e0133235. <https://doi.org/10.1371/journal.pone.0133235>.
- [21] A. Alderkamp, G.L. van Dijken, K.E. Lowry, K.M. Lewis, H.L. Joy-Warren, W. van de Poll, P. Laan, L. Gerringa, T.O. Delmont, B.D. Jenkins, K.R. Arrigo, Effects of iron and light availability on phytoplankton photosynthetic properties in the Ross Sea, *Mar. Ecol. Prog. Ser.* 621 (2019) 33–50. <https://doi.org/10.3354/meps13000>.
- [22] A.-C. Alderkamp, G. Kulk, A.G.J. Buma, R.J.W. Visser, G.L.

- Van Dijken, M.M. Mills, K.R. Arrigo, The effect of iron limitation on the photophysiology of *Phaeocystis antarctica* (Prymnesiophyceae) and *Fragilariopsis cylindrus* (Bacillariophyceae) under dynamic irradiance, *J. Phycol.* 48 (2012) 45–59. <https://doi.org/10.1111/j.1529-8817.2011.01098.x>.
- [23] S. White, A. Anandraj, F. Bux, PAM fluorometry as a tool to assess microalgal nutrient stress and monitor cellular neutral lipids, *Bioresour. Technol.* 102 (2011) 1675–1682. <https://doi.org/10.1016/j.biortech.2010.09.097>.
- [24] O. Herlory, J. Bonzom, R. Gilbin, Sensitivity evaluation of the green alga *Chlamydomonas reinhardtii* to uranium by pulse amplitude modulated ( PAM ) fluorometry, *Aquat. Toxicol.* 140–141 (2013) 288–294. <https://doi.org/10.1016/j.aquatox.2013.06.007>.
- [25] A.T. Lombardi, M.T. Maldonado, The effects of copper on the photosynthetic response of *Phaeocystis cordata*, *Photosynth. Res.* 108 (2011) 77–87. <https://doi.org/10.1007/s11120-011-9655-z>.
- [26] A. Nikolaou, A. Bernardi, A. Meneghesso, F. Bezzo, T. Morosinotto, B. Chachuat, A model of chlorophyll fluorescence in microalgae integrating photoproduction, photoinhibition and photoregulation, *J. Biotechnol.* 194 (2015) 91–99. <https://doi.org/10.1016/j.jbiotec.2014.12.001>.
- [27] E.D. Fleming, B.M. Bebout, R.W. Castenholz, Effect of salinity and light intensity on the resumption of photosynthesis in rehydrated cyanobacterial mats from Baja California Sur, Mexico, *J. Phycol.* 43 (2007) 15–24. <https://doi.org/10.1111/j.1529-8817.2006.00297.x>.
- [28] J. Pruvost, G. Van Vooren, G. Cogne, J. Legrand, Investigation of biomass and lipids production with *Neochloris oleoabundans* in photobioreactor, *Bioresour. Technol.* 100 (2009) 5988–5995. <https://doi.org/10.1016/j.biortech.2009.06.004>.
- [29] V.S. Ferreira, R.F. Pinto, C. Sant’ Anna, Low light intensity and nitrogen starvation modulate the chlorophyll content of *Scenedesmus dimorphus*, *J. Appl. Microbiol.* 120 (2015) 661–

670. <https://doi.org/10.1111/jam.13007>.
- [30] R.J. Ritchie, Consistent sets of spectrophotometric chlorophyll equations for acetone, methanol and ethanol solvents, *Photosynth. Res.* 89 (2006) 27–41. <https://doi.org/10.1007/s11120-006-9065-9>.
- [31] A.R. Wellburn, The spectral determination of chlorophylls *a* and *b*, as well as total carotenoids, using various solvents with spectrophotometers of different resolution, *J. Plant Physiol.* 144 (1994) 307–313. [https://doi.org/10.1016/S0176-1617\(11\)81192-2](https://doi.org/10.1016/S0176-1617(11)81192-2).
- [32] K. Oxborough, N.R. Baker, Resolving chlorophyll *a* fluorescence images of photosynthetic efficiency into photochemical and non-photochemical components—calculation of  $qP$  and  $Fv'/Fm'$  without measuring  $Fo'$ , *Photosynth. Res.* 54 (1997) 135–142. <https://doi.org/10.1023/A:1005936823310>.
- [33] Y. Kodama, Time gating of chloroplast autofluorescence allows clearer fluorescence imaging in planta, *PLoS One.* 11 (2016) e0152484. <https://doi.org/10.1371/journal.pone.0152484>.
- [34] Z. Kim, K. Kim, H. Park, C.S. Lee, S.W. Nam, K.J. Yim, J.Y. Jung, S. Hong, C. Lee, Enhanced fatty acid productivity by *Parachlorella* sp., a freshwater microalga, via adaptive laboratory evolution under salt stress, *Biotechnol. Bioprocess Eng.* 26 (2021) 223–231. <https://doi.org/10.1007/s12257-020-0001-1>.
- [35] J.A. Raven, M.C.W. Evans, R.E. Korb, The role of trace metals in photosynthetic electron transport in  $O_2$ -evolving organisms, *Photosynth. Res.* 60 (1999) 111–149. <https://doi.org/10.1023/A:1006282714942>.
- [36] J.C. Pushnik, G.W. Miller, J.H. Manwaring, The role of iron in higher plant chlorophyll biosynthesis, maintenance and chloroplast biogenesis, *J. Plant Nutr.* 7 (1984) 733–758. <https://doi.org/10.1080/01904168409363238>.
- [37] G.E. Kroh, M. Pilon, Regulation of iron homeostasis and use in chloroplasts, *Int. J. Mol. Sci.* 21 (2020) 3395.



<https://doi.org/10.3390/ijms21093395>.

- [38] J.A. Berges, D.O. Charlebois, D.C. Mauzerall, P.G. Falkowski, Differential effects of nitrogen limitation on photosynthetic efficiency of photosystems I and II in microalgae, *Plant Physiol.* 110 (1996) 689–696. <https://doi.org/10.1104/pp.110.2.689>.
- [39] S. Jazzar, N. Berrejeb, C. Messaoud, M.N. Marzouki, I. Smaali, Growth parameters, photosynthetic performance, and biochemical characterization of newly isolated green microalgae in response to culture condition variations, *Appl. Biochem. Biotechnol.* 179 (2016) 1290–1308. <https://doi.org/10.1007/s12010-016-2066-z>.
- [40] Y. Zhang, H. Chen, C. He, Q. Wang, Nitrogen starvation induced oxidative stress in an oil-producing green alga *Chlorella sorokiniana* C3, *PLoS One.* 8 (2013) e69225. <https://doi.org/10.1371/journal.pone.0069225>.
- [41] Y. Gao, M. Yang, C. Wang, Nutrient deprivation enhances lipid content in marine microalgae, *Bioresour. Technol.* 147 (2013) 484–491. <https://doi.org/10.1016/j.biortech.2013.08.066>.
- [42] H.V. Perales-Vela, R. Velasco García, E.A. Gómez-Juárez, M.O. Salcedo-Álvarez, R.O. Cañizares-Villanueva, Streptomycin affects the growth and photochemical activity of the alga *Chlorella vulgaris*, *Ecotoxicol. Environ. Saf.* 132 (2016) 311–317. <https://doi.org/10.1016/j.ecoenv.2016.06.019>.
- [43] P. Juneau, P.J. Harrison, Comparison by PAM fluorometry of photosynthetic activity of nine marine phytoplankton grown under identical conditions, *Photochem. Photobiol.* 81 (2005) 649–653. <https://doi.org/10.1111/j.1751-1097.2005.tb00239.x>.
- [44] S.M. Rincon, N.F. Urrego, K.J. Avila, H.M. Romero, H. Beyenal, Photosynthetic activity assessment in mixotrophically cultured *Chlorella vulgaris* biofilms at various developmental stages, *Algal Res.* 38 (2019) 101408. <https://doi.org/10.1016/j.algal.2019.101408>.

- [45] E.A. Gwózdź, J.D. Bewley, E.B. Tucker, Studies on protein synthesis in *Tortula ruralis*, *J. Exp. Bot.* 25 (1974) 599–608. <https://doi.org/10.1093/jxb/25.4.599>.
- [46] M.J. Oliver, J.D. Bewley, Plant desiccation and protein synthesis. IV. RNA synthesis, stability and recruitment of RNA into protein synthesis during desiccation and rehydration of the desiccation-tolerant moss, *Tortula ruralis*, *Plant Physiol.* 74 (1984) 21–25. <https://doi.org/10.1104/pp.74.1.21>.
- [47] M. Loebel, A.M. Cockshutt, D.A. Campbell, Z. V Finkel, Physiological basis for high resistance to photoinhibition under nitrogen depletion in *Emiliania huxleyi*, *Limnol. Oceanogr.* 55 (2010) 2150–2160. <https://doi.org/10.4319/lo.2010.55.5.2150>.
- [48] M. Kamalanathan, M. Pierangelini, L.A. Shearman, R. Gleadow, J. Beardall, Impacts of nitrogen and phosphorus starvation on the physiology of *Chlamydomonas reinhardtii*, *J. Appl. Phycol.* 28 (2016) 1509–1520. <https://doi.org/10.1007/s10811-015-0726-y>.
- [49] U. Schreiber, Pulse-amplitude-modulation (PAM) fluorometry and saturation pulse method: an overview., in: G. Papageorgiou G.C. (Ed.), *Chlorophyll a Fluoresc. Adv. Photosynth. Respir.* Vol 19, 1st ed., Springer Netherlands, Dordrecht, 2004: pp. 279–319. [https://doi.org/10.1007/978-1-4020-3218-9\\_11](https://doi.org/10.1007/978-1-4020-3218-9_11).
- [50] G.P.M.K. Ciniciato, F.-L. Ng, S.-M. Phang, M. Musoddig Jaafar, A.C. Fisher, K. Yunus, V. Periasamy, Investigating the association between photosynthetic efficiency and generation of biophotocurrent in autotrophic microbial fuel cells, *Sci. Rep.* 6 (2016) 31193. <https://doi.org/10.1038/srep31193>.
- [51] G.H. Krause, E. Weis, Chlorophyll fluorescence and photosynthesis: the basics, *Annu. Rev. Plant Physiol. Plant Mol. Biol.* 42 (1991) 313–349. <https://doi.org/10.1146/annurev.pp.42.060191.001525>.
- [52] S. Takahashi, N. Murata, How do environmental stresses accelerate photoinhibition?, *Trends Plant Sci.* 13 (2008) 178–182. <https://doi.org/10.1016/j.tplants.2008.01.005>.

- [53] D. Lazár, Parameters of photosynthetic energy partitioning, *J. Plant Physiol.* 175 (2015) 131–147. <https://doi.org/10.1016/j.jplph.2014.10.021>.
- [54] V. Giovagnetti, A. V Ruban, Discerning the effects of photoinhibition and photoprotection on the rate of oxygen evolution in *Arabidopsis* leaves, *J. Photochem. Photobiol. B Biol.* 152 (2015) 272–278. <https://doi.org/10.1016/j.jphotobiol.2015.09.010>.
- [55] Z. Li, S. Wakao, B.B. Fischer, K.K. Niyogi, Sensing and responding to excess light, *Annu. Rev. Plant Biol.* 60 (2009) 239–260. <https://doi.org/10.1146/annurev.arplant.58.032806.103844>.
- [56] L. Guidi, E. Lo Piccolo, M. Landi, Chlorophyll fluorescence, photoinhibition and abiotic stress: does it make any difference the fact to be a C3 or C4 species?, *Front. Plant Sci.* 10 (2019) 1–11. <https://doi.org/10.3389/fpls.2019.00174>.
- [57] E. Aro, I. Virgin, B. Andersson, Photoinhibition of photosystem II . Inactivation, protein damage and turnover, *Biochim. Biophys. Acta (BBA)- Bioenerg.* 1143 (1993) 113–134. [https://doi.org/10.1016/0005-2728\(93\)90134-2](https://doi.org/10.1016/0005-2728(93)90134-2).
- [58] W.. Adams III, B. Demmig-Adams, T.. Rosenstiel, A.. Brightwell, V. Ebbert, Photosynthesis and photoprotection in overwintering plants, *Plant Biol.* 4 (2002) 545–557. <https://doi.org/10.1055/s-2002-35434>.
- [59] P. Horton, A. V Ruban, R.G. Walters, Regulation of light harvesting in green plants, *Annu. Rev. Plant Physiol. Plant Mol. Biol.* 47 (1996) 655–84. <https://doi.org/10.1146/annurev.arplant.47.1.655>.
- [60] P. Horton, M. Wentworth, A. Ruban, Control of the light harvesting function of chloroplast membranes : The LHCII-aggregation model for non-photochemical quenching, *FEBS Lett.* 579 (2005) 4201–4206. <https://doi.org/10.1016/j.febslet.2005.07.003>.
- [61] O. Van Kooten, J.F.H. Snel, The use of fluorescence nomenclature in plant stress physiology, *Photosynth. Res.* 25 (1990) 147–150. <https://doi.org/10.1007/BF00033156>.

- [62] U. Schreiber, U. Schliwa, W. Bilger, Continuous recording of photochemical and non-photochemical chlorophyll fluorescence quenching with a new type of modulation fluorometer, *Photosynth. Res.* 10 (1986) 51–62. <https://doi.org/10.1007/BF00024185>.
- [63] A. V Ruban, E.H. Murchie, Assessing the photoprotective effectiveness of non-photochemical chlorophyll fluorescence quenching: A new approach, *BBA - Bioenerg.* 1817 (2012) 977–982. <https://doi.org/10.1016/j.bbabi.2012.03.026>.
- [64] A. Trebst, Inhibitors in the functional dissection of the photosynthetic electron transport system, *Photosynth. Res.* 92 (2007) 217–224. <https://doi.org/10.1007/s11120-007-9213-x>.
- [65] W. Oettmeier, H.J. Soll, Competition between plastoquinone and 3-(3,4-dichlorophenyl)-1,1-dimethylurea at the acceptor side of Photosystem II, *Biochim. Biophys. Acta - Bioenerg.* 724 (1983) 287–290. [https://doi.org/10.1016/0005-2728\(83\)90147-0](https://doi.org/10.1016/0005-2728(83)90147-0).
- [66] T. Ikeda, H. Takeda, Species-specific differences of pyrenoids in *Chlorella* (Chlorophyta), *J. Phycol.* 31 (1995) 813–818. <https://doi.org/10.1111/j.0022-3646.1995.00813.x>.
- [67] Y. Němcová, T. Kalina, Cell wall development, microfibril and pyrenoid structure in type strains of *Chlorella vulgaris*, *C. kessleri*, *C. sorokiniana* compared with *C. luteoviridis* (Trebouxiophyceae, Chlorophyta), *Appl. Stud.* 100 (2000) 95–105. [https://doi.org/10.1127/ALGOL\\_STUD/100/2000/95](https://doi.org/10.1127/ALGOL_STUD/100/2000/95).
- [68] H.G. Gerken, B. Donohoe, E.P. Knoshaug, Enzymatic cell wall degradation of *Chlorella vulgaris* and other microalgae for biofuels production, *Planta.* 237 (2013) 239–253. <https://doi.org/10.1007/s00425-012-1765-0>.
- [69] E. Kapaun, W. Reisser, A chitin-like glycan in the cell wall of a *Chlorella* sp. (Chlorococcales, Chlorophyceae), *Planta.* 197 (1995) 577–582. <https://doi.org/10.1007/BF00191563>.
- [70] N. Petrova, S. Todinova, M. Paunov, L. Kovács, S. Taneva, S. Krumova, Thylakoid membrane unstacking increases LHCII thermal stability and lipid phase fluidity, *J. Bioenerg. Biomembr.* 50 (2018) 425–435.

<https://doi.org/10.1007/s10863-018-9783-7>.

- [71] Z. Gojkovic, C. Vílchez, R. Torronteras, J. Vígara, V. Gómez-Jacinto, N. Janzer, J.-L. Gómez-Ariza, I. Márová, I. Garbayo, Effect of selenate on viability and selenomethionine accumulation of *Chlorella sorokiniana* grown in batch culture, *Sci. World J.* 2014 (2014) 401265. <https://doi.org/10.1155/2014/401265>.

## Conclusions and Future work

The overall goal of this thesis was to enhance the cell-to-electrode electron transfer of cellular-based BPV's bioanodes. To achieve that, we considered to approach strategies at the level of the anode's architecture and the ability of the cell to exoelectrogenesis.

Chapter 2 and 4 were focused on designing novel bioanode architectures based on boronic acid residues, which can covalently bind to saccharides of the cell surface. In more detail, a poly(3-aminophenylboronic acid) nanostructured electrode was constructed in chapter 2 with outstanding photocurrent generation from *C. vulgaris*. The current was confirmed to be originated from the photoexcitation of PSII and no excreted electron shuttles were detected. ESEM images showed that the cells were embedded within the conducting polymer, which appeared to establish intimate contact with the cell surface. These findings suggest that PAPBA electrochemically wires the electron transfer from the cell to the electrode. Furthermore, PAPBA proved to enhanced the electron transfer of another 5 photosynthetic microorganisms. Nevertheless, this biophotocathode exhibited poor stability compromising their application in BPVs.

Other ICPs related with PAPBA were evaluated as platforms to construct bioanodes in Chapter 3. Polymers of un- and substituted anilines were successfully synthesized by electrochemical and chemical methods. The polymers' structure, the effect of the electronic properties and the position of the substituents in the aniline

ring were assessed by CV, XPS and UPS. All polymers with electron donor substituents were photoactive and the photoresponse observed was rather due to the polymer than to the *C. vulgaris*. Conversely, photocurrent from *C. vulgaris* was obtained when cells were immobilized on PANI and all polymers with electron acceptors substituents. Among all of them, PAPBA outperformed the photocurrent generation of *C. vulgaris*.

Exploiting the ability of boronic acid to bind to the cell surface, a bioanode consisting of *C. vulgaris* functionalized with 3-APBA and embedded in a POs hydrogel was constructed in chapter 4. An improved integration of the cells with the redox polymer was observed when cells were functionalized with 3-APBA, which resulted in an enhanced photocurrent and stability of the hydrogel. A proof-of-concept BPV cell was assembled by coupling the bioanode to a BOD-based biocathode. The ET mechanism was investigated by comparing the action spectrum of the bioanode with that of the Chl *a*, adding electron mediators and inhibitors and by SPECM. It was found that electrons might stem from alternative electron transport pathways linked to PSI that are activated under stress conditions (e.g., high light intensity). It is noteworthy that the ET mechanism of *C. vulgaris* immobilized on PAPBA-modified electrodes was different to that of *C. vulgaris* embedded in POs hydrogel.

In the last part of the present thesis, we studied the effect of different [REDACTED] stresses on the exoelectrogenesis of GCE/oCNT/PAPBA\_ *C. vulgaris* biophotoelectrodes by combining

CA and PAM-fluorometry. [REDACTED] starvation and [REDACTED] produced a decline in the photosynthetic efficiency indicating that cells were under stress. However, photocurrent was only generated when cells were [REDACTED]. TEM images showed that [REDACTED] cells presented thinner cell wall than not-desiccated cells and certain degree of cell wall disruption, which might promote the exoelectrogenesis. Nevertheless, TEM and PAM -fluorometry revealed that [REDACTED] cells exhibited photoinhibition compromising the integrity of the photosynthetic machinery.

Overall, this thesis provides additional knowledge about the structure-properties relationships of materials to be used in the development of bioanodes for their application in BPVs and other bioelectrochemical systems. Moreover, this work encourages the use of boronic acid derivatives to construct tailor-made bioanodes for cellular-based BPVs.

### **Future work**

- ⚙ To increase the stability of PAPBA-based bioanodes by copolymerization with molecules that modify the local pH improving the doping of the polymer.
- ⚙ To evaluate other ICPs (like PEDOT:PSS and PP) as anchoring and wiring materials to construct bioanodes for cellular-based BPVs.
- ⚙ To assess the photocurrent performance of [REDACTED] tolerant species with PAPBA-based bioanodes under [REDACTED] conditions.



- ⚙ To explore other mild disruption techniques and stressing agents to improve the photocurrent performance and stability of *C. vulgaris*-based bioanodes.

## Appendix A:

### Supplementary material of Chapter 2

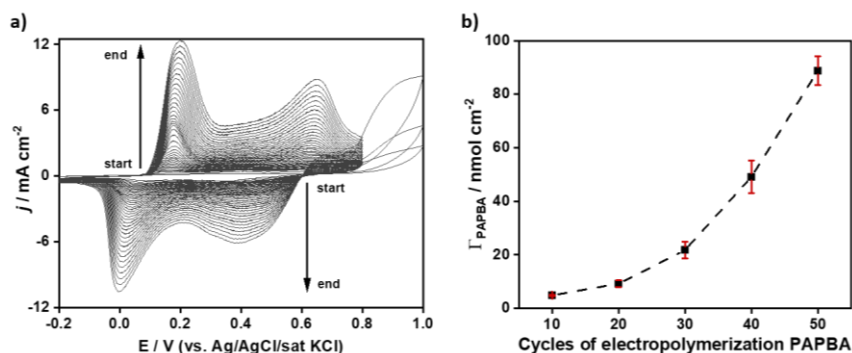


**Figure Appendix A.1.** (a) Cyclic voltammograms of the electropolymerization 40 mM 3-aminophenylboronic acid (3-APBA) with [redacted] ([redacted]). Scan rate:  $0.1 \text{ V s}^{-1}$ . (b) Surface area coverage of poly(3-aminophenylboronic acid) PAPBA at different number of electropolymerization cycles determined from the cyclic voltammograms in 0.2 M HCl monomer free solution ( $n = 3$ ). Error bars represent the standard deviation.

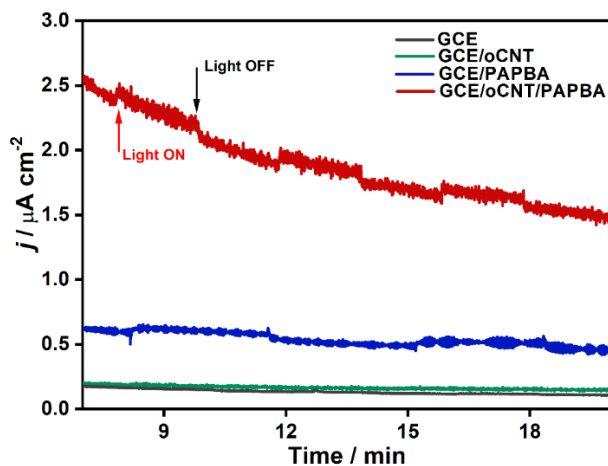


**Figure Appendix A.2.** Chronoamperograms recorded in 0.1 M PB pH 7 at 0.2 V vs. Ag/AgCl/sat KCl of bare GCE, GCE/oCNT, GCE/PAPBA and GCE/oCNT/PAPBA electrodes incubated with the supernatant of *C. vulgaris*. Irradiation of [redacted] incident white light. Red and black arrows indicate light ON and OFF, respectively.

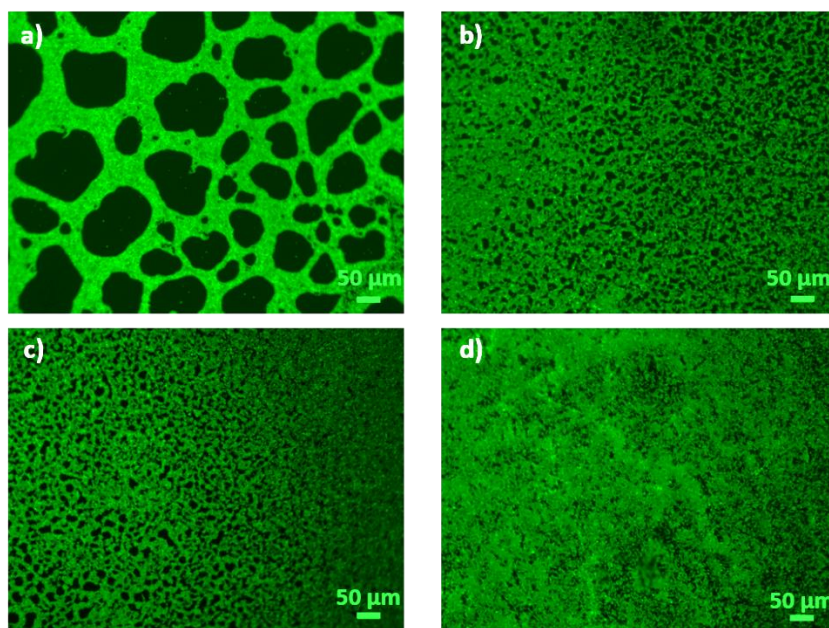


**Figure Appendix A.3.** Fluorescence micrographs of *C. vulgaris* attached on (a) GCE, (b) GCE/oCNT, (c) GCE/PAPBA and (d) GCE/oCNT/PAPBA electrodes excited with red light.

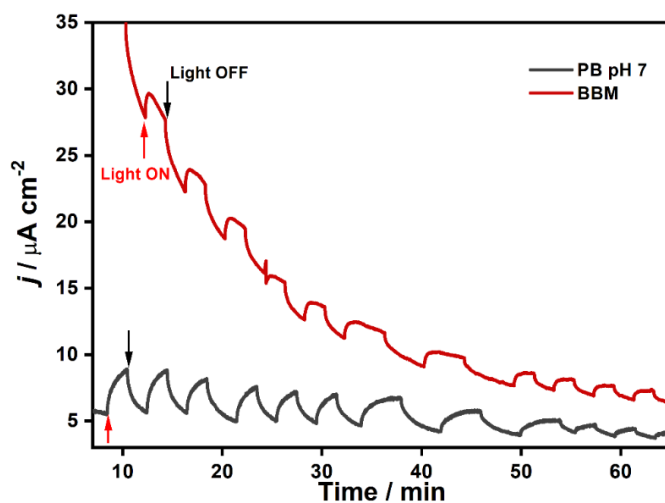


**Figure Appendix A.4.** Chronoamperogram of *C. vulgaris* immobilized on GCE/oCNT/PAPBA electrodes recorded in 0.1M PB pH 7 and in fresh BBM for 1 h of successive illumination cycles.  $E_{\text{app}} = 0.2 \text{ V vs (Ag/AgCl/sat KCl)}$ . Irradiation of  $90 \mu\text{mol photons m}^{-2} \text{ s}^{-1}$  incident white light. Red and black arrows indicate light ON and OFF, respectively.

**Table Appendix A.1.** Comparative profile of photocurrent densities reported for *Chlorella vulgaris* in a mediator-less system.

<i>Working electrode/ anode</i>	<i>Counter electrode/ cathode</i>	<i>Cell setup</i>	<i>Maximum current density (<math>\mu\text{A cm}^{-2}</math>)</i>	<i>Ref.</i>
<b>ITO/alginate</b>	Pt coated glass	BPV	$0.10 \pm 0.04^{\text{a}}$	[1]
<b>FTO/ceramic</b>	Activated carbon cloth	BPV	$0.20^{\text{b}}$	[2]
<b>ITO/alginate</b>	Pt coated glass	BPV	$0.64^{\text{b}}$	[3]
<b>ITO coated glass</b>	Pt coated glass	BPV	$0.10 \pm 0.05^{\text{a}}$	[4]
<b>RGO coated glass</b>	Pt coated glass	BPV	$0.03 \pm 0.05^{\text{a}}$	[4]
<b>ITO/alginate</b>	Pt coated glass	BPV	$0.68 \pm 0.03^{\text{b}}$	[5]
<b>GCE/oCNT/PAPBA</b>	Pt wire	CA	$1.98 \pm 0.65^{\text{c}}$	*

<sup>a)</sup> Data calculated from article <sup>b)</sup> Without current density in dark subtracted <sup>c)</sup> Current density from the third cycle of light, not maximum current density. \* stands for “this work”.

#### References:

- [1] F.L. Ng, S.M. Phang, V. Periasamy, K. Yunus, A.C. Fisher, Enhancement of power output by using alginate immobilized algae in biophotovoltaic Devices, *Sci. Rep.* 7 (2017) 16237. <https://doi.org/10.1038/s41598-017-16530-y>.
- [2] R. Thorne, H. Hu, K. Schneider, P. Bombelli, A. Fisher, L.M. Peter, A. Dent, P.J. Cameron, Porous ceramic anode materials for photo-microbial fuel cells, *J. Mater. Chem.* 21 (2011) 18055–18060. <https://doi.org/10.1039/c1jm13058g>.

- [3] C. Thong, S. Phang, F. Ng, V. Periasamy, T. Ling, K. Yunus, A.C. Fisher, Effect of different irradiance levels on bioelectricity generation from algal biophotovoltaic (BPV) devices, *Energy Sci. Eng.* 7 (2019) 2086–2097. <https://doi.org/10.1002/ese3.414>.
- [4] F.-L. Ng, M.M. Jaafar, S.-M. Phang, Z. Chan, N.A. Salleh, S.Z. Azmi, K. Yunus, A.C. Fisher, V. Periasamy, Reduced graphene oxide anodes for potential application in algae biophotovoltaic platforms, *Sci. Rep.* 4 (2014) 7562. <https://doi.org/10.1038/srep07562>.
- [5] F.L. Ng, S.M. Phang, B.L. Lan, V. Kalavally, C.H. Thong, K.T. Chong, V. Periasamy, K. Chandrasekaran, G.G. Kumar, K. Yunus, A.C. Fisher, Optimised spectral effects of programmable LED arrays (PLA)s on bioelectricity generation from algal-biophotovoltaic devices, *Sci. Rep.* 10 (2020) 16105. <https://doi.org/10.1038/s41598-020-72823-9>.

## Appendix B:

### Supplementary material of Chapter 3

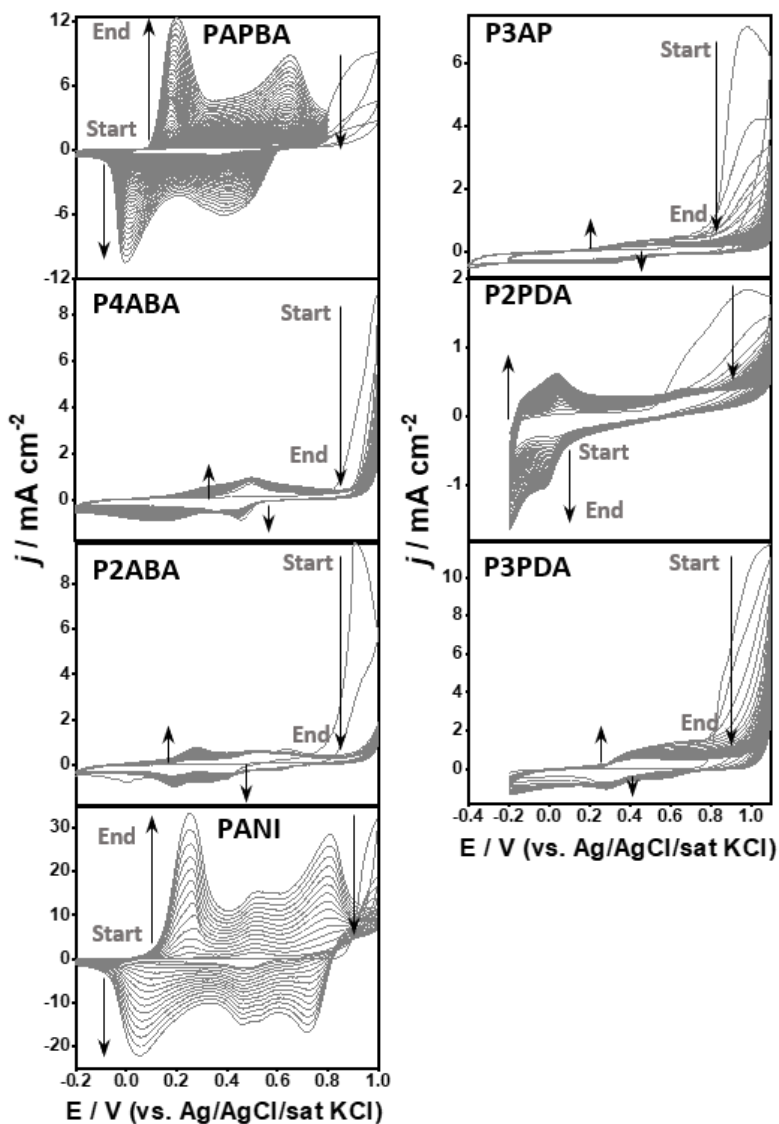


**Figure Appendix B.1.** Cyclic voltammograms of the electropolymerization of homopolymers of aniline (PANI) and substituted aniline (i.e., PAPBA, P4ABA, P2ABA, P3AP, P2PDA and P3PDA). Arrows indicate the timecourse of the electropolymerization.

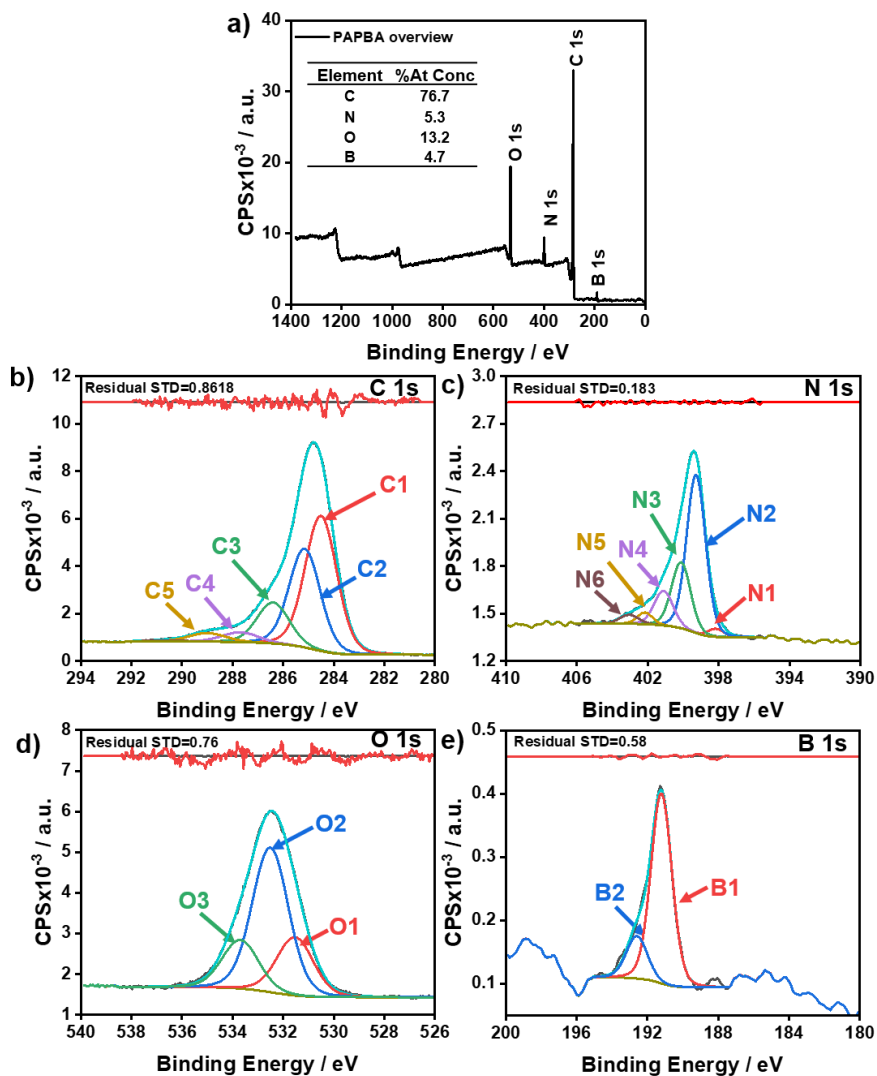


**Figure Appendix B.2.** (a) Survey XPS spectra of GCE/oCNT/PAPBA. Inset: table of element composition. High resolution XPS spectra in the (b) C 1s, (c) N 1s, (d) O 1s and (e) B 1s regions of GCE/oCNT/PAPBA electrodes.

**Table Appendix B.2.** Contribution (in %) of all components resulting from the fitting of high resolution XPS spectra in each element region of the GCE/oCNT/PAPBA:

<i>Name</i>	<i>Assignment</i>	<i>Position</i>	<i>Line Shape</i>	<i>FWHM</i>	<i>%Area</i>
<b>C1</b>	C-C/C-H	284.5	LA(1.53,243)	1.47	45.6
<b>C2</b>	C-C/C-H	285.2	LA(1.53,243)	1.45	32.8
<b>C3</b>	C-N/C=N	286.4	LA(1.53,243)	1.50	14.1
<b>C4</b>	C-N <sup>+</sup> /C=N <sup>+</sup>	287.7	LA(1.53,243)	1.70	3.8
<b>C5</b>	O-C=O	289.0	LA(1.53,243)	1.70	3.3
<b>C6</b>	Shake-up	290.6	LA(1.53,243)	1.43	0.4
<b>N1</b>	-N=	398.2	LA(1.53,243)	1.05	2.4
<b>N2</b>	-HN-	399.3	LA(1.53,243)	1.26	55.7
<b>N3</b>	-HN <sup>+</sup> -	400.1	LA(1.53,243)	1.26	23.3
<b>N4</b>	=N <sup>+</sup> -	401.1	LA(1.53,243)	1.26	12.2
<b>N5</b>	-HN <sup>+</sup> -	402.2	LA(1.53,243)	1.00	3.3
<b>N6</b>	H <sub>2</sub> N <sup>+</sup> -	403.0	LA(1.53,243)	1.26	3.1
<b>O1</b>	O=C	531.5	LA(1.53,243)	1.70	23.2
<b>O2</b>	O-B	532.5	LA(1.53,243)	1.69	57.4
<b>O3</b>	O-C	533.7	LA(1.53,243)	1.70	19.4
<b>B1</b>	B-OH tetrahedral	191.2	LA(1.53,243)	1.39	81.8
<b>B2</b>	B-OH trigonal	192.6	LA(1.53,243)	1.39	18.2



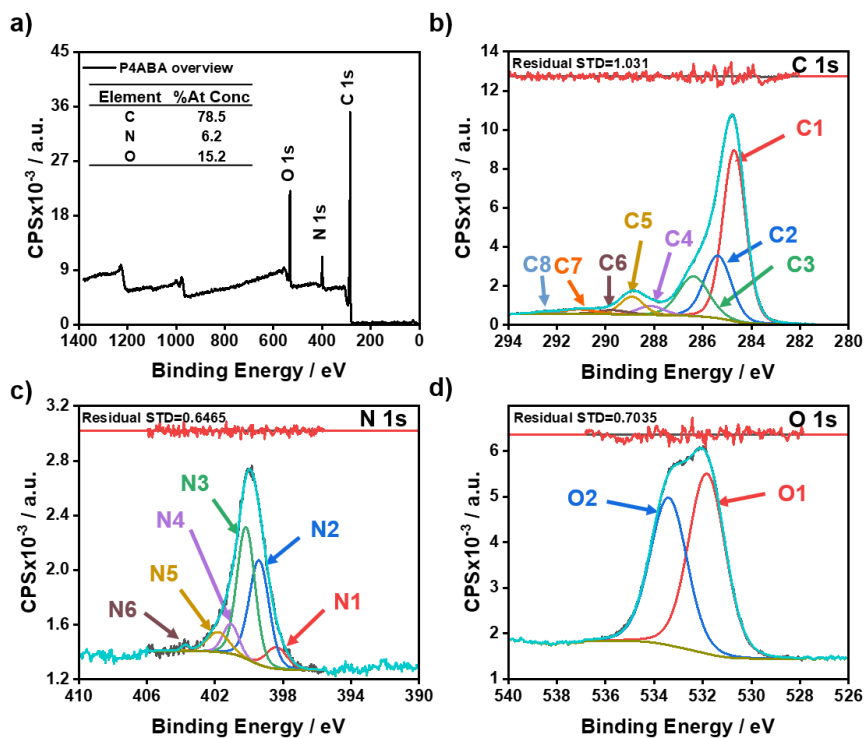


**Figure Appendix B.3.** (a) Survey XPS spectra of GCE/oCNT/P4ABA. Inset: table of element composition. High resolution XPS spectra in the (b) C 1s, (c) N 1s, (d) O 1s regions of GCE/oCNT/P4ABA electrodes.

**Table Appendix B.3.** Contribution (in %) of all components resulting from the fitting of high resolution XPS spectra in each element region of the GCE/oCNT/P4ABA:

<i>Name</i>	<i>Assignment</i>	<i>Position</i>	<i>Line Shape</i>	<i>FWHM</i>	<i>%Area</i>
<b>C1</b>	C-C/C-H	284.7	LA(1.53,243)	1.11	50.3
<b>C2</b>	C-C/C-H	285.4	LA(1.53,243)	1.30	21.6
<b>C3</b>	C-N/C=N	286.4	LA(1.53,243)	1.47	15.5
<b>C4</b>	C-N <sup>+</sup> /C=N <sup>+</sup>	288.1	LA(1.53,243)	1.29	3.0
<b>C5</b>	C=O	288.9	LA(1.53,243)	1.13	5.4
<b>C6</b>	O-C=O	289.7	LA(1.53,243)	1.54	1.7
<b>C7</b>	Shake-up	291.1	LA(1.53,243)	1.64	2.0
<b>C8</b>	Shake-up	292.4	LA(1.53,243)	1.23	0.6
<b>N1</b>	-N=	398.4	LA(1.53,243)	1.46	7.8
<b>N2</b>	-HN-	399.4	LA(1.53,243)	1.38	35.5
<b>N3</b>	-HN <sup>+</sup> -	400.2	LA(1.53,243)	1.25	40.6
<b>N4</b>	=N <sup>+</sup> -	401.1	LA(1.53,243)	1.09	8.0
<b>N5</b>	-HN <sup>+</sup> -	401.8	LA(1.53,243)	1.51	7.5
<b>N6</b>	H <sub>2</sub> N <sup>+</sup> -	403.8	LA(1.53,243)	0.50	0.7
<b>O1</b>	O=C	531.8	LA(1.53,243)	1.78	55.0
<b>O2</b>	O-C	533.4	LA(1.53,243)	1.78	45.0

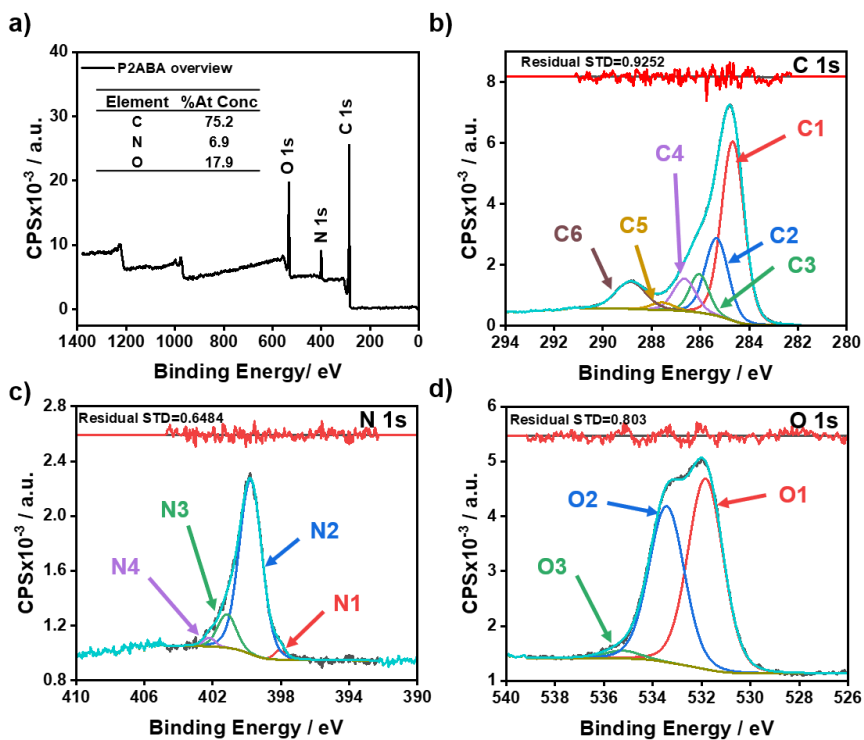


**Figure Appendix B.4.** (a) Survey XPS spectra of GCE/oCNT/P2ABA. Inset: table of element composition. High resolution XPS spectra in the (b) C 1s, (c) N 1s, (d) O 1s regions of GCE/oCNT/P2ABA electrodes.

**Table Appendix B.4.** Contribution (in %) of all components resulting from the fitting of high resolution XPS spectra in each element region of the GCE/oCNT/P2ABA:

<i>Name</i>	<i>Assignment</i>	<i>Position</i>	<i>Line Shape</i>	<i>FWHM</i>	<i>%Area</i>
<b>C1</b>	C-C/C-H	284.7	LA(1.53,243)	1.09	49.0
<b>C2</b>	C-C/C-H	285.3	LA(1.53,243)	1.11	21.6
<b>C3</b>	C-N/C=N	286.1	LA(1.53,243)	0.92	8.8
<b>C4</b>	C-N <sup>+</sup> /C=N <sup>+</sup>	286.7	LA(1.53,243)	1.08	8.7
<b>C5</b>	C=O, O-C-O	287.6	LA(1.53,243)	1.10	2.1
<b>C6</b>	O-C=O	288.9	LA(1.53,243)	1.45	9.8
<b>N1</b>	-N=	398.1	LA(1.53,243)	0.73	2.1
<b>N2</b>	-HN-	399.8	LA(1.53,243)	1.56	82.8
<b>N3</b>	=N <sup>+</sup> -	401.2	LA(1.53,243)	1.27	13.0
<b>N4</b>	-HN <sup>+</sup> -	402.2	LA(1.53,243)	0.80	2.1
<b>O1</b>	O=C	531.8	LA(1.53,243)	1.70	53.8
<b>O2</b>	O-C	533.4	LA(1.53,243)	1.70	44.0
<b>O3</b>	H <sub>2</sub> O/Na KLL	535.3	LA(1.53,243)	1.70	2.0

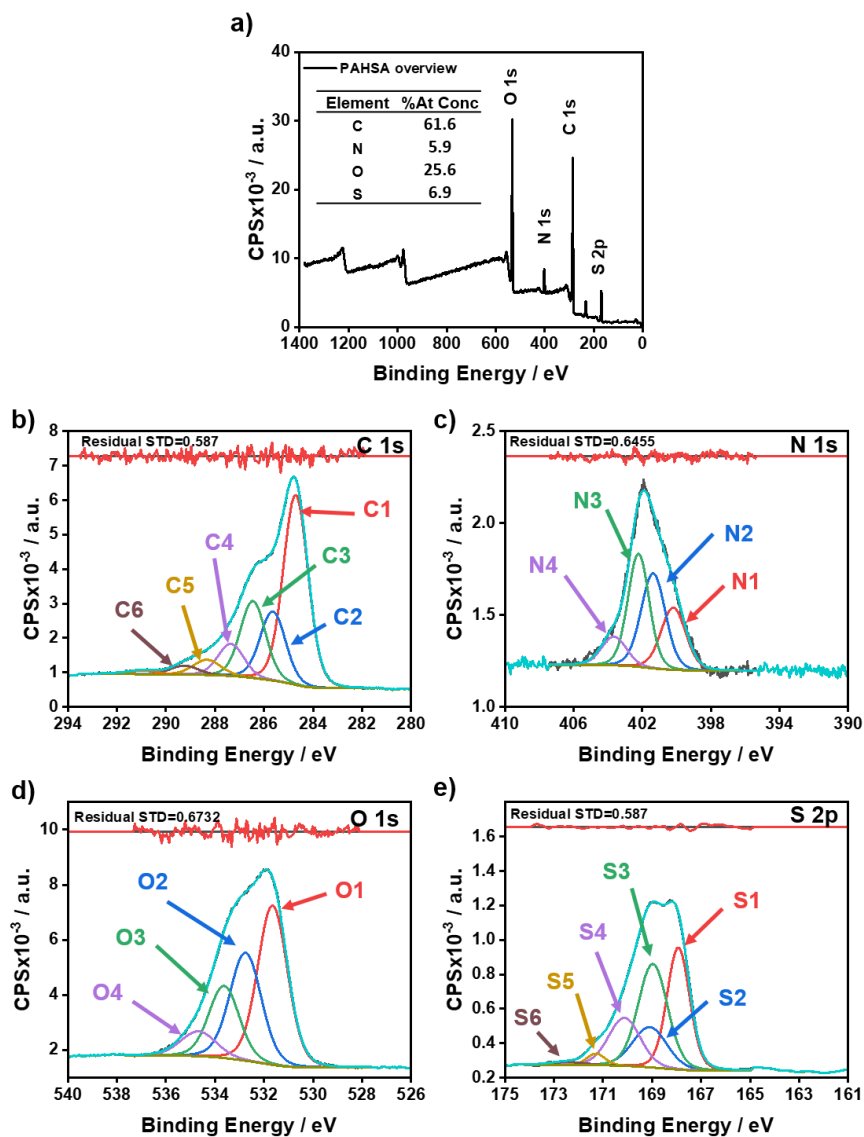


**Figure Appendix B.5.** (a) Survey XPS spectra of GCE/oCNT/PAHSA. Inset: table of element composition. High resolution XPS spectra in the (b) C 1s, (c) N 1s, (d) O 1s and (e) S 2p regions of GCE/oCNT/PAHSA electrodes.

**Table Appendix B.5.** Contribution (in %) of all components resulting from the fitting of high resolution XPS spectra in each element region of the GCE/oCNT/PAHSA:

<i>Name</i>	<i>Assignment</i>	<i>Position</i>	<i>Line Shape</i>	<i>FWHM</i>	<i>%Area</i>
<b>C1</b>	C-C/C-H	284.7	LA(1.53,243)	1.19	46.9
<b>C2</b>	C-C/C-H	285.6	LA(1.53,243)	1.22	17.5
<b>C3</b>	C-N/C=N/C-O	286.5	LA(1.53,243)	1.21	19.4
<b>C4</b>	C-N <sup>+</sup> /C=N <sup>+</sup>	287.4	LA(1.53,243)	1.24	8.3
<b>C5</b>	O-C-O	288.3	LA(1.53,243)	1.33	4.2
<b>C6</b>	O=C=O	289.3	LA(1.53,243)	1.37	2.5
<b>C7</b>	Shake-up	290.9	LA(1.53,243)	1.30	1.0
<b>C8</b>	Shake-up	292.1	LA(1.53,243)	1.63	0.3
<b>N1</b>	-HN <sup>+</sup> -	400.2	LA(1.53,243)	1.70	22.1
<b>N2</b>	=N <sup>+</sup> -	401.4	LA(1.53,243)	1.67	33.1
<b>N3</b>	-HN <sup>+</sup> -	402.2	LA(1.53,243)	1.46	34.5
<b>N4</b>	H <sub>2</sub> N <sup>+</sup> -	403.7	LA(1.53,243)	1.70	10.3
<b>O1</b>	O-S	531.7	LA(1.53,243)	1.43	42.3
<b>O2</b>	O=C-O	532.8	LA(1.53,243)	1.51	30.4
<b>O3</b>	O-C	533.6	LA(1.53,243)	1.46	19.5
<b>O4</b>	Adsorbed H <sub>2</sub> O	534.7	LA(1.53,243)	1.70	7.8
<b>S1</b>	S 2p 3/2 -SO <sub>3</sub> H	167.9	LA(1.53,243)	1.08	30.5
<b>S2</b>	S 2p 1/2	169.1	LA(1.53,243)	1.64	15.3
<b>S3</b>	S 2p 3/2 -SO <sub>3</sub> <sup>-</sup>	169.0	LA(1.53,243)	1.41	33.8
<b>S4</b>	S 2p 1/2	170.1	LA(1.53,243)	1.52	16.9
<b>S5</b>	S 2p 3/2 SO <sub>4</sub> <sup>2-</sup>	171.3	LA(1.53,243)	0.87	2.3
<b>S6</b>	S 2p 1/2	172.5	LA(1.53,243)	1.70	1.2

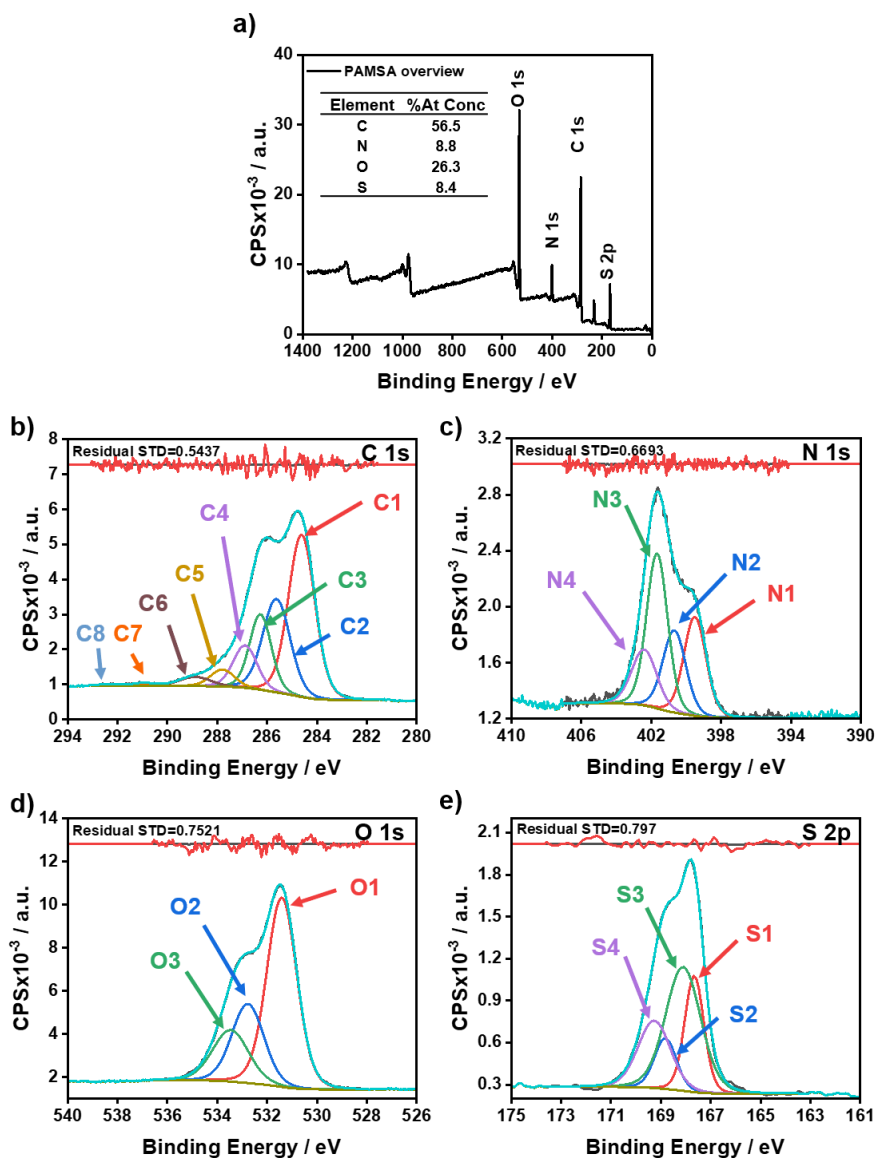


**Figure Appendix B.6.** (a) Survey XPS spectra of GCE/oCNT/PAMSA. Inset: table of element composition. High resolution XPS spectra in the (b) C 1s, (c) N 1s, (d) O 1s and (e) S 2p regions of GCE/oCNT/PAMSA electrodes.

**Table Appendix B.6.** Contribution (in %) of all components resulting from the fitting of high resolution XPS spectra in each element region of the GCE/oCNT/PAMSA:

<i>Name</i>	<i>Assignment</i>	<i>Position</i>	<i>Line Shape</i>	<i>FWHM</i>	<i>%Area</i>
<b>C1</b>	C-C/C-H	284.6	LA(1.53,243)	1.25	41.8
<b>C2</b>	C-C/C-H	285.6	LA(1.53,243)	1.29	24.9
<b>C3</b>	C-N/C=N/C-O	286.3	LA(1.53,243)	1.02	15.9
<b>C4</b>	C-N <sup>+</sup> /C=N <sup>+</sup>	286.9	LA(1.53,243)	1.12	9.8
<b>C5</b>	C=O	287.8	LA(1.53,243)	1.14	4.0
<b>C6</b>	O-C-O	288.9	LA(1.53,243)	1.48	2.8
<b>C7</b>	Shake-up	291.0	LA(1.53,243)	0.99	0.5
<b>C8</b>	Shake-up	292.4	LA(1.53,243)	1.04	0.3
<b>N1</b>	-HN-	399.5	LA(1.53,243)	1.49	25.1
<b>N2</b>	-HN <sup>+</sup> -	400.7	LA(1.53,243)	1.55	21.6
<b>N3</b>	=N <sup>+</sup> -	401.7	LA(1.53,243)	1.41	37.2
<b>N4</b>	-HN <sup>+</sup> -	402.4	LA(1.53,243)	1.70	16.1
<b>O1</b>	O-S	531.4	LA(1.53,243)	1.42	56.4
<b>O2</b>	O=C-O	532.8	LA(1.53,243)	1.51	25.2
<b>O3</b>	O-C	533.5	LA(1.53,243)	1.70	18.4
<b>S1</b>	S 2p 3/2 -SO <sub>3</sub> H	167.7	LA(1.53,243)	0.91	22.6
<b>S2</b>	S 2p 1/2	168.8	LA(1.53,243)	1.04	11.3
<b>S3</b>	S 2p 3/2 -SO <sub>3</sub> <sup>-</sup>	168.1	LA(1.53,243)	1.66	44.1
<b>S4</b>	S 2p 1/2	169.3	LA(1.53,243)	1.52	22.0



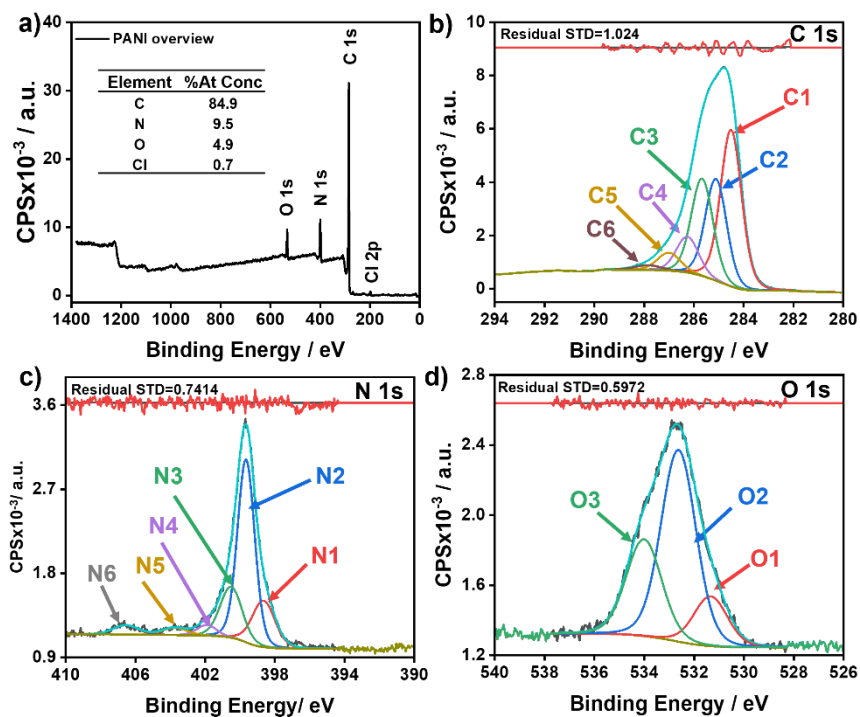


**Figure Appendix B.7.** (a) Survey XPS spectra of GCE/oCNT/PANI. Inset: table of element composition. High resolution XPS spectra in the (b) C 1s, (c) N 1s and (d) O 1s regions of GCE/oCNT/PANI electrodes.

**Table Appendix B.7.** Contribution (in %) of all components resulting from the fitting of high resolution XPS spectra in each element region of the GCE/oCNT/PANI:

<i>Name</i>	<i>Assignment</i>	<i>Position</i>	<i>Line Shape</i>	<i>FWHM</i>	<i>%Area</i>
<b>C1</b>	C-C/C-H	284.5	LA(1.53,190)	0.99	37.3
<b>C2</b>	C-C/C-H	285.1	LA(1.53,243)	1.01	24.3
<b>C3</b>	C-N/C=N	285.7	LA(1.53,243)	1.03	23.6
<b>C4</b>	C-N+/C=N+	286.3	LA(1.53,243)	1.05	8.9
<b>C5</b>	C-O	287.0	LA(1.53,243)	1.08	4.6
<b>C6</b>	C=O	287.8	LA(1.53,243)	1.25	1.4
<b>N1</b>	-N=	398.7	LA(1.53,243)	1.54	17.7
<b>N2</b>	-HN-	399.7	LA(1.53,243)	1.17	52.9
<b>N3</b>	-HN <sup>+</sup> -	400.5	LA(1.53,243)	1.49	18.8
<b>N4</b>	=N <sup>+</sup> -	401.9	LA(1.53,243)	1.31	3.5
<b>N4</b>	H <sub>2</sub> N <sup>+</sup> -	403.8	LA(1.53,243)	1.70	3.1
<b>N5</b>	Shake-up	406.6	LA(1.53,243)	1.70	4.0
<b>O1</b>	C=O	531.3	LA(1.53,243)	1.60	14.2
<b>O2</b>	C-O	532.6	LA(1.53,243)	1.65	56.6
<b>O3</b>	H <sub>2</sub> O ads	534.0	LA(1.53,243)	1.68	29.2

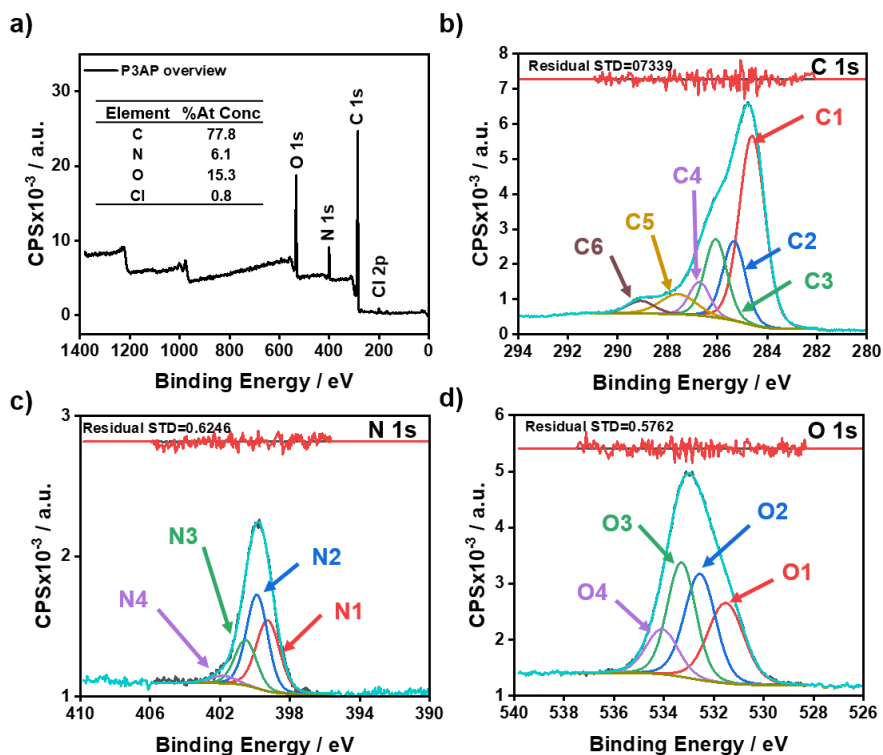


**Figure Appendix B.8.** (a) Survey XPS spectra of GCE/oCNT/P3AP. Inset: table of element composition. High resolution XPS spectra in the (b) C 1s, (c) N 1s and (d) O 1s regions of GCE/oCNT/P3AP electrodes.

**Table Appendix B.8.** Contribution (in %) of all components resulting from the fitting of high resolution XPS spectra in each element region of the GCE/oCNT/P3AP:

<i>Name</i>	<i>Assignment</i>	<i>Position</i>	<i>Line Shape</i>	<i>FWHM</i>	<i>%Area</i>
<b>C1</b>	C-C/C-H	284.6	LA(1.53,243)	1.22	47.8
<b>C2</b>	C-C/C-H	285.3	LA(1.53,243)	1.07	17.7
<b>C3</b>	C-N/C=N	286.1	LA(1.53,243)	1.06	17.2
<b>C4</b>	C-N+/C=N+	286.7	LA(1.53,243)	0.99	6.9
<b>C5</b>	C=O	287.6	LA(1.53,243)	1.70	7.1
<b>C6</b>	O-C-O	289.1	LA(1.53,243)	1.28	3.3
<b>N1</b>	-HN-	399.3	LA(1.53,243)	1.57	34.4
<b>N2</b>	-HN <sup>+</sup> -	399.9	LA(1.53,243)	1.43	41.2
<b>N3</b>	-HN <sup>+</sup> -	400.5	LA(1.53,243)	1.47	20.5
<b>N4</b>	=N <sup>+</sup> -	401.8	LA(1.53,243)	1.70	4.0
<b>O1</b>	O=C	531.5	LA(1.53,243)	1.71	26.6
<b>O2</b>	O-N/C-O-C	532.6	LA(1.53,243)	1.47	30.3
<b>O3</b>	O-C	533.3	LA(1.53,243)	1.35	29.9
<b>O4</b>	Adsorbed H <sub>2</sub> O	534.1	LA(1.53,243)	1.51	13.2

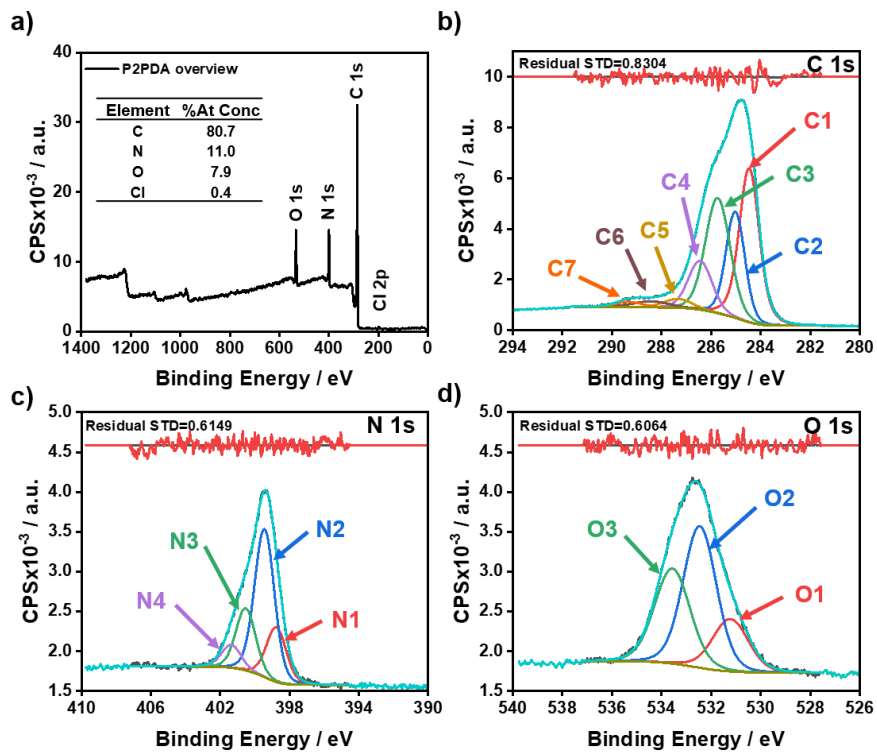


**Figure Appendix B.9.** (a) Survey XPS spectra of GCE/oCNT/P2PDA. Inset: table of element composition. High resolution XPS spectra in the (b) C 1s, (c) N 1s and (d) O 1s regions of GCE/oCNT/P2PDA electrodes.

**Table Appendix B.9.** Contribution (in %) of all components resulting from the fitting of high resolution XPS spectra in each element region of the GCE/oCNT/P2PDA:

<i>Name</i>	<i>Assignment</i>	<i>Position</i>	<i>Line Shape</i>	<i>FWHM</i>	<i>%Area</i>
<b>C1</b>	C-C/C-H	284.5	LA(1.62,120)	0.95	32.5
<b>C2</b>	C-C/C-H	285.0	LA(1.53,243)	0.89	20.5
<b>C3</b>	C-N/C=N	285.7	LA(1.53,243)	1.18	29.0
<b>C4</b>	C-N+/C=N+	286.4	LA(1.53,243)	1.13	11.9
<b>C5</b>	O-C-O	287.3	LA(1.53,243)	1.34	2.6
<b>C6</b>	C=O	288.4	LA(1.53,243)	1.7	2.2
<b>C7</b>	O-C=O	289.3	LA(1.53,243)	1.29	1.4
<b>N1</b>	=N-	398.8	LA(1.53,243)	1.36	19.1
<b>N2</b>	-HN-	399.5	LA(1.53,243)	1.34	51.5
<b>N3</b>	-HN <sup>+</sup> -	400.5	LA(1.53,243)	1.34	21.5
<b>N4</b>	=N <sup>+</sup> -	401.4	LA(1.53,243)	1.33	7.9
<b>O1</b>	O=C	531.2	LA(1.53,243)	1.69	18.8
<b>O2</b>	O-N/C-O-C	532.5	LA(1.53,243)	1.58	47.4
<b>O3</b>	O-C	533.6	LA(1.53,243)	1.68	33.8

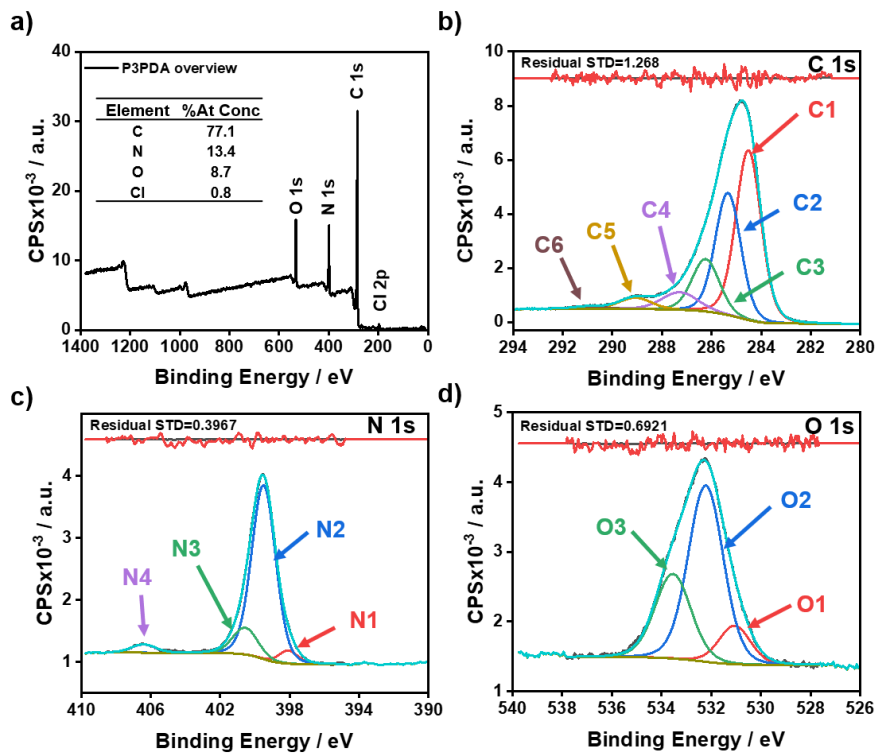


**Figure Appendix B.10.** (a) Survey XPS spectra of GCE/oCNT/P3PDA. Inset: table of element composition. High resolution XPS spectra in the (b) C 1s, (c) N 1s and (d) O 1s regions of GCE/oCNT/P3PDA electrodes.

**Table Appendix B.10.** Contribution (in %) of all components resulting from the fitting of high resolution XPS spectra in each element region of the GCE/oCNT/P3PDA:

<i>Name</i>	<i>Assignment</i>	<i>Position</i>	<i>Line Shape</i>	<i>FWHM</i>	<i>%Area</i>
<b>C1</b>	C-C/C-H	284.5	LA(1.53,200)	1.20	43.6
<b>C2</b>	C-C/C-H	285.3	LA(1.53,243)	1.21	31.5
<b>C3</b>	C-N/C=N	286.2	LA(1.53,243)	1.30	14.4
<b>C4</b>	C-N+/C=N+/C=O	287.3	LA(1.53,243)	1.70	6.3
<b>C5</b>	O-C=O	289.1	LA(1.53,243)	1.52	3.6
<b>C6</b>	Shake-up	290.9	LA(1.53,243)	1.31	0.6
<b>N1</b>	=N-	398.1	LA(1.53,243)	1.27	4.7
<b>N2</b>	-HN-	399.5	LA(1.53,243)	1.62	78.8
<b>N3</b>	-HN <sup>+</sup> -	400.6	LA(1.53,243)	1.70	12.7
<b>N4</b>	Shake-up	406.4	LA(1.53,243)	1.68	3.8
<b>O1</b>	O=C	531.1	LA(1.53,243)	1.49	11.7
<b>O2</b>	O-N/C-O-C	532.2	LA(1.53,243)	1.66	59.2
<b>O3</b>	O-C	533.5	LA(1.53,243)	1.70	29.1



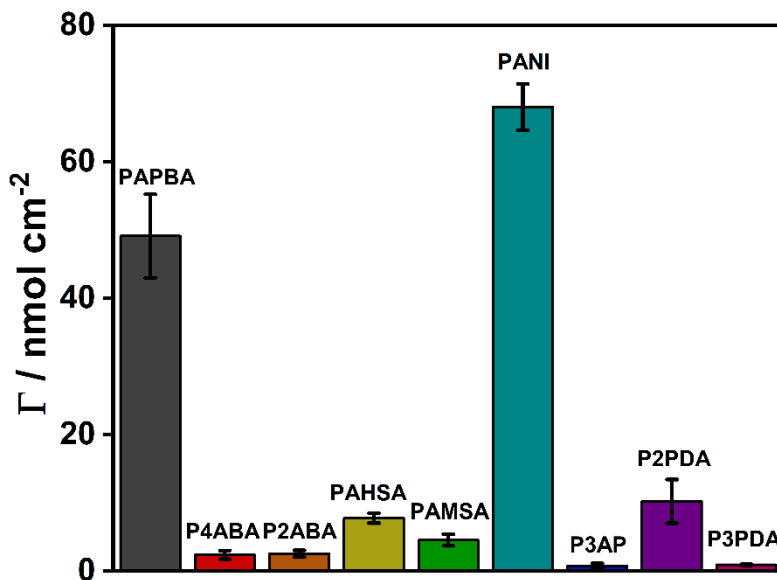


**Figure Appendix B.11.** Surface area coverage of the electrodepositing polymers of un- and substituted aniline on oCNT-modified glassy carbon electrodes calculated from CV recorded in acidic monomer-free solution ( $n = 3$ ). Error bars represent the standard deviation.

## Appendix C:

### Supplementary material of Chapter 4

**Table Appendix C.1.** Photocurrent generation and stability (percentage of remaining photocurrent after 3<sup>rd</sup> illumination cycle) for P-Os modified electrodes with and without *Chlorella* with and without 3-APBA. Calculated from chronoamperometric measurements. Mean (n = 3) ± standard deviation

<i>Electrode</i>	<i>Photocurrent (<math>\mu\text{A cm}^{-2}</math>)</i>		
	<i>Maximum</i>	<i>3<sup>rd</sup> cycle</i>	<i>Stability</i>
<b>Au/POs_APBA+Chlorella<sup>a</sup></b>	6.0 ± 0.8	3.8 ± 0.3	62 ± 2
<b>Au/POs_APBA_Chlorella<sup>b</sup></b>	4.0	2.3	58
<b>Au/POs_Chlorella<sup>c</sup></b>	3.2	1.5	47
<b>Au/POs</b>	1.15 ± 0.26	1.0 ± 0.2	91 ± 11

<sup>a</sup> Preincubation of *Chlorella* with 3-APBA, <sup>b</sup> without preincubation, <sup>c</sup> without 3-APBA

**Table Appendix C.2.** Anodic and cathodic peak currents (*I*<sub>pa</sub> and *I*<sub>pc</sub>, respectively) and peak-to-peak separation for P-Os modified electrodes with and without *Chlorella* with and without 3-APBA. Calculated from cyclic voltammetry measurements. Mean (n = 2) ± standard deviation.

<i>Electrode</i>	<i>I</i> <sub>pa</sub> ( $\mu\text{A cm}^{-2}$ )	<i>I</i> <sub>pc</sub> ( $\mu\text{A cm}^{-2}$ )	<i>Peak-to-peak</i> (mV)
<b>Au/POs_APBA+Chlorella<sup>a</sup></b>	29 ± 3	-28.4 ± 0.7	55 ± 7
<b>Au/POs_APBA_Chlorella<sup>b</sup></b>	21 ± 5	-20 ± 4	55 ± 7
<b>Au/POs_Chlorella<sup>c</sup></b>	12 ± 3	-11 ± 2	59.9 ± 0.1
<b>Au/POs</b>	21 ± 3	-21 ± 3	26 ± 2

<sup>a</sup> Preincubation of *Chlorella* with 3-APBA, <sup>b</sup> without preincubation, <sup>c</sup> without 3-APBA

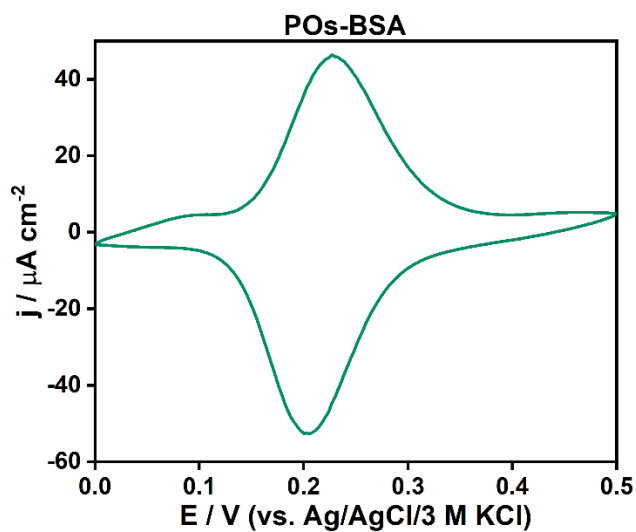


**Figure Appendix C.1.** Cyclic voltammogram of a P-Os modified electrode integrating BSA recorded at  $10 \text{ mV s}^{-1}$  in 0.1 M PB buffer pH 7.

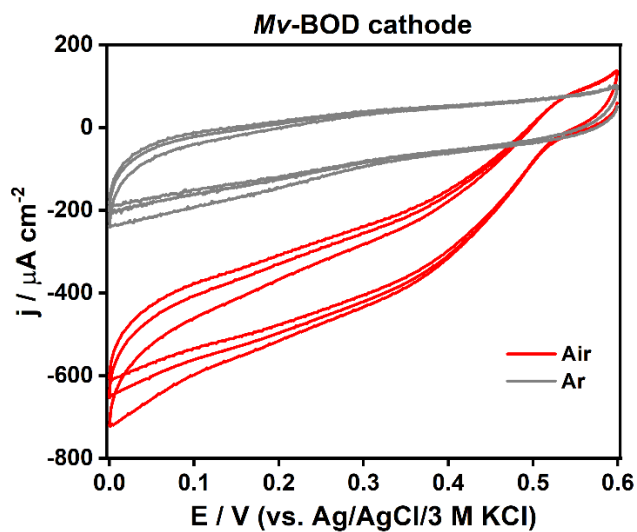


**Figure Appendix C.2.** Cyclic voltammograms of the *Mv*-BOD cathode under air and Ar atmosphere recorded at  $10 \text{ mV s}^{-1}$  in 0.1 M PB buffer pH 7.

---

**Calculation of the power input of reported photobioelectrochemical cells:**

Conversion of photon flux ( $\Phi$ ) [ $\mu\text{mol photons m}^{-2} \text{s}^{-1}$ ] to power density [ $\text{mW cm}^{-2}$ ] considering that the energy of a photon ( $E_p$ ) is calculated using the equation Appendix C.1:

$$E_p = \frac{hc}{\lambda} \quad (\text{Appendix C.1})$$

where  $h$  is the Planck constant ( $= 6.63 \times 10^{-34} \text{ J s}$ ),  $c$  is the speed of light ( $= 2.998 \times 10^8 \text{ m s}^{-1}$ ) and  $\lambda$  is the wavelength in [m]. Therefore, to calculate the power input density the equation Appendix C.2 is used:

$$\text{Power input} = \Phi \times E_p \times N_A \times 100 \quad (\text{Appendix C.2})$$

where  $N_A$  is the Avogadro's number ( $= 6.023 \times 10^{23} \text{ mol}^{-1}$ ).

## Appendix D:

### Supplementary material of Chapter 5

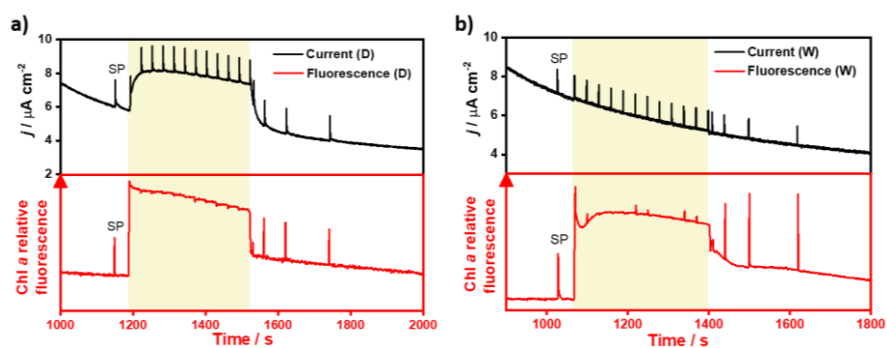


**Figure Appendix D.1.** Chronoamperograms (black lines) and simultaneous Chl *a* fluorescence measurements (red lines) of *C. vulgaris* immobilized by (a) [redacted] D and (b) [redacted] immobilization (W) on GCE/oCNT/PAPBA electrodes.  $E_{\text{app}} = 0.2$  V vs. Ag/AgCl/sat KCl. Electrolyte: PB pH 7. Yellow shadows indicate actinic light ([redacted]).

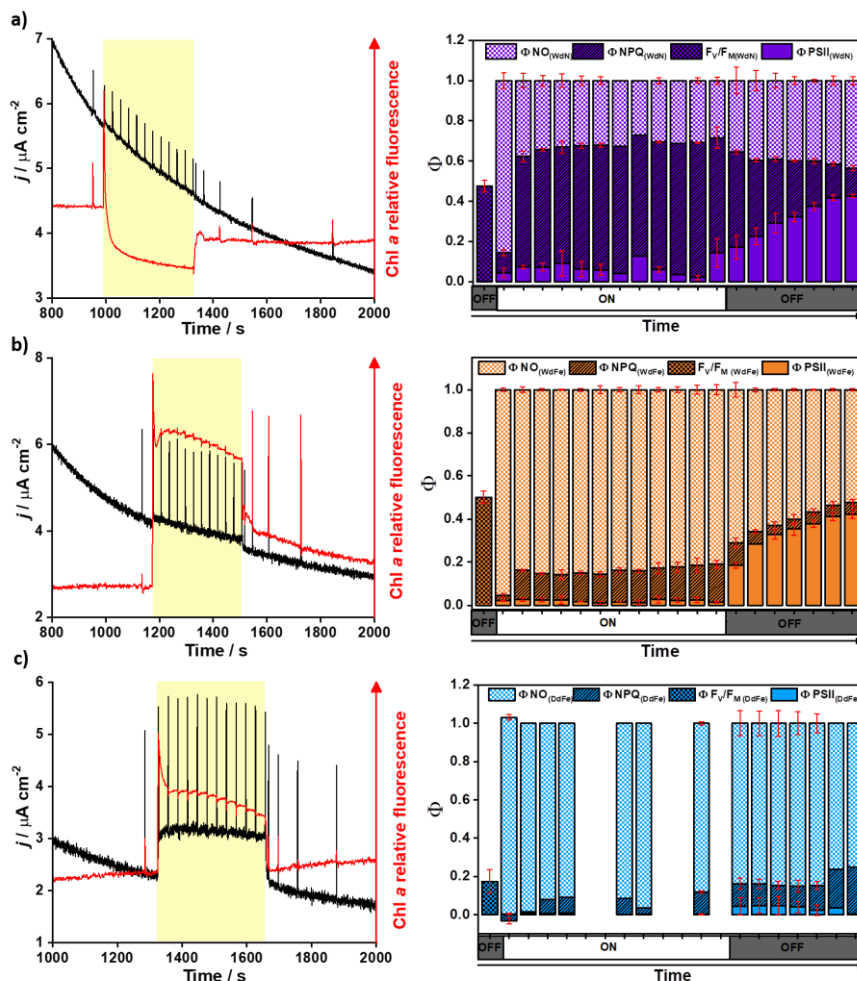


**Figure Appendix D.2.** (right) Simultaneous chronoamperograms and fluorescence measurements (black and red lines, respectively) and (left) average photochemical, light-regulated non-photochemical and non-regulated non-photochemical quantum yields ( $F_V/F_M$ ,  $\Phi$  PSII,  $\Phi$  NPQ and  $\Phi$  NO, respectively) of *C. vulgaris* grown in (a) [redacted] deficient and (b) [redacted] deficient media and further immobilized in [redacted] conditions on GCE/oCNT/PAPBA electrodes, and (c) cells grown in [redacted] deficient medium and further immobilized by [redacted] on GCE/oCNT/PAPBA electrodes. Error bars indicate standard deviation ( $n = 3$ ).  $E_{app} = 0.2$  V vs. Ag/AgCl/sat KCl. Electrolyte: PB pH 7. Yellow shadows indicate actinic light ([redacted]).

**Table Appendix D.1.** One-way ANOVA table for  $F_V/F_M$  by growth conditions and immobilization method with 95% confidence level

<i>Source</i>	<i>Sum of Squares</i>	<i>Df</i>	<i>Mean Square</i>	<i>F-Ratio</i>	<i>P-Value</i>
<b>Between groups</b>	0.341396	4	0.0853489	<b>60.45</b>	<b>0.0000</b>
<b>Within groups</b>	0.0146172	9	0.00162413		
<b>Total (Corr.)</b>	0.356013	13			

**Table Appendix D.2.** Post-hoc Tuckey HSD for  $F_V/F_M$  by growth conditions and immobilization method with 95% confidence level

<i>Treatment</i>	<i>Count</i>	<i>Mean</i>	<i>Homogeneous Groups</i>
<b>Dd</b>	3	0.174333	X
<b>D</b>	3	0.370667	X
<b>Wd</b>	2	0.4755	XX
<b>Wd</b>	3	0.498333	X
<b>W</b>	3	0.627333	X
<b>suspension</b>	2	0.67	X

<i>Contrast</i>	<i>Sig.</i>	<i>Difference</i>	<i>+/- Limits</i>
<b>Dd</b> - <b>D</b>	*	<b>-0.196333</b>	0.108716
<b>Dd</b> - <b>Wd</b>	*	<b>-0.324</b>	0.108716
<b>Dd</b> - <b>Wd</b>	*	<b>-0.301167</b>	0.121549
<b>Dd</b> - <b>W</b>	*	<b>-0.453</b>	0.108716
<b>Dd</b> - <b>suspension</b>	*	<b>-0.495667</b>	0.121549
<b>D</b> - <b>Wd</b>	*	<b>-0.127667</b>	0.108716
<b>D</b> - <b>Wd</b>		-0.104833	0.121549
<b>D</b> - <b>W</b>	*	<b>-0.256667</b>	0.108716
<b>D</b> - <b>suspension</b>	*	<b>-0.299333</b>	0.121549
<b>Wd</b> - <b>Wd</b>		0.0228333	0.121549
<b>Wd</b> - <b>W</b>	*	<b>-0.129</b>	0.108716
<b>Wd</b> - <b>suspension</b>	*	<b>-0.171667</b>	0.121549
<b>Wd</b> - <b>W</b>	*	<b>-0.151833</b>	0.121549
<b>Wd</b> - <b>suspension</b>	*	<b>-0.1945</b>	0.13315
<b>W</b> - <b>suspension</b>		-0.0426667	0.121549

\* denotes a statistically significant difference.

**Table Appendix D.3.** One-way ANOVA table for  $\Phi$ PSII during recovery by growth conditions and immobilization method with 95% confidence level

<i>Source</i>	<i>Sum of Squares</i>	<i>Df</i>	<i>Mean Square</i>	<i>F-Ratio</i>	<i>P-Value</i>
<b>Between groups</b>	1.53135	4	0.382836	<b>95.54</b>	<b>0.0000</b>
<b>Within groups</b>	0.03707	9	0.00411889		
<b>Total (Corr.)</b>	1.56842	13			

**Table Appendix D.4.** Post-hoc Tuckey HSD for  $\Phi$ PSII during recovery by growth conditions and immobilization method with 95% confidence level

<i>Treatment</i>	<i>Count</i>	<i>Mean</i>	<i>Homogeneous Groups</i>
Dd	3	22.2333	X
D	3	23.2333	X
Wd	3	84.9333	X
Wd	2	89.8	X
W	3	93.4	X
suspension	2	97.9	X

<i>Contrast</i>	<i>Sig.</i>	<i>Difference</i>	<i>+/- Limits</i>
Dd - D		-1.0	17.2452
Dd - Wd	*	-62.7	17.2452
Dd - Wd	*	-67.5667	19.2808
Dd - W	*	-71.1667	17.2452
Dd - suspension	*	-75.6667	19.2808
D - Wd	*	-61.7	17.2452
D - Wd	*	-66.5667	19.2808
D - W	*	-70.1667	17.2452
D - suspension	*	-74.6667	19.2808
Wd - Wd		-4.86667	19.2808
Wd - W		-8.46667	17.2452
Wd - suspension		-12.9667	19.2808
Wd - W		-3.6	19.2808
Wd - suspension		-8.1	21.121
W - suspension		-4.5	19.2808

\* denotes a statistically significant difference.



**Table Appendix D.5.** One-way ANOVA table for photocurrent generation by growth conditions and immobilization method with 95% confidence level

<i>Source</i>	<i>Sum of Squares</i>	<i>Df</i>	<i>Mean Square</i>	<i>F-Ratio</i>	<i>P-Value</i>
<b>Between groups</b>	9.4632	5	1.89264	<b>25.68</b>	<b>0.0000</b>
<b>Within groups</b>	0.810791	11	0.0737083		
<b>Total (Corr.)</b>	10.274	16			

**Table Appendix D.6.** Post-hoc Tuckey HSD for photocurrent generation by growth conditions and immobilization method with 95% confidence level

<i>treatment</i>	<i>Count</i>	<i>Mean</i>	<i>Homogeneous Groups</i>
Wd	2	0.06785	X
W	3	0.1393	X
no cells	3	0.146667	X
W	3	0.243333	XX
Dd	3	0.926667	X
D	3	2.1241	X

<i>Contrast</i>	<i>Sig.</i>	<i>Difference</i>	<i>+/- Limits</i>
Dd - D	*	-1.19744	0.755422
Dd - Wd		0.683333	0.755422
Dd - W	*	0.858817	0.844587
Dd - no cells	*	0.787367	0.755422
Dd - Wd	*	0.78	0.755422
D - Wd	*	1.88077	0.755422
D - W	*	2.05625	0.844587
D - no cells	*	1.9848	0.755422
D - Wd	*	1.97744	0.755422
Wd - Wd		0.175483	0.844587
Wd - W		0.104033	0.755422
Wd - no cells		0.0966667	0.755422
W - W		-0.07145	0.844587
W - no cells		-0.0788167	0.844587
W - no cells		-0.00736667	0.755422

\* denotes a statistically significant difference.

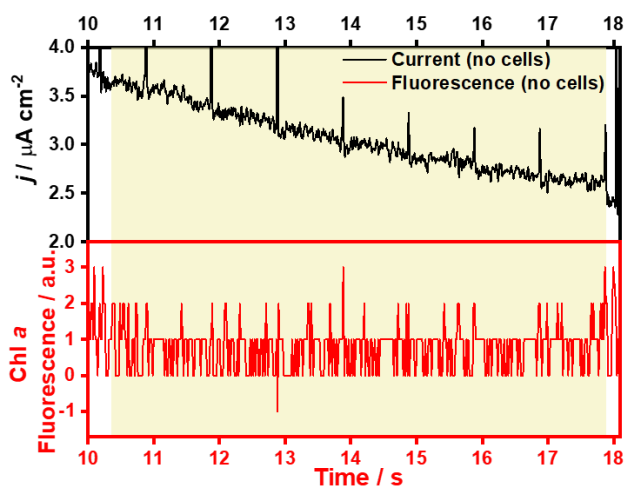


**Figure Appendix D.3.** Chronoamperogram (black line) and simultaneous Chl *a* fluorescence measurement (red line) of GCE/oCNT/PAPBA electrodes in the absence of cells.  $E_{\text{app}} = 0.2 \text{ V}$  vs. Ag/AgCl/sat KCl. Electrolyte: PB pH 7. Yellow shadows indicate actinic light ( ).

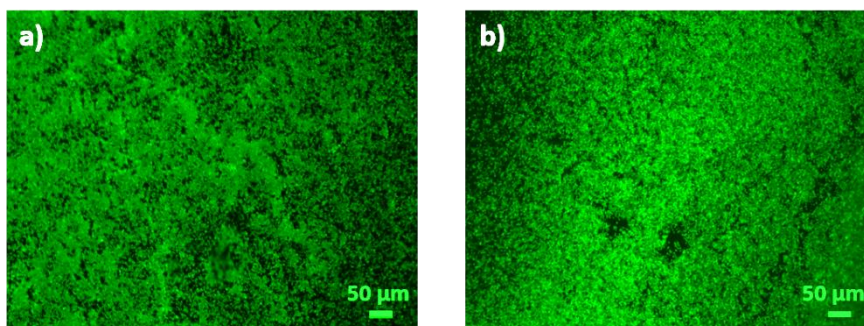


**Figure Appendix D.4.** Fluorescence micrographs of *C. vulgaris* immobilized on GCE/oCNT/PAPBA electrodes by (a) and (b) immobilization. Excitation/emission wavelengths of 630/(650-700) nm. Images were coloured in Image J.

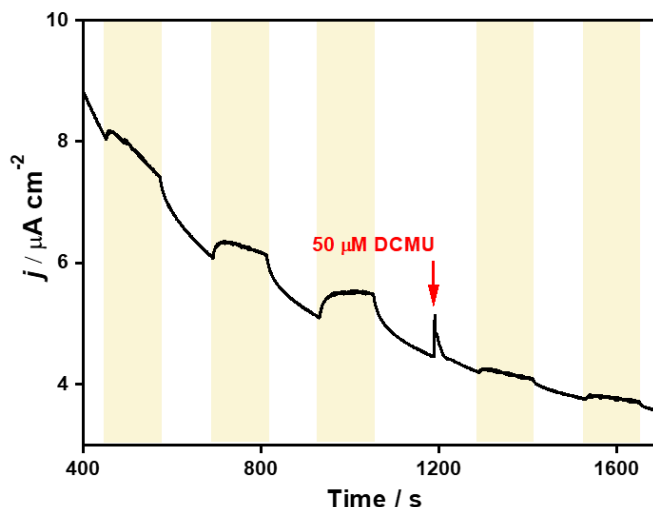


**Figure Appendix D.5.** Chronoamperogram of *C. vulgaris* immobilized on GCE/oCNT/PAPBA electrodes by desiccation recorded in PB pH 7 at 0.2 V vs. Ag/AgCl/sat KCl. Red arrow indicates the addition of DCMU at a final concentration of 50  $\mu\text{M}$ . Yellow shadows indicate irradiation with white light at 90  $\mu\text{mol photons m}^{-2} \text{s}^{-1}$ .

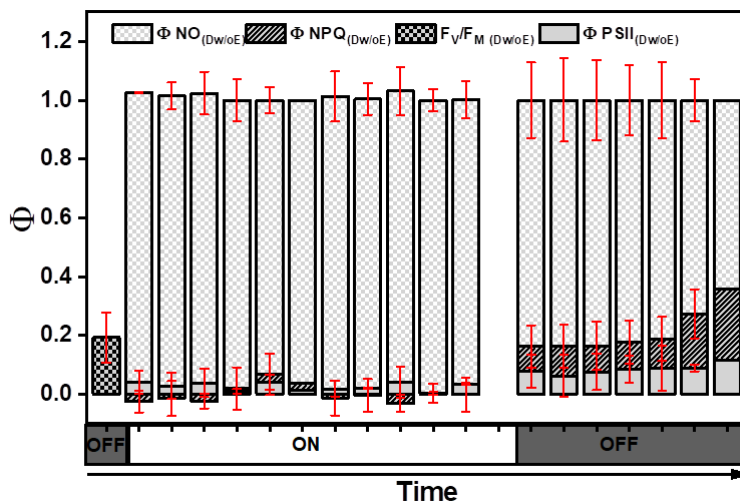


**Figure Appendix D.6.** Average photochemical, light-regulated non-photochemical, light-regulated non-photochemical and non-regulated non-photochemical quantum yields ( $F_v/F_m$ ,  $\Phi$  PSII,  $\Phi$  NPQ and  $\Phi$  NO, respectively) of *C. vulgaris* immobilized by [redacted] on GCE/oCNT/PAPABA without applying potential (no simultaneous chronoamperometry). Error bars indicate standard deviation ( $n = 3$ ). Electrolyte: PB pH 7.





UNIVERSITAT  
ROVIRA i VIRGILI